VOLTAGE DEVIATION IMPROVEMENT IN ACTIVE DISTRIBUTION NETWORK USING BATTERY ENERGY STORAGE SYSTEM OPTIMAL VOLTAGE DROOP CONTROL

THANARAT PHIMTAKHOB

A Thesis Submitted in Partial Fulfillment of the Requirements for
the Degree of Master of Engineering in Electrical Engineering
Suranaree University of Technology
Academic Year 2024

การปรับปรุงการเบี่ยงเบนของแรงดันไฟฟ้าในโครงข่ายจำหน่ายแบบแอคทีฟ โดยใช้การควบคุมแรงดันของระบบกักเก็บพลังงานที่เหมาะที่สุด

นายธนรัตน์ พิมตะขบ

วิทยานิพนธ์นี้เป็นส่วนหนึ่งของการศึกษาตามหลักสูตรปริญญาวิศวกรรมศาสตรมหาบัณฑิต
สาขาวิชาวิศวกรรมไฟฟ้า
มหาวิทยาลัยเทคโนโลยีสุรนารีปี
การศึกษา 2567

VOLTAGE DEVIATION IMPROVEMENT IN ACTIVE DISTRIBUTION NETWORK USING BATTERY ENERGY STORAGE SYSTEM OPTIMAL VOLTAGE DROOP CONTROL

Suranaree University of Technology has approved this thesis submitted in partial fulfillment of the requirements for a Master's Degree.

Thesis Examining Committee

.....

(Asst. Prof. Dr. Chai Chompoo-Inwai)

Chairperson

.....

(Assoc. Prof. Dr. Keerati Chayakulkheeree)

Member (Thesis Advisor)

.....

(Prof. Dr. Thanatchai Kulworawanichpong)

Member

Tosaphol Ratniyomchai

.....

(Asst. Prof. Dr. Tosaphol Ratniyomchai)

Member

.....

(Assoc. Prof. Dr. Yupaporn Ruksakulpiwat)

Vice Rector for Academic Affairs and

Quality Assurance

.....

(Assoc. Prof. Dr. Pornsiri Jongkol)

Dean of Institute of Engineering

ธนรัตน์ พิมตะขบ: การปรับปรุงการเบี่ยงเบนของแรงดันไฟฟ้าในโครงข่ายจำหน่ายแบบแอคทีฟโดยใช้การควบคุมแรงดันของระบบกักเก็บพลังงานที่เหมาะที่สุด
อาจารย์ที่ปรึกษา : รองศาสตราจารย์ ดร. กีรติ ชยะกุลคีรี, 171 หน้า.

คำสำคัญ : voltage stability/ battery energy storage Systems/ L-index/ State of Charge/ SoC restoration

งานวิจัยนี้เสนอการนำระบบกักเก็บพลังงานด้วยแบตเตอรี่มาใช้ในการควบคุมแรงดันไฟฟ้าในเครือข่ายจำหน่ายไฟฟ้าเชิงรุกที่มีการแทรกซึมของพลังงานหมุนเวียนในระดับสูง เพื่อเพิ่มเสถียรภาพของระบบไฟฟ้า โดยมีวัตถุประสงค์หลักเพื่อ ลดค่าความเบี่ยงเบนของแรงดันไฟฟ้ารวมที่เกิดขึ้นกับทุกบัสและลดความเบี่ยงเบนของสถานะการประจุจากค่าที่กำหนดไว้ เพื่อให้ระบบกักเก็บพลังงานด้วยแบตเตอรี่สามารถดำเนินการต่อเนื่องได้อย่างมีประสิทธิภาพ

เพื่อบรรลุเป้าหมายนี้ ได้มีการใช้ดัชนี L-index เพื่อระบุจุดอ่อนของบัส และติดตั้งระบบกักเก็บพลังงานด้วยแบตเตอรี่หลักในตำแหน่งดังกล่าว จากนั้นจึงควบคุมการทำงานของระบบกักเก็บพลังงานด้วยแบตเตอรี่ด้วยเทคนิคการควบคุมแบบ Adaptive Droop Control เพื่อให้สามารถจัดการพลังงานได้อย่างมีประสิทธิภาพ พร้อมทั้งเสนอเทคนิคการฟื้นฟูค่า SoC ให้กลับสู่ระดับที่กำหนดในขณะเดียวกันก็ยังคงรักษาแรงดันไฟฟ้าให้อยู่ในเกณฑ์

ในงานนี้ยังได้นำเทคนิค Particle Swarm Optimization (PSO) และ Fuzzy Multi-Objective Optimization (FMOO) มาใช้เพื่อหาค่าพารามิเตอร์ที่เหมาะสมที่สุดในการควบคุมระบบกักเก็บพลังงานด้วยแบตเตอรี่วิธีการที่เสนอได้ถูกทดสอบในระบบ IEEE 33-bus และ IEEE 69-bus โดยแบ่งการทดลองออกเป็น 4 กรณี ได้แก่ กรณีพื้นฐาน, กรณีที่เพิ่มการแทรกซึมของพลังงานแสงอาทิตย์และพลังงานลม, กรณีที่มีพลังงานแสงอาทิตย์ พลังงานลมและติดตั้งระบบกักเก็บพลังงานด้วยแบตเตอรี่และกรณีที่มีพลังงานแสงอาทิตย์ พลังงานลมและติดตั้งระบบกักเก็บพลังงานด้วยแบตเตอรี่และพิจารณาการฟื้นฟู SoC

ผลการจำลองแสดงให้เห็นถึง ประสิทธิภาพ ของวิธีที่เสนออย่างชัดเจน โดยในทุกกรณีแรงดันไฟฟ้าในระบบดีขึ้นเมื่อเทียบกับกรณีที่ใช้เพียงพลังงานหมุนเวียน และสถานะการประจุสุดท้ายของแบตเตอรี่ยังคงอยู่ใกล้เคียงกับค่าเริ่มต้น แสดงให้เห็นว่าวิธีนี้สามารถควบคุมแรงดันและจัดการ SoC ได้อย่างมีประสิทธิภาพในเวลาเดียวกัน

สาขาวิชาวิศวกรรมไฟฟ้า ลายมือชื่อนักศึกษา ธนรัตน์ พิมตะขบ

ปีการศึกษา 2567 ลายมือชื่ออาจารย์ที่ปรึกษา.....

THANARAT PHIMTAKHOB: VOLTAGE DEVIATION IMPROVEMENT IN ACTIVE DISTRIBUTION NETWORK USING BATTERY ENERGY STORAGE SYSTEM OPTIMAL VOLTAGE DROOP CONTROL

THESIS ADVISOR: ASSOC. PROF. DR. KEERATI CHAYAKULKHEEREE, D.Eng. 171 PP.

Keyword: voltage stability/ battery energy storage Systems/ L-index/ State of Charge/ SoC restoration

This work proposed the implementation of battery energy storage system (BESS) management for voltage regulation in the active distribution network (ADN) with high penetration of renewable energy sources to enhance the stability of the power system. The main objective is to reduce the total voltage deviation (VD) at all buses and minimize the deviation of the state of charge (SoC) from the nominal level to ensure that the BESS can continue to operate. To achieve this, the L-index is introduced to identify weak buses and install the main BESS. Subsequently, the BESS is operated using adaptive droop control to manage its operation efficiently. Moreover, a SoC restoration technique is proposed to maintain the BESS at nominal charge levels while regulating voltage. Particle swarm optimization (PSO) and fuzzy multi objective optimization (FMOO) are used to obtain optimal parameters for controlling the BESS. The proposed method is tested on the IEEE 33-bus system and IEEE 69-bus system, divided into four cases as follows: base case, modified IEEE 33-bus and IEEE 69-bus with PV and wind power penetration, modified IEEE 33-bus and IEEE 69-bus with PV and wind power penetration and BESS, and modified IEEE 33-bus and IEEE 69-bus with PV and wind power penetration and BESS considering SoC restoration.

The simulation results clearly demonstrate the effectiveness and robustness of the proposed approach. In all tested scenarios, voltage profiles improved when compared to only renewable energy. At the same time, the final state of charge (SoC) of each battery remained within its initial value, confirming that the method achieves both voltage control and SoC management successfully

School of Electrical Engineering Student's Signature ธนรัตน์ พิมตะขบ

Academic Year 2024 Advisor's Signature .....

ACKNOWLEDGEMENT

I would like to express my sincere gratitude to Assoc. Prof. Dr. Keerati Chayakulkheeree, my thesis advisor, for his invaluable support, insightful guidance, and continuous encouragement throughout every stage of this research. His expertise and thoughtful advice have been essential to the completion of this thesis.

My sincere thanks also go to the thesis committee members: Asst. Prof. Dr. Chai Chompoo-Inwai, Prof. Dr. Thanatchai Kulworawanichpong, and Asst. Prof. Dr. Tosaphol Ratniyomchai, for their valuable time, comments, and suggestions that helped improve the quality and depth of this work.

I am also grateful to the faculty and staff of the School of Electrical Engineering, Suranaree University of Technology, for their academic support and for providing a learning environment that has helped me grow both personally and professionally.

I would like to extend my appreciation to Suranaree University of Technology for awarding me the Distinguished Graduate Scholarship, which provided essential financial support throughout my master's studies. This scholarship allowed me to focus entirely on my research and academic development.

Special thanks to my friends and fellow graduate students, whose support and companionship made this journey more enjoyable and less stressful. Their encouragement during the challenging moments has meant a lot to me.

Last but certainly not least, I am deeply thankful to my family for their unconditional love, understanding, and constant support. Without their encouragement and belief in me, this achievement would not have been possible.

Thanarat Phimtakhob

TABLE OF CONTENTS

Page

ABSTRACT (THAI)....I
ABSTRACT (ENGLISH)....II
ACKNOWLEDGEMENT....III
TABLE OF CONTENTS....IV
LIST OF TABLES....IX
LIST OF FIGURES....XII
LIST OF ABBREVIATION....XVIII
LIST OF NOMENCLATURE....XIX

CHAPTER

I INTRODUCTION....1

1.1 General Introduction....1
1.2 Problem Statement....2
1.3 Research Objectives....3
1.4 Scope and Limitations....3
1.5 Conception....4
1.6 Research Benefits....5
1.7 Organization of Proposal....5

II LITERATURE REVIEWS....7

2.1 Introduction....7
2.2 Voltage Stability in Modern Power Systems....8
2.3 Power System Analysis Overview....9
2.4 Power Flow Analysis Fundamentals: Newton-Raphson Method....10

TABLE OF CONTENTS (Continued)

Page

2.4.1 System Variables and Bus Classifications 11
2.4.2 Mathematical Formulation of Power Flow Equations 12
2.4.3 Computational Algorithm of the Newton-Raphson Load Flow 14
2.5 Voltage Stability Indices: L-index and Others (Comparison) 17
2.6 Conventional Voltage Control Methods (STATCOM, Capacitor, Tap Changer) 21
2.7 Battery Energy Storage System (BESS) for Voltage Regulation 22
2.8 Voltage Droop Control and Its Variants (Adaptive, Fuzzy, etc.) 23
2.9 State of Charge (SoC) Management in BESS 25
2.10 Optimization Techniques for BESS Control (PSO, Fuzzy, Multi-objective) 26
2.11 Research Gap and Motivation 28
2.12 Summary and Research Contribution 30

III MICROGRID VOLTAGE STABILITY INDICES IMPROVEMENT USING PARTICLE SWARM OPTIMIZATION 31

3.1 Introduction 31
3.2 L-index 31
3.3 P-V curve 33
3.4 Voltage Stability Improvement Using PSO 34
3.5 Results and Discussion 35
3.5.1 IEEE 33-bus base case 35
3.5.2 IEEE 33-bus with L-index improvement 37
3.5.3 IEEE 33-bus modified 38

TABLE OF CONTENTS (Continued)

Page

3.5.4 Modified IEEE 33-bus system with L-index improvement 40
3.6 Chapter Summary 46

IV VOLTAGE DEVIATION IMPROVEMENT IN ACTIVE DISTRIBUTION NETWORK USING BETTERY ENERGY STORAGE SYSTEM OPTIMAL VOLTAGE DROOP CONTROL 48

4.1 Introduction 48
4.2 BESS with Adaptive Droop Control 49
4.3 PSO Based Voltage Deviation Improvement 54
4.4 BESS Selection Criteria and Sizing 56
4.5 Results and Discussion 58
4.5.1 IEEE 33-bus base case 59
4.5.2 Modified IEEE 33-bus with PV and wind power penetration 60
4.5.3 Modified IEEE 33-bus with PV and wind power penetration and BESS with optimal VDC 60
4.5.4 Sensitivity Analysis of Renewable Energy Placement and Sizing 64
4.6 Chapter Summary 67

V BESS VOLTAGE REGULATION CONSIDERING SoC RESTORATION 69

5.1 Introduction 69
5.2 SoC Restoration Formulation 69
5.3 Objective Function 70
5.3 Objective Function 70
5.3.1 PSO Based TSoC Improvement 70

TABLE OF CONTENTS (Continued)

Page

5.3.2 PSO Based TVD Improvement 71
5.4 FMOO-based PSO 71
5.5 PSO Parameter Selection and Tuning 74
5.6 Results and Discussion 79
5.6.1 modified IEEE 33-bus with PV and wind power penetration and BESS considering SoC restoration results 79
5.6.1.1 Scenario 1 Wind power only: 1.25 MW wind, no PV installed 79
5.6.1.2 Scenario 2 0.25 MW PV and 1.00 MW wind 85
5.6.1.3 Scenario 3 0.50 MW PV and 0.75 MW wind 89
5.6.1.4 Scenario 4 0.75 MW PV and 0.50 MW wind 94
5.6.1.5 Scenario 5MW PV and 0.25 MW wind 99
5.6.1.6 Scenario 6 PV only: 1.25 MW PV, no wind installed 103
5.6.2 modified IEEE 69-bus with PV and wind power penetration and BESS considering SoC restoration results 107
5.7 Chapter Summary 114

VI CONCLUSION 115

REFERENCE 117

APPENDIX

APPENDIX A The BESS Operating Result 123
APPENDIX B Energy Profile for Test Simulation 139
APPENDIX C IEEE 33-bus system test data 145
APPENDIX D IEEE 69-bus system test data 149

TABLE OF CONTENTS (Continued)

Page

APPENDIX E List of publications 155
BIOGRAPHY 171

LIST OF TABLES

Table **Page**

2.1 Key Research on Voltage Stability and Renewable Integration 8
2.2 Power System Bus Classifications and Variables 12
2.3 Comparison of Voltage Stability Indices 18
2.4 Comparison of Conventional Voltage Control Methods 21
2.5 Droop Control Methods for BESS 24
2.6 Optimization Techniques for BESS 27
3.1 Comparison of IEEE 33-bus Base Case and L-index Improvement Results 40
3.2 Comparison of IEEE 33-bus Modified Case and Modified IEEE 33-bus system with L-index improvement Results 42
3.3 Comparing L-index value 44
3.4 Comparison Real Power All Cases 46
4.2 Specification of the BESS 59
4.3 Adjust exponent, Droop coefficient and BEES regulating power of BESS 62
4.4 Adjust exponent, Droop coefficient and BEES regulating power of BESS 63
4.5 Adjust exponent, Droop coefficient and BEES regulating power of BESS in sensitivity analysis case 66
4.6 Adjust exponent, Droop coefficient and BEES regulating power of BESS in sensitivity analysis case 67
5.1 PSO Parameter Ranges for Testing 76
5.2 PSO Parameter for TVD objective 78
5.3 PSO Parameter for TSoC objective 78
5.4 PSO Parameter for Fuzzy Multi-objective 78
5.5 Optimal adjust-exponent values obtained with the fuzzy multi-objective PSO algorithm scenario 1 84

LIST OF TABLES (Continued)

Table **Page**

5.6 Optimal adjust-exponent values obtained with the fuzzy multi-objective PSO algorithm scenario 2 88
5.7 Optimal adjust-exponent values obtained with the fuzzy multi-objective PSO algorithm scenario 3 93
5.8 Optimal adjust-exponent values obtained with the fuzzy multi-objective PSO algorithm scenario 4 98
5.9 Optimal adjust-exponent values obtained with the fuzzy multi-objective PSO algorithm scenario 5 102
5.10 Optimal adjust-exponent values obtained with the fuzzy multi-objective PSO algorithm scenario 6 106
5.11 The Maximum, Minimum, and Fuzzy Multi-Objective of Voltage Deviation 108
5.12 The Maximum, Minimum, and Fuzzy Multi-Objective of SoC Deviation 108
B.1 Load profile 139
B.2 PV profile, rated 0.25 MW 139
B.3 PV profile, rated 0.50 MW 140
B.4 PV profile, rated 0.75 MW 140
B.5 PV profile, rated 1.00 MW 141
B.6 PV profile, rated 1.25 MW 141
B.7 Wind profile, rated 0.25 MW 142
B.8 Wind profile, rated 0.50 MW 142
B.9 Wind profile, rated 0.75 MW 143
B.10 Wind profile, rated 1.00 MW 143
B.11 Wind profile, rated 1.25 MW 144
C.1 Line parameter of IEEE 33-bus test system 145

LIST OF TABLES (Continued)

Table **Page**

C.2 Power parameter of IEEE 33-bus test system 147
D.1 Line parameter of IEEE 69-bus test system 149
D.2 Power parameter of IEEE 69-bus test system 152

LIST OF FIGURES

Figure **Page**

1.1 The concept of study 5

3.1 PV curve procedure 33

3.2 Computation Procedure 35

3.3 IEEE 33-bus system 36

3.4 L-index of IEEE 33-bus base case 36

3.5 PV-curve of IEEE 33-bus base case 37

3.6 L-index of IEEE 33-bus with L-index improvement 37

3.7 PV-curve of IEEE 33-bus system with L-index improvement 38

3.8 Modified IEEE 33-bus system 39

3.9 L-index of modified IEEE 33-bus. 40

3.10 PV-curve of modified IEEE 33-bus. 40

3.11 L-index of modified IEEE 33-bus system with L-index improvement. 42

3.12 PV-curve of modified IEEE 33-bus system with L-index improvement. 42

4.1 BESS configuration 49

4.2 VDC strategies 51

4.3 Adaptive VDC strategy 52

4.4 The Relationship between SoC and k_{BES} with the SoC is within the range of $SoC_{\min}$ and $SoC_{\max}$ 53

4.5 The Relationship between SoC and n with the SoC is within the range of $SoC_{\min}$ and $SoC_{\max}$ 54

4.6 The PSO based BESS optimal VDC computation procedure 55

4.7 The modified IEEE 33-bus with PV and wind power penetration and BESS 57

4.8 The modified IEEE 69-bus with PV and wind power penetration and BESS 57

LIST OF FIGURES (Continued)

Figure **Page**

4.9 The PV and Wind profile 24 hour 58
4.10 Comparative Voltage Profile of modified IEEE 33-bus system 62
4.11 the convergence plot of the proposed PSO-based BESS optimal VDC 63
4.12 the result of 30 trials of the proposed method 63
4.13 The result of 30 trials of the computation time 64
4.14 The modified IEEE 33-bus with PV and wind power penetration and BESS in sensitivity analysis case 65
4.15 Comparative Voltage Profile of modified IEEE 33-bus system in sensitivity analysis case 66
5.1 The PSO based BESS optimal TSoC computation procedure 72
5.2 The Fuzzy membership function of total SoC deviation 73
5.3 The Fuzzy membership function of total voltage deviation 74
5.4 The FMOO-based PSO computation procedure 75
5.5 PSO parameter for TVD objective 77
5.6 PSO parameter for TSoC objective 77
5.7 PSO parameter for Fuzzy Multi-objective 77
5.8 Overview of BESS Operation for Voltage Support scenario 1 81
5.9 Time-Series Profiles of Voltage, Regulation Power and Battery SoC at Bus 18 Scenario 1 82
5.10 Comparison of Maximum, Minimum, and Fuzzy Multi-Objective Voltage Deviation scenario 1 83
5.11 Comparison of Maximum, Minimum, and Fuzzy Multi-Objective SoC Deviation scenario 1 83

LIST OF FIGURES (Continued)

Figure **Page**

5.12 Time-Series Profiles of Voltage, Regulation Power and Battery SoC at Bus 18 Scenario 2 86
5.13 Overview of BESS Operation for Voltage Support scenario 2 87
5.14 Comparison of Maximum, Minimum, and Fuzzy Multi-Objective Voltage Deviation scenario 2 87
5.15 Comparison of Maximum, Minimum, and Fuzzy Multi-Objective SoC Deviation scenario 2 88
5.16 Time-Series Profiles of Voltage, Regulation Power and Battery SoC at Bus 18 Scenario 3 91
5.17 Overview of BESS Operation for Voltage Support scenario 3 92
5.18 Comparison of Maximum, Minimum, and Fuzzy Multi-Objective Voltage Deviation scenario 3 92
5.19 Comparison of Maximum, Minimum, and Fuzzy Multi-Objective SoC Deviation scenario 3 93
5.20 Overview of BESS Operation for Voltage Support Scenario 4 95
5.21 Time-Series Profiles of Voltage, Regulation Power and Battery SoC at Bus 18 Scenario 4 96
5.22 Comparison of Maximum, Minimum, and Fuzzy Multi-Objective Voltage Deviation scenario 4 97
5.23 Comparison of Maximum, Minimum, and Fuzzy Multi-Objective SoC Deviation scenario 4 97
5.24 Overview of BESS Operation for Voltage Support Scenario 5 99
5.25 Time-Series Profiles of Voltage, Regulation Power and Battery SoC at Bus 18 Scenario 5 100

LIST OF FIGURES (Continued)

Figure **Page**

5.26 Comparison of Maximum, Minimum, and Fuzzy Multi-Objective Voltage Deviation scenario 5 101
5.27 Comparison of Maximum, Minimum, and Fuzzy Multi-Objective SoC Deviation scenario 5 101
5.28 Overview of BESS Operation for Voltage Support Scenario 6 103
5.29 Time-Series Profiles of Voltage, Regulation Power and Battery SoC at Bus 18 Scenario 6 104
5.30 Comparison of Maximum, Minimum, and Fuzzy Multi-Objective Voltage Deviation scenario 6 105
5.31 Comparison of Maximum, Minimum, and Fuzzy Multi-Objective SoC Deviation scenario 6 105
5.32 Time-Series Profiles of Voltage, Regulation Power and Battery SoC at Bus 65 Scenario 1 109
5.33 Time-Series Profiles of Voltage, Regulation Power and Battery SoC at Bus 65 Scenario 2 110
5.34 Time-Series Profiles of Voltage, Regulation Power and Battery SoC at Bus 65 Scenario 3 111
5.35 Time-Series Profiles of Voltage, Regulation Power and Battery SoC at Bus 65 Scenario 4 112
5.36 Time-Series Profiles of Voltage, Regulation Power and Battery SoC at Bus 65 Scenario 5 113
A.1 Time-Series Profiles of Voltage, Regulation Power and Battery SoC at Bus 22, 25 and 33 in IEEE 33-bus system Scenario 1 123

LIST OF FIGURES (Continued)

Figure **Page**

A.2 Time-Series Profiles of Voltage, Regulation Power and Battery SoC at Bus 22, 25 and 33 in IEEE 33-bus system Scenario 2 124
A.3 Time-Series Profiles of Voltage, Regulation Power and Battery SoC at Bus 22, 25 and 33 in IEEE 33-bus system Scenario 3 125
A.4 Time-Series Profiles of Voltage, Regulation Power and Battery SoC at Bus 22, 25 and 33 in IEEE 33-bus system Scenario 4 126
A.5 Time-Series Profiles of Voltage, Regulation Power and Battery SoC at Bus 22, 25 and 33 in IEEE 33-bus system Scenario 5 127
A.6 Time-Series Profiles of Voltage, Regulation Power and Battery SoC at Bus 22, 25 and 33 in IEEE 33-bus system Scenario 6 128
A.7 Time-Series Profiles of Voltage, Regulation Power and Battery SoC at Bus 27, 35, 46 and 50 in IEEE 69-bus system Scenario 1 129
A.8 Time-Series Profiles of Voltage, Regulation Power and Battery SoC at Bus 52, 67 and 69 in IEEE 69-bus system Scenario 1 130
A.9 Time-Series Profiles of Voltage, Regulation Power and Battery SoC at Bus 27, 35, 46 and 50 in IEEE 69-bus system Scenario 2 131
A.10 Time-Series Profiles of Voltage, Regulation Power and Battery SoC at Bus 52, 67 and 69 in IEEE 69-bus system Scenario 2 132
A.11 Time-Series Profiles of Voltage, Regulation Power and Battery SoC at Bus 27, 35, 46 and 50 in IEEE 69-bus system Scenario 3 133
A.12 Time-Series Profiles of Voltage, Regulation Power and Battery SoC at Bus 52, 67 and 69 in IEEE 69-bus system Scenario 3 134
A.13 Time-Series Profiles of Voltage, Regulation Power and Battery SoC at Bus 27, 35, 46 and 50 in IEEE 69-bus system Scenario 4 135

LIST OF FIGURES (Continued)

Figure **Page**

A.14 Time-Series Profiles of Voltage, Regulation Power and Battery SoC at Bus 52, 67 and 69 in IEEE 69-bus system Scenario 4 136
A.15 Time-Series Profiles of Voltage, Regulation Power and Battery SoC at Bus 27, 35, 46 and 50 in IEEE 69-bus system Scenario 5 137
A.16 Time-Series Profiles of Voltage, Regulation Power and Battery SoC at Bus 52, 67 and 69 in IEEE 69-bus system Scenario 5 138
C.1 IEEE 33-bus system data 145
D.1 IEEE 69-bus system data 149

LIST OF ABBREVIATION

ADN	Active Distribution Network
BESS	Battery energy storage system
FMOO	Fuzzy Multi-Objective Optimization
LV	Low Voltage
NRLF	Newton-Raphson Load Flow
PSO	Particle Swarm Optimization
PV	Photovoltaic
SoC	State of Charge
TSoC	Total SoC deviation
TVD	Total voltage deviation
VC	Voltage Collpse
VD	Voltage Deviation
VDC	Voltage Droop Control
VI	Voltage Instability
VP	Voltage Profile
VS	Voltage Stability
VSI	Voltage Stability Index

LIST OF NOMENCLATURE

$\mathbf{I^G}$	current at generator bus
$\mathbf{I^L}$	current at load bus
$\mathbf{V^G}$	voltage at generator bus
$\mathbf{V^L}$	voltage at load bus
g	the total number of generators
L_j	the L-index value of the bus
V_i	the voltage at the generator bus
V_j	the voltage at the load bus j
F_{ij}	the element of the $\mathbf{F_{LG}}$ matrix obtained by (3.9)
$\mathbf{Y_{LL}}$ and $\mathbf{Y_{LG}}$	the submatrix of $\mathbf{Y_{bus}}$
$\mathbf{F_{LG}}$	the Y-bus converting matrix
P_{BES}	The electrical power that a battery charges or discharges
$P_{BES}^{\max}$	The maximum power that the battery can supply.
$k_{BES,c}$	The droop coefficient controls energy charge.
$k_{BES,d}$	The droop coefficient controls energy discharge.
ΔV	voltage deviation
V_k	Bus voltage
V_0	Nominal voltage
V_h	The sum of Voltage deviation 24 hour
$V_{\text{th}}^{\min}$	The minimum voltage thresholds
$V_{\text{th}}^{\max}$	The maximum voltage thresholds
$V_{\min}$	The minimum voltage

LIST OF NOMENCLATURE (Continued)

$V_{\max}$	The maximum voltage
$K_{\max}$	The maximum droop coefficient
$K_{\min}$	The minimum droop coefficient
n_d	The adjust exponent for $k_{BES,d}$
n_c	The adjust exponent for $k_{BES,c}$
$SoC(t)$	state of charge at the current step
$SoC(t-1)$	state of charge at the previous step
E	Battery capacity
N	Number of buses
SoC	State of charge
SoC	The sum of SoC 24 hour
$SoC_{\min}$	Minimum state of charge
$SoC_{\max}$	Maximum state of charge
$P_{BES,\min}$	The minimum power that the battery can supply
$P_{BES,\max}$	The maximum power that the battery can supply
Z	Number of batteries
h	The hour
P_{SoC}	The power of SoC restoration
$P_{SoC,\max}$	The maximum power of SoC restoration
$P_{SoC,\min}$	The minimum power of SoC restoration
$P_{SoC,d}$	The discharge power of SoC restoration
$P_{SoC,c}$	The charge power of SoC restoration
n_{ds}	The adjust exponent for $P_{SoC,d}$
n_{cs}	The adjust exponent for $P_{SoC,c}$

LIST OF NOMENCLATURE (Continued)

n_s	The adjust exponent of SoC restoration
$pBest_i$	The best value of each particle i
$gBest$	The best value of all particles
t	The iteration
v_i	The velocity for a particle i
c_1 and c_2	Constant numbers
r_1 and r_2	Random parameters
w	Inertial weight
x_i	The population of particles
$TSoC_{\max}$	The maximum total SoC deviation
$TSoC_{\min}$	The minimum total SoC deviation
$TVD_{\max}$	The maximum total voltage deviation
$TVD_{\min}$	The minimum total voltage deviation
μ_T	The membership function
μ_{TSoC}	The membership function of total SoC deviation
μ_{TVD}	The membership function of total voltage deviation

CHAPTER I

INTRODUCTION

1.1 General Introduction

At present, the electrical network is being rapidly expanded to meet energy demand, which is increasing at an average rate of over 4 percent per year. Therefore, it is critically important to focus on maintaining the system's Voltage Stability (VS) to prevent Voltage Instability (VI), which can lead to severe system disturbances. Today's systems are extremely complicated, with widespread usage of renewable energy sources such as wind and solar power. Most renewable energy sources function in tandem with distribution electrical systems, influencing system parameters such as Voltage Profile (VP) and Voltage Deviation (VD). As a result, VS is a key element contributing to VI, must be considered because it has an impact on the system.

Voltage Stability is an important tool for considering electrical systems because it can indicate how the system operates or other design aspects. As a result, VI can cause system failure or power outages. For example, in 1978, Thailand experienced a huge blackout due to generator failures caused by VI, affecting the people statewide for several hours and badly damaging the economy. Thus, considering VS contributes to the system's efficiency.

To assess and improve VS, system operators and researchers utilize analytical tools such as Voltage Stability Indices (VSIs). From several VSIs, the L-index is one of the methods used to determine the weakest bus that causes the system's Voltage Collapse (VC). The L-index is calculated from power flow analysis and the system's admittance matrix (Y-bus), with values ranging from 0 to 1. A value approaching 1 indicates a high risk of voltage instability. By identifying and reinforcing

these weak buses, it is possible to prevent VC and improve the resilience of the overall system.

In addition to analytical methods, technological solutions like Battery Energy Storage Systems (BESS) are another useful instrument for current electrical systems in resolving voltage stability issues. BESS operates to supply or receive active power at the weakest bus identified through L-index analysis, allowing it to address a variety of difficulties such as Voltage Profile and Voltage Drop. Furthermore, BESS improves the stability of the electrical system by collaborating with Renewable Energy, which has intermittent energy systems. Integrating BESS at strategically critical places is thus a promising strategy for reducing voltage instability and ensuring a consistent and dependable power supply.

1.2 Problem Statement

Voltage instability poses serious threats to the stability of power systems around the world. Maintaining voltage stability has become an increasingly difficult task. Conventional solutions for dealing with voltage instability usually rely on system improvements or actual power adjustment techniques, which may be insufficiently successful. Precise identification of important spots in the electrical grid is critical. The L-index has been shown to be an effective technique for measuring voltage stability, identifying the most sensitive buses to voltage collapse. Despite its usefulness, the L-index's practical applications in operations are restricted.

Battery Energy Storage Systems are an appealing alternative because of their quick response times and diverse operational properties. BESS can provide rapid voltage assistance by absorbing or injecting actual power. However, studies on BESS have investigated a variety of topics, including establishing appropriate installation sites in power systems to reduce losses and reducing dependency on older devices such as load tap-changing transformers and capacitor banks. In this study, BESS is used to increase voltage stability specifically VP and VD via battery management techniques. Among the strategies investigated, adaptive droop voltage control, which is an

adaptation of droop frequency control, is used. The advantage of this technology is that it considers the battery's State of Charge (SoC) to avoid saturation, hence increasing the efficiency of BESS utilization. Furthermore, optimization procedures are used to accomplish the most efficient process.

This study seeks to provide a technique that combines the analytical precision of the L-index with the practical advantages of BESS implementation. VD are optimized, and the system's VP further improved, by selecting the most suitable buses for battery installation using the L-index and then managing the batteries with adaptive droop voltage control while taking the SoC into account. This strategy helps to strengthen the stability of the power system.

1.3 Research Objectives

The main objective of this research is to enhance voltage stability in power systems by integrating BESS at critical bus points identified by the L-index. The specific objectives of the research include:

1.3.1 To apply the method to identify critical buses that lead to voltage collapse using L-index.

1.3.2 To apply the method for BESS management using particle swarm optimization (PSO) to minimize voltage deviation and enhance voltage profile.

1.3.3 To manage BESS with adaptive droop voltage control while maintaining SoC at an appropriate level.

Achieving these objectives will provide a systematic approach for improving voltage stability through the use of BESS at critical points in power systems.

1.4 Scope and Limitations

1.4.1 In the IEEE 33-bus system, BESS are installed at four locations: 4.25 MW at bus 18, 1.75 MW at bus 22, 3.5 MW at bus 25, and 3.5 MW at bus 33. In the IEEE 69-bus system, BESS units are installed at eight locations: 1.75 MW at bus 27, 0.5 MW at

bus 35, 0.75 MW at bus 46, 2.75 MW at bus 50, 0.25 MW at bus 52, 5.75 MW at bus 65, 0.25 MW at bus 67, and 0.25 MW at bus 69.

1.4.2 The IEEE 33-bus and IEEE 69-bus distribution system is employed for testing and analysis purposes. Including four cases as follows:

- case I: IEEE 33-bus base case,
- case II: modified IEEE 33-bus with PV and wind power penetration,
- case III: modified IEEE 33-bus with PV and wind power penetration and BESS and
- case IV: modified IEEE 33-bus and IEEE 69-bus with PV and wind power penetration and BESS considering SoC restoration

1.4.3 Economic considerations related to BESS, including battery costs and investment expenses, are not considered in this study.

1.4.4 The study does not cover dynamic or transient stability analysis, focusing solely on steady-state conditions.

1.5 Conception

This study originated from the need to enhance the stability of electrical systems, particularly voltage stability. Consequently, various relevant methodologies were investigated. It was discovered that weak buses may lead to VC. Therefore, the L-index, which can identify weak buses, was employed for calculation and assessment to determine optimal locations for BESS installation. This research hypothesizes that installing BESS at weak buses will significantly improve the stability and reliability of the electrical system. Furthermore, it is posited that incorporating BESS management through optimization techniques will yield even greater improvements in system stability. Fig. 1.1 shows the concept of the study.

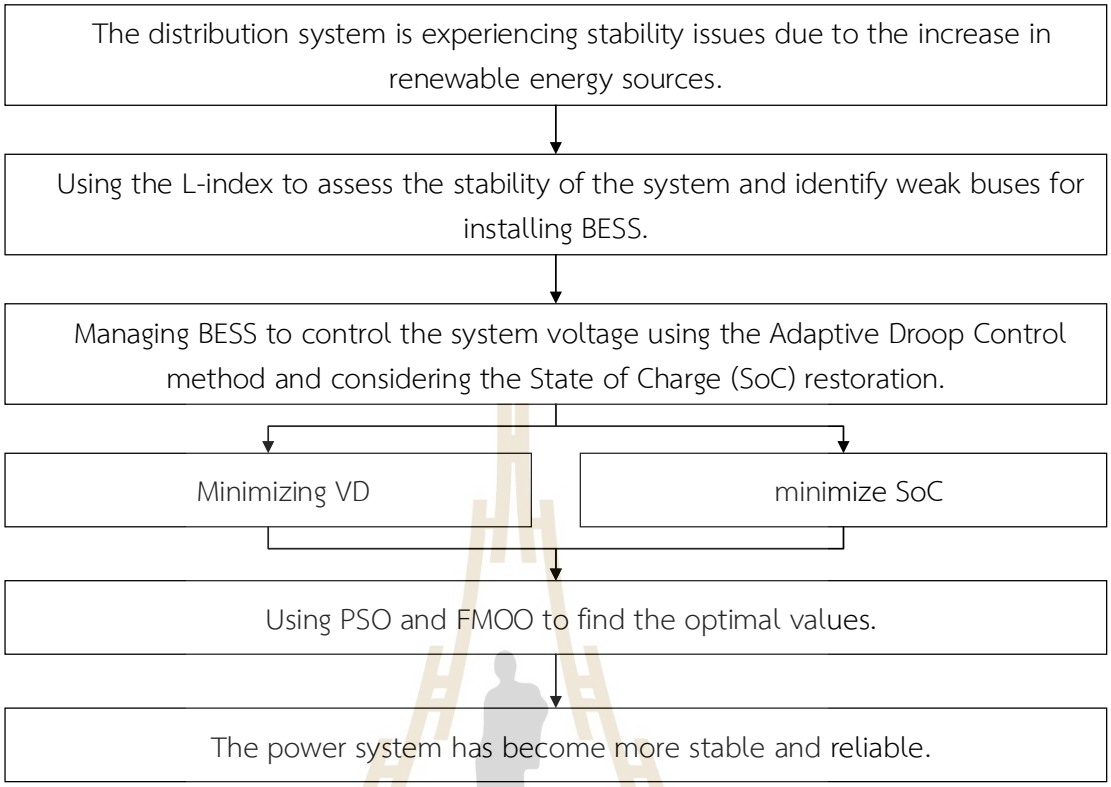

Figure 1.1 The concept of study

1.6 Research Benefits

The L-index can effectively identify vulnerable buses within an electrical system, thereby enabling the assessment and prevention of system stability issues before they manifest. Furthermore, it facilitates the optimal placement of BESS on appropriate buses. The efficient management of BESS through PSO and Fuzzy Multi-objective contributes to the enhancement of VP and the reduction of VD. These parameters contribute to the heightened stability of the electrical system.

1.7 Organization of Proposal

This Proposal is organized as follows:

Chapter 2 involves presenting an overview of studies related to the research. In sections 2.2 to 2.11, a literature review is conducted on topics related to VS, VSI, Conventional Methods of Voltage Control, and BESS.

Chapter 3 examines the use of the L-index to identify weak buses in the power system. Section 3.2 presents the formula and calculation method for the L-index, and in Section 3.5, the experimental results are analyzed to identify weak buses in the power system.

Chapter 4 introduces methods for voltage control in power systems using BESS in systems with renewable energy. Section 4.2 proposes a method for managing BESS with VDC to ensure efficient operation, and Section 4.3 applies optimization to find optimal values for BESS management. Finally, Section 4.5 presents the results from BESS management.

Chapter 5 proposes a method for SoC restoration of BESS. Sections 5.2 to 5.3 demonstrate the calculation methods and optimization processes using Multi-objective Fuzzy Logic. Finally, Section 5.6 presents the results.

Chapter 6 summarizes all the work conducted in this study.

CHAPTER II

LITERATURE REVIEWS

2.1 Introduction

In recent years, the enormous increase in renewable energy integration has had a significant impact on power system stability. As a result, it is critical to emphasize the design and control of system stability, particularly voltage stability. This chapter discusses voltage stability and its assessment methodologies, as well as the research of BESS, which improves the system's voltage stability. Finally, the main points of the content and research are summarized.

This research is divided into 8 sections that address the following themes. An overview of voltage stability and the implications of incorporating renewable energy into the system, a study of voltage stability indices for evaluating system stability, with a focus on the L-index as a critical measure for identifying weak buses, an analysis of traditional voltage control methods, their implementation and benefits, an exploration of the applications of batteries and Examine the management of BESS for energy supply or absorption with the goal to resolve system stability issues. The entire study emphasizes maintaining system stability, from assessment to control, to enhance system reliability. The various research efforts are presented in the following sections: 2.2 presents research relating to Voltage Stability in Modern Power Systems, 2.3 presents Power Flow Analysis Fundamentals: Newton-Raphson Method , 2.4 presents research on Voltage Stability Indices: L-index and Others (Comparison), 2.5 presents research on Conventional Voltage Control Methods (STATCOM, Capacitor, Tap Changer), 2.6 presents research on Battery Energy Storage System (BESS) for Voltage Regulation, 2.7 presents research on Voltage Droop Control and Its Variants (Adaptive, Fuzzy, etc.), 2.8 presents research on State of Charge (SoC) Management in BESS, 2.9

Optimization Techniques for BESS Control (PSO, Fuzzy, Multi-objective), 2.10 present Research Gap and Motivation and 2.11 Summary and Research Contribution

2.2 Voltage Stability in Modern Power Systems

Due to increased demand loads and renewable energy integration, electrical systems are becoming more complicated and difficult to operate and plan effectively. VS is an important concern for electrical systems since it indicates efficiency and reliability. Several research studies investigated into systems that integrate renewable energy sources.

Table 2.1 Key Research on Voltage Stability and Renewable Integration

Year	Author	Objective	Description
2018	(Xu et al., 2018)	To evaluate the impact of renewable energy variabilities on power system voltage stability.	Renewable power variabilities significantly impact the probability distributions of load margins.
2018	(Adnan et al., 2018)	To investigate the impact of installing Distributed Generation (DG), specifically solar photovoltaic (PV) systems.	Use the IEEE 30 bus test system and carefully selecting DG locations and penetration levels.
2021	(Dondariya & Sakravdia, 2021)	To assess and improve voltage stability in power systems with the integration of solar photovoltaic (PV) generation.	The integration of solar PV generators at suitable locations significantly increases the critical load ability limit of the system. If installed PV at weak buses, it can improve voltage stability.

Table 2.1 Key Research on Voltage Stability and Renewable Integration (Continued)

Year	Author	Objective	Description
2024	(Malik et al., 2024)	To provide a comprehensive review of voltage stability issues in power systems with integrated wind energy.	To address the challenges associated with voltage instability and its implications for wind power integration and Various voltage stability indices have been developed to identify weak buses and assess overall system stability.
2024	(Wang et al., 2024)	To develop a method for analyzing static voltage stability in distribution power systems with integrated renewable energy sources.	-The study aims to address the challenges posed by large-scale renewable energy integration on static voltage stability and propose a simpler, more effective analysis method compared to traditional approaches.

2.3 Power System Analysis Overview

Power system analysis is a key tool for electrical engineers to ensure the grid we rely on is reliable, safe, and efficient. This analysis looks at the grid under two main conditions: normal operation and abnormal operation. Normal Operation is when the power system is running smoothly, just as it was designed to. Key values like voltage and frequency stay within their standard limits. Analysis in this state focuses on routine planning to keep the system running at its best. Abnormal Operation refers to unexpected events that disturb the system, like a lightning strike, a downed power line, or a power plant suddenly going offline. These events can lead to major issues like blackouts.

Beyond these conditions, the analysis can also be classified by its timeframe into two types: Steady-State Analysis and Transient-State Analysis. Steady-State Analysis looks at the system's condition after things have settled down and become stable. It's like taking a snapshot of the grid to see if everything is balanced. The study of Voltage Stability, which is the focus of this thesis, is a type of steady-state analysis. It deals with the system's ability to maintain a steady voltage under changing load conditions. The primary tool for this is Power Flow Analysis, which calculates voltage levels and power flows in the network. The results are used to calculate a Voltage Stability Index (VSI), an indicator that helps gauge how close the system might be to a voltage collapse. Transient-State Analysis studies what happens in the brief moments right after a disturbance. This helps understand the rapid changes and design protective systems that can react in time.

Therefore, this research focuses exclusively on steady-state analysis to understand and solve voltage stability problems. It uses data from power flow analysis as a critical foundation, providing a clearer and more complete picture of the underlying theories involved.

2.4 Power Flow Analysis Fundamentals: Newton-Raphson Method

In power system engineering, power flow analysis, often called a load flow study, is one of the most essential and widely used computational tools. It plays a crucial role in system planning, operation, economic dispatch, and overall control. The main goal of a power flow study is to numerically analyze how electric power flows through an interconnected network under steady-state conditions. This analysis provides the voltage magnitude and phase angle at each bus in the system, which are then used to calculate the real and reactive power flowing through transmission lines and transformers, as well as overall system losses. By offering a detailed snapshot of issues and a system's operating status under specific load and generation scenarios, power flow analysis helps engineers ensure the system is running safely and efficiently,

detect potential overload or voltage issues and make informed decisions for future system upgrades and expansions.

2.4.1 System Variables and Bus Classifications

In power system analysis, the steady-state condition of any bus i within a network is fully characterized by four fundamental variables: the real power injection (P_i), the reactive power injection (Q_i), the voltage magnitude ($|V_i|$), and the voltage phase angle (δ_i). For the power flow problem to be mathematically well-posed and solvable, exactly two of these four variables must be specified for each bus, leaving the remaining two to be determined through computation. This requirement underpins the standard classification of buses into three distinct types, which consequently defines the structure of the system of nonlinear algebraic equations to be solved. The standard bus classifications are presented in Table 2.2.

The designation of a slack bus is not merely a matter of computational convenience but represents a fundamental necessity within the power flow formulation. The analysis is governed by power balance equations, which require that total power generation equals the sum of total system load and transmission losses. However, real power losses primarily resulting from I^2R losses in transmission lines are a function of the current flow, which itself depends on bus voltage magnitudes and phase angles. Since these quantities are initially unknown, the total system losses cannot be determined a priori, thereby making it infeasible to predefine the exact real power output of every generator in the system.

To resolve this issue, a single bus referred to as the slack (or swing) bus is designated to absorb the mismatch between the specified generation and the total system demand plus losses. The real and reactive power injections at the slack bus are treated as unknowns, allowing it to adjust dynamically during the solution process. This ensures that the power balance equations are satisfied upon convergence of the power flow algorithm, thereby maintaining consistency with physical and operational constraints.

Table 2.2 Power System Bus Classifications and Variables

Bus Type	Description	Specified (Known) Variables	Unknown Variables to be Solved
Slack Bus (Swing or Reference Bus)	A single reference bus, typically connected to a large generator, that compensates for system power losses and provides the angle reference for all other buses.	Voltage Magnitude and voltage phase angle	Real Power (P) and Reactive Power (Q).
Load Bus (PQ Bus)	Represents a point of consumption in the network where real and reactive power are drawn from the system. Most buses in a power system fall into this category.	Real Power (P) and Reactive Power (Q).	Voltage Magnitude and voltage phase angle
Generator Bus (PV Bus)	Represents a bus where a generator is connected. The real power output is controlled via the prime mover, and the voltage magnitude is maintained by the generator's excitation system.	Real Power (P) and Voltage Magnitude	Reactive Power (Q) and voltage phase angle

2.4.2 Mathematical Formulation of Power Flow Equations

The mathematical model for the power flow problem is derived from fundamental circuit theory, specifically Kirchhoff's Current Law applied at each node of the power system. For a multi-bus network, this relationship is systematically expressed using the bus admittance matrix ($\mathbf{Y_{BUS}}$), which relates the vector of bus current injections ($\mathbf{I}$) to the vector of bus voltages ($\mathbf{V}$).

$$\mathbf{I} = \mathbf{Y_{BUS}}\mathbf{V} \tag{2.1}$$

For any given bus i in an n-bus system, the injected current I_i is the sum of the currents flowing from that bus into the connected branches:

$$I_i = \sum_{j=1}^{n} Y_{ij} V_j \tag{2.2}$$

However, in power flow studies, the specified quantities are typically real and reactive power injections, not currents. The complex power injected into bus *i* is defined as:

$$S_i = P_i + jQ_i = V_i I_i^* \tag{2.3}$$

where I_i^* is the complex conjugate of the injected current I_i. Rearranging this equation yields an expression for the current injection in terms of power and voltage:

$$I_i = \frac{P_i - jQ_i}{V_i^*} \tag{2.4}$$

By substituting this expression for current back into the nodal admittance equation, we formulate the fundamental power flow equations. These equations relate the specified powers at each bus to the bus voltages throughout the network.

$$\frac{P_i - jQ_i}{V_i^*} = \sum_{j=1}^{n} Y_{ij} V_j \tag{2.5}$$

To facilitate an iterative solution, these complex equations are typically expressed in polar coordinates. Let the voltage at bus i be $V_i = |V_i| \angle \delta_i$ and the element of the admittance matrix between bus i and bus j be $Y_{ij} = |Y_{ij}| \angle \theta_{ij}$. By substituting these polar forms into the power flow equation and separating the real and imaginary parts, we arrive at the final set of non-linear, coupled algebraic equations that must be solved:

Real Power Injection Equation:

$$P_i = \sum_{j=1}^{n} |V_i||V_j||Y_{ij}| \cos(\delta_i - \delta_j - \theta_{ij}) \tag{2.6}$$

Reactive Power Injection Equation:

$$Q_i = \sum_{j=1}^{n} |V_i||V_j||Y_{ij}|\sin(\delta_i - \delta_j - \theta_{ij}) \quad (2.7)$$

This system of non-linear equations forms the core of the power flow problem. Due to their non-linearity and the coupling between variables, an analytical solution is not feasible for any practical power system. Therefore, iterative numerical methods are required to find the unknown voltage magnitudes $|V|$ and angles δ that satisfy these equations within a specified tolerance.

2.4.3 Computational Algorithm of the Newton-Raphson Load Flow

The implementation of the Newton-Raphson method follows a structured, iterative procedure. The algorithm begins with an initial guess and repeatedly refines the solution until the power mismatches at all buses fall below a specified convergence tolerance. The detailed computational steps are as follows:

Step 1: Initialization

- Construct the system's bus admittance matrix, Y_{bus}, from the line and transform impedance data.
- Assume an initial voltage profile for all buses. A "flat start" is commonly used, where the voltage magnitude is set to 1.0 p.u. and the phase angle is set to 0° for all PQ and PV buses. The slack bus voltage is fixed at its specified value.
- Set the iteration counter, k, to 0 and define the convergence tolerance, ε.

Step 2: Calculate Power Mismatches

- Using the bus voltage values from the current iteration, $|V|^{(k)}$ and $\delta^{(k)}$, calculate the real power injection ($P_i^{(k)}$) for all buses except the slack bus, and the reactive power injection ($Q_i^{(k)}$) for all PQ buses using the power flow equations.
- Compute the power mismatch vectors by subtracting the calculated powers from the specified (scheduled) powers:

$$\Delta P_i^{(k)} = P_i^{spec} - P_i^{(k)} \tag{2.8}$$

$$\Delta Q_i^{(k)} = Q_i^{spec} - Q_i^{(k)} \tag{2.9}$$

Step 3: Check for Convergence

- Find the maximum absolute value among all elements of the power mismatch vectors.
- If max $\max(|\Delta P|, |\Delta Q|) < \varepsilon$ the solution has converged. The algorithm terminates the iterative loop and proceeds to Step 7. Otherwise, continue to the next step.

Step 4: Compute the Jacobian Matrix

- Calculate the elements of the four sub-matrices of the Jacobian, $j^{(k)}$, using the partial derivative formulas and the voltage values from the current iteration, $|V|^{(k)}$ and $\delta^{(k)}$.

$$\begin{bmatrix} \Delta P^{(k)} \\ \Delta Q^{(k)} \end{bmatrix} = \begin{bmatrix} J_{11}^{(k)} & J_{12}^{(k)} \\ J_{21}^{(k)} & J_{22}^{(k)} \end{bmatrix} \begin{bmatrix} \Delta \delta^{(k)} \\ \Delta |V|^{(k)} \end{bmatrix} \tag{2.10}$$

  - $J_{11} = \dfrac{\partial P}{\partial \delta}$: This sub-matrix relates changes in real power injections to changes in bus voltage angles. The diagonal and off-diagonal elements are given by:
    - Off-diagonal ($i \neq k$)

$$\frac{\partial P_i}{\partial \delta_k} = -|V_i||V_k||Y_{ik}|\sin(\theta_{ik} + \delta_k - \delta_i) \tag{2.11}$$

    - Diagonal ($i = k$)

$$\frac{\partial P_i}{\partial \delta_i} = \sum_{\substack{j=1 \\ j \neq i}}^{n} |V_i||V_j||Y_{ij}|\sin(\theta_{ij} + \delta_j - \delta_i) \tag{2.12}$$

  - $J_{12} = \dfrac{\partial P}{\partial |V|}$: This sub-matrix relates changes in real power injections to changes in bus voltage magnitudes. The diagonal and off-diagonal elements are:

- Off-diagonal ($i \neq k$)

$$\frac{\partial P_i}{\partial |V_k|} = |V_i||Y_{ik}|\cos(\theta_{ik} + \delta_k - \delta_i) \tag{2.13}$$

- Diagonal ($i = k$)

$$\frac{\partial P_i}{\partial \delta_i} = 2|V_i||Y_{ii}|\cos(\theta_{ii}) + \sum_{\substack{j=1 \\ j \neq i}}^{n} |V_j||Y_{ij}|\cos(\theta_{ij} + \delta_j - \delta i) \tag{2.14}$$

- $J_{21} = \frac{\partial Q}{\partial \delta}$: This sub-matrix relates changes in reactive power injections to changes in bus voltage angles. The diagonal and off-diagonal elements are:
  - Off-diagonal ($i \neq k$)

$$\frac{\partial Q_i}{\partial \delta_k} = -|V_i||V_k||Y_{ik}|\cos(\theta_{ik} + \delta_k - \delta_i) \tag{2.15}$$

  - Diagonal ($i = k$)

$$\frac{\partial Q_i}{\partial \delta_i} = \sum_{\substack{j=1 \\ j \neq i}}^{n} |V_i||V_j||Y_{ij}|\cos(\theta_{ij} + \delta_j - \delta_i) \tag{2.16}$$

- $J_{22} = \frac{\partial Q}{\partial |V|}$: This sub-matrix relates changes in real power injections to changes in bus voltage magnitudes. The diagonal and off-diagonal elements are:
  - Off-diagonal ($i \neq k$)

$$\frac{\partial P_i}{\partial |V_k|} = -|V_i||Y_{ik}|\sin(\theta_{ik} + \delta_k - \delta_i) \tag{2.17}$$

  - Diagonal ($i = k$)

$$\frac{\partial Q_i}{\partial \delta_i} = -2|V_i||Y_{ii}|\sin(\theta_{ii}) - \sum_{\substack{j=1 \\ j \neq i}}^{n} |V_j||Y_{ij}|\sin(\theta_{ij} + \delta_j - \delta i) \tag{2.18}$$

Step 5: Solve for Voltage Corrections

- Solve the system of linear equations to find the voltage correction vector.

$$\begin{bmatrix} \Delta\delta^{(k)} \\ \Delta|V|^{(k)} \end{bmatrix} = \left[J^{(k)}\right]^{-1} \begin{bmatrix} \Delta P^{(k)} \\ \Delta Q^{(k)} \end{bmatrix} \tag{2.19}$$

Step 6: Update Voltages and Iterate

- Update the voltage magnitudes and angles for the next iteration:

$$\delta^{(k+1)} = \delta^{(k)} + \Delta\delta^{(k)} \quad (2.20)$$

$$|V|^{(k+1)} = |V|^{(k)} + \Delta|V|^{(k)} \quad (2.21)$$

- Increment the iteration counter, k = k+1, and return to Step 2 to begin the next iteration.

Step 7: Final Calculations

- Once convergence is achieved, use the final bus voltage solution to calculate the real and reactive power injections at the slack bus.
- Calculate the real and reactive power flows on all transmission lines and transformers, as well as the power losses in each component.

2.5 Voltage Stability Indices: L-index and Others (Comparison)

To address the many concerns with voltage stability (VS) that occur as a result of renewable energy integration, instruments for assessing system stability are required. Numerous research has looked into these techniques, one of which is the voltage stability indices (VSI). VSI is used to compare the current operating state of the system to the voltage collapse point; in other words, it indicates how close the system's voltage stability is to collapsing. VSI can also detect important buses and analyze the stability of transmission lines.

Voltage stability index is classified into three types based on the calculation method: system parameters (variable)-based, Jacobian matrix-based, and phasor measurement units (PMU)-based. Each type has characteristics. The Jacobian matrix-based approach can be used to calculate the voltage collapse point and load margin. The system parameters (variable)-based method is used to identify weak buses or

places that need to be assessed, and it considers the line loadability limit. The PMU-based technique, which relies on local measurements and Thevenin impedance computations, is used to monitor voltage stability indices rather than to anticipate instability. Table 2.2 shows a comparison of various VSIs.

Table 2.3 Comparison of Voltage Stability Indices

Index	Advantages	Disadvantages	Example Application	References
L-index	The L-Index can be easily implemented in real-time monitoring systems. Identify strong/weak buses using L-index coeff.	Not suitable for dynamic analysis	IEEE 10, 14, 39, 118 test system., the WSCC 9 bus system	(Karn et al., 2023; Kessel & Glavitsch, 1986; Ram & M, 2016; Ramanareddy, 2011)

Table 2.3 Comparison of Voltage Stability Indices (Continued)

Index	Advantages	Disadvantages	Example Application	References
FSVI	The Fast Voltage Stability Index (FVSI) can identify "weak buses" that are close to voltage collapse based on index values approaching 1.00. The calculation is straightforward.	Low efficiency for large systems requires multiple power flow iterations.	IEEE 30-bus	(Isaiah et al., 2015)
Jacobian-based	It can accurately estimate the collapse point and Voltage Stability Margin (VSM).	The calculations are extensive and complex, making it unsuitable for real-time monitoring and not ideal for identifying weak buses/lines.	-	(Danish et al., 2019; Yadav et al., 2024)

Table 2.3 Comparison of Voltage Stability Indices (Continued)

Index	Advantages	Disadvantages	Example Application	References
PMU-based	It offers high accuracy, excellent real-time performance, and the ability to perform online monitoring, providing alerts before voltage collapse occurs.	The Thevenin-based (local) method has a drawback in that parameter changes between two measurement periods can lead to inaccurate estimations.	-	(Yadav et al., 2024; Zaheb et al., 2020)

Based on Table 2.3, the L-index is suitable for selecting buses for BESS installation due to its simplicity and ability to identify weak buses in the system. the L-index, introduced by (Kessel & Glavitsch, 1986) who investigated power system voltage stability and presented a novel analytical method based on the Indicator L, which assesses voltage stability on a scale from 0 (no load) to 1 (voltage collapse). The method reliably forecasts voltage stability limits and identifies important nodes prone to voltage collapse. Radial network designs provided the best voltage stability, whereas increasing transmission capacity and optimizing system topology increased the Indicator L and overall system stability. Furthermore, selecting node locations with higher Indicator L values helped to improve the voltage stability of the power distribution system. This study provides useful information for building and operating power systems to ensure voltage stability and avoid voltage collapse.

2.6 Conventional Voltage Control Methods (STATCOM, Capacitor, Tap Changer)

Once the weak bus has been identified through the L-index, enhancing the system's voltage stability (VS) requires system control to guarantee that it operates correctly. One way to accomplish this is by voltage regulation. Voltage levels in the electrical system can be maintained within acceptable limits by controlling the voltage, enhancing stability and reliability. Several approaches for voltage regulation have been investigated, including STATCOM, capacitor banks and tap-changing transformers. The primary premise of voltage regulation is to provide reactive power to the system in order to increase the voltage to normal levels. (Soni & Gaur, 2018)

Table 2.4 Comparison of Conventional Voltage Control Methods

Device	Principle	Advantages	Disadvantages	References
STATCOM	Reactive power compensation (VSC)	STATCOMs are better suited for short-term stability issues. effective voltage regulation and designing both linear and nonlinear controllers to manage load voltage effectively	It involves high costs and investment.	(Jain et al., 2006; Taylor, 2003; Xu & Li, 2014)
Capacitor Banks	Reactive power compensation	Mechanically switched capacitor banks are effective for long-term voltage stability	Slow response, not for transients	(Swe et al., 2011; Taylor, 2003)

Table 2.4 Comparison of Conventional Voltage Control Methods (Continued)

Device	Principle	Advantages	Disadvantages	References
Tap-Changing Transformer	Adjust transformer winding ratio	Continuous voltage adjustment	Slow, mechanical wear	(Swe et al., 2011; Taylor, 2003)

From the three presented methods of voltage control, each method has its own advantages and disadvantages. However, the aforementioned voltage control is still not suitable for power systems with high levels of renewable energy penetration. Therefore, in the next section, we will present a voltage control method using Battery Energy Storage Systems (BESS).

2.7 Battery Energy Storage System (BESS) for Voltage Regulation

Battery Energy Storage Systems (BESS) are devices that can store, or supply energy as needed. One of their key advantages is their ability to help manage load and fluctuating renewable energy, which gives BESS an edge over voltage control as mentioned in the previous section. The primary function of BESS is to store excess energy when electricity production exceeds demand. Conversely, if the system experiences an energy shortage, BESS can help supply energy and can respond quickly to changes. (Zhang & Srivastava, 2021)

Several studies have investigated methods to address voltage regulation issues in distribution networks with high PV penetration. (Wang et al., 2016) proposed a coordinated control strategy for distributed energy storage systems (ESS) to regulate voltages in low-voltage (LV) distribution networks with high PV penetration. Their approach involves coordinating the power outputs of ESS based on distributed control and localized state-of-charge (SoC) management. Simulation results demonstrated that

the proposed method effectively maintains voltages within specified ranges during daily operations and enhances system stability.

In another approach, (Alam et al., 2013) addressed the impacts of rooftop solar PV on voltage profiles and proposed a new strategy for charging and discharging distributed energy storage systems to mitigate these effects. Their method utilizes the available capacity of storage devices to reduce voltage rise during peak PV generation, mitigate voltage fluctuations due to sudden changes in PV output, and support evening peak loads by discharging stored energy. Simulation results showed that this strategy effectively mitigates negative impacts of PV, supports peak-time load demand, and optimizes the utilization of storage capacity.

Furthermore, (Zeraati et al., 2016) proposed a coordinated control strategy for battery energy storage systems (BESS) to address voltage rise and drop issues in low voltage distribution networks with high photovoltaic (PV) penetration. The research highlights the challenges of voltage regulation due to reverse power flow from PV systems. The proposed strategy combines local droop-based control with distributed consensus algorithms to manage the charge and discharge of BES. Two consensus algorithms are employed: the Weighted Consensus Control (WCC) algorithm, which allocates BES participation based on capacity, and the Dynamic Consensus Control (DCC) algorithm, which adjusts participation based on the state of charge (SoC) to prevent saturation or depletion. Simulation results using real data from a radial distribution feeder demonstrate the effectiveness of the approach in maintaining voltage within permissible limits and optimizing the use of storage capacity.

2.8 Voltage Droop Control and Its Variants (Adaptive, Fuzzy, etc.)

One method of controlling BESS is voltage droop control. This control method allows for the adjustment of the power supplied or received as needed. Adaptive droop control and fuzzy logic-based droop control have been developed to enhance performance, prevent battery saturation, and improve system resilience.

Table 2.5 Droop Control Methods for BESS

Method	Principle	Strengths	Example	References
Conventional Droop	Linear adjustment by deviation	Smooth power-sharing, no oscillations Keeps feeder voltages inside limits	The CIGRE B4 dc grid test system, A 6-bus distribution feeder and a 13-bus distribution network, a realistic 7-bus LV radial feeder modeled.	(Rouzbehi et al., 2015; Wang et al., 2016; Zeraati et al., 2016)
Adaptive Droop	Dynamic coefficient adjustment	Sustains SoC, eases generator burden	-	(Tan et al., 2020)
Fuzzy Droop	Fuzzy logic-based adaptation	Cuts voltage deviation, avoids overload Holds voltage band, prevents saturation	Test on a simplified LV microgrid simulated.	(Chen et al., 2017; Jamroen et al., 2018)

Therefore, voltage droop control is crucial for managing BESS to achieve maximum efficiency and is suitable for power systems with high renewable energy

fluctuations, such as wind energy with its inherent uncertainty or solar energy, which also exhibits variability. The adaptability of droop control makes it the best and most appropriate choice.

2.9 State of Charge (SoC) Management in BESS

One important aspect of using BESS is considering the SoC. If neglected, it may result in the system's inability to control voltage effectively. There are several research studies that examine BESS with a focus on SoC. (Ota et al., 2012) investigated an autonomous distributed Vehicle-to-Grid (V2G) control scheme designed to integrate electric vehicles (EVs) into the power grid while satisfying users' scheduled charging requirements. They proposed a V2G control that utilizes frequency deviation at the plug-in terminal to provide distributed spinning reserves, enabling EVs to respond quickly and synchronously to grid fluctuations. The study examined the impact of SoC balance control, scheduled charging requests, and battery characteristics on V2G performance. Results showed that the proposed scheme effectively contributes to grid frequency regulation without compromising user convenience or interfering with traditional load frequency control by thermal power plants. The smart charging control ensures that EVs meet their scheduled charging demands while leveraging idle plug-in times for V2G operations.

(Jamroen et al., 2018) presented an adaptive droop-based control of BESS for voltage regulation in microgrids with high PV penetration. Their strategy aims to eliminate voltage rise caused by peak PV generation and voltage drop due to PV intermittency or high loading conditions. By employing fuzzy logic to adjust the droop coefficient based on allowable voltage deviation limits and the SoC of the BESS, the proposed control strategy enhances performance and avoids undesired battery saturation. Simulation studies demonstrated the effectiveness of the method in regulating voltages within allowable limits and improving system resilience.

In controlling BESS, the SoC should be managed to ensure continued operation. These research studies have explored methods for restoring the SoC to enable efficient continued use. (Liu et al., 2013) explored decentralized Vehicle-to-Grid (V2G) control systems for primary frequency regulation, emphasizing charging demands of electric vehicles (EVs). They proposed two strategies: the Battery SoC Holder (BSH) and Charging with Frequency Regulation (CFR). The BSH maintains the battery SOC while participating in frequency regulation, while CFR combines scheduled charging and frequency regulation. Simulation results on a two-area interconnected system, including wind power integration, demonstrated that these methods effectively enhance frequency stability and meet charging demands. The study concluded that decentralized control offers greater flexibility and efficiency compared to centralized approaches, improving both system stability and EV battery management.

(Jamroen & Sirisukprasert, 2022) proposed a voltage regulation strategy using BESS with SoC management optimized by a self-learning particle swarm optimization (SLPSO) algorithm. The study addresses voltage deviations in distribution networks with high PV penetration. The proposed strategy employs an adaptive droop characteristic to manage voltage deviations while considering SoC constraints. SoC management is designed to restore SoC to nominal levels by compensating BES power based on restoring power and restriction coefficient characteristics. The SLPSO algorithm optimizes the operation of BES by balancing voltage regulation and SoC restoration. Simulation results demonstrate that the proposed strategy outperforms existing methods, achieving up to 12.09% improvement in performance by effectively maintaining voltage within permissible limits and optimizing SoC management.

2.10 Optimization Techniques for BESS Control (PSO, Fuzzy, Multi-objective)

Optimal control of BESS is essential for maximizing their benefits in voltage regulation. Optimization techniques such as PSO, fuzzy logic, and multi-objective

optimization are commonly used to determine the best locations for BESS installation and to optimize their control strategies

Table 2.6 Optimization Techniques for BESS

Technique	Principle	Strengths	Example	References
PSO	Population-based search that updates particle "velocity" & "position" toward the global-best and personal-best solutions.	• Simple to code, few hyper-parameters • Fast convergence on nonlinear problems • Easily hybridised with other methods	PSO fine-tunes the V-P / V-Q droop-control slopes of BESS-equipped soft-open-points in a multi-time-scale voltage-control scheme for a 33-bus distribution network.	(Ding et al., 2024)
Fuzzy Logic	Rule-based inference using linguistic variables and membership functions; no precise mathematical model needed.	• Handles uncertainty and imprecise measurements • Can embed expert knowledge directly • Very fast real-time computation	Type-2 fuzzy-logic direct-power control of a PV–Battery inverter; provides voltage regulation and frequency support in a micro-grid prototype, outperforming classical PI.	(Maroua et al., 2024; Zainal Abidin & A. Danapalasingam, 2022)

Table 2.6 Optimization Techniques for BESS (Continued)

Technique	Principle	Strengths	Example	References
Multi-objective	Simultaneous optimizaation of conflicting goals (losses, voltage deviation, cost, risk) producing a Pareto front; selection via decision criteria (CVaR, fuzzy ranking, etc.).	• Yields trade-off solutions instead of a single point • Can incorporate uncertainty (stochastic, robust, DRO)	Distributionally-robust model-predictive control allocates BESS capacity while minimising operating cost and CVaR-based voltage-violation risk on an IEEE-37 feeder.	(Duan et al., 2024; Li et al., 2024; Wang et al., 2024)

2.11 Research Gap and Motivation

Despite the extensive research on voltage stability assessment and control, several gaps remain in the literature, particularly in the context of distribution networks with high renewable energy penetration:

- Limitations of Traditional Voltage Control Methods: Traditional methods such as capacitor banks and tap-changing transformers may not be sufficient to address the voltage fluctuations caused by intermittent renewable energy sources.
- Application for BESS for Voltage Control: While BESS has been shown to be effective for voltage regulation, there is a need for more research on the optimal control strategies for BESS in distribution networks with high renewable penetration.

- BESS Siting Considerations: The optimal placement of BESS in distribution networks is a complex problem that depends on various factors, including network topology, load profiles, and renewable energy generation patterns.
- Joint SoC Restoration and Voltage Deviation: Most studies focus on either voltage regulation or SoC management, but there is a need for integrated control strategies that consider both objectives simultaneously.
- Multi-Objective Optimization Frameworks: Multi-objective optimization techniques can be used to balance competing objectives such as voltage regulation and SoC management but there is a need for more research on the application of these techniques to BESS control in distribution networks.
- Test Cases and Validation: Many studies rely on small test systems or simplified models, but there is a need for more research on the validation of BESS control strategies in large distribution networks with high renewable penetration.

Therefore, there is a need for a comprehensive framework that:

a) Utilizes the L-index for optimal BESS placement, considering the specific characteristics of distribution networks with high renewable penetration.

b) Employs an adaptive droop control strategy that adjusts the BESS output based on the SoC and voltage deviation.

c) Integrates SoC restoration as a primary objective alongside voltage deviation minimization.

d) Evaluates the performance of the proposed framework on standard distribution networks over a 24-hour period under high renewable energy penetration scenarios.

This research proposes an integrated approach combining L-index, BESS Adaptive Droop, and FMOO-PSO to address these gaps and provide a comprehensive solution for voltage stability enhancement in distribution networks with high renewable energy penetration.

2.12 Summary and Research Contribution

This chapter has provided a comprehensive review of the literature on voltage stability assessment and control, highlighting the challenges posed by renewable energy integration and the potential of BESS for voltage regulation. The review has identified several gaps in the literature, including the need for more research on optimal BESS control strategies, BESS sitting considerations, joint SoC restoration and voltage deviation, multi-objective optimization frameworks, and test cases and validation. The following chapters will present the proposed framework for voltage stability enhancement in distribution networks with high renewable energy penetration, which aims to address these gaps and provide a comprehensive solution for voltage stability management.

CHAPTER III

MICROGRID VOLTAGE STABILITY INDICES IMPROVEMENT USING PARTICLE SWARM OPTIMIZATION

3.1 Introduction

In section 2.2, voltage stability was presented. When the system integrates with renewable energy, it is evident that renewable energy affects the power system, especially in terms of voltage. Therefore, tools for monitoring the system's voltage stability are necessary to assess its stability. In section 2.4, a tool for evaluating VS is proposed, which is VSI. There are various VSIs used differently in this study, the L-index is presented because its calculation is not complex. It is suitable for rapid monitoring as it can compute using data from load flow analysis directly.

In this study, L-index values are used to detect the weakest buses in the electrical power system, with lower values suggesting better voltage stability. Each load bus is assigned a unique L-index depending on the power network's admittance characteristics. Using PSO, the ideal generator voltage that minimizes the L-index value is found. Finally, PV curves for the system's weakest buses are created to assess overall system performance.

3.2 L-index

The L-index predicts the occurrence of electrical collapse and provides a simple method for calculating and identifying weak buses in the power system. As a result, it is an adaptable tool for increasing system stability. The L-index is computed using the following equation:

$$I_{bus} = Y_{bus} V_{bus} \tag{3.1}$$

Furthermore, since the system comprises multiple buses, they can be incorporated into a matrix representation.

$$\begin{bmatrix} \mathbf{I}^{\mathbf{G}} \\ \mathbf{I}^{\mathbf{L}} \end{bmatrix} = \begin{bmatrix} \mathbf{Y}^{\mathbf{GG}} & \mathbf{Y}^{\mathbf{GL}} \\ \mathbf{Y}^{\mathbf{LG}} & \mathbf{Y}^{\mathbf{LL}} \end{bmatrix} \begin{bmatrix} \mathbf{V}^{\mathbf{G}} \\ \mathbf{V}_{\mathbf{L}} \end{bmatrix} \tag{3.2}$$

$$\mathbf{I}^{\mathbf{G}} = \mathbf{Y}^{\mathbf{GG}}\mathbf{V}^{\mathbf{G}} + \mathbf{Y}^{\mathbf{GL}}\mathbf{V}^{\mathbf{L}} \tag{3.3}$$

$$\mathbf{I}^{\mathbf{L}} = \mathbf{Y}^{\mathbf{LG}}\mathbf{V}^{\mathbf{G}} + \mathbf{Y}^{\mathbf{LL}}\mathbf{V}^{\mathbf{L}} \tag{3.4}$$

After performing further mathematical manipulations, Eq. (3.2) can be reformulated and expressed as Eq. (3.5) to (3.7).

$$\mathbf{V}^{\mathbf{L}} = [\mathbf{Y}^{\mathbf{LL}}]^{-1}\mathbf{I}^{\mathbf{L}} - [\mathbf{Y}^{\mathbf{LL}}]^{-1}\mathbf{Y}^{\mathbf{LG}}\mathbf{V}^{\mathbf{G}} \tag{3.5}$$

$$\mathbf{I}^{\mathbf{G}} = \mathbf{Y}^{\mathbf{GL}}[\mathbf{Y}^{\mathbf{LL}}]^{-1}\mathbf{I}^{\mathbf{L}} + (\mathbf{Y}^{\mathbf{GG}} - \mathbf{Y}^{\mathbf{GL}}[\mathbf{Y}^{\mathbf{LL}}]^{-1}\mathbf{Y}^{\mathbf{LG}})\mathbf{V}^{\mathbf{G}} \tag{3.6}$$

As a result, Eq. (3.5) and (3.6) can be expressed in matrix form.

$$\begin{bmatrix} \mathbf{V}^{\mathbf{L}} \\ \mathbf{I}^{\mathbf{G}} \end{bmatrix} = \begin{bmatrix} [\mathbf{Y}^{\mathbf{LL}}]^{-1} & -[\mathbf{Y}^{\mathbf{LL}}]^{-1}\mathbf{Y}^{\mathbf{LG}} \\ \mathbf{Y}^{\mathbf{GL}}[\mathbf{Y}^{\mathbf{LL}}]^{-1} & \mathbf{Y}^{\mathbf{GG}} - \mathbf{Y}^{\mathbf{GL}}[\mathbf{Y}^{\mathbf{LL}}]^{-1}\mathbf{Y}^{\mathbf{LG}} \end{bmatrix} \begin{bmatrix} \mathbf{I}^{\mathbf{L}} \\ \mathbf{V}^{\mathbf{G}} \end{bmatrix} \tag{3.7}$$

By rearranging the aforementioned matrix, we obtain:

$$\begin{bmatrix} \mathbf{V}^{\mathbf{L}} \\ \mathbf{I}^{\mathbf{G}} \end{bmatrix} = \begin{bmatrix} \mathbf{Z}^{\mathbf{LL}} & \mathbf{F}^{\mathbf{LG}} \\ \mathbf{K}_{\mathbf{GL}} & \mathbf{Y}^{\mathbf{GG}} \end{bmatrix} \begin{bmatrix} \mathbf{I}^{\mathbf{L}} \\ \mathbf{V}^{\mathbf{G}} \end{bmatrix} \tag{3.8}$$

$$\mathbf{F}_{\mathbf{LG}} = -\mathbf{Y}_{\mathbf{LL}}^{-1}\mathbf{Y}_{\mathbf{LG}} \tag{3.9}$$

$$L_j = \left| 1 - \sum_{i=1}^{i=g} F_{ij} \frac{V_i}{V_j} \right| \tag{3.10}$$

Before calculating the L-Index, the voltage values for each system bus and the Y-bus admittance matrix must be determined using the Newton-Raphson Load Flow (NRLF) approach. Finally, the required matrix is obtained by converting it from the Y-bus. The L-Index value is then computed using Eq. (3.10). It should be emphasized that the L-Index is solely determined for loaded buses. Furthermore, an L-Index value around 1 implies that the related bus is the weakest, which could result in a voltage collapse in the system. In contrast, a bus with an L-Index value near to zero is considered to be the most reliable.

3.3 P-V curve

The P-V curve, or Power-Voltage curve, is a graphical tool used to show how the voltage at a specific bus change as the real power (P) supplied to that bus increases. To create this curve, the load at the chosen bus gradually increased in small steps. After each increase, a load flow calculation is performed to determine the new voltage at that bus. This process continues until the load flow calculation can no longer find a solution, which indicates the system has reached its stability limit or is about to experience voltage collapse. The calculation can be done according to the graph details as fig. 3.1.

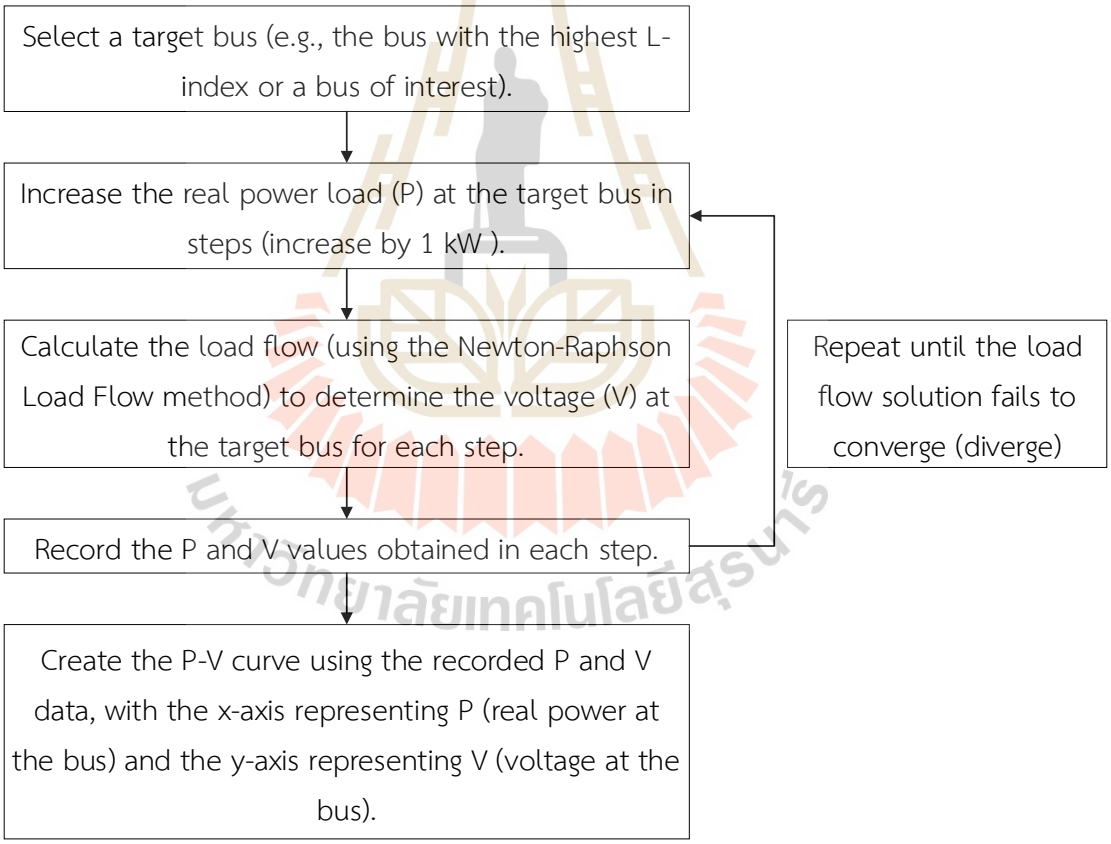

Figure 3.1 PV curve procedure

3.4 Voltage Stability Improvement Using PSO

PSO is a well-known metaheuristic algorithm inspired by birds' flocking behavior during food looking for. It iteratively explores the solution space by altering particle positions, integrating individual and shared experiences to determine the personal and global optimal positions. This technique incorporates velocity updates and seeks to arrive at a perfect solution.

PSO has emerged as a promising approach to improving voltage stability in microgrid systems. It accomplishes this by identifying the best generator bus voltages to reduce the L-index, a key indicator of the voltage stability margin. PSO's inherent characteristics such as its simplicity, computational efficiency, and adaptability make it appropriate for this application.

The fitness function that minimizes the L-index value of the weakest bus can be mentioned as,

$$\text{minimize } f(x_i^t) = \max\{\text{L-index}\}, \tag{3.11}$$

The computation of velocity and position is performed using the following equations:

$$v_i^{t+1} = wv_i^t + c_1 r_1 (pBest_i^t - x_i^t) + c_2 r_2 (gBest^t - x_i^t) \tag{3.12}$$

$$x_i^{t+1} = x_i^t + v_i^t \tag{3.13}$$

In this case, the population of particles reflects the generator voltage values. The generator voltage is listed as 0.95 and 1.05 per unit, respectively. Fig 3.2 depicts the proposed PSO-based computational approach for improving VSI.

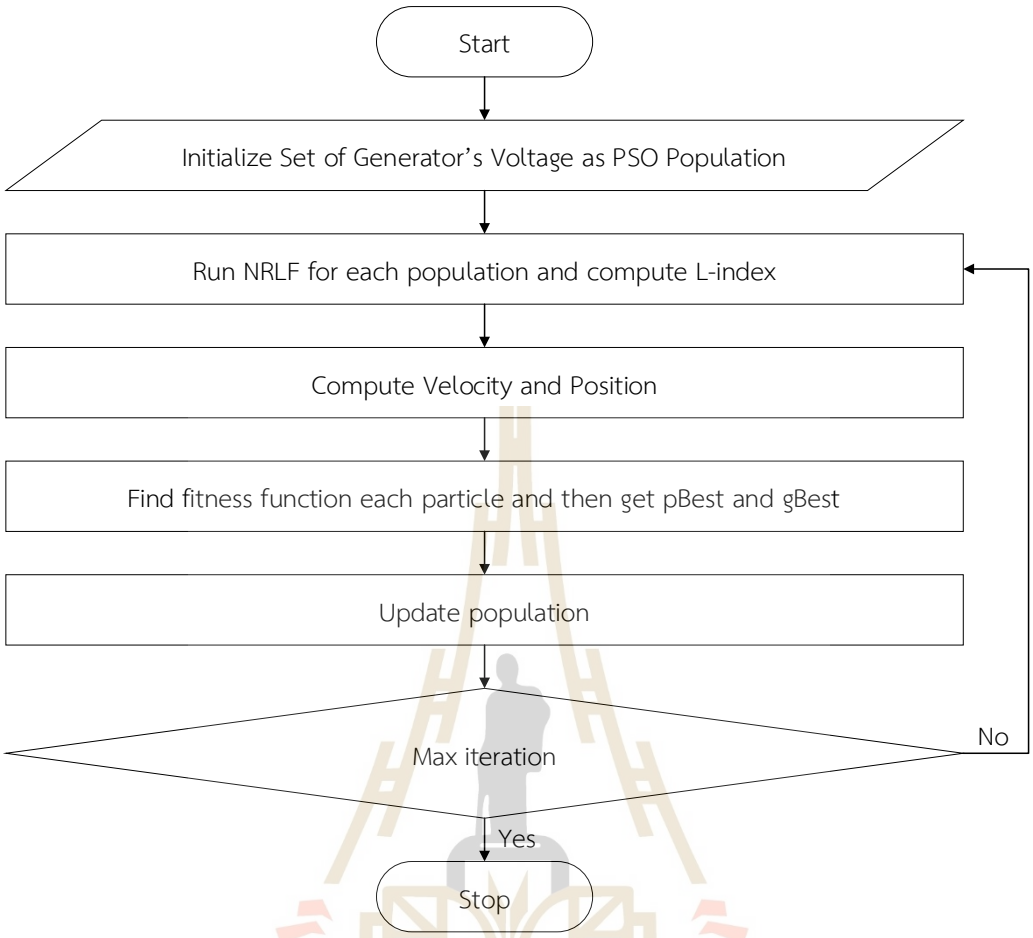

Figure 3.2 Computation Procedure

3.5 Results and Discussion

This section presents the results of the proposed method applied to the IEEE 33-bus distribution system. The analysis is segmented into four distinct cases, which are detailed below.

- IEEE 33-bus base case
- IEEE 33-bus with L-index improvement
- IEEE 33-bus modified
- Modified IEEE 33-bus system with L-index improvement

3.5.1 IEEE 33-bus base case

Figure 3.3 depicts the base case of the IEEE 33-bus system, which consists of one slack bus and 32 load buses, with the slack bus voltage set to 1.0 per

unit (p.u.). Fig 3.4 shows the L-Index values calculated for each bus in the system. Bus 18 has the greatest L-Index value, making it the weakest bus in the network. Bus 2 has the lowest L-Index value, indicating it is the strongest bus. Bus 18's elevated L-Index value indicates a significant susceptibility to voltage collapse in the system. Furthermore, Fig 3.5 depicts the PV curve for Bus 18, demonstrating that voltage collapse occurs when the real power loading hits 2,672 kW.

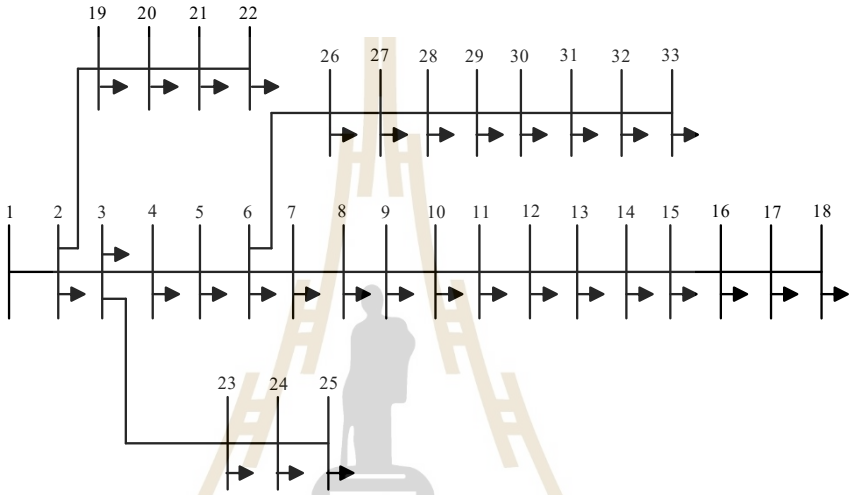

Figure 3.3 IEEE 33-bus system

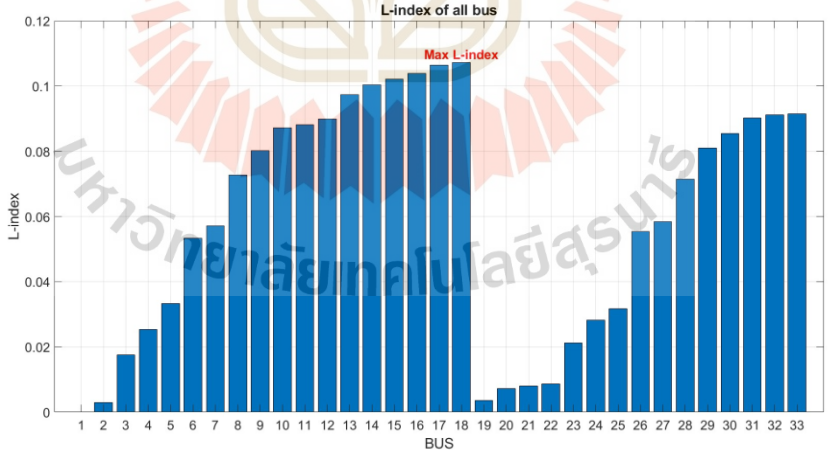

Figure 3.4 L-index of IEEE 33-bus base case

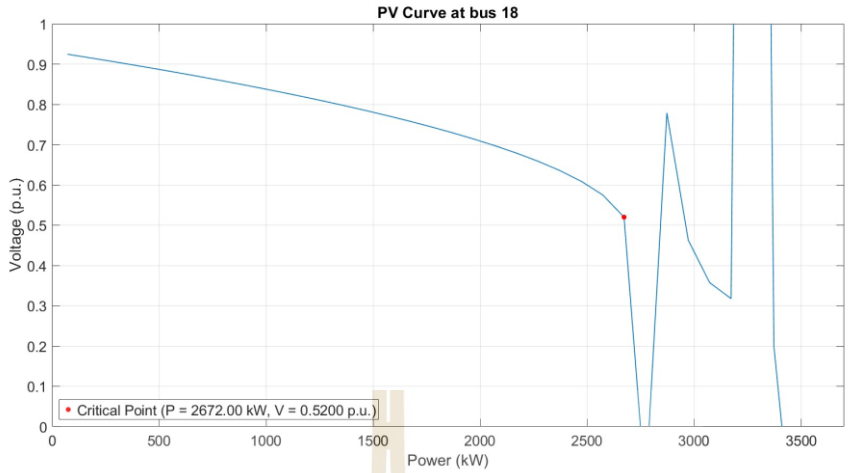

Figure 3.5 PV-curve of IEEE 33-bus base case

3.5.2 IEEE 33-bus with L-index improvement

Using the proposed method, the best generator voltage at the slack bus is calculated to be 1.05 per unit. Figure 3.6 demonstrates that in this improved system, the L-index values have decreased. Bus 18 is the weakest bus, while Bus 2 remains the strongest in the network. However, when compared to the prior scenario, the buses' L-index values are significantly lower. Figure 3.7 depicts the PV curve of the modified system, which shows that Bus 18's maximum loading capability has increased to 3,072 kW.

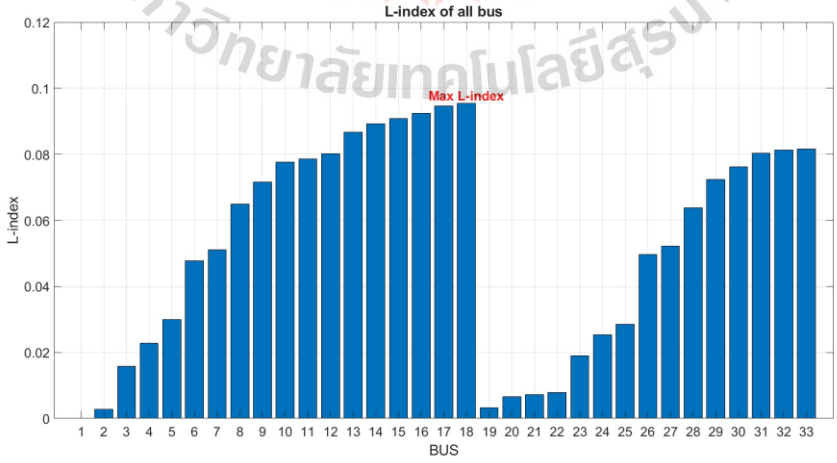

Figure 3.6 L-index of IEEE 33-bus with L-index improvement

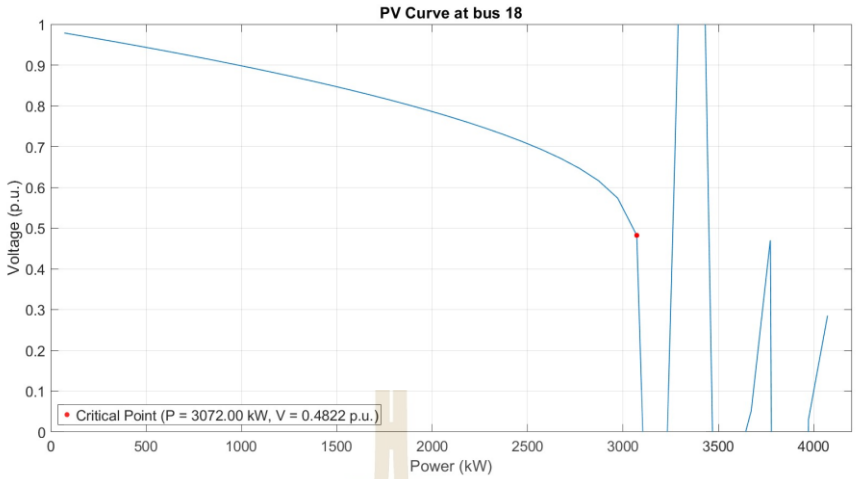

Figure 3.7 PV-curve of IEEE 33-bus system with L-index improvement

3.5.3 IEEE 33-bus modified

In this case, the IEEE 33-bus system is modified by installing four distributed generators (DGs) at buses 18, 22, 25, and 31, with power outputs of 1.075 MW, 0.36 MW, 0.93 MW, and 0.92 MW, respectively. The locations for DG installation are selected based on the lowest L-index value in each branch, while the DG capacities are determined according to the total power demand of each branch. For the microgrid (MG) case study, Bus 1 is disconnected from the main power grid. The voltage at all generator buses is set to 1 p.u., and Bus 18 is designated as the slack bus, as illustrated in Fig. 3.8.

Figure 3.9 shows the L-index of the modified IEEE 33-bus, similarly Bus 8 is a weaker bus, while bus 17 is a stronger bus. As observed, the weak bus is the farthest bus from the power sources. On the other hand, the strong bus is the nearest to the power sources. Fig 3.10 shows the PV-curve of bus 8, The maximum loading capability is 1,100 kW.

From table 3.1, in the base case, the voltage magnitude at bus 1 is set to 1.0 per unit, resulting in a maximum L-index of 0.1072 and a power output at the slack bus of 3.926 MW. After applying PSO, the voltage magnitude increases at bus 1 to 1.05 per unit, the maximum L-index is reduced to 0.0954, indicating an improvement

in voltage stability. Additionally, the power at the slack bus slightly decreases to 3.9035 MW.

This demonstrates that optimizing the voltage magnitude using PSO can effectively reduce the maximum L-index, thereby enhancing the voltage stability of the system. The slight reduction in power at the slack bus also suggests a more efficient power flow, as losses may be reduced. Overall, the results confirm that the proposed method can improve system stability with minimal impact on the overall power supplied by the slack bus.

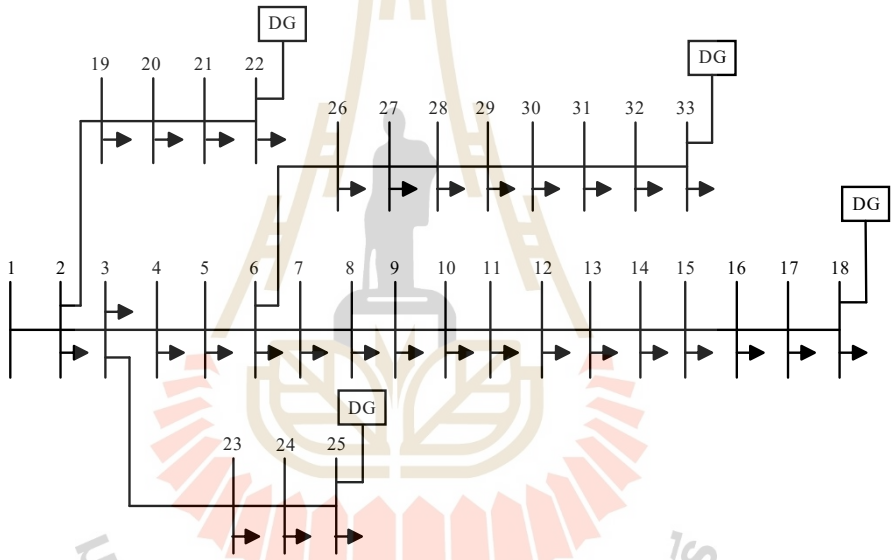

Figure 3.8 Modified IEEE 33-bus system

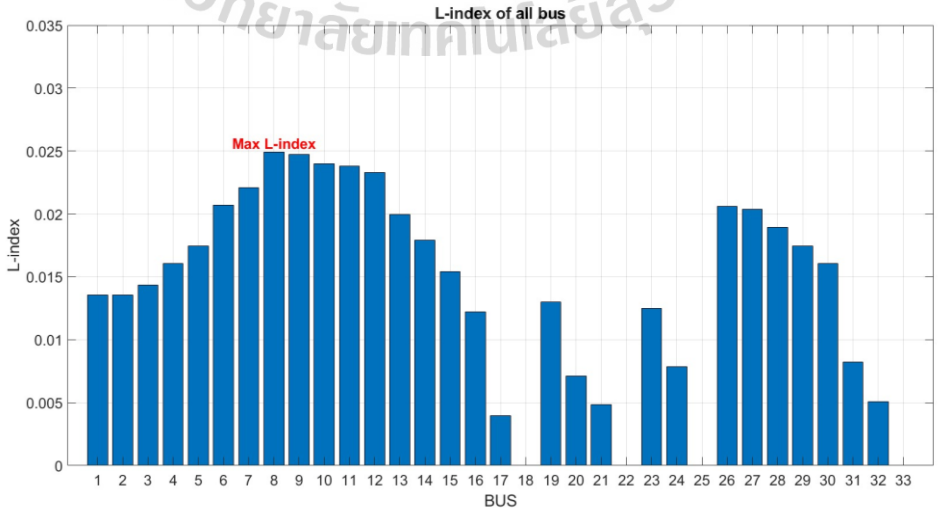

Figure 3.9 L-index of modified IEEE 33-bus.

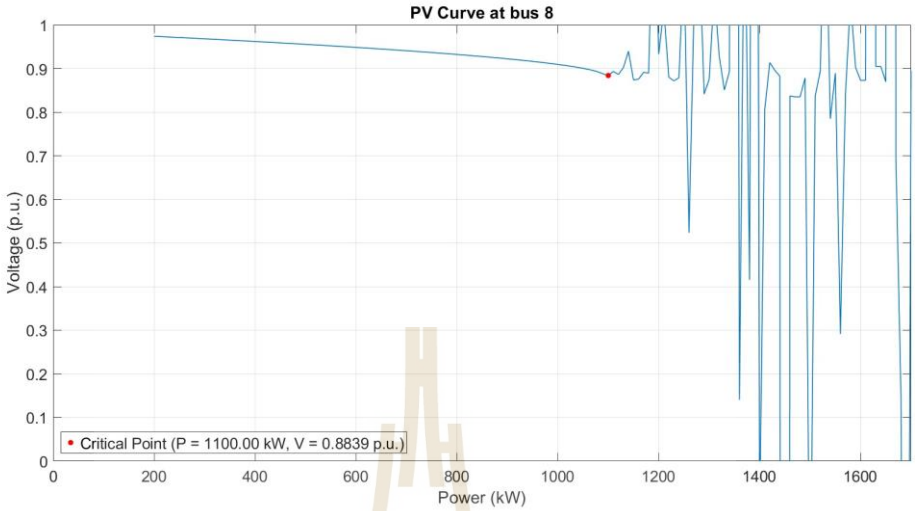

Figure 3.10 PV-curve of modified IEEE 33-bus.

Table 3.1 Comparison of IEEE 33-bus Base Case and L-index Improvement Results

Case	Bus	Voltage Magnitude	Max L-index	Power at Slack Bus (MW)
IEEE 33-bus base case	1	1	0.1072	3.926
IEEE 33-bus with L-index improvement	1	1.05	0.0954	3.9035

3.5.4 Modified IEEE 33-bus system with L-index improvement

In this case, PSO is used to find the optimal solution for the objective, which is to minimize the maximum L-index of the buses. The optimization is performed by adjusting the voltage levels of generator buses or designated buses, with the voltage search space constrained within the standard voltage limits of 0.95 to 1.05 p.u. The test is conducted on a modified power system, based on the same configuration as Case 3, making the system under study effectively resemble a microgrid.

Figure 3.11 depicts the L-index values for each bus of the modified IEEE 33-bus system. When compared to previous cases, L-index values are significantly lower, indicating that voltage stability has improved. Bus 8 is established as a weak bus, whereas Bus 17 remains the strongest bus in the network.

Figure 3.12 shows the PV curve for the improved IEEE 33-bus system following the L-index optimization. The investigation shows that the system's maximum loading capacity has increased to 1,260 kW, indicating its ability to handle higher loading levels. This increase in loading capacity shows the system's increased stability, demonstrating the successful result of the proposed optimization strategy in reinforcing voltage stability.

Table 3.2 presents a comparison between the IEEE 33-bus Modified case and the case where the L-index is improved by increasing the voltage magnitude at buses 18, 22, 25, and 33 from 1.00 pu to 1.05 pu.

In the base case, where the voltage magnitude at these four buses is set to 1.00 pu, the maximum L-index is 0.0249, and the power at the slack bus is 3.2596 MW. After increasing the voltage magnitude at buses 18, 22, 25, and 33 to 1.05 pu, the maximum L-index decreases to 0.0225, indicating an improvement in voltage stability. Additionally, the power at the slack bus slightly decreases to 3.2354 MW, suggesting a reduction in system losses and a more efficient power supply.

These results demonstrate that optimizing the voltage magnitude at selected buses can effectively reduce the maximum L-index, thereby enhancing the voltage stability of the system. The slight reduction in slack bus power also indicates improved system efficiency. Overall, the proposed method improves system stability without negatively impacting the overall power supply.

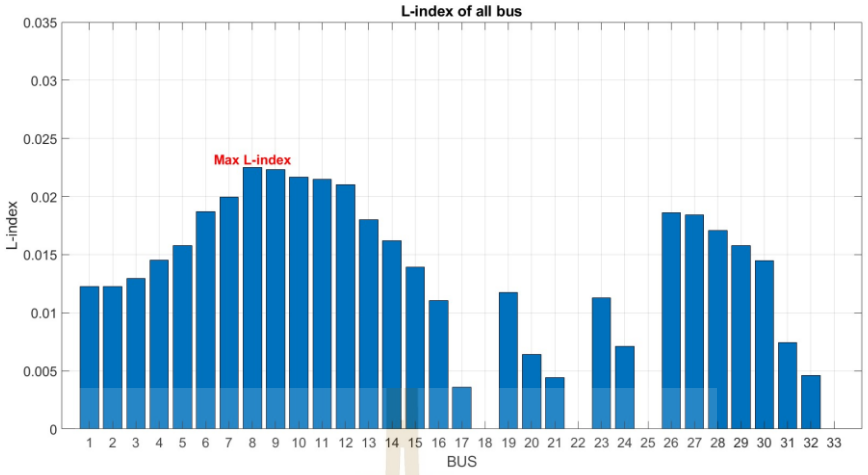

Figure 3.11 L-index of modified IEEE 33-bus system with L-index improvement.

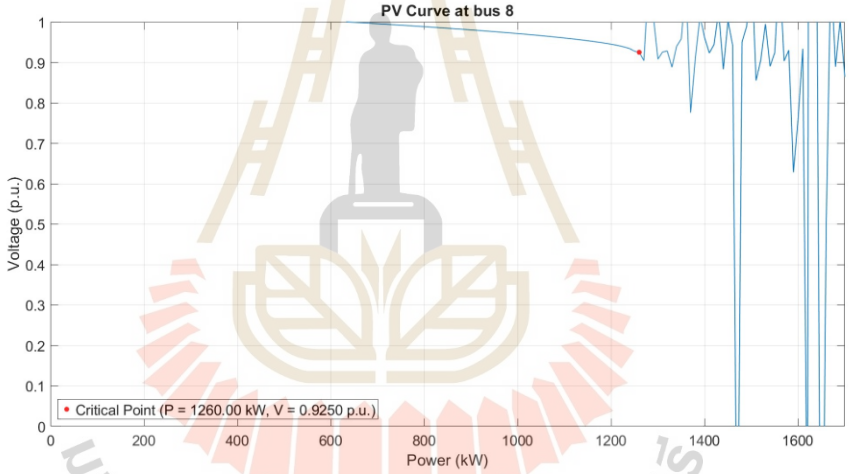

Figure 3.12 PV-curve of modified IEEE 33-bus system with L-index improvement.

Table 3.2 Comparison of IEEE 33-bus Modified Case and Modified IEEE 33-bus system with L-index improvement Results

Case	Bus	Voltage Magnitude	Max L-index	Power at Slack Bus (MW)
IEEE 33-bus Modified	18	1.00	0.0249	3.2596
	22	1.00		
	25	1.00		
	33	1.00		

Table 3.2 Comparison of IEEE 33-bus Modified Case and Modified IEEE 33-bus system with L-index improvement Results (Continued)

Case	Bus	Voltage Magnitude	Max L-index	Power at Slack Bus (MW)
Modified IEEE 33-bus system with L-index improvement	18	1.05	0.0225	3.2354
	22	1.05		
	25	1.05		
	33	1.05		

Table 3.3 demonstrates that the system's voltage stability has improved, as indicated by the lower L-Index values. The reduction in L-Index values significantly enhances system stability during the optimization process. It is important to note that the table does not include L-Index values for PV buses, since the L-Index calculation is only applicable to load buses. In the IEEE 33-bus base case, Bus 1 is identified as a PV bus, while in the modified IEEE 33-bus system, Buses 18, 22, 25, and 33 are classified as PV buses.

When analyzing system stability, it is evident that in the base case, Bus 18 consistently exhibits the highest L-Index value, followed by Buses 17, 16, and 15. This suggests that Bus 18 is the least reliable and has the greatest potential to contribute to system instability. In the modified IEEE 33-bus system, Bus 8 has the highest L-Index value, indicating similarly low reliability. If an abnormal event occurs, there is a high likelihood that voltage collapse would originate from this bus.

Therefore, to ensure system stability, special attention should be given to Bus 18 in the base case and Bus 8 in the modified case. Improving the operational conditions of these buses is crucial for maintaining the overall stability of the IEEE 33-bus system.

Additionally, the PV curves indicate that the modified IEEE 33-bus system achieves the highest level of stability, as it can accommodate a greater load

capacity compared to the other cases analyzed. This improvement highlights the effectiveness of the proposed optimization strategy in enhancing voltage stability within the system.

Table 3.3 Comparing L-index value

BUS	L-index			
	IEEE 33-bus base case	IEEE 33-bus with L-index improvement	IEEE 33-bus Modified	IEEE 33-bus Modified with L-index improvement
1	-	-	0.013538	0.012246
2	0.003004	0.002708	0.013538	0.012246
3	0.017498	0.015742	0.014334	0.012964
4	0.025411	0.022832	0.016056	0.014515
5	0.033364	0.029944	0.017475	0.015794
6	0.053276	0.047698	0.020685	0.018688
7	0.057172	0.051161	0.022083	0.019952
8	0.072771	0.064999	0.024913	0.022498
9	0.080183	0.071556	0.024711	0.022318
10	0.087129	0.077691	0.023974	0.021655
11	0.088143	0.078586	0.023783	0.021484
12	0.089917	0.080151	0.023296	0.021046
13	0.097415	0.086758	0.01994	0.018023
14	0.100304	0.089300	0.017937	0.016216
15	0.102096	0.090877	0.015424	0.013949
16	0.103813	0.092386	0.012216	0.011053
17	0.10646	0.094713	0.003944	0.003572
18	0.107227	0.095386	-	-
19	0.003527	0.003181	0.013009	0.011769
20	0.00723	0.006535	0.007095	0.006424

Table 3.3 Comparing L-index value (Continued)

BUS	L-index			
	IEEE 33-bus base case	IEEE 33-bus with L-index improvement	IEEE 33-bus Modified	IEEE 33-bus Modified with L-index improvement
21	0.007993	0.007225	0.004864	0.004405
22	0.008698	0.007864	-	-
23	0.021172	0.019053	0.012484	0.011293
24	0.028149	0.025332	0.007876	0.00713
25	0.031696	0.028521	-	-
26	0.055454	0.049636	0.020612	0.018622
27	0.058377	0.052235	0.020373	0.018407
28	0.071425	0.063818	0.018922	0.017099
29	0.081028	0.072323	0.01744	0.015762
30	0.085367	0.076160	0.016048	0.014506
31	0.090123	0.080360	0.008235	0.007452
32	0.091174	0.081288	0.005073	0.004592
33	0.091500	0.081576	-	-

From the comparison table 3.4 of the 33-bus distribution system under different scenarios, the base case, L-index improvement, network modification, and network modification combined with L-index improvement it is evident that both L-index and network improvements have a significant impact on system performance.

In the base case, the system exhibits a total power loss of 0.2110 MW and a power supply from the slack bus of 3.926 MW. When the L-index improvement is applied, the power loss decreases to 0.1804 MW, and the power supplied by the slack bus is reduced to 3.2596 MW. This demonstrates that L-index improvement can significantly reduce system losses and enhance the efficiency of power delivery.

In the Modification case, when both network modification and L-index improvement are applied together, the results are optimal. The power loss is minimized to 0.1804 MW, and the slack bus power is reduced to 3.2596 MW, which is the lowest value among all studied cases.

Additionally, the total generation power required tends to decrease as the system is improved, reflecting a reduction in system losses and overall energy savings.

Based on these results, it can be concluded that the combination of L-index and network improvements provides the highest efficiency for the distribution system. This approach effectively reduces power losses and the burden on the slack bus, thereby enhancing the overall performance of the power distribution network.

Table 3.4 Comparison Real Power All Cases

Case	Total Power Loss (MW)	Total Power Load (MW)	Power at Slack Bus (MW)	Total Generation Power (MW)
IEEE 33-bus base case	0.211	3.715	3.926	3.926
IEEE 33-bus with L-index improvement	0.1885	3.715	3.9035	3.9035
IEEE 33-bus modified	0.2046	3.055	1.6196	3.2596
Modified IEEE 33-bus system with L-index improvement	0.1804	3.055	1.5954	3.2354

3.6 Chapter Summary

This chapter demonstrates that improving both the L-index and the network configuration in the IEEE 33-bus distribution system can greatly enhance the system's overall performance. By applying these two strategies together, the system experiences the lowest power losses and the least burden on the slack bus compared to all other

scenarios studied. This means that not only is the system more efficient, but it also saves more energy overall.

A key finding is that certain buses specifically Bus 18 in the original system and Bus 8 in the modified system are the most vulnerable points in terms of voltage stability. These buses have the highest L-index values, which makes them the most likely spots for voltage instability or even collapse if something goes wrong. Therefore, focusing on improving the conditions at these buses is essential for keeping the whole system stable.

The chapter also highlights the results from the PV-curve analysis, which shows that the L-index improvement can handle a higher load before reaching its stability limit. This is a clear sign that the proposed optimization methods are effective at making the system more robust.

CHAPTER IV

VOLTAGE DEVIATION IMPROVEMENT IN ACTIVE DISTRIBUTION NETWORK USING BETTERY ENERGY STORAGE SYSTEM OPTIMAL VOLTAGE DROOP CONTROL

4.1 Introduction

From Chapter 3, once the voltage stability of the system has been assessed using the L-index, which is a tool capable of identifying weak buses, the weak buses identified by the L-index become the locations where BESS is installed. This chapter proposes methods for voltage control to enhance system stability and reliability. In section 2.5, there are three methods of voltage control: STATCOM, capacitor banks, and tap-changing transformers. Each method has its own advantages and disadvantages but is still not suitable for systems with renewable energy, as such systems require energy storage and the ability to supply or absorb real power. Therefore, in section 2.6 and 2.7, a method of voltage control using BESS is proposed.

This study provides a way to solve the impact of renewable energy on VD of the Active Distribution Network (AND). The optimum BESS management is achieved by adopting a Voltage Droop Control (VDC) approach that employs BESS to charge and discharge energy into the system. The adaptive droop control approach was chosen for BESS management because it allows the droop coefficient to be chosen as desired and appropriate, as well as taking into account the SoC level. In addition, the PSO is used to get the most appropriate droop coefficient value for battery control. The IEEE 33-bus test system was chosen as a test system because it is a distribution system with voltage levels lower than the standard criterion, making it acceptable for testing.

4.2 BESS with Adaptive Droop Control

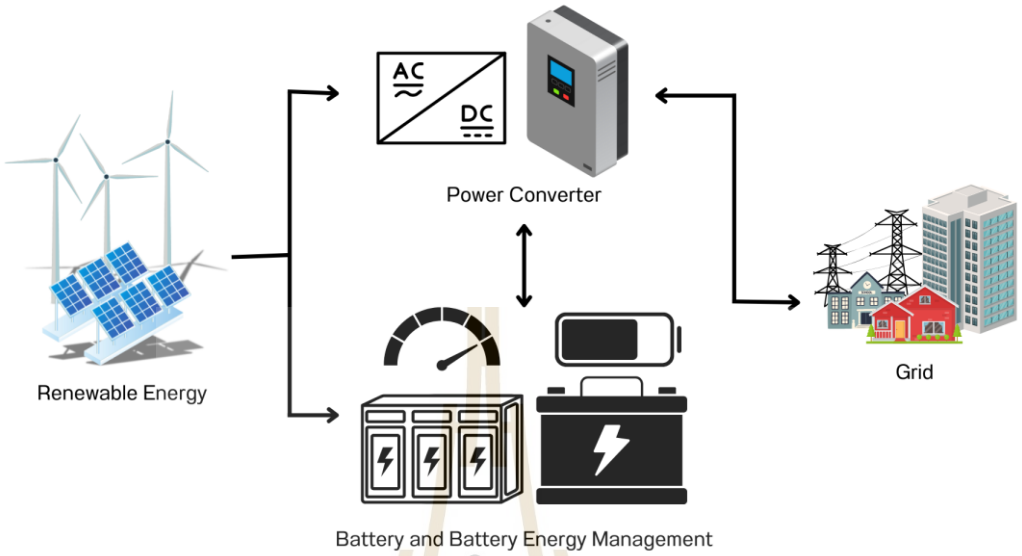

Figure. 4.1 BESS configuration

The BESS configuration is shown in Fig. 4.1, which includes the following main elements: a battery for storing energy, a battery energy management system for controlling BESS operation, and a power converter for energy conversion.

In this study, we focus on the battery and its energy management system. This study presents a method for controlling battery operations to resolve the VD issue. The battery can either provide or receive active power from the grid. When the BESS supplies active power to the grid, the voltage level rises, whereas when it absorbs active power from the grid, the voltage level drops. Thus, the BESS's operation can affect the voltage when the active power changes. Therefore, effective BESS operation relies heavily on battery energy management. According to a review, Fig. 4.2 shows that the VDC has three modes: (1) Mode 1 (Fixed Voltage): Keeps the voltage at a predetermined level and allows the battery power to adjust as needed, (2) Mode 2 (Fixed Power): Keeps the battery's power output constant, (3) Mode 3 (Droop Control): Uses a droop coefficient to determine how much power the battery delivers or consumes depending on the grid voltage.

This study uses the droop control method (Mode 3) to regulate battery operation because it can adjust the droop coefficient, allowing the voltage level to be freely regulated. Fig. 4.3 illustrates the operating concept as follows:

• 1: If the bus voltage of the battery exceeds the maximum voltage ($V_{\max}$), the battery will charge the maximum power into the system.

• 2: If the bus voltage value of the battery is less than the maximum voltage ($V_{\max}$) but larger than the maximum voltage thresholds ($V_{\text{th}}^{\max}$), the battery will charge power based on VD, which is governed by the droop coefficient.

• 3: If the battery's bus voltage value falls within the range of the minimum voltage thresholds ($V_{\text{th}}^{\min}$) and the maximum voltage thresholds ($V_{\text{th}}^{\max}$) or the deadband range, the battery will not charge or discharge at all.

• 4: If the bus voltage value of the battery is larger than the minimum voltage ($V_{\min}$) but less than the minimum voltage thresholds ($V_{\text{th}}^{\min}$), the battery will discharge the power based on VD, which is governed by the droop coefficient.

• 5: If the battery's bus voltage value is less than the minimum voltage ($V_{\min}$), it will discharge the maximum power back.

It can be represented mathematically as an equation given below:

$$P_{BES} = \begin{cases} -P_{BES}^{\max} & \text{if } V_k \geq V^{\max} \\ k_{BES,c(SoC)}\Delta V & \text{if } V_{\text{th}}^{\max} < V_k < V^{\max} \\ 0 & \text{if } V_{\text{th}}^{\min} \leq V_k \leq V_{\text{th}}^{\max} \\ k_{BES,d(SoC)}\Delta V & \text{if } V^{\min} < V_k < V_{\text{th}}^{\min} \\ P_{BES}^{\max} & \text{if } V_k \leq V^{\min} \end{cases} \tag{4.1}$$

$$\Delta V = V_k - V_0 \tag{4.2}$$

Since the battery may be saturated, it cannot be utilized further, causing the system to have a VD value that exceeds the required limit. As a result of the investigation, the SoC level was examined, as shown in the equation below.

$$k_{BES,d} = \begin{cases} 0 & \text{if } 0 < \text{SoC} \leq \text{SoC}_{\min} \\ \dfrac{K_{\max}K_{\min}e^{n_d(SoC-SoC_{\min})}}{K_{\max}+K_{\min}e^{n_d(SoC-SoC_{\min})}-1} & \text{if } \text{SoC}_{\min} < \text{SoC} \leq 1 \end{cases} \tag{4.3}$$

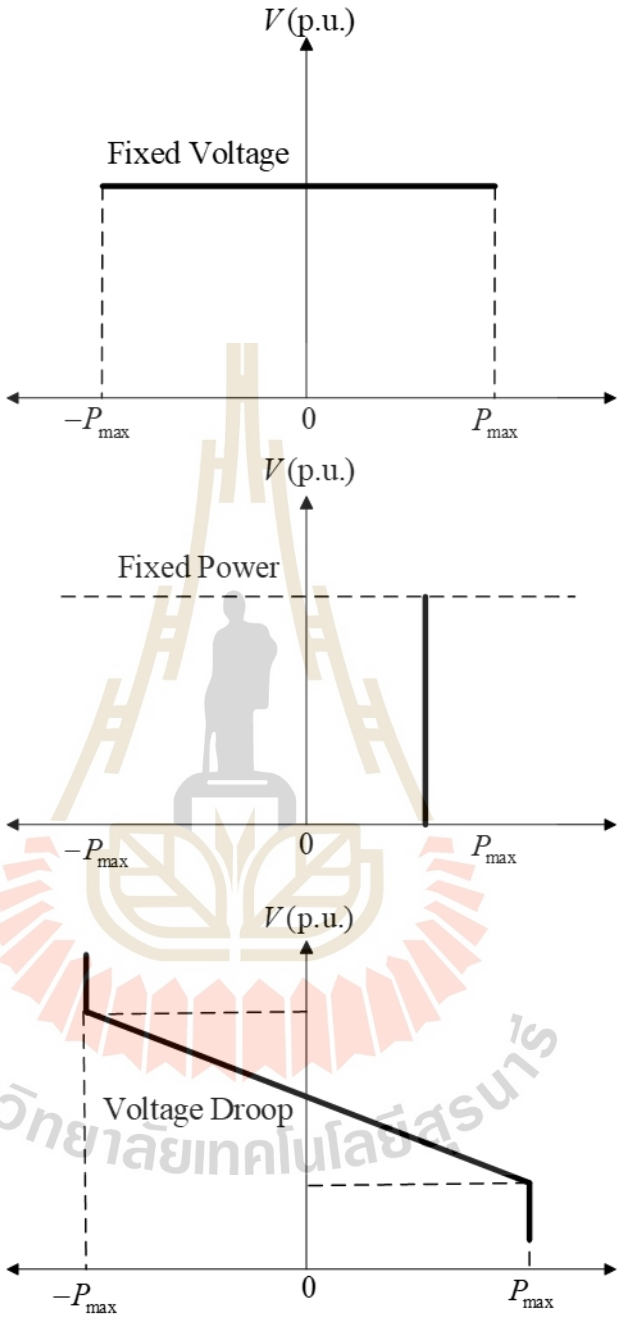

Figure 4.2 VDC strategies

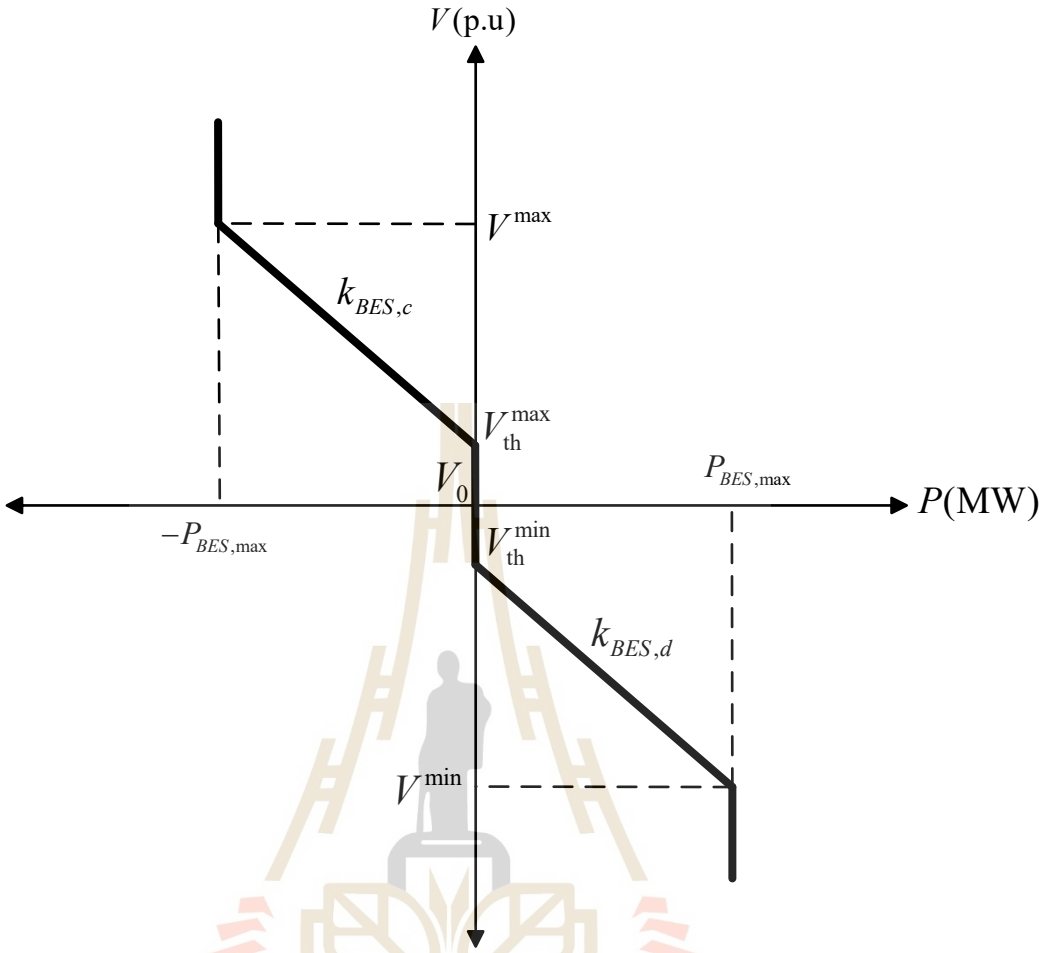

Figure 4.3 Adaptive VDC strategy

$$k_{BES,c} = \begin{cases} 0 & \text{if } \mathrm{SoC}_{\max} \le \mathrm{SoC} < 1 \\ \dfrac{K_{\max} K_{\min} e^{n_c (SoC_{\max} - SoC)}}{K_{\max} + K_{\min} e^{n_c (SoC_{\max} - SoC)} - 1} & \text{if } 0 < \mathrm{SoC} < \mathrm{SoC}_{\max} \end{cases} \quad (4.4)$$

$$SoC(t) = SoC(t-1) - \frac{1}{E}\int P_{BES}(t)dt \quad (4.5)$$

$$k_{droop} = \begin{cases} k_{BES,c}, \text{ charging} \\ k_{BES,d}, \text{ discharging} \end{cases} \quad (4.6)$$

$$n = \begin{cases} n_c, \text{ charging} \\ n_d, \text{ discharging} \end{cases} \quad (4.7)$$

The control of the BESS using VDC can be modeled into the Newton-Raphson load flow analysis through the following equations:

$$P_{BES} + P_k^{gen} - P_k^{load} - \sum_{j=1}^{n}[V_k V_j (G_{ij}\cos\theta_{ij} + B_{ij}\sin\theta_{ij})] = 0 \quad (4.8)$$

As shown in Equation (4.8), the real power output of the BESS, denoted as P_{BES}, which is obtained from the VDC strategy, is incorporated into the NRLF's power equations. This allows for the calculation of bus voltages after the contribution from the BESS has been integrated into the system. A negative P_{BES} value indicates that the battery is charging, while a positive P_{BES} value indicates that the battery is discharged.

When evaluating k_{droop}, it is discovered that this value is related to the determination of $K_{\max}$, $K_{\min}$, SoC, and n As a result, while examining (4.1), (4.3), and (4.4), it can be represented in Fig. 4.4 and 4.5. From Fig. 4.4, it has been discovered that as the SoC of the battery increase, the $k_{BES,d}$ value gradually increases, the $k_{BES,c}$ value gradually decrease. This is because adaptive droop management is intended to protect the battery's functionality, which increases the SoC range, resulting in less charging and discharging. On the other hand, a low SoC level in the battery causes it to charge more and discharge less. The aforementioned relationship leads to the design of $K_{\max}$, $K_{\min}$ and n values, demonstrating that $K_{\max}$ and $K_{\min}$ will have a relationship with the desired power output, and n will be the factor determining the battery's power distribution, which is related to SoC, as shown in Fig. 4.5.

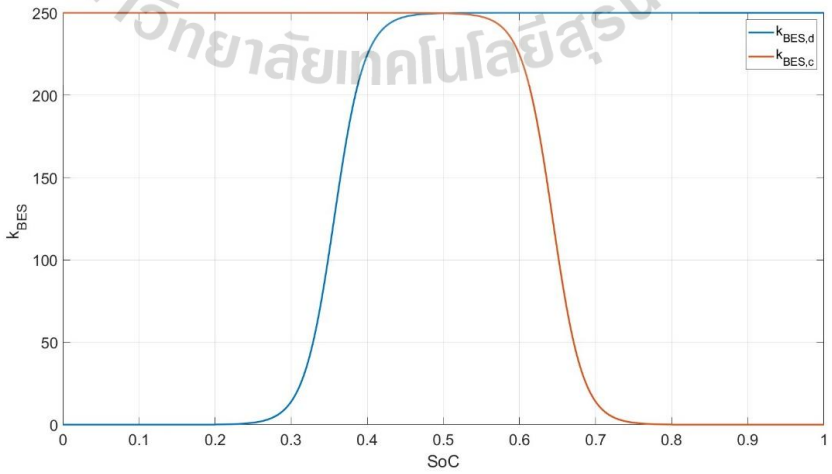

Figure 4.4 The Relationship between SoC and k_{BES} with the SoC is within the range of $SoC_{\min}$ and $SoC_{\max}$

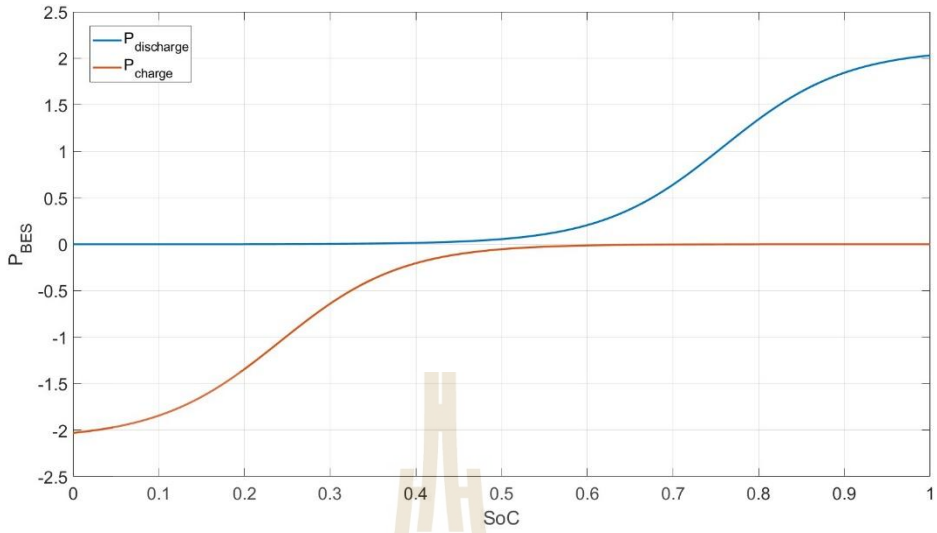

Figure 4.5 The Relationship between SoC and n with the SoC is within the range of $SoC_{\min}$ and $SoC_{\max}$

4.3 PSO Based Voltage Deviation Improvement

This study aims to minimize the system's total voltage deviation (TVD) through the objective function. By reducing the TVD, the stability of the power system can be greatly enhanced. The objective function employed in this study is shown in the following equation.

$$\text{minimize } TVD = \sum_{k=1}^{N} (|V_k - V_0|) \tag{4.9}$$

and the constraints are defined as follows:

$$P_k^{gen} - P_k^{load} - \sum_{j=1}^{n} [V_k V_j (G_{kj} \cos\theta_{kj} + B_{kj} \sin\theta_{kj})] = 0 \tag{4.10}$$

$$Q_k^{gen} - Q_k^{load} - \sum_{j=1}^{n} [V_k V_j (G_{kj} \sin\theta_{kj} - B_{kj} \cos\theta_{kj})] = 0 \tag{4.11}$$

$$V_{\min} \le V_k \le V_{\max} \tag{4.12}$$

$$SoC_{\min} \le SoC \le SoC_{\max} \tag{4.13}$$

$$P_{BES,\min} \le P_{BES} \le P_{BES,\max} \tag{4.14}$$

$$k_{BES,d}^{\min} \le k_{BES,d} \le k_{BES,d}^{\max} \tag{4.15}$$

$$k_{BES,c}^{\min} \le k_{BES,c} \le k_{BES,c}^{\max} \tag{4.16}$$

The working equation of PSO is as follows Eq. (3.12) and Eq. (3.13).

where x_i is the population of particles that represent the adjust exponent of $k_{BES,d}$ and $k_{BES,c}$, which are n_d and n_c, respectively. The proposed PSO-based VD improvement computational procedure is illustrated in Fig 4.6.

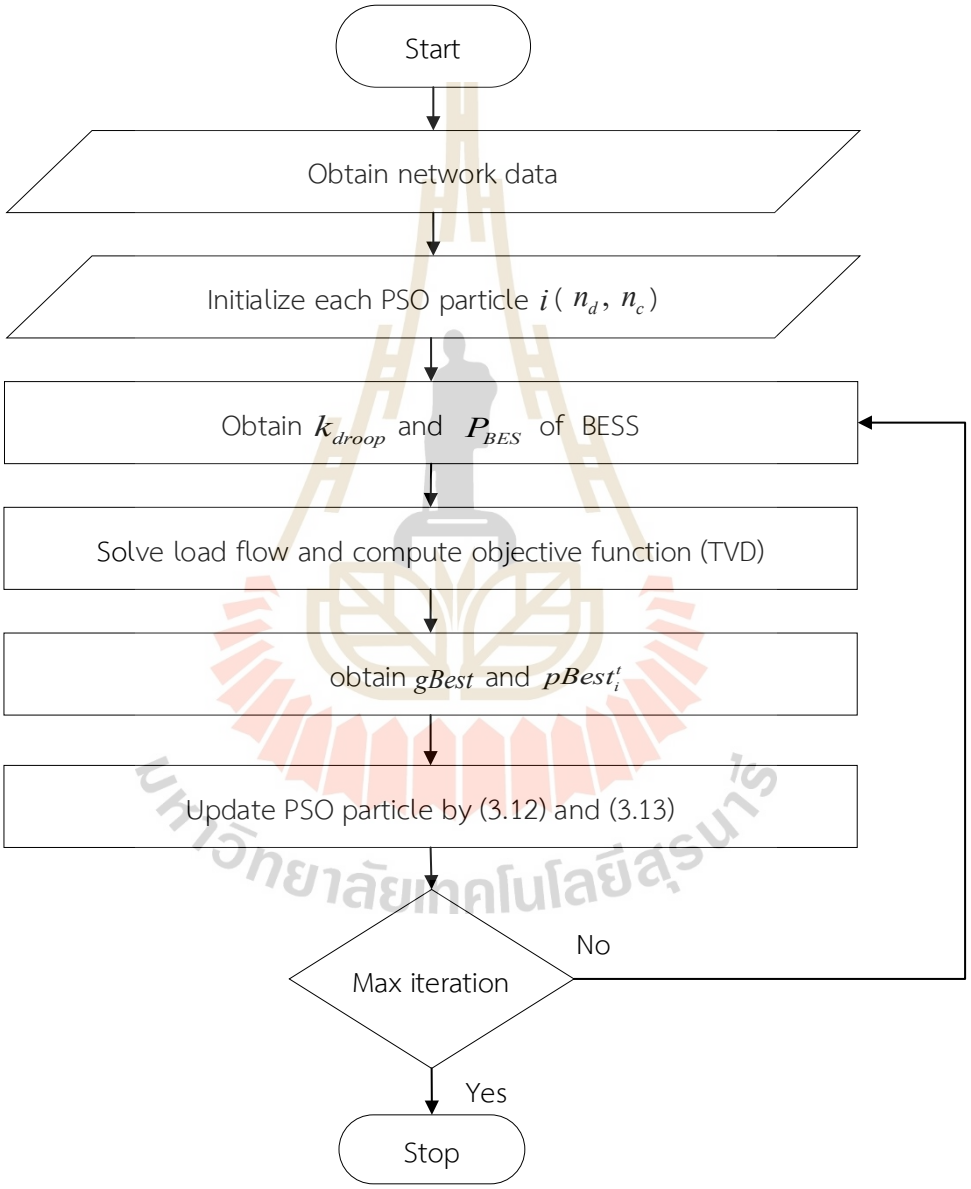

Figure 4.6 The PSO based BESS optimal VDC computation procedure

4.4 BESS Selection Criteria and Sizing

The selection of buses and sizing for BESS installation is based on two main criteria. The bus locations for BESS installation are determined using the L-index, which identifies the buses most susceptible to voltage collapse. These are considered the weakest buses in the system and require the most attention. In the IEEE 33-bus system, there are four branches: Branch 1 includes buses 7–18, Branch 2 includes buses 19–22, Branch 3 includes buses 23–25, and Branch 4 includes buses 26–33. This means that a total of four BESS units are needed. Based on the L-index calculation from table 3.3, the optimal buses for BESS installation are buses 18, 22, 25, and 33, as these have the highest L-index values in each branch. The installation will be considered from the base case only.

The size of each BESS is determined by the total load of each branch. The total loads are as follows: Branch 1 has a total load of 1.075 MW, Branch 2 has 0.36 MW, Branch 3 has 0.93 MW, and Branch 4 has 0.92 MW. For effective voltage control, it is desirable for the BESS to operate continuously, maintaining voltage stability at all times. Therefore, the SoC of the BESS should be set at 0.5, allowing it to absorb energy from PV and wind sources when available, and discharge energy back to the system when generation is low. In this study, the maximum and minimum SoC levels are set at 0.8 and 0.2, respectively, which are considered optimal for BESS operation. This means that only 0.3 p.u. of the SoC is usable, so the BESS capacity must be larger than the total load of each branch. The resulting BESS sizes are as follows: 4.25 MW at bus 18, 1.75 MW at bus 22, 3.5 MW at bus 25, and 3.5 MW at bus 33. The system with renewable energy and BESS is shown on Fig. 4.7.

Similarly, for the IEEE 69-bus system, BESS and renewable energy sources are installed at buses 27, 35, 46, 50, 52, 65, 67, and 69, with capacities of 1.75 MW, 0.5 MW, 0.75 MW, 2.75 MW, 0.25 MW, 5.75 MW, 0.25 MW, and 0.25 MW, respectively, is shown on Fig. 4.8.

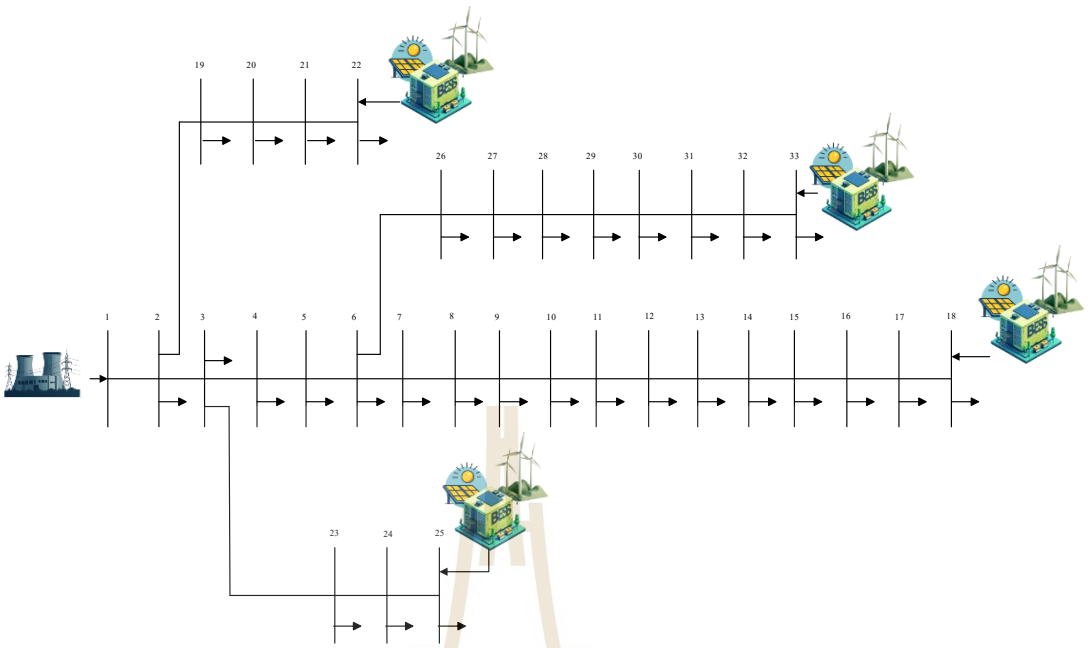

Figure 4.7 The modified IEEE 33-bus with PV and wind power penetration and BESS

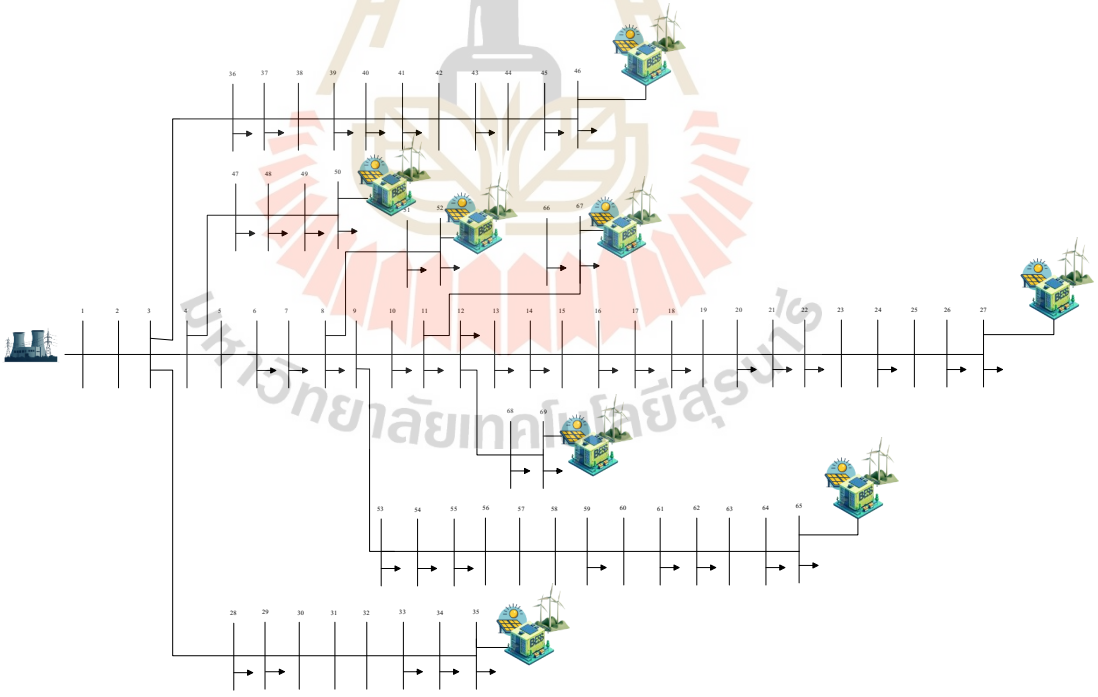

Figure 4.8 The modified IEEE 69-bus with PV and wind power penetration and BESS

In this study, photovoltaic (PV) and wind power, as renewable energy sources, were integrated into the IEEE 33-bus and IEEE 69-bus distribution networks. The sizing of the renewable energy (RE) sources was determined by simulating overvoltage conditions in the power system. This was achieved by incrementally increasing the output of the RE sources and observing whether the voltage magnitude exceeded the specified limit of 1.05 p.u. As a result, the optimal size of the RE sources was found to be 1.25 MW for the IEEE 33-bus system and 1 MW for the IEEE 69-bus system. The PV and wind profiles for these systems are shown in Figure 4.9. (Renewables.ninja).

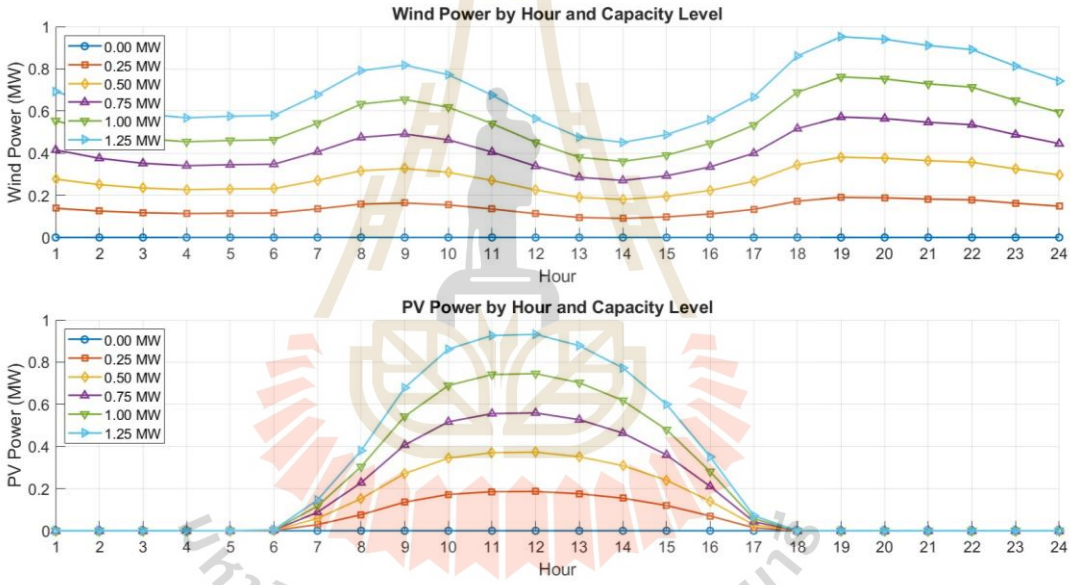

Figure 4.9 The PV and Wind profile 24 hour

4.5 Results and Discussion

The test was conducted on the IEEE 33-bus system, which includes one generator bus and 32 load buses, where bus 1 is designated as the slack bus. The system's voltage restrictions range from 0.95 to 1.05 p.u. The system contains 3.715 MW of real power load and 2.3 MVar of reactive power load. The substation's nominal voltage is configured at 13.8 kV, with the transformer at bus 1 having a capacity of 3 MW.

Table 4.2 also provides the study's parameters, which were evaluated and adjusted as needed, mostly through trial and error. The variable n specifies how quickly the battery can charge or discharge. A larger n allows faster charging or discharging when the BESS SoC is near its maximum or minimum, whereas a smaller n slows charging or discharging when the SoC is near the nominal level. Therefore, we conducted trials to adjust these ranges, as illustrated in Fig 4.5.

The test is divided into three scenarios, as follows:

- case I: IEEE 33-bus base case,
- case II: modified IEEE 33-bus with PV and wind power penetration, and
- case III: modified IEEE 33-bus with PV and wind power penetration and BESS with optimal VDC.

4.5.1 IEEE 33-bus base case.

An initial test was conducted on an IEEE 33-bus distribution system. The voltage of each bus in the system ranges from 0.9038 p.u. to 1.0000 p.u., and the TVD is 1.8047 p.u. This significant deviation indicates that the bus voltages are not within the typical standard range of 0.95 p.u. to 1.05 p.u. The bus with the lowest value is Bus 18. Consequently, the lower-voltage bus should be prioritized to prevent power system instability, which could potentially lead to blackouts.

Table 4.2 Specification of the BESS

Parameter	Specification
Range of the adjust exponent (n)	0.1 to 20
The maximum power of battery ($P_{BES}^{\max}$)	4.25 MW
The maximum droop coefficient ($K_{\max}$)	2182.03
The minimum droop coefficient ($K_{\min}$)	0.1
Nominal Voltage (V_0)	1.00 p.u.
Battery capacity (E)	4.25 MWh
The maximum voltage ($V_{\max}$)	1.05 p.u.
The minimum voltage ($V_{\min}$)	0.95 p.u.

Table 4.2 Specification of the BESS (Continued)

Parameter	Specification
Maximum state of charge ($SoC_{\max}$)	0.8 p.u.
Minimum state of charge ($SoC_{\min}$)	0.2 p.u.

4.5.2 Modified IEEE 33-bus with PV and wind power penetration

In this study, PV and wind power, as renewable energy sources, were integrated into an IEEE 33-bus distribution network. A total of 1.25 MW of PV and wind power was installed at buses 8, 12, 28, and 33. As a result of these renewable energy installations, the system's real power from RE is 6 MW. It was observed that the system voltage ranged from 0.9854 p.u. to 1.0223 p.u. and that TVD was 0.2610 p.u. These findings indicate that high levels of renewable energy penetration affect the power system, causing overvoltages when there is excess power from renewable energy sources and significant voltage fluctuations that negatively affect the electrical network. Therefore, appropriate energy management strategies should be implemented.

4.5.3 Modified IEEE 33-bus with PV and wind power penetration and BESS with optimal VDC.

In case III, the proposed method incorporates a battery into the system and employs PSO to optimize the system to obtain the best value that minimizes TVD. The PSO parameters are configured as follows w ranges from 0.1 to 1.1, both c_1 and c_2 are set to 1.49 and the maximum iterations is 50, which was selected through multiple trial runs. It was observed that the values generally start to converge around 50 iterations, so this value was set accordingly. The results show that the voltage levels on all buses in the system are within the prescribed range, with TVD being 0.2440 p.u. This adjustment was made using the variables presented in Table 4.3, specifically the values of the adjust exponent (n), droop coefficient (k_{droop}) and regulating power (

P_{BES}) for each battery. The sign of P_{BES} for each value indicates whether the battery is charging or discharging. Specifically, a negative sign denotes that the BESS is charging, whereas a positive sign signifies that it is discharging.

Figure 4.10 illustrates the voltage profile for all three scenarios, showing that the proposed method maintains the voltage profile within the specified range through efficient battery charging and discharging. Table 4.4. depicts the 3 scenarios of TVD, indicating that the proposed method also produces the best results by reducing VD compared to case 1 and 2. Furthermore, Fig. 4.11 shows the convergence plot of the proposed PSO-based BESS optimal VDC. it is clear that the value of the objective function progressively converges toward the optimal solution. Fig. 4.12 presents the results of 30 trials conducted using the proposed method that have the average value is 0.2440, standard deviation value is 0.0000, maximum value is 0.2440 and minimum value is 0.2440. The low standard deviation of the objective function values indicates that they are closely clustered, suggesting that the results obtained from PSO algorithm are reliable. The runtime of the proposed method was evaluated over 30 runs on a computer equipped with an AMD Ryzen 5 6600H CPU (3.30 GHz up to 4.50 GHz) and 16 GB of RAM. On average, the method took 54.38 seconds to complete, with a standard deviation of 1.94 seconds. The minimum runtime observed was 52.70 seconds, while the maximum reached 58.28 seconds. Thus, although the PSO method typically requires about 54.38 seconds, it can occasionally take as long as 58.28 seconds, likely due to unfavorable random initializations delaying convergence. These results are illustrated in Figure 4.13.

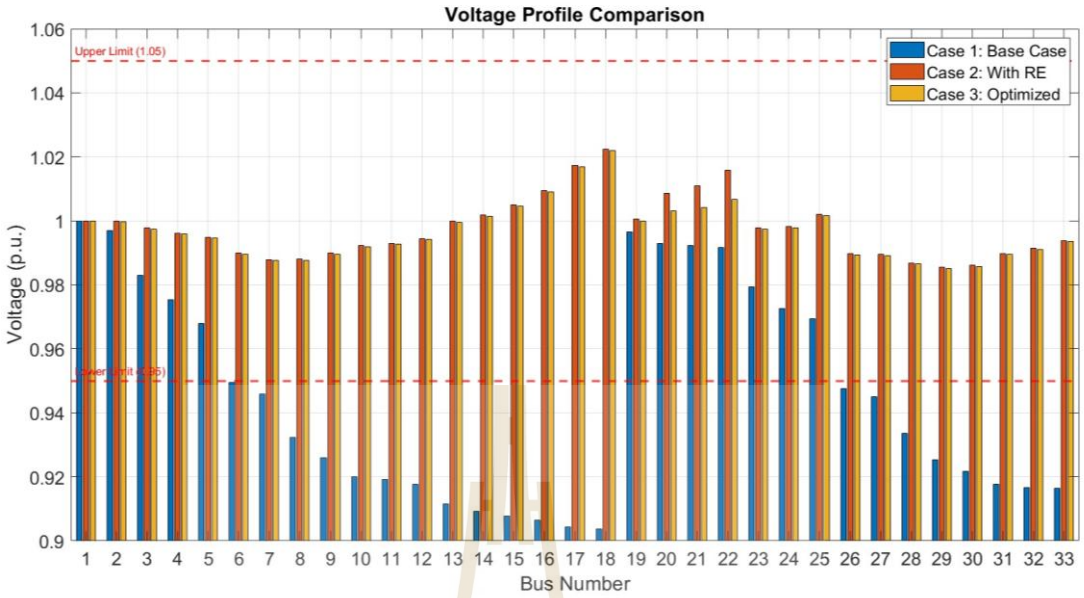

Figure 4.10 Comparative Voltage Profile of modified IEEE 33-bus system

Table 4.3 Adjust exponent, Droop coefficient and BEES regulating power of BESS

Bus with Battery Installed	n	k_{droop}	P_{BES} (MW)	SoC
18	0.1000	0.1031	-0.0023	0.5005
22	20.0000	39.6160	-0.5250	0.8000
25	0.1000	0.1031	-0.0002	0.5001
33	20.0000	39.6160	-0.0000	0.5000

Table 4.4 Adjust exponent, Droop coefficient and BEES regulating power of BESS

Scenarios	TVD (p.u.)
IEEE 33-bus base case	1.8047
Modified IEEE 33-bus with PV and wind power penetration	0.2610
Modified IEEE 33-bus with PV and wind power penetration and BESS with optimal VDC.	0.2440

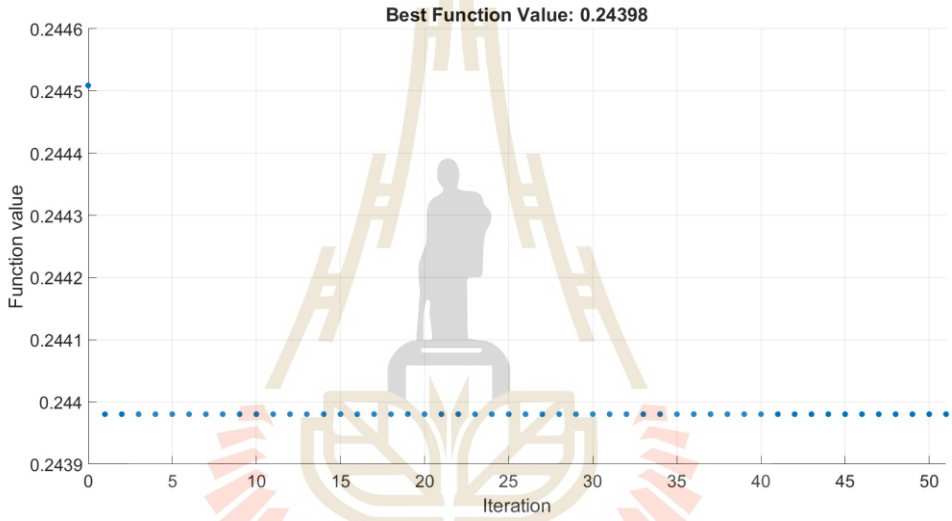

Figure 4.11 the convergence plot of the proposed PSO-based BESS optimal VDC

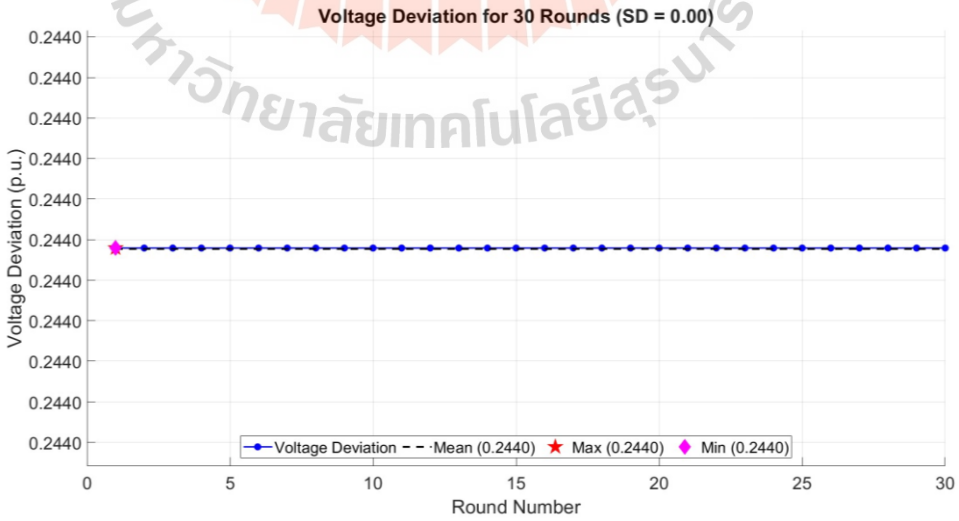

Figure 4.12 the result of 30 trials of the proposed method

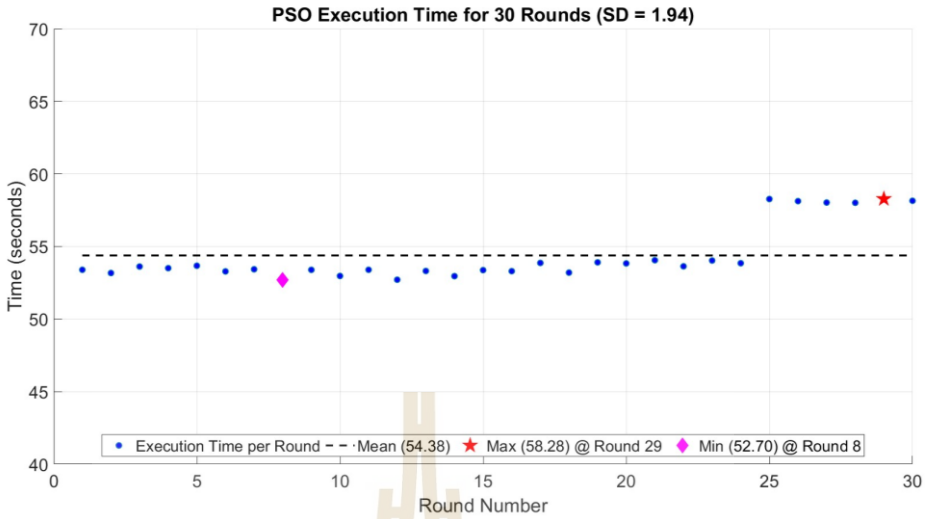

Figure 4.13 The result of 30 trials of the computation time

4.5.4 Sensitivity Analysis of Renewable Energy Placement and Sizing

To further evaluate the robustness and practical applicability of the proposed BESS optimal voltage droop control, this section presents a sensitivity analysis. The primary results demonstrated that the control strategy was highly effective for a specific system configuration, successfully reducing the Total Voltage Deviation (TVD) to 0.2440 p.u. in Case III. However, in real-world distribution networks, the placement and sizing of both Renewable Energy (RE) sources and the BESS units can vary significantly. Therefore, this analysis investigates the performance of the control algorithm when the system configuration deviates from the baseline case. The objective is to determine if the proposed method remains effective under sub-optimal conditions.

To establish the baseline for this analysis, renewable energy, including PV and wind power, was integrated into the IEEE 33-bus distribution system. The configuration includes two 1 MW wind turbine generators on buses 18 and 24; three 1 MW PV systems on buses 5, 21, and 31; and four 500 kW PV systems on buses 8, 12, 28, and 33. Additionally, four 2 MWh BESS units were installed at buses 18, 21, 24, and 32, with their placement determined through a trial-and-error process show in figure

4.14. In this configuration with high RE penetration but without BESS control, the system voltage ranged from 1.0000 p.u. to 1.0534 p.u.

In this scenario, the results show that the voltage levels on all buses in the system are within the prescribed range, with the total voltage deviation (TVD) being 0.0385 p.u. This adjustment was made using the variables presented in Table 4.5, specifically the values of the adjust exponent (n), droop coefficient (k_{droop}), and regulating power (P_{BES}) for each battery.

As shown in Figure 4.15, our proposed method keeps the voltage profile within the required range through efficient battery charging and discharging. Table 4.6 further demonstrates that this method provides the best outcome, reducing voltage deviation more effectively than the other two cases.

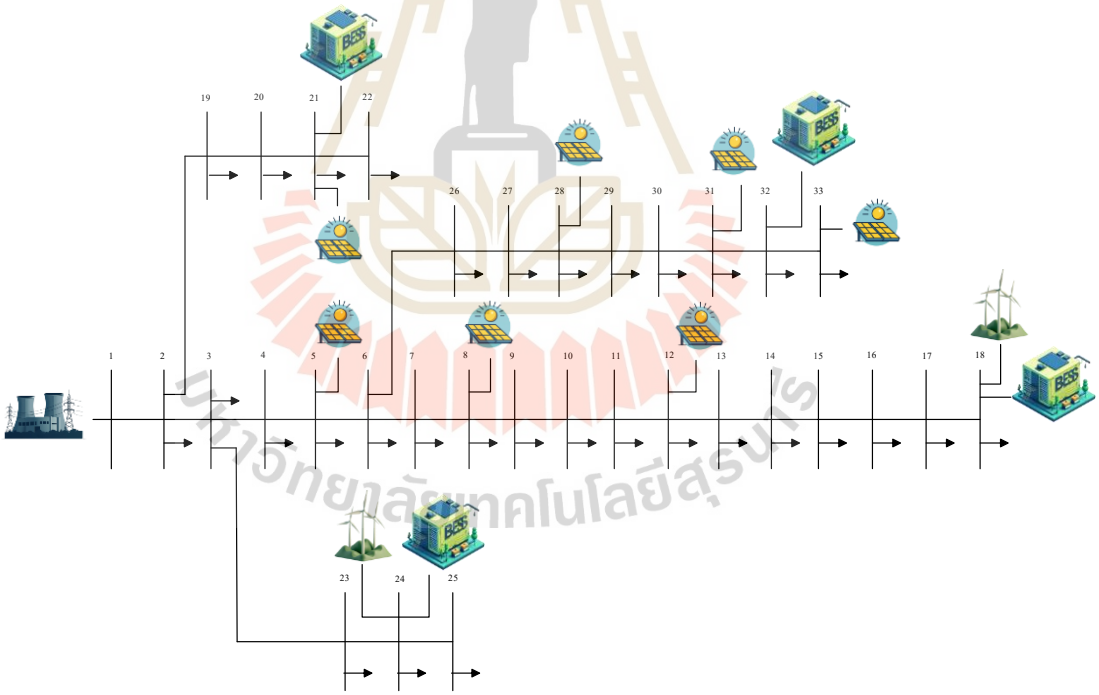

Figure 4.14 The modified IEEE 33-bus with PV and wind power penetration and BESS in sensitivity analysis case

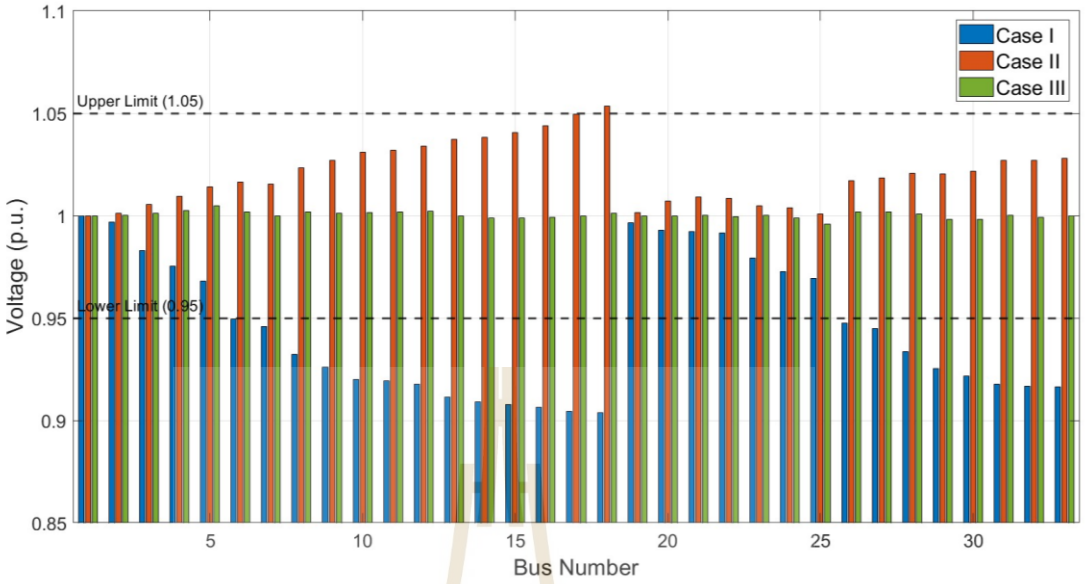

Figure 4.15 Comparative Voltage Profile of modified IEEE 33-bus system in sensitivity analysis case

Table 4.5 Adjust exponent, Droop coefficient and BEES regulating power of BESS in sensitivity analysis case

Bus with Battery Installed	n	k_{droop}	P_{BES} (MW)
18	13.6531	12.3498	-0.6591
22	17.1637	67.4965	-0.6139
25	5.8498	16.0991	-0.0627
33	0.1000	19.5058	-0.5282

Table 4.6 Adjust exponent, Droop coefficient and BEES regulating power of BESS in sensitivity analysis case

Scenarios	TVD (p.u.)
IEEE 33-bus base case	1.8047
Modified IEEE 33-bus with PV and wind power penetration in sensitivity analysis case	0.6879
Modified IEEE 33-bus with PV and wind power penetration and BESS with optimal VDC in sensitivity analysis case	0.0385

4.6 Chapter Summary

This chapter introduces a method for enhancing VS in an active distribution network by installing BESS at weak buses, which were previously identified using the L-index method. The study utilizes an adaptive voltage droop control strategy to manage the BESS, which adjusts its operation based on the battery's SoC to improve efficiency and prevent saturation. To determine the optimal control parameters, PSO is employed to minimize TVD across the system.

The proposed methodology was tested on the IEEE 33-bus system under three scenarios: a base case, a case with high penetration of renewable energy (PV and wind), and a final case that included the BESS with optimized control. The results demonstrated that while the integration of renewables alone caused significant voltage fluctuations, the implementation of the BESS with optimal VDC successfully maintained the voltage profile within the acceptable range of 0.95 to 1.05 p.u. The PSO algorithm proved effective and reliable in finding the optimal parameters, as evidenced by the consistent results over 30 trial runs and the clear convergence of the objective function. A sensitivity analysis further confirmed that the proposed

control strategy remains robust and effective even when the placement and sizing of renewable sources and BESS units are altered.

CHAPTER V

BESS VOLTAGE REGULATION CONSIDERING SoC RESTORATION

5.1 Introduction

This chapter proposes a management strategy for SoC Restoration of BESS to eliminate saturation concerns and produce optimal VD in ADN. It begins by presenting an overview technique for calculating SoC Restoration and control strategies. Then the chapter defines the objective function for evaluating the effectiveness of the suggested solutions and includes numerous case studies that demonstrate the practical application of SoC restoration in real-world circumstances.

Effective management of SoCs can greatly enhance voltage profiles and minimize voltage drift by using advanced control methods and optimization techniques. The insights shared here play a vital role in the ongoing conversation about enhancing the stability of today's energy networks, particularly as we see a rise in the use of renewable energy sources.

5.2 SoC Restoration Formulation

SoC restoration is the process of bringing the SoC level back to the nominal level to enable more efficient operation.

From equation Eq. (4.1), the equation for the discharge and charge of the BESS can be rewritten considering SoC restoration, as shown in Eq. (5.1).

$$P_{BESS} = P_{BES} + P_{SoC} \tag{5.1}$$

The principle is to check the remaining SoC level compared to the nominal SoC as follows: If the SoC is between 0 and 0.45, the battery will charge to increase the SoC

level for future operations. Meanwhile, if the SoC is between 0.55 and 1, the battery will discharge to prevent the SoC level from becoming too high and causing battery saturation. This operation can be represented by Eq. (5.2) and Eq. (5.3).

$$P_{SoC,d} = \begin{cases} 0 & \text{if } 0 < \text{SoC} < 0.55 \\ \dfrac{P_{SoC,\max} P_{SoC,\min} e^{n_{ds}(SoC-0.5)}}{P_{SoC,\max} + P_{SoC,\min} e^{n_{ds}(SoC-0.5)} - 1} & \text{if } 0.55 < \text{SoC} < 1 \end{cases} \tag{5.2}$$

$$P_{SoC,c} = \begin{cases} 0 & \text{if } 0.45 < \text{SoC} < 1 \\ \dfrac{P_{SoC,\max} P_{SoC,\min} e^{n_{cs}(0.5-SoC)}}{P_{SoC,\max} + P_{SoC,\min} e^{n_{cs}(0.5-SoC)} - 1} & \text{if } 0 < \text{SoC} < 0.45 \end{cases} \tag{5.3}$$

$$P_{SoC} = \begin{cases} P_{SoC,d}, & \text{discharge} \\ P_{SoC,c}, & \text{charge} \end{cases} \tag{5.4}$$

As shown in Equation (4.8), after the voltage deviation has been reduced, the BESS aims to maintain its SoC within an appropriate range typically between 0.45 and 0.55 for effective voltage control. This consideration allows the BESS operation to be further modeled and integrated into the NRLF analysis. Consequently, the bus voltage can be recalculated with this updated model, as expressed in Equation (5.5).

$$P_{BESS} + P_k^{gen} - P_k^{load} - \sum_{j=1}^{n} [V_k V_j (G_{kj} \cos\theta_{kj} + B_{kj} \sin\theta_{kj})] = 0 \tag{5.5}$$

5.3 Objective Function

5.3.1 PSO Based TSoC Improvement

In this study, an additional objective function will be introduced to maintain the SoC level at the nominal level. The objective function used in the study is illustrated in the following equation.

$$\text{minimize } \text{T}SoC = \sum_{k=1}^{N} \left(\left| SoC_k - SoC_0 \right| \right) \tag{5.6}$$

This objective is to reduce the sum deviation of SoC from the nominal level. Reducing this deviation will allow BESS to control the voltage continuously,

thereby improving the system's performance. The working equation of PSO is following Eq. (3.12) and Eq. (3.13). where x_i is the population of particles that represent the adjust exponent of $P_{SoC,d}$ and $P_{SoC,c}$, which are n_{ds} and n_{cs}, respectively. The proposed PSO computational procedure is illustrated in Fig 5.1.

5.3.2 PSO Based TVD Improvement

From Eq. (4.9), the equation is as follows:

$$\text{minimize TVD} = \sum_{k=1}^{N}(V_k - V_0) \tag{5.7}$$

The proposed PSO computational procedure is illustrated in Fig 4.5. The constraints are defined as follows Eq. (4.10) – Eq. (4.16).

5.4 FMOO-based PSO

In this study, the FMOO-based PSO algorithm uses a linear Max-Min method. This approach sets the boundaries using the maximum and minimum values of each objective, creating a straight-line trade-off region between the two goals (Muangkhiew, 2022).

The two main objectives in this study are:

- Minimizing TVD (Total Voltage Deviation)
- Minimizing TSoC (Total State of Charge deviation)

The FMOO-based PSO helps find the best balance between these two competing objectives. It is searching for the most suitable solution that offers a good trade-off between reducing TVD and TSoC.

Based on the objective functions in Eq. (5.6) and Eq. (5.7), membership functions are created, as shown in Fig. (5.2) and Fig. (5.3). These functions help measure how well each solution meets the objectives. The functions can be expressed as follows:

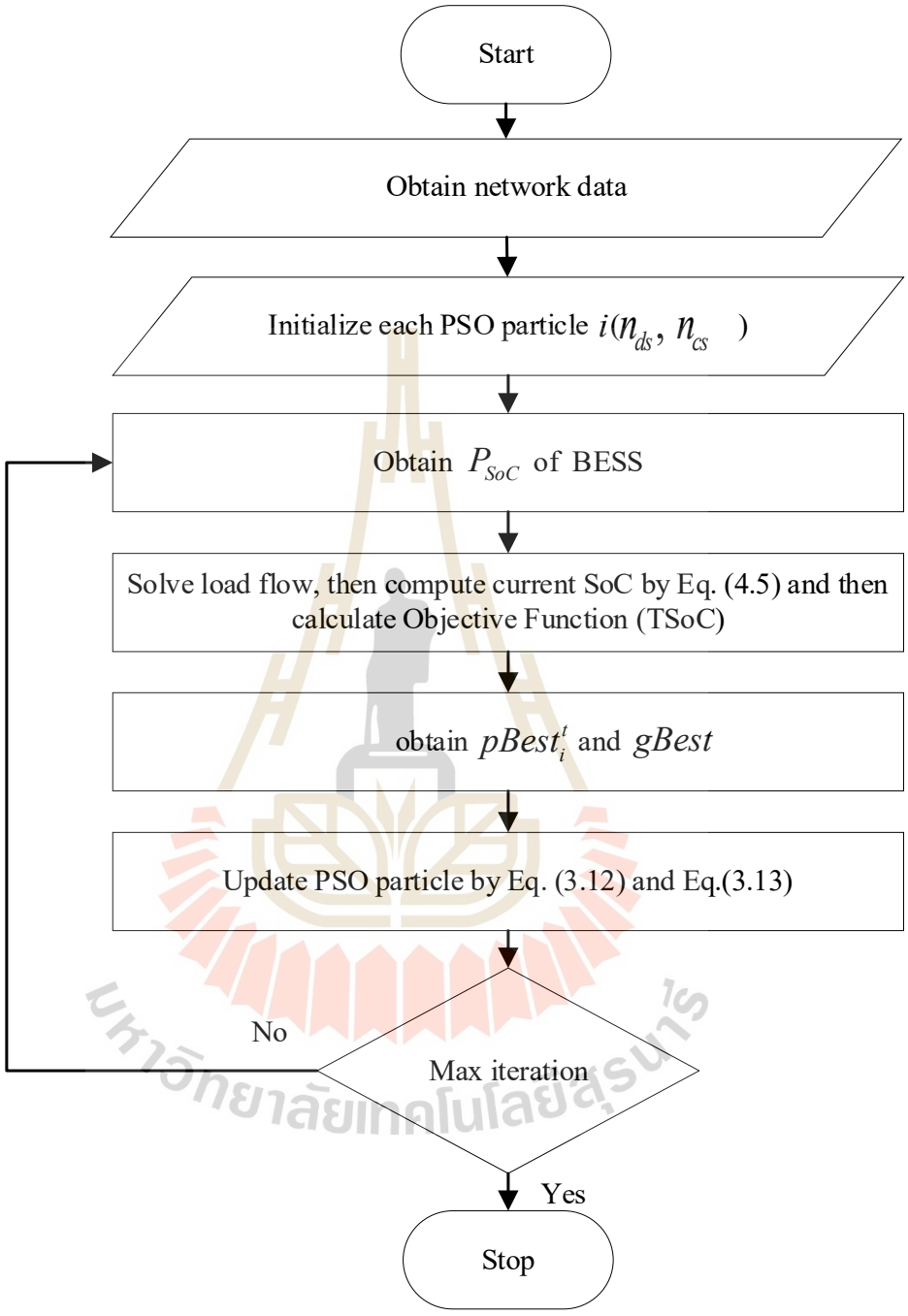

Figure 5.1 The PSO based BESS optimal TSoC computation procedure

membership function for Eq. (5.6)

$$\mu_{TSoC}(x)=\begin{cases}1, & \text{if } TSoC(x)\le TSoC_{\min}\\ \dfrac{TSoC_{\max}-TSoC(x)}{TSoC_{\max}-TSoC_{\min}}, & \text{if } TSoC_{\min}<TSoC(x)\le TSoC_{\max}\\ 0 & \text{if } TSoC(x)\ge TSoC_{\max}\end{cases} \quad (5.8)$$

membership function for Eq. (5.7)

$$\mu_{TVD}(x)=\begin{cases}1, & \text{if } TVD(x)\le TVD_{\min}\\ \dfrac{TVD_{\max}-TVD(x)}{TVD_{\max}-TVD_{\min}}, & \text{if } TVD_{\min}<TVD(x)\le TVD_{\max}\\ 0 & \text{if } TVD(x)\ge TVD_{\max}\end{cases} \quad (5.9)$$

The optimum fuzzy function can be obtained as follows:

$$\text{Maximize } \mu_T=\min\left\{\mu_{TSoC}(x),\mu_{TVD}(x)\right\} \quad (5.10)$$

The proposed computational procedure for the FMOO-based PSO is illustrated in Fig. 5.4.

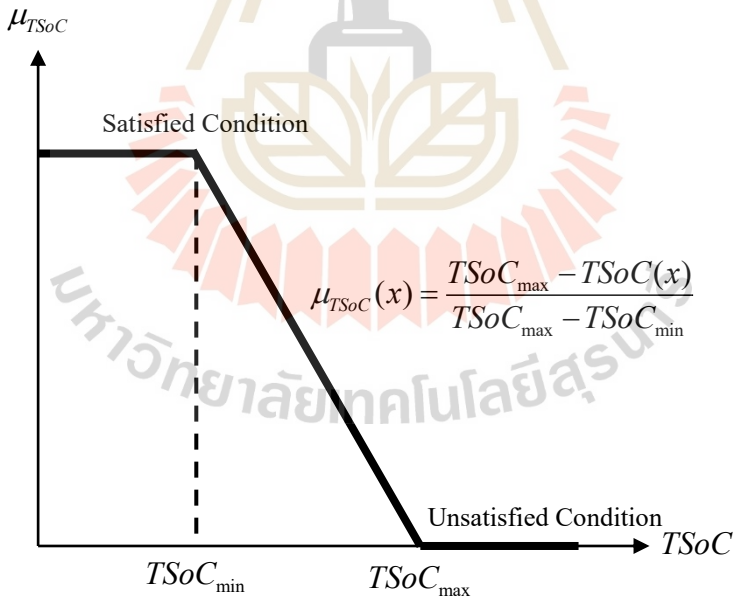

Figure 5.2 The Fuzzy membership function of total SoC deviation

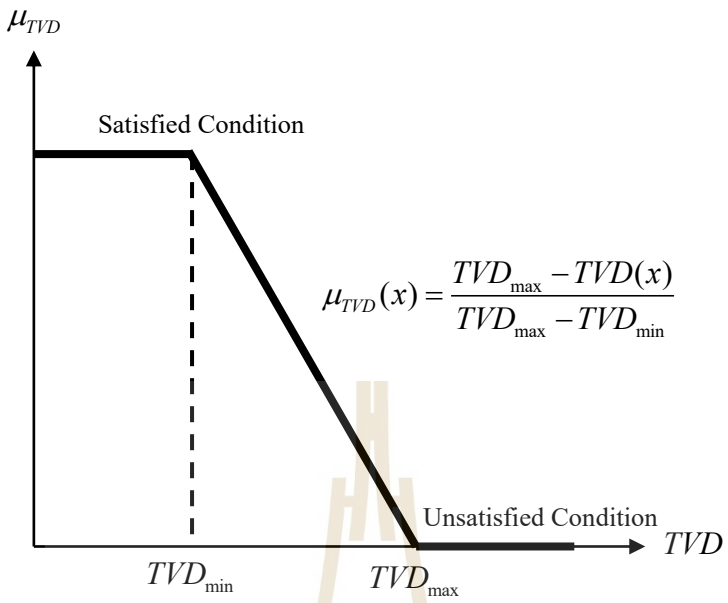

Figure 5.3 The Fuzzy membership function of total voltage deviation

5.5 PSO Parameter Selection and Tuning

For the PSO process, it is essential to carefully tune several key parameters to ensure optimal performance. These parameters include the self-adjustment weight, social-adjustment weight, inertia weight range, maximum number of iterations, and the size of the swarm. Each of these factors plays a significant role in determining both the quality of the solution and the computational efficiency of the optimization process. To systematically investigate the effects of these parameters, we conducted a comprehensive full factorial exploration, as detailed in Table 5.1. This exploration covered a total of 1,176 different parameter combinations, allowing us to thoroughly assess the impact of each setting. The results of this extensive study are summarized and presented in Figure 5.5 and Table 5.2, providing valuable insights into the parameter configurations that yield the best performance.

In the proposed method, a battery is integrated into the system, and PSO is utilized with the specific objective of minimizing the total voltage deviation . Through numerous trial runs and iterative adjustments, the PSO parameters were ultimately set as follows: the inertia weight was varied within the range of 0.3 to 0.7,

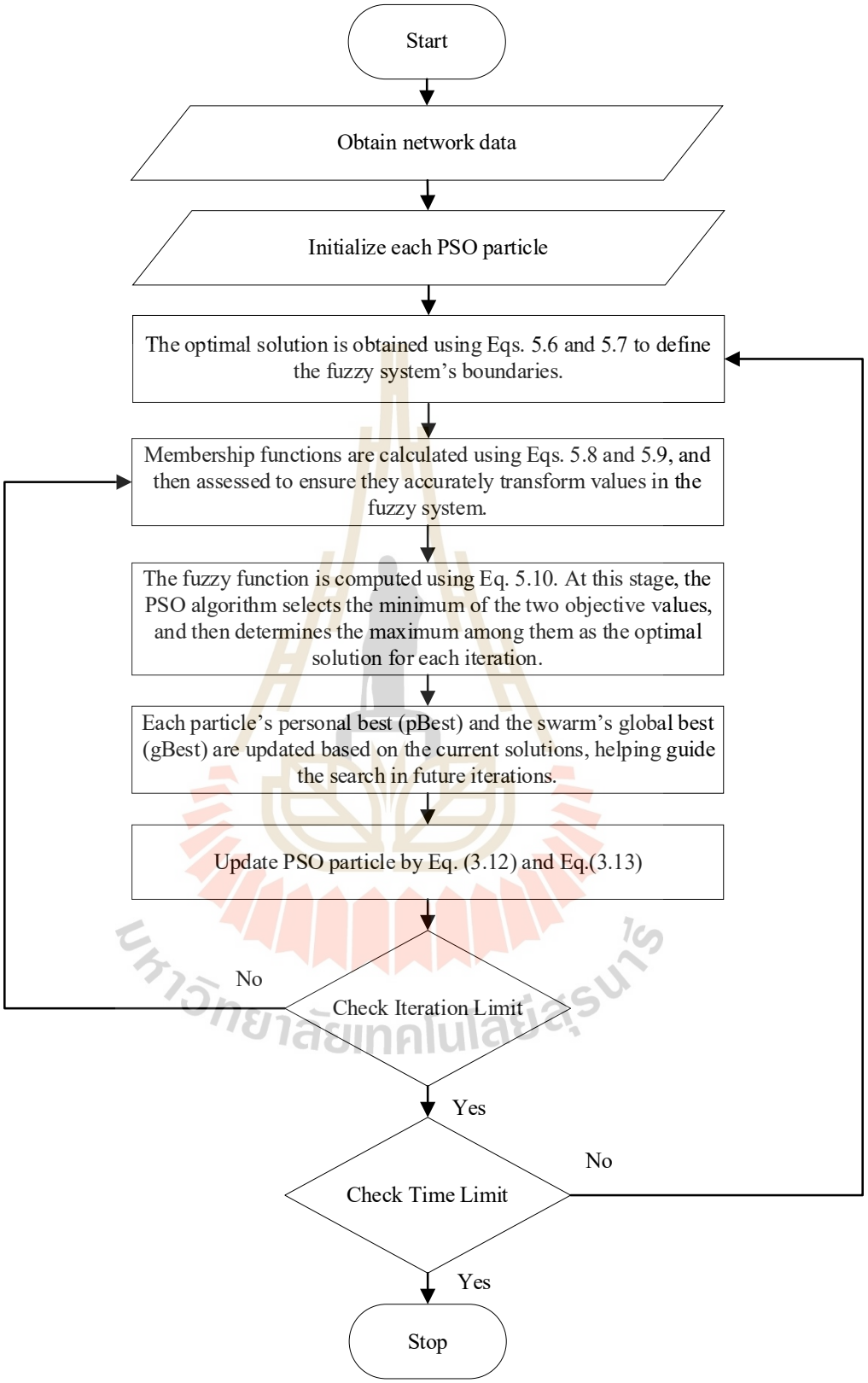

Figure 5.4 The FMOO-based PSO computation procedure

while both the self-adjustment weight and the social-adjustment weight were assigned values of 1 and 2, respectively. Additionally, the maximum number of iterations was fixed at 100, and the swarm size was also set to 100.

In addition, the minimization of the total SoC deviation was also considered. For this objective, the inertia weight was varied within the range of 0.1 to 1.1, while the self-adjustment weight and the social-adjustment weight were set to 1 and 2, respectively. This configuration resulted in an optimal objective function value of 0.90023, with a computation time of 20 seconds, as illustrated in Figure 5.6 and table 5.3.

For the Fuzzy Multi-objective approach, the inertia weight varied from 0.1 to 0.9, and both the self-adjustment weight and the social-adjustment weight were set to 2. This setup yielded an optimal objective function value of 0.8924, with a computation time of 30 seconds, as shown in Figure 5.7 and table 5.4.

These parameter values were selected based on their consistent ability to deliver optimal results across multiple experimental runs. With this carefully chosen configuration, the PSO algorithm was able to achieve the best possible outcome for the given objective function, effectively minimizing the total voltage deviation within the system.

Table 5.1 PSO Parameter Ranges for Testing

Parameter	Symbols	Values in Test Set
Self-Adjustment Weight	c_1	[1.1, 1.0, 0.9, 0.8, 0.7, 0.6]
Social Adjustment Weight	c_2	[0.1, 0.2, 0.3, 0.4]
Inertia Range	w	[1.0, 1.5, 2.0, 2.5, 3.0, 3.5, 4.0]

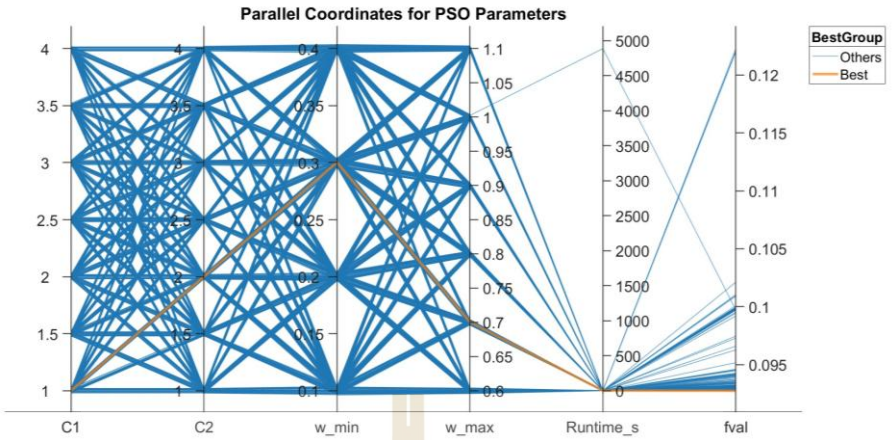

Figure 5.5 PSO parameter for TVD objective

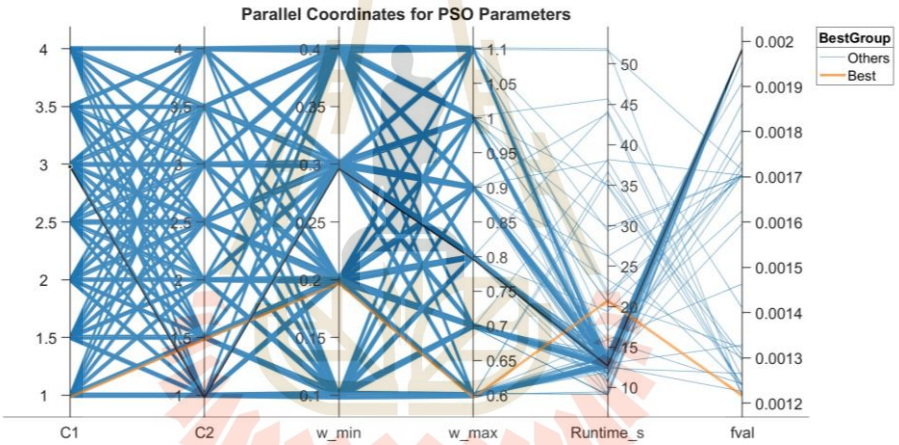

Figure 5.6 PSO parameter for TSoC objective

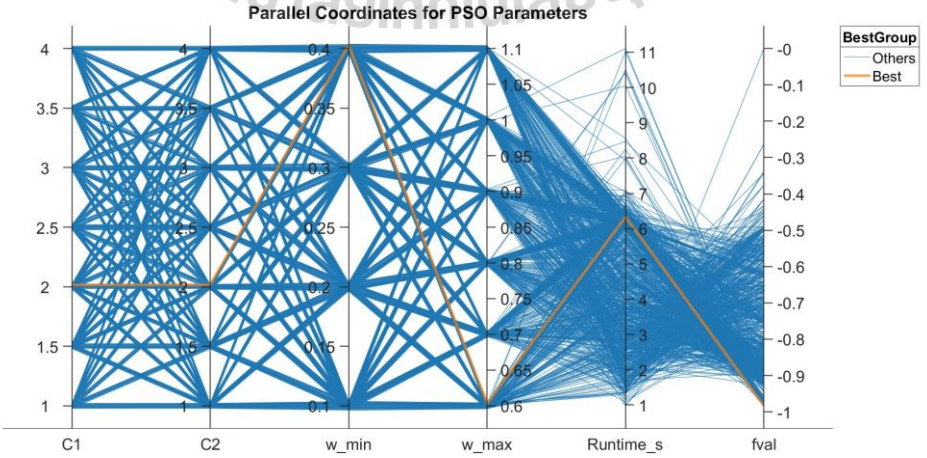

Figure 5.7 PSO parameter for Fuzzy Multi-objective

Table 5.2 PSO Parameter for TVD objective

Parameter	Symbols	Settings
Self-Adjustment Weight	c_1	1
Social Adjustment Weight	c_2	2
Max Inertia Range	$w_{\max}$	0.7
Min Inertia Range	$w_{\min}$	0.3
Max Iteration	-	100
Swarm Size	-	100

Table 5.3 PSO Parameter for TSoC objective

Parameter	Symbols	Settings
Self-Adjustment Weight	c_1	1
Social Adjustment Weight	c_2	1.5
Max Inertia Range	$w_{\max}$	0.6
Min Inertia Range	$w_{\min}$	0.2
Max Iteration	-	100
Swarm Size	-	100

Table 5.4 PSO Parameter for Fuzzy Multi-objective

Parameter	Symbols	Settings
Self-Adjustment Weight	c_1	2
Social Adjustment Weight	c_2	2
Max Inertia Range	$w_{\max}$	0.6
Min Inertia Range	$w_{\min}$	0.4
Max Iteration	-	100
Swarm Size	-	100

5.6 Results and Discussion

The operation will be tested using the IEEE 33-bus and IEEE 69-bus distribution system, where scenarios of voltage rise, and voltage drop will be simulated to observe the performance of the proposed method. Furthermore, the tests are divided into 2 comparative cases as follows:

• case 5.5.3.1 modified IEEE 33-bus with PV and wind power penetration and BESS considering SoC restoration results

• case 5.5.3.2: modified IEEE 69-bus with PV and wind power penetration and BESS considering SoC restoration results

5.6.1 modified IEEE 33-bus with PV and wind power penetration and BESS considering SoC restoration results

In this case six scenarios considered, in which RE sources with a total capacity of 1.25 MW and BESS were installed at bus 18, 1.75 MW at bus 22, 3.5 MW at bus 25, and 3.5 MW at bus 33. The scenarios are as follows:

- Scenario 1 Wind power only: 1.25 MW wind, no PV installed
- Scenario 2 0.25 MW PV and 1.00 MW wind
- Scenario 3 0.50 MW PV and 0.75 MW wind
- Scenario 4 0.75 MW PV and 0.50 MW wind
- Scenario 5 1.00 MW PV and 0.25 MW wind
- Scenario 6 PV only: 1.25 MW PV, no wind installed

5.6.1.1 Scenario 1 Wind power only: 1.25 MW wind, no PV installed

In this study, the IEEE 33-bus distribution system was modeled with the integration of four 1.25 MW wind turbines installed at buses 18, 22, 25, and 33. Notably, no PV generation was included in this scenario, allowing for a focused assessment of the impact of wind power alone. Each wind turbine site was equipped with a BESS, which was managed by a FMOO-based PSO controller. The controller was designed to optimize the “adjust-exponent” parameter, as detailed in Table 5.5, in order to

balance two key objectives: minimizing TVD across the network and maintaining the TSoC among the BESS units within acceptable limits.

Figure 5.9 illustrates the operational profile of the BESS at bus 18 over a 24-hour period. Due to the variable nature of wind generation, the power supplied to the grid fluctuates throughout the day, occasionally leading to over-voltage conditions, particularly during hours 8–10 and at hour 18. Figure 5.8 provides a detailed BESS Operation at a single time point to illustrate this multi-objective control. The process begins with the bus voltage at a high of 1.0278 p.u. At this moment, the FMOO based PSO controller determines a net power action by balancing two simultaneous objectives. As shown in the middle plot, the primary objective of voltage control requires a significant charge action (-0.2834 p.u.), while the secondary objective of restoring the SoC towards its 0.5 reference (from an initial 55.03%) calls for a discharge action (0.1277 p.u.).

The controller synthesizes these conflicting requirements into a single net charging action. This resulting net action effectively reduces the bus voltage to its final value of 1.0158 p.u., as shown in the "After Control" bar. The impact on the State of Charge, detailed in the right-hand plot, reflects this combined action. While the charging component for voltage control alone would raise the SoC to 61.70%, the actual net operation results in a final SoC of 58.70%. This demonstrates the controller's ability to successfully mitigate the over-voltage condition while simultaneously managing the battery's state of charge, ensuring it remains prepared for future grid events.

The effectiveness of the FMOO based PSO approach is further demonstrated in Figures 5.10 and 5.11. For example, at hour 15, the maximum and minimum TVD values obtained from single-objective optimizations are 0.4939 p.u. and 0.3023 p.u., respectively. The FMOO solution achieves a TVD of 0.3686 p.u., which lies between these extremes. Similarly, for the TSoC metric, the maximum and minimum values are 0.2353 and 0.0029, while the fuzzy solution yields 0.0832. These results indicate that the controller successfully balances the trade-off between voltage

regulation and battery state-of-charge management, avoiding excessive deviation in either objective.

Overall, the findings confirm that the proposed FMOO based PSO controller enables robust voltage regulation and effective energy management in a wind-only scenario. By maintaining the BESS state of charge near the midpoint, the system ensures that storage resources are consistently available, contributing to the stability of the distribution network. This approach demonstrates the potential for integrating renewable energy sources with advanced control strategies to enhance the performance of modern power systems.

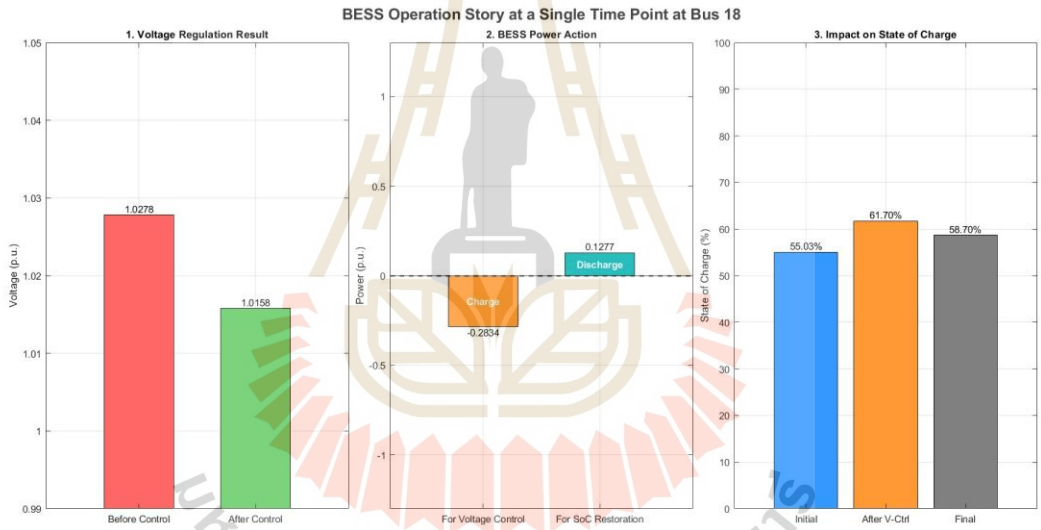

Figure 5.8 Overview of BESS Operation for Voltage Support scenario 1

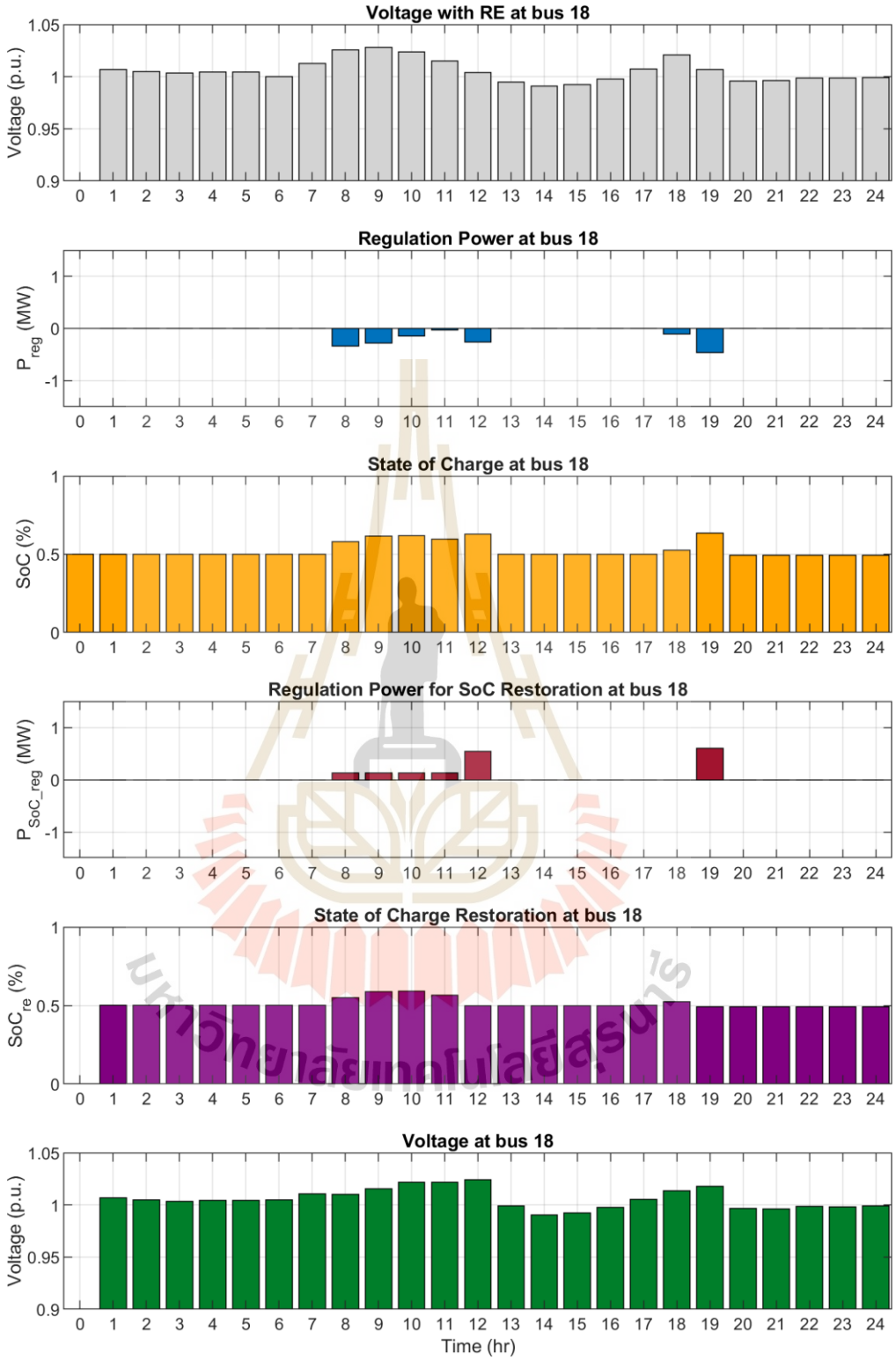

Figure 5.9 Time-Series Profiles of Voltage, Regulation Power and Battery SoC at Bus 18 Scenario 1

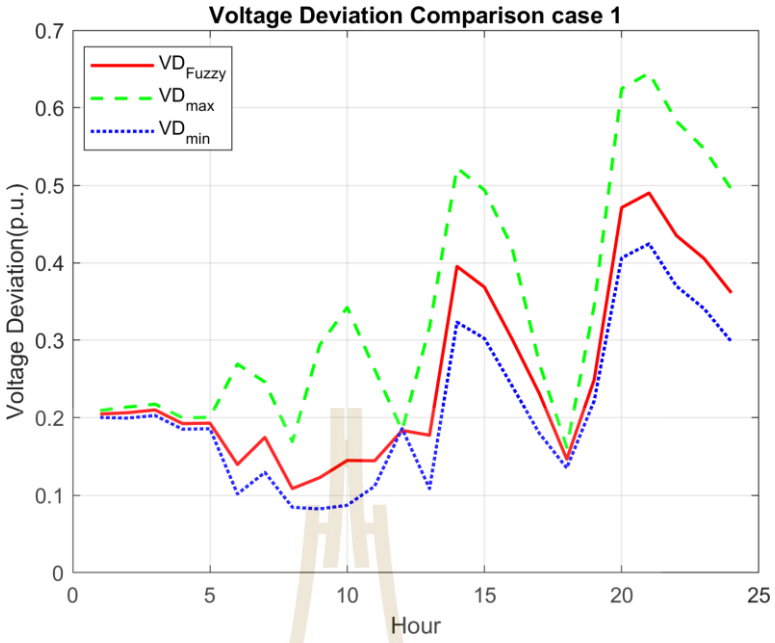

Figure 5.10 Comparison of Maximum, Minimum, and Fuzzy Multi-Objective Voltage Deviation scenario 1

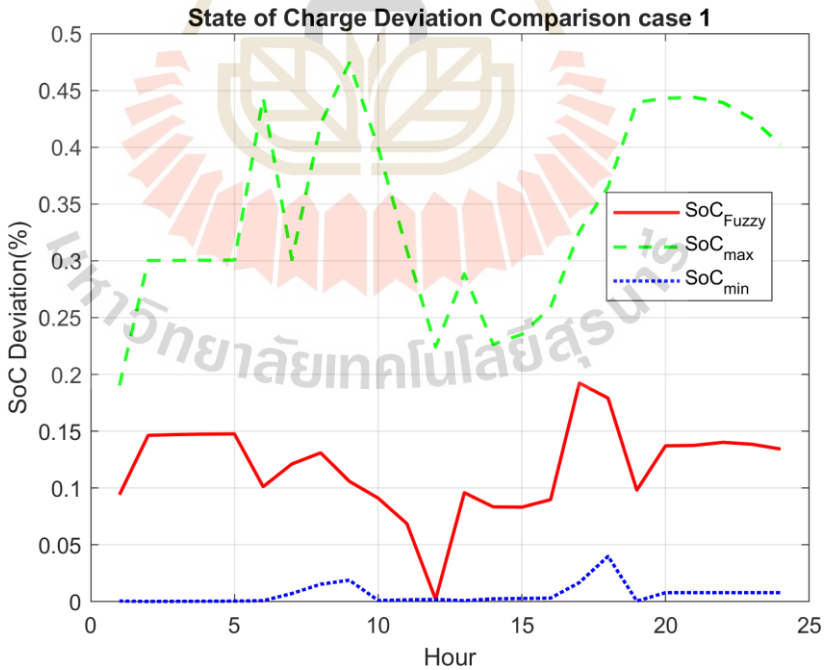

Figure 5.11 Comparison of Maximum, Minimum, and Fuzzy Multi-Objective SoC Deviation scenario 1

Table 5.5 Optimal adjust-exponent values obtained with the fuzzy multi-objective PSO algorithm scenario 1

Hour	Control	Bus	n	Power (MW)	SoC
8	Voltage Deviation	18	16.2303	-0.3373	0.5803
		22	12.1134	-0.0828	0.6034
		25	0.1000	-0.0005	0.5002
		33	18.8230	-0.0498	0.4500
	SoC Deviation	18	0.1000	0.1272	0.5503
		22	0.1000	0.1275	0.5305
		25	3.4116	0.0000	0.5002
		33	0.1000	0.0000	0.4500
9	Voltage Deviation	18	13.1980	-0.2834	0.6170
		22	12.5637	-0.0737	0.5727
		25	0.1000	-0.0006	0.5003
		33	20.0000	-0.1098	0.4814
	SoC Deviation	18	0.1000	0.1277	0.5870
		22	0.1000	0.1271	0.5000
		25	8.1443	0.0000	0.5003
		33	17.1891	0.0000	0.4814
18	Voltage Deviation	18	13.1198	-0.1071	0.5254
		22	19.9961	-0.2595	0.8000
		25	0.1000	-0.0003	0.5006
		33	0.1000	-0.0000	0.4600
	SoC Deviation	18	0.1000	0.0000	0.5254
		22	3.9865	0.3270	0.6131
		25	4.4869	0.0000	0.5006
		33	0.1000	0.0000	0.4600

5.6.1.2 Scenario 2 0.25 MW PV and 1.00 MW wind

By adding a small photovoltaic (PV) system just 0.25 MW per site alongside the existing 1.00 MW wind turbines, the overall renewable generation profile now shows two distinct peaks. The first is a PV-driven rise between 9:00 AM and 3:00 PM, while the second, a wind-dominated peak, occurs in the early evening around 7:00 to 8:00 PM. At bus 18, these peaks push the voltage up to about 1.0255 p.u.

During peak generation periods, the BESS is set to charge, helping to pull the voltage back within acceptable limits, ensuring the voltage stays close to its nominal value throughout the entire 24-hour period, as illustrated in Figure 5.12. However, the controller is equally effective during times of low generation. To illustrate the controller's versatility, Figure 5.13 presents a BESS Operation during a moment of under-voltage at bus 18. At this specific time, the voltage has dropped to 0.9791 p.u. The FMOO PSO controller determines a net power action by balancing two conflicting objectives. The primary response to correct the under-voltage is to discharge power into the grid (0.9531 p.u.). Simultaneously, with the initial SoC slightly high at 51.99%, the secondary objective of SoC restoration calls for a charging action (-0.4225 p.u.) to move it closer to the 50% target. The controller synthesizes these opposing needs into a net discharge command, which successfully raises the bus voltage to 1.0134 p.u. The impact of this balanced action on the SoC is shown in the right-hand plot while discharging for voltage control alone would have caused the SoC to plummet to 29.56%, the actual net operation results in a more moderate final SoC of 39.51%. At the most challenging time around 9:00 AM the single-objective optimization methods produce a maximum TVD of 0.1541 p.u. and a minimum of 0.0880 p.u., while the fuzzy logic controller lands somewhere in between at 0.1070 p.u. Similarly, the TSoC ranges from 0.0036 to 0.3842 across the single-objective runs, with the fuzzy controller achieving a more balanced result of 0.1129 as shown in Figures 5.14 and 5.15.

These results highlight how the algorithm tuned using PSO effectively balances performance by selecting an optimal n, detailed in Table 5.6. In

summary, while the small addition of PV slightly increases the evening over-voltage, it has little effect on midday conditions. The proposed controller continues to manage voltage effectively throughout the day.

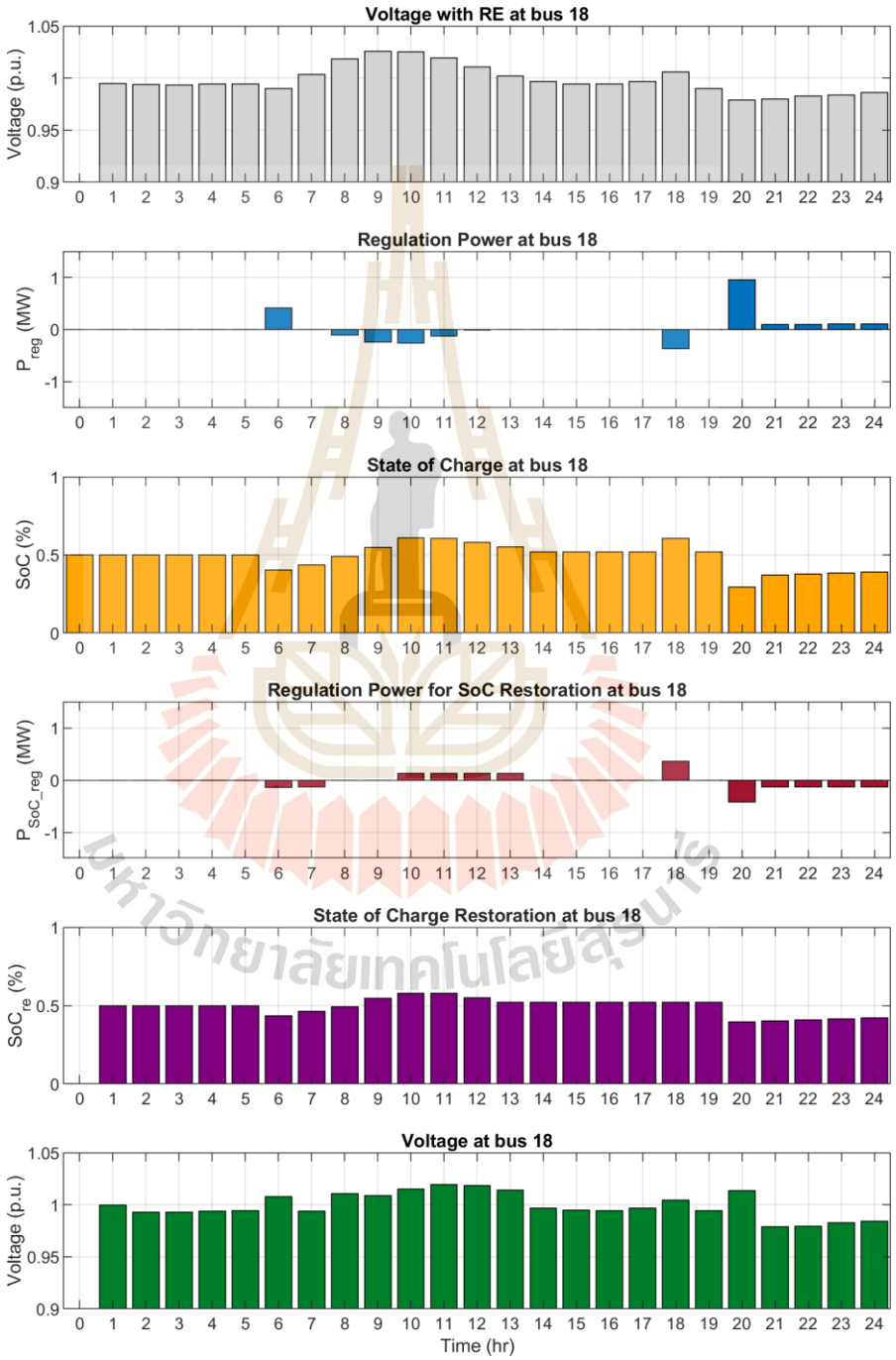

Figure 5.12 Time-Series Profiles of Voltage, Regulation Power and Battery SoC at Bus 18 Scenario 2

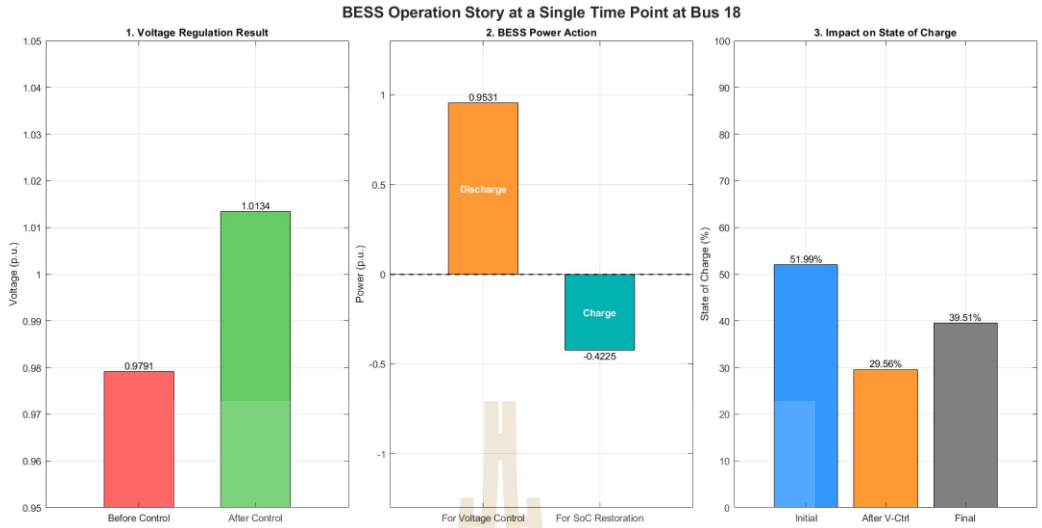

Figure 5.13 Overview of BESS Operation for Voltage Support scenario 2

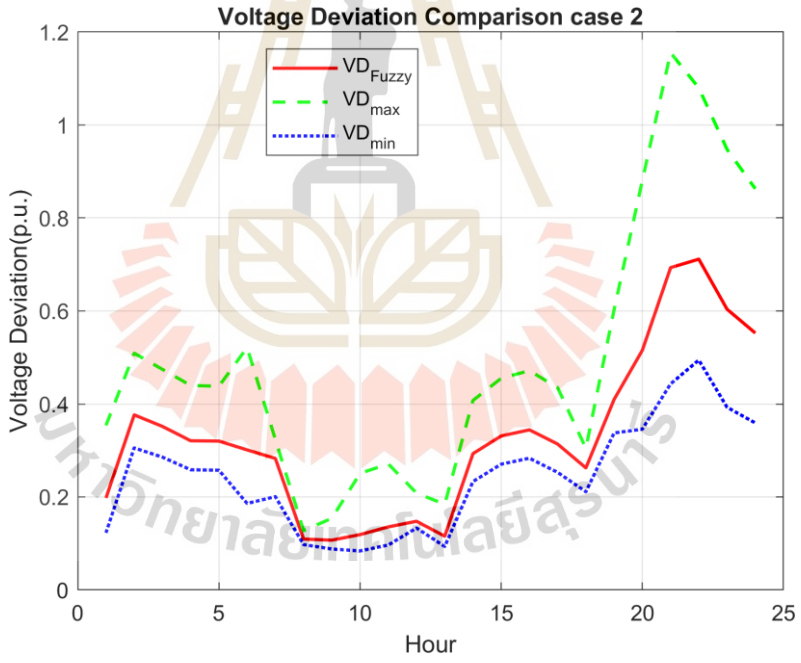

Figure 5.14 Comparison of Maximum, Minimum, and Fuzzy Multi-Objective Voltage Deviation scenario 2

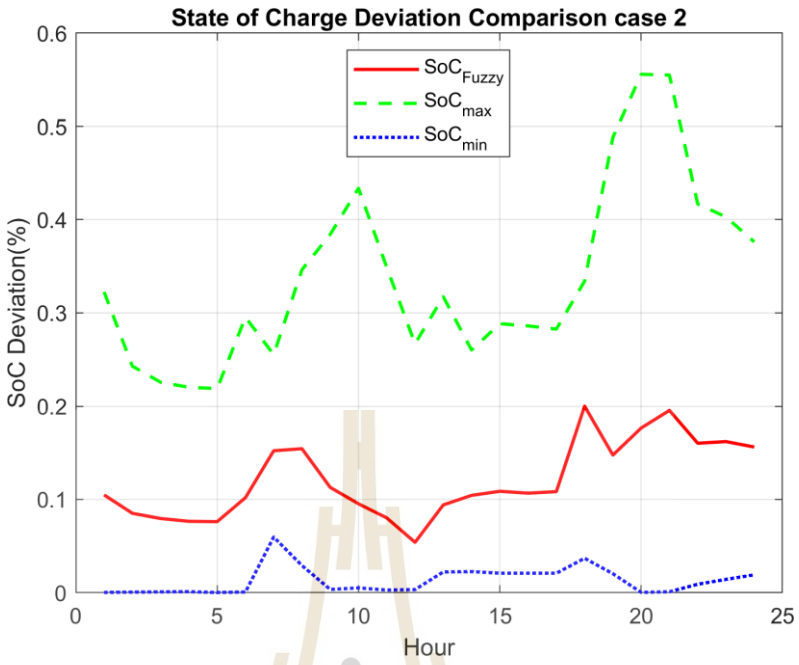

Figure 5.15 Comparison of Maximum, Minimum, and Fuzzy Multi-Objective SoC Deviation scenario 2

Table 5.6 Optimal adjust-exponent values obtained with the fuzzy multi-objective PSO algorithm scenario 2

Hour	Control	Bus	n	Power (MW)	SoC
6	Voltage Deviation	18	20.0000	0.4132	0.4028
		22	0.1000	-0.0004	0.5005
		25	19.9967	0.0000	0.5000
		33	0.1000	0.0020	0.4235
	SoC Deviation	18	1.4877	-0.1358	0.4347
		22	0.1000	0.0000	0.5005
		25	0.1000	0.0000	0.5000
		33	4.1943	-0.1413	0.4639

Table 5.6 Optimal adjust-exponent values obtained with the fuzzy multi-objective PSO algorithm scenario 2 (Continued)

Hour	Control	Bus	n	Power (MW)	SoC
9	Voltage Deviation	18	15.6228	-0.2392	0.5471
		22	0.1000	-0.0012	0.6097
		25	0.1000	-0.0005	0.5002
		33	0.1000	-0.0006	0.4641
	SoC Deviation	18	0.1202	0.0000	0.5471
		22	1.6964	0.1399	0.5297
		25	20.0000	0.0000	0.5002
		33	0.1000	0.0000	0.4641
20	Voltage Deviation	18	19.1362	0.9531	0.2956
		22	0.1000	-0.0007	0.5004
		25	1.4836	0.0016	0.5000
		33	0.2062	0.0036	0.3718
	SoC Deviation	18	8.2757	-0.4225	0.3951
		22	0.1000	0.0000	0.5004
		25	19.4877	0.0000	0.5000
		33	6.0080	-0.1994	0.4287

5.6.1.3 Scenario 3 0.50 MW PV and 0.75 MW wind

From Figure 5.16, Increasing the PV rating to 0.50 MW shifts more of the generation to the middle of the day, creating a noticeable voltage hump between 9:00 and 11:00 AM. Although the evening wind peak is still present, it's now less dominant. Over-voltage conditions first occur at hour 10, reaching a value of 1.0266 p.u. The BESS steps in to absorb this excess energy and later discharges in the late afternoon to bring its SoC back to the target level. The BESS Operation for this scenario at hour 10 is detailed in Figure 5.17. At this moment, the system faces a significant

over-voltage of 1.0237 p.u. due to high solar generation. The controller's multi-objective logic weighs two powerful, conflicting actions: To correct the high voltage, a very strong charging action is required (-1.0313 p.u.). Conversely, to restore the already high initial SoC of 55.73% back towards the 50% target, a strong discharge action is needed (0.9226 p.u.).

The controller balances these opposing demands, resulting in a small net charging action. This nuanced response successfully lowers the voltage to 1.0153 p.u. while preventing severe overcharging of the battery. The right-hand plot starkly illustrates this trade-off: while the voltage control component alone would have driven the SoC to a critical level of 80.00%, the final, balanced action results in an actual SoC of just 58.29%.

Figures 5.18 and 5.19, along with Table 5.7, illustrate how the system operates under these new conditions using PSO. At hour 10, the TVD ranges from a maximum of 0.1258 p.u. to a minimum of 0.0861 p.u., while the fuzzy logic controller produces a well-balanced result of 0.1080 p.u. For SoC, the values span from 0.0213 to 0.3503 p.u., with the fuzzy controller again settling at 0.1093 p.u.

In short, increasing the solar share shifts the primary voltage regulation challenge to midday. However, the fuzzy PSO-based control scheme handles this transition smoothly, staying well within its operational limits.

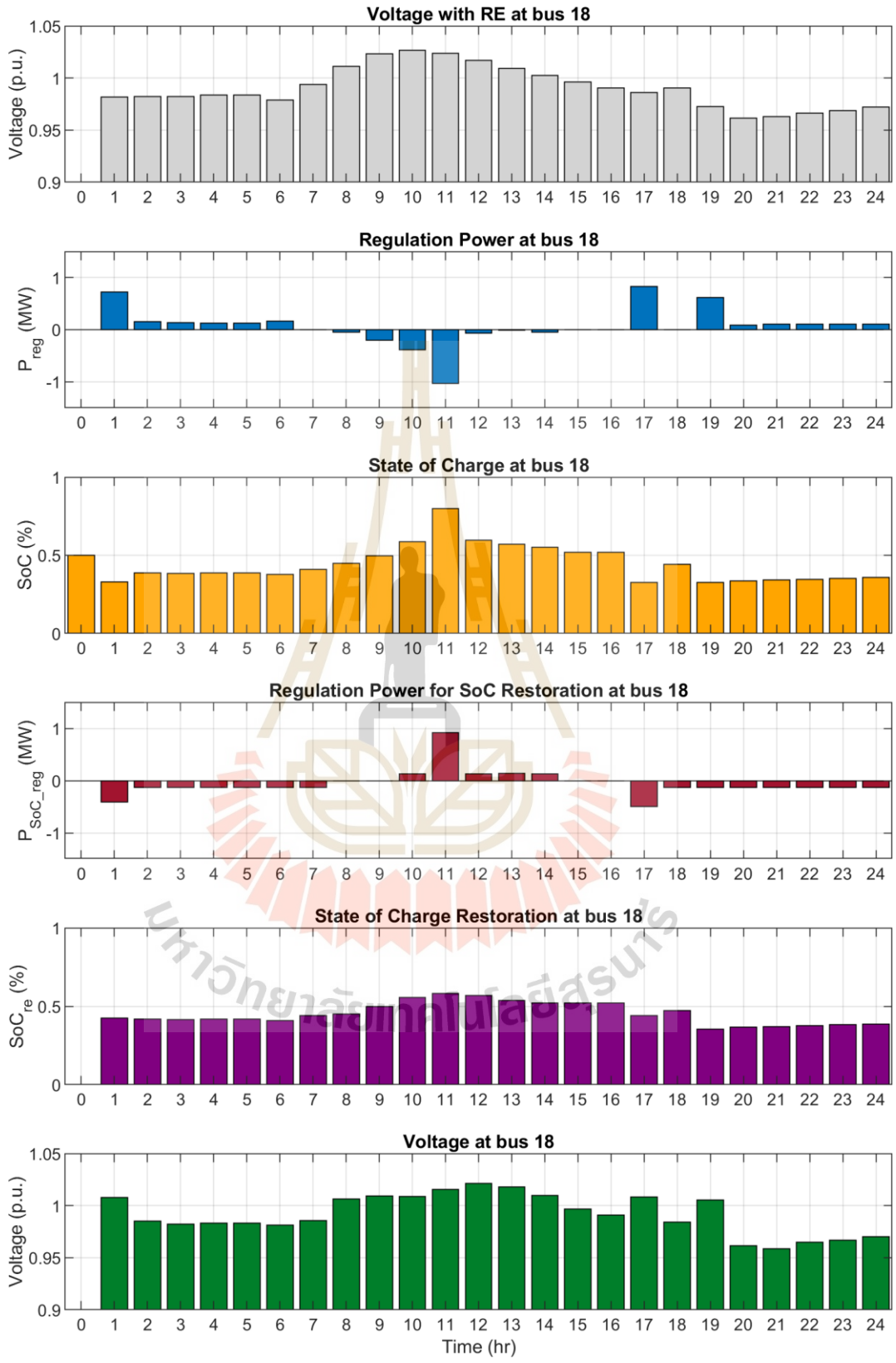

Figure 5.16 Time-Series Profiles of Voltage, Regulation Power and Battery SoC at Bus 18 Scenario 3

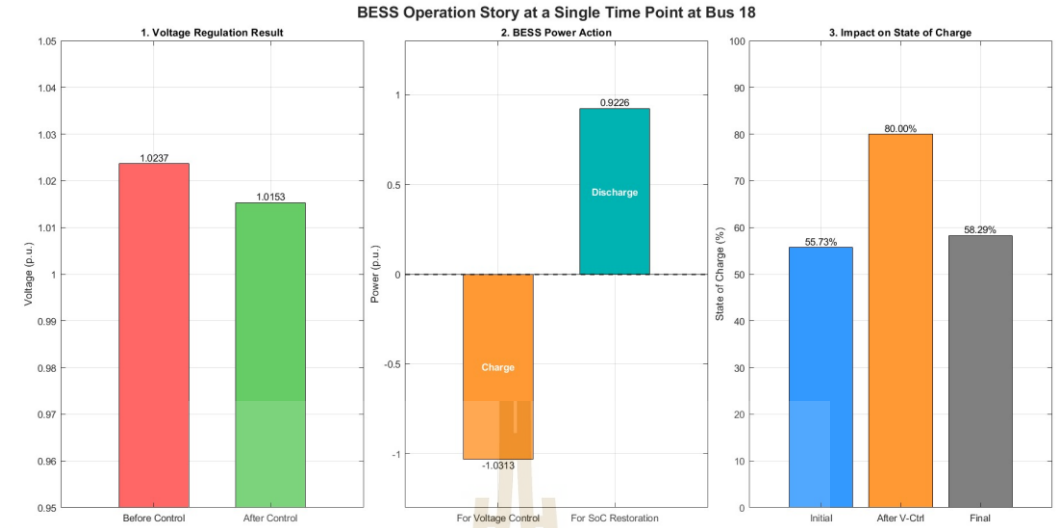

Figure 5.17 Overview of BESS Operation for Voltage Support scenario 3

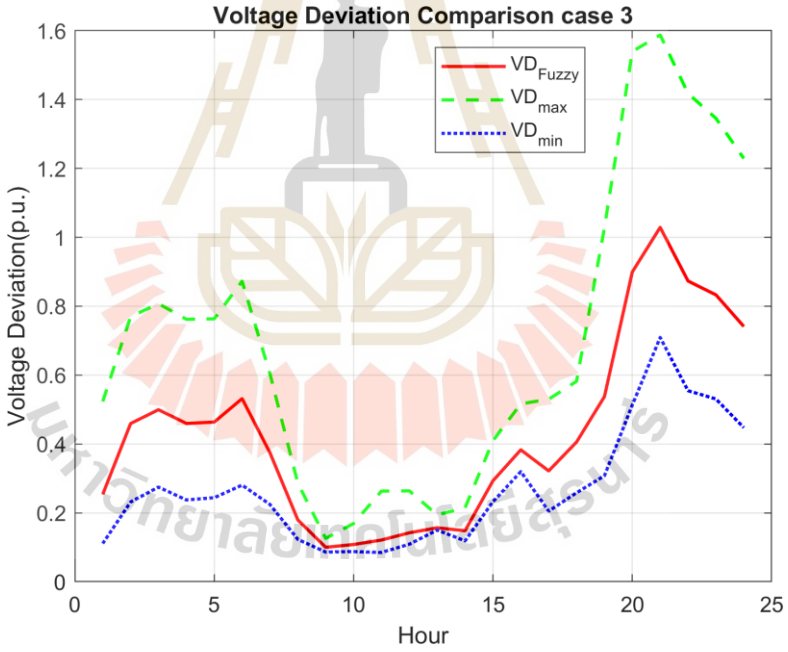

Figure 5.18 Comparison of Maximum, Minimum, and Fuzzy Multi-Objective Voltage Deviation scenario 3

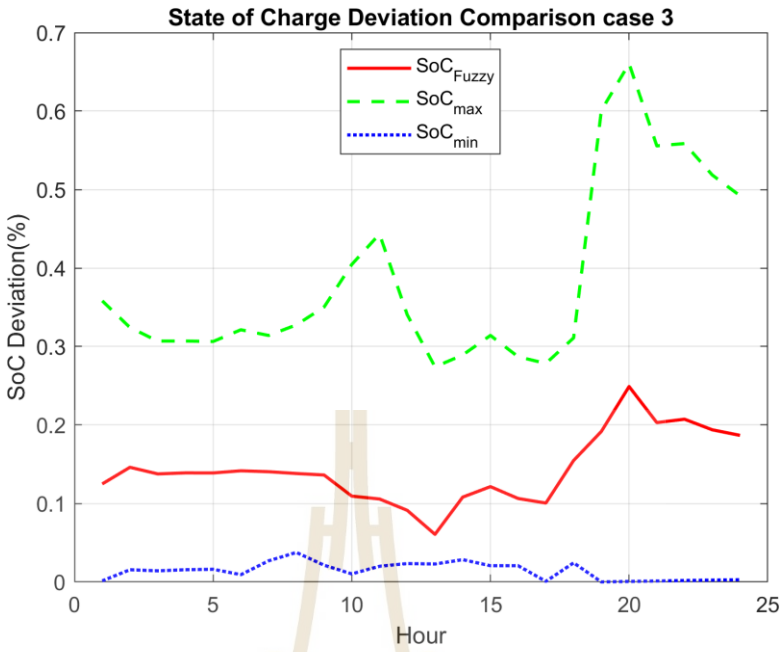

Figure 5.19 Comparison of Maximum, Minimum, and Fuzzy Multi-Objective SoC Deviation scenario 3

Table 5.7 Optimal adjust-exponent values obtained with the fuzzy multi-objective PSO algorithm scenario 3

Hour	Control	Bus	n	Power (MW)	SoC
6	Voltage Deviation	18	20.0000	0.1614	0.3794
		22	0.1000	-0.0002	0.5008
		25	20.0000	0.0000	0.5000
		33	20.0000	0.3470	0.3454
	SoC Deviation	18	0.1000	-0.1277	0.4094
		22	18.2114	0.0000	0.5008
		25	0.1000	0.0000	0.5000
		33	10.6838	-0.3655	0.4498

Table 5.7 Optimal adjust-exponent values obtained with the fuzzy multi-objective PSO algorithm scenario 3 (Continued)

Hour	Control	Bus	n	Power (MW)	SoC
11	Voltage Deviation	18	18.6100	-1.0313	0.8000
		22	17.4886	-0.2413	0.6475
		25	0.1000	-0.0004	0.5004
		33	19.4789	-0.0690	0.4777
	SoC Deviation	18	8.7942	0.9226	0.5829
		22	7.6169	0.2582	0.5000
		25	0.1111	0.0000	0.5004
		33	12.4026	0.0000	0.4777
20	Voltage Deviation	18	20.0000	0.0864	0.3353
		22	0.1000	-0.0003	0.5002
		25	0.1000	0.0016	0.4995
		33	17.2260	0.3607	0.3496
	SoC Deviation	18	0.1000	-0.1283	0.3654
		22	20.0000	0.0000	0.5002
		25	0.1000	0.0000	0.4995
		33	0.1000	-0.1281	0.3862

5.6.1.4 Scenario 4 0.75 MW PV and 0.50 MW wind

From figure 5.20 and figure 5.21, When PV generation becomes dominant at 0.75 MW the feeder begins to experience sustained over-voltage for several hours, particularly between 9:00 AM and noon, with the voltage peaking around 1.0281 p.u. To manage this, the BESS is required to charge over a longer period, pushing its SoC closer to the upper limit. Later in the day, the system discharges to restore the SoC to its reference level.

Figures 5.22 and 5.23, along with Table 5.8, present the system's performance under these conditions, optimized using PSO. At the most critical time, hour 10, the TVD ranges from a maximum of 0.1289 p.u. to a minimum of 0.0859 p.u., while the fuzzy controller achieves a balanced value of 0.1019 p.u. The SoC varies between 0.0002 and 0.3734 p.u., with the fuzzy solution settling at 0.1388 p.u.

Even with the heavier PV loading, the controller effectively limits the voltage rise and ensures that no single battery becomes fully saturated, demonstrating the robustness of the fuzzy PSO-based approach.

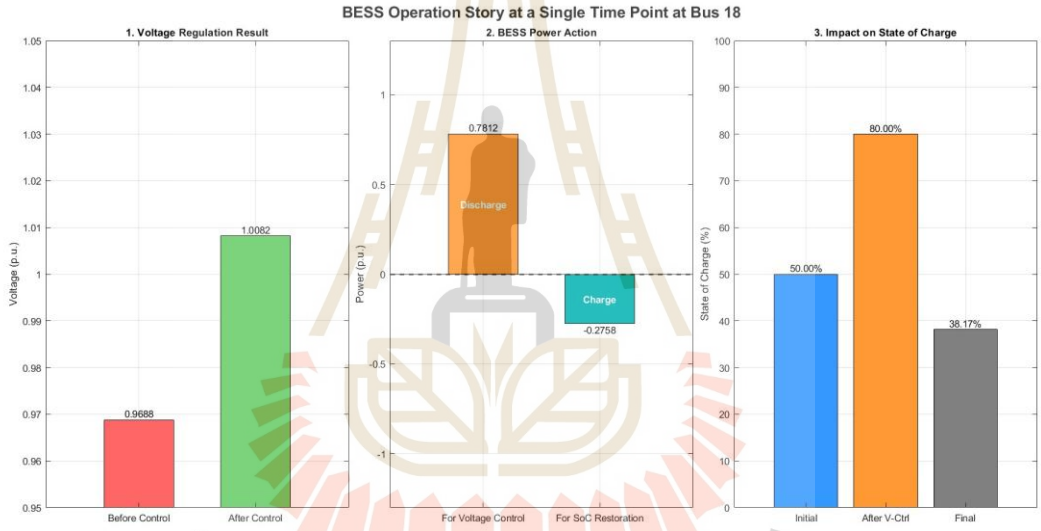

Figure 5.20 Overview of BESS Operation for Voltage Support Scenario 4

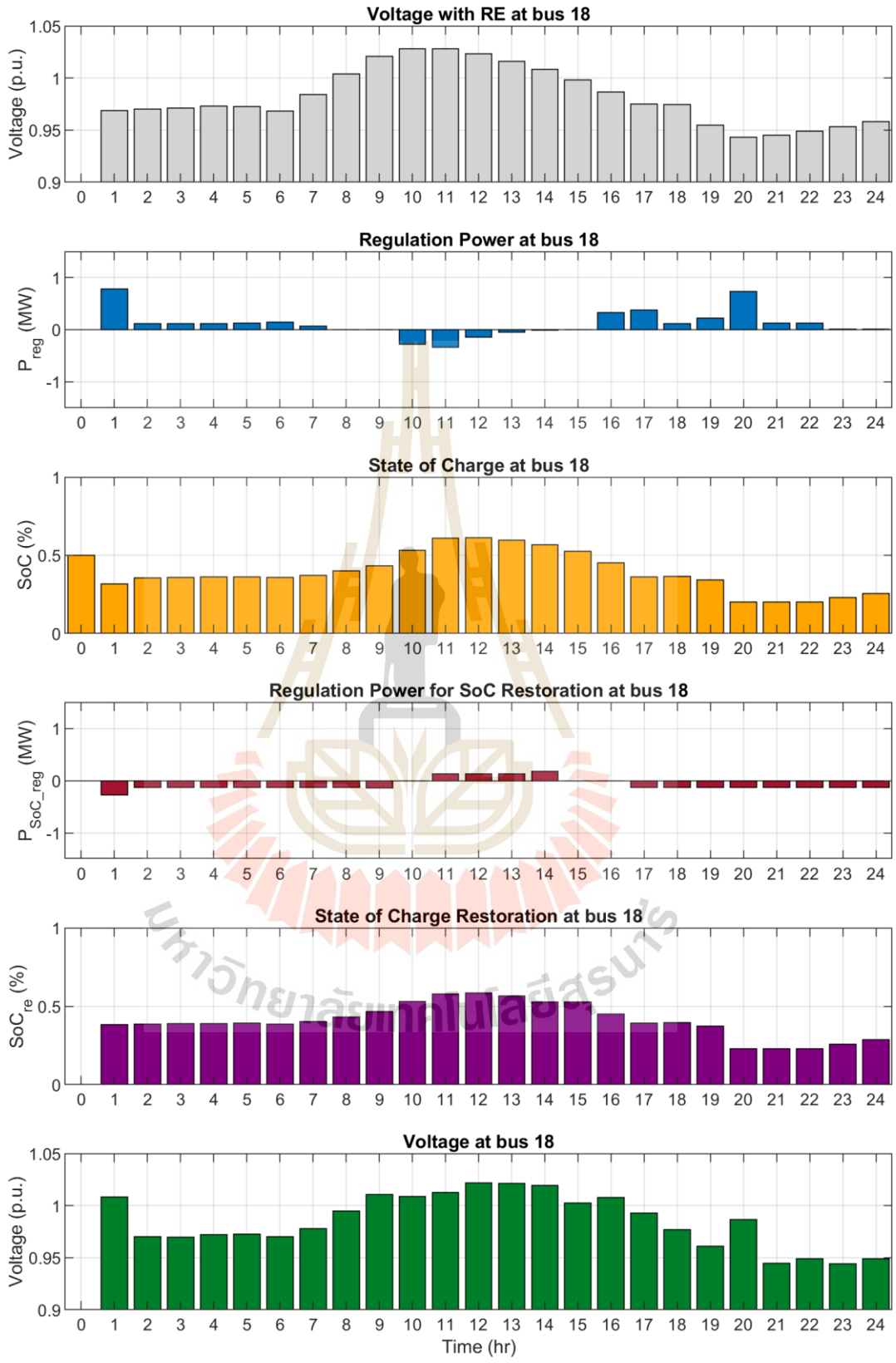

Figure 5.21 Time-Series Profiles of Voltage, Regulation Power and Battery SoC at Bus 18 Scenario 4

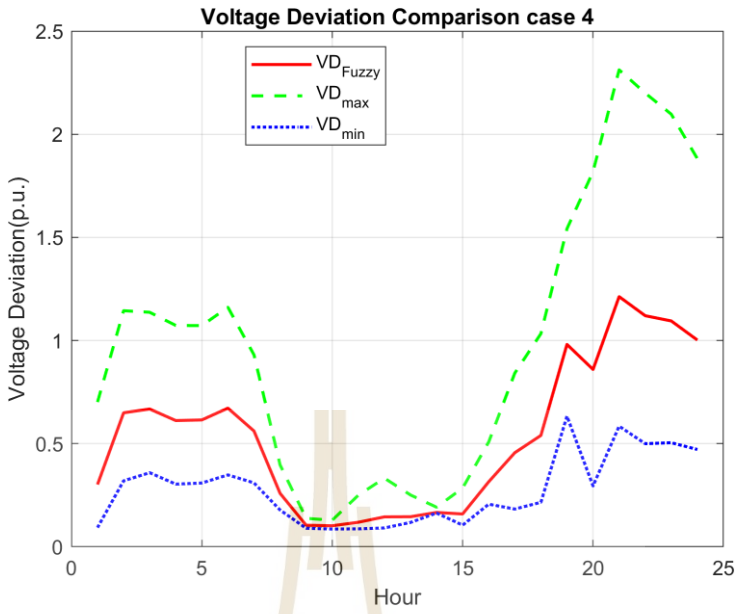

Figure 5.22 Comparison of Maximum, Minimum, and Fuzzy Multi-Objective Voltage Deviation scenario 4

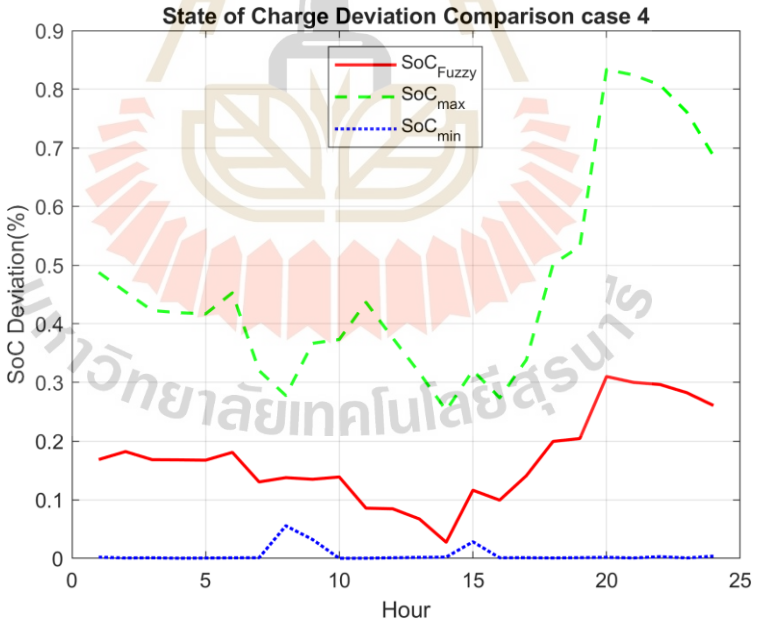

Figure 5.23 Comparison of Maximum, Minimum, and Fuzzy Multi-Objective SoC Deviation scenario 4

Table 5.8 Optimal adjust-exponent values obtained with the fuzzy multi-objective PSO algorithm scenario 4

Hour	Control	Bus	n	Power (MW)	SoC
6	Voltage Deviation	18	20.0000	0.1473	0.3571
		22	0.1000	0.0000	0.5000
		25	0.1000	0.0012	0.4991
		33	15.9882	0.1572	0.3965
	SoC Deviation	18	0.1000	-0.1280	0.3872
		22	0.2599	0.0000	0.5000
		25	20.0000	0.0000	0.4991
		33	0.1000	-0.1275	0.4329
10	Voltage Deviation	18	17.2894	-0.2783	0.5312
		22	19.5058	-0.4024	0.8000
		25	0.1000	-0.0006	0.5002
		33	0.1000	-0.0008	0.4696
	SoC Deviation	18	0.1000	0.0000	0.5312
		22	4.7576	0.3902	0.5771
		25	20.0000	0.0000	0.5002
		33	1.9742	0.0000	0.4696
21	Voltage Deviation	18	4.0004	0.1300	0.2000
		22	7.3837	0.0000	0.5007
		25	0.1000	0.0020	0.4983
		33	14.8233	0.9138	0.2000
	SoC Deviation	18	0.1000	-0.1300	0.2306
		22	14.1961	0.0000	0.5007
		25	16.4983	0.0000	0.4983
		33	8.9480	-0.9507	0.4716

5.6.1.5 Scenario 5MW PV and 0.25 MW wind

From figure 5.24 and 5.25, With 1.00 MW of PV and only a small contribution from wind (0.25 MW), renewable generation becomes heavily concentrated around midday. As a result, the feeder voltage rises above 1.0 p.u. as early as 9:00 AM and peaks around 1.0321 p.u. near solar noon. Since wind generation in the evening is minimal, the BESS mainly discharges after 4:00 PM to bring its SoC back into balance.

Figures 5.26 to 5.27 and Table 5.9 present the system's behavior and optimization results using PSO. At hour 11, which is representative of peak solar input, the TVD ranges from a maximum of 0.1184 p.u. to a minimum of 0.0821 p.u., while the fuzzy controller achieves a more moderate value of 0.0965 p.u. The SoC varies from 0.0156 to 0.3721 p.u., with the fuzzy solution settling at 0.1575 p.u.

These results confirm that the BESS fleet can still handle a PV-dominated generation profile, though it comes at the cost of more intense cycling during midday hours.

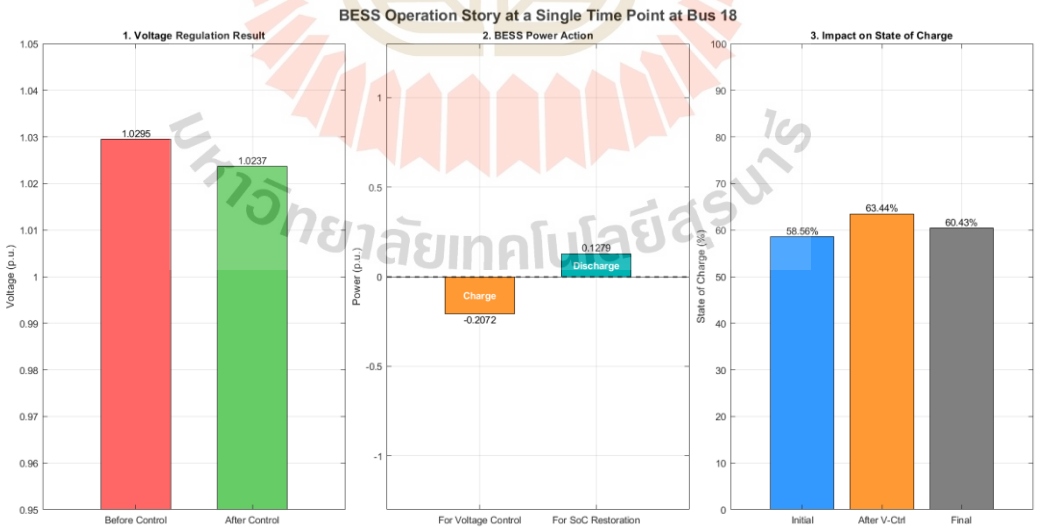

Figure 5.24 Overview of BESS Operation for Voltage Support Scenario 5

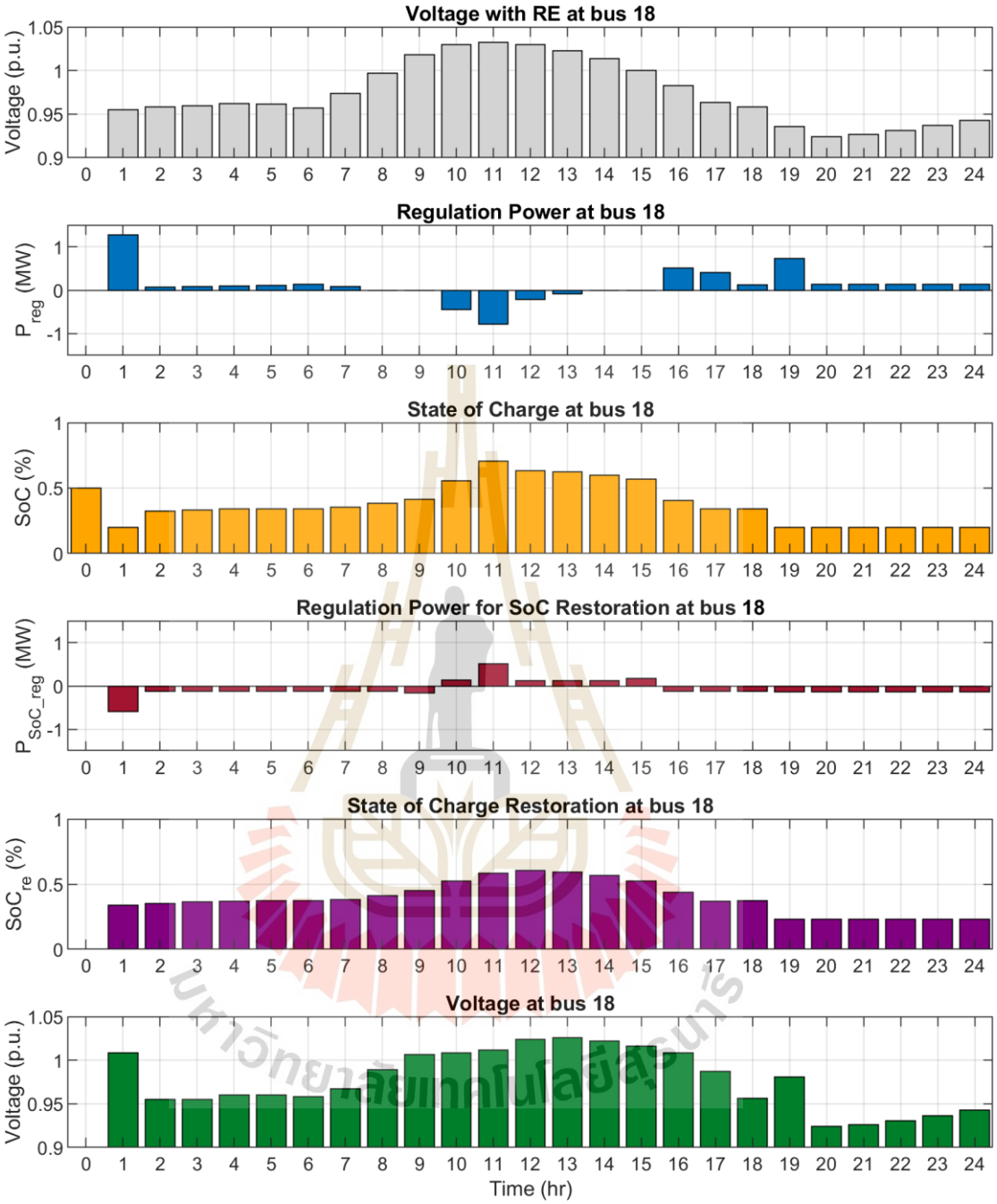

Figure 5.25 Time-Series Profiles of Voltage, Regulation Power and Battery SoC at Bus 18 Scenario 5

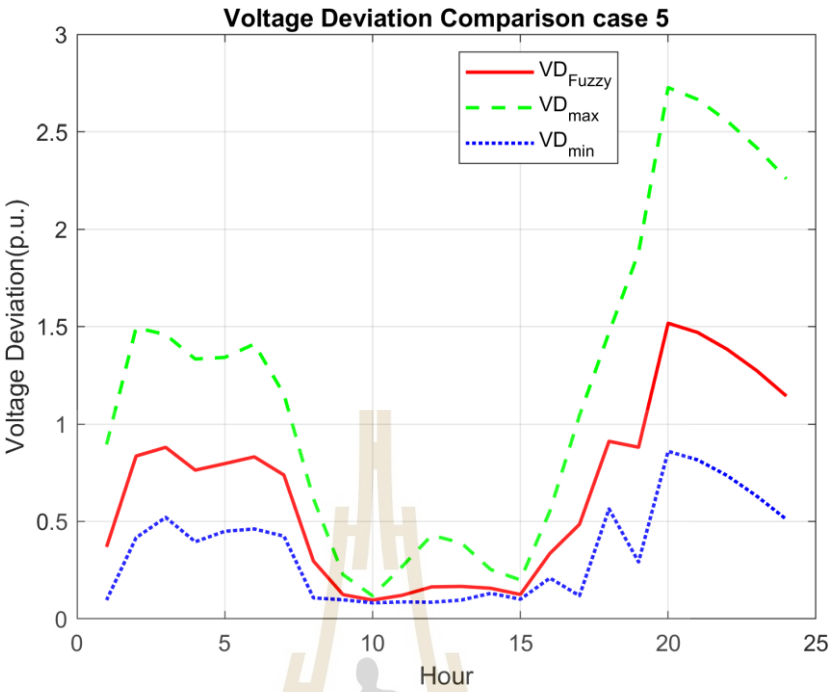

Figure 5.26 Comparison of Maximum, Minimum, and Fuzzy Multi-Objective Voltage Deviation scenario 5

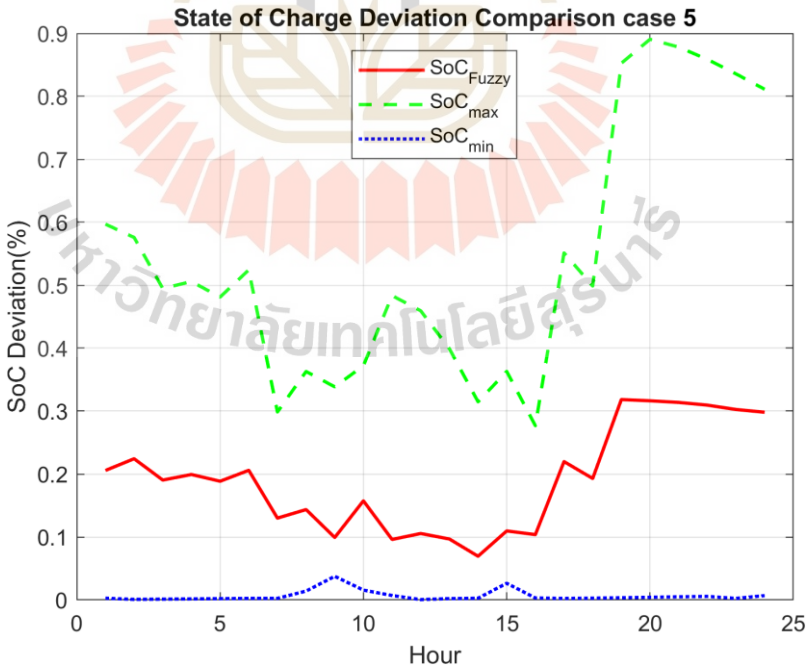

Figure 5.27 Comparison of Maximum, Minimum, and Fuzzy Multi-Objective SoC Deviation scenario 5

Table 5.9 Optimal adjust-exponent values obtained with the fuzzy multi-objective PSO algorithm scenario 5

Hour	Control	Bus	n	Power (MW)	SoC
3	Voltage Deviation	18	20.0000	0.0849	0.3326
		22	0.1000	0.0000	0.5000
		25	0.1000	0.0014	0.4987
		33	10.8639	0.0430	0.4117
	SoC Deviation	18	0.1000	-0.1283	0.3628
		22	19.9287	0.0000	0.5000
		25	20.0000	0.0000	0.4987
		33	0.1000	-0.1273	0.4481
10	Voltage Deviation	18	19.8917	-0.4420	0.5556
		22	20.0000	-0.4937	0.7830
		25	0.1000	-0.0006	0.5002
		33	0.1000	-0.0009	0.4503
	SoC Deviation	18	20.0000	0.1414	0.5223
		22	4.5422	0.3461	0.5852
		25	0.1000	0.0000	0.5002
		33	19.6330	0.0000	0.4503
19	Voltage Deviation	18	20.0000	0.7256	0.2000
		22	4.9004	0.0000	0.5024
		25	0.1000	0.0023	0.4989
		33	0.1162	0.8371	0.2000
	SoC Deviation	18	0.1000	-0.1300	0.2306
		22	15.9159	0.0000	0.5024
		25	0.1206	0.0000	0.4989
		33	8.6168	-0.8910	0.4546

5.6.1.6 Scenario 6 PV only: 1.25 MW PV, no wind installed

From figure 5.28 and 5.29, In the PV-only scenario, the entire 1.25 MW of renewable output is concentrated during daylight hours, resulting in a single, broad over-voltage plateau between 9:00 AM and 2:00 PM, peaking at around 1.0363 p.u. During this period, all BESS units charge aggressively, driving their SoC close to the upper limit. A staged discharge follows in the late afternoon, gradually bringing each battery back to around 0.50 by sunset.

Figures 5.30 to 5.31 and Table 5.10 present the system's response under this condition, optimized using PSO. At peak hour 11 the TVD ranges from a maximum of 0.2729 p.u. to a minimum of 0.0816 p.u., with the fuzzy controller achieving a more balanced result of 0.1128 p.u. SoC values vary from 0.0033 to 0.4279 p.u., and the fuzzy solution settles at 0.0724 p.u.

Despite the intense midday stress, the fuzzy multi-objective PSO controller is able to maintain voltages within acceptable limits for most of the day. However, slight under-voltage is observed during hours 20 and 21, likely due to the limited BESS capacity being unable to support voltage at those late hours. Even so, the controller successfully prevents long-term SoC drift, highlighting the resilience of the control strategy even in a scenario powered entirely by solar energy.

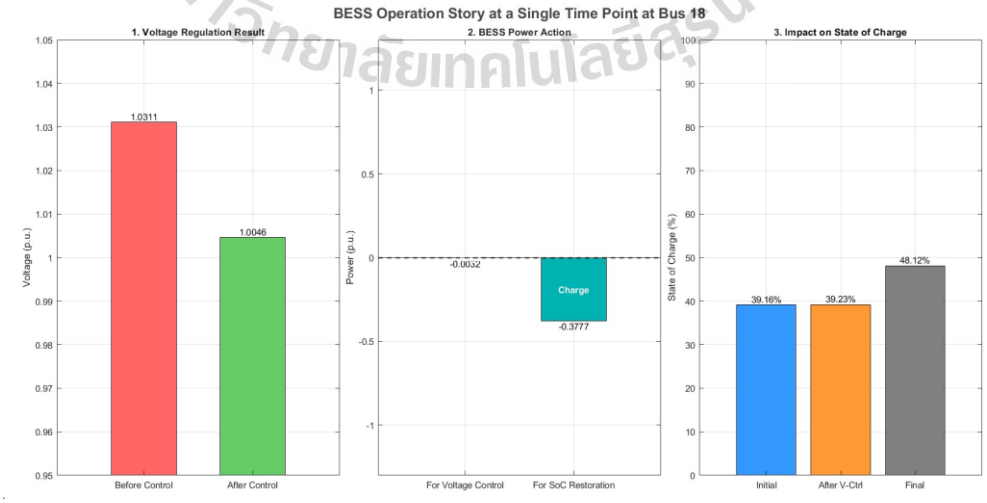

Figure 5.28 Overview of BESS Operation for Voltage Support Scenario 6

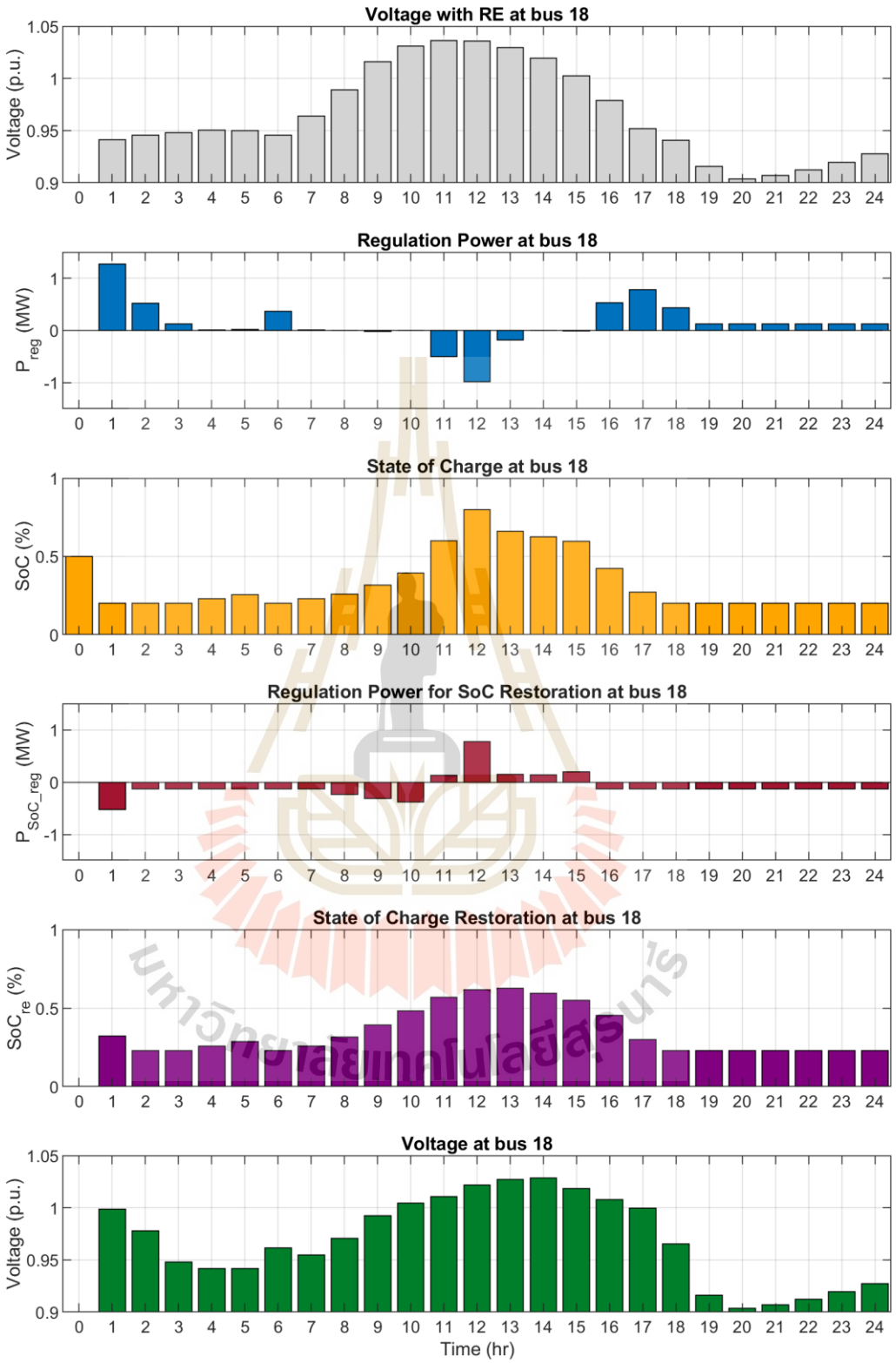

Figure 5.29 Time-Series Profiles of Voltage, Regulation Power and Battery SoC at Bus 18 Scenario 6

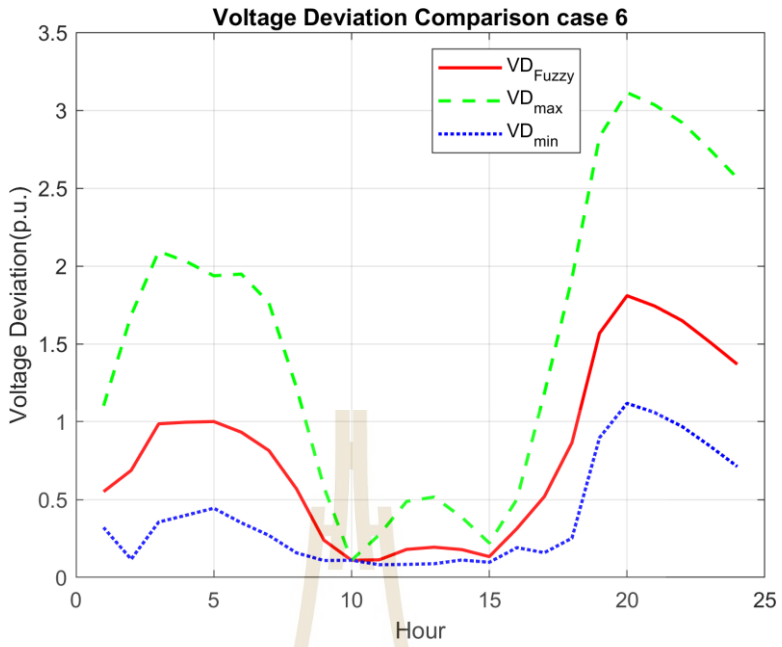

Figure 5.30 Comparison of Maximum, Minimum, and Fuzzy Multi-Objective Voltage Deviation scenario 6

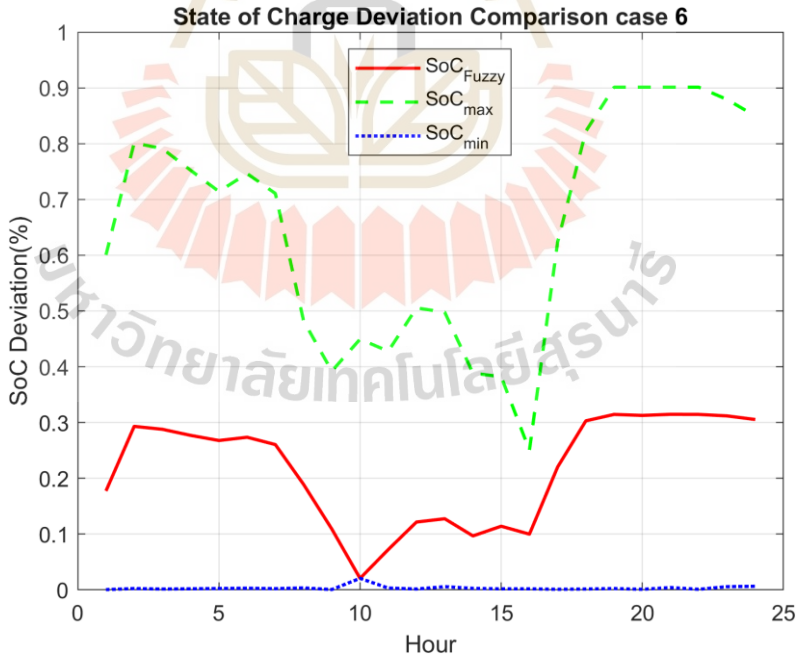

Figure 5.31 Comparison of Maximum, Minimum, and Fuzzy Multi-Objective SoC Deviation scenario 6

Table 5.10 Optimal adjust-exponent values obtained with the fuzzy multi-objective PSO algorithm scenario 6

Hour	Control	Bus	n	Power (MW)	SoC
3	Voltage Deviation	18	0.6991	0.1300	0.2000
		22	20.0000	0.0000	0.5000
		25	0.1000	0.0017	0.4984
		33	12.7077	0.1534	0.4335
	SoC Deviation	18	0.1000	-0.1300	0.2306
		22	18.1804	0.0000	0.5000
		25	0.1000	0.0000	0.4984
		33	19.6737	-0.1736	0.4831
10	Voltage Deviation	18	0.1000	-0.0032	0.3923
		22	0.1000	-0.0013	0.5014
		25	0.1000	-0.0007	0.5002
		33	0.1000	-0.0010	0.5003
	SoC Deviation	18	20.0000	-0.3777	0.4812
		22	2.4770	0.0000	0.5014
		25	19.9587	0.0000	0.5002
		33	0.1000	0.0000	0.5003
19	Voltage Deviation	18	20.0000	0.1300	0.2000
		22	0.4581	0.0000	0.5011
		25	0.1000	0.0028	0.4986
		33	13.4846	0.9379	0.2000
	SoC Deviation	18	0.1000	-0.1300	0.2306
		22	9.3085	0.0000	0.5011
		25	0.1000	0.0000	0.4986
		33	8.6705	-0.9005	0.4573

5.6.2 modified IEEE 69-bus with PV and wind power penetration and BESS considering SoC restoration results

In this case five scenarios considered, in which RE sources with a total capacity of 1.00 MW were installed at buses 27, 35, 46, 50, 52, 65, 67, and 69 and BESS with capacities of 1.75 MW, 0.5 MW, 0.75 MW, 2.75 MW, 0.25 MW, 5.75 MW, 0.25 MW, and 0.25 MW, respectively. The scenarios are as follows:

- Scenario 1 Wind power only: 1.00 MW wind, no PV installed
- Scenario 2 0.25 MW PV and 1.00 MW wind
- Scenario 3 0.50 MW PV and 0.75 MW wind
- Scenario 4 0.75 MW PV and 0.50 MW wind
- Scenario 5 PV only: 1.00 MW PV, no wind installed

The IEEE 69-bus system is a standard benchmark for distribution network studies, featuring 69 buses at a base voltage of 12.66 kV, with total loads of 3,801 kW and 2,694 kVAR, and a base apparent power of 10 MVA. Its minimum voltage is 0.9097 pu at bus 54, highlighting voltage drop issues. Compared to the IEEE 33-bus system, it is larger and more complex, making it ideal for testing advanced control strategies like BESS.

The results in Tables 5.11 and 5.12 show that the Fuzzy Multi-objective PSO algorithm effectively balances TVD and TSoC. Its fuzzy multi-objective PSO controller simultaneously handles system uncertainties and optimizes for multiple objectives, ensuring a balanced and adaptive response. This leads to better voltage regulation and BESS utilization, maintaining both voltage stability and SoC.

Figures 3.32 to 3.36 show how the BESS manages voltage control under different scenarios. The BESS absorbs excess energy during high solar or high wind output to prevent overvoltage and discharges during low renewable periods to support voltage levels. These results demonstrate that, with the proposed algorithm, the BESS effectively regulates voltage and improves distribution system reliability an essential function for modern grids with high renewable integration.

Table 5.11 The Maximum, Minimum, and Fuzzy Multi-Objective of Voltage Deviation

Scenarios	Minimum TVD	Fuzzy TVD	Maximum TVD
Scenario 1 Wind power only: 1.00 MW wind, no PV installed	0.4704	0.4997	0.6334
Scenario 2 0.25 MW PV and 1.00 MW wind	0.5705	0.5949	0.7395
Scenario 3 0.50 MW PV and 0.75 MW wind	0.6766	0.7043	0.8492
Scenario 4 0.75 MW PV and 0.50 MW wind	0.7792	0.8141	1.0094
Scenario 5 PV only: 1.00 MW PV, no wind installed	0.8979	0.9285	1.0874

Table 5.12 The Maximum, Minimum, and Fuzzy Multi-Objective of SoC Deviation

Scenarios	Minimum TSoC	Fuzzy TSoC	Maximum TSoC
Scenario 1 Wind power only: 1.00 MW wind, no PV installed	0.0827	0.3873	1.7769
Scenario 2 0.25 MW PV and 1.00 MW wind	0.1183	0.3563	1.7613
Scenario 3 0.50 MW PV and 0.75 MW wind	0.0904	0.3719	1.8434
Scenario 4 0.75 MW PV and 0.50 MW wind	0.0886	0.3486	1.8023
Scenario 5 PV only: 1.00 MW PV, no wind installed	0.0514	0.3379	1.8232

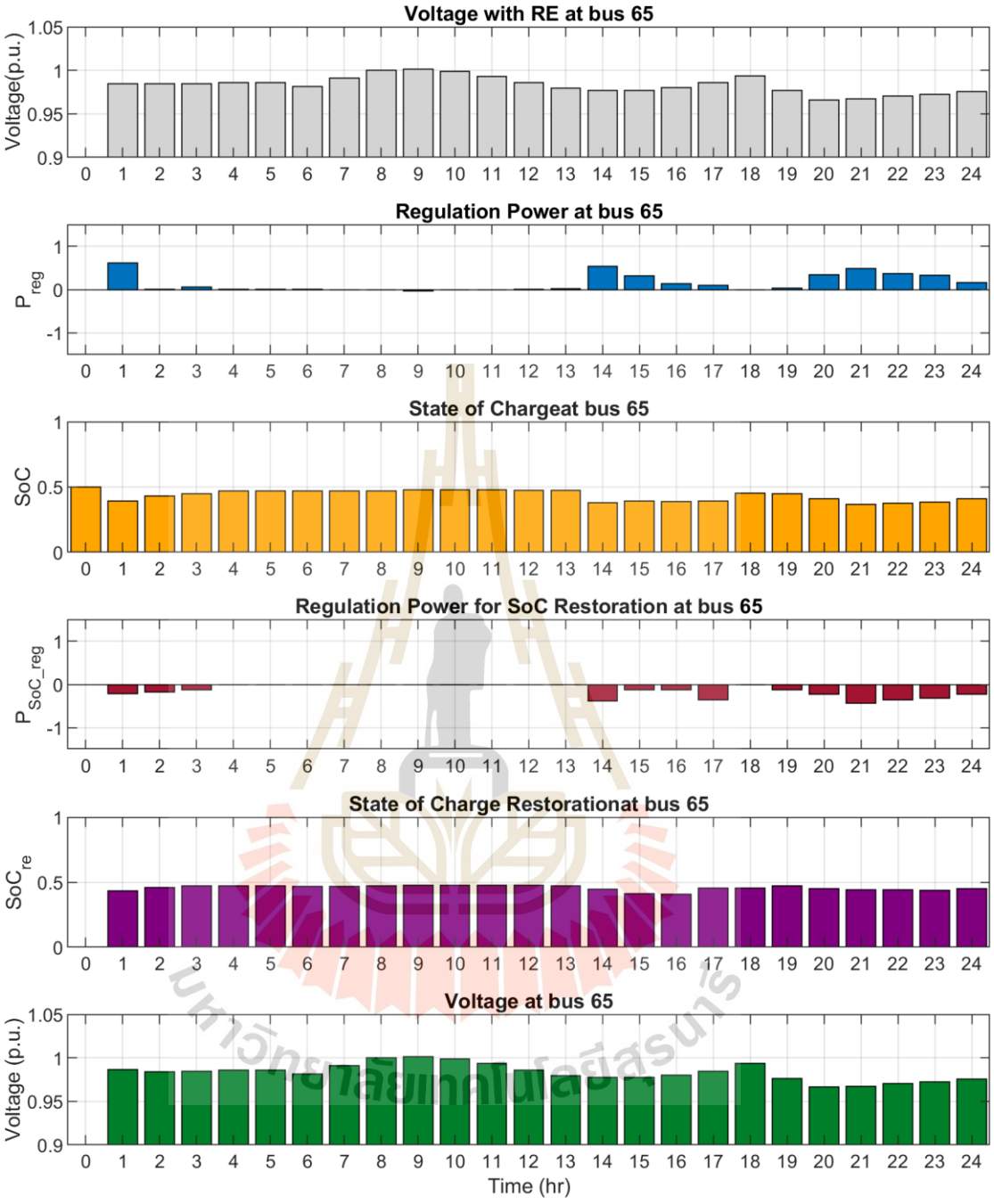

Figure 5.32 Time-Series Profiles of Voltage, Regulation Power and Battery SoC at Bus 65 Scenario 1

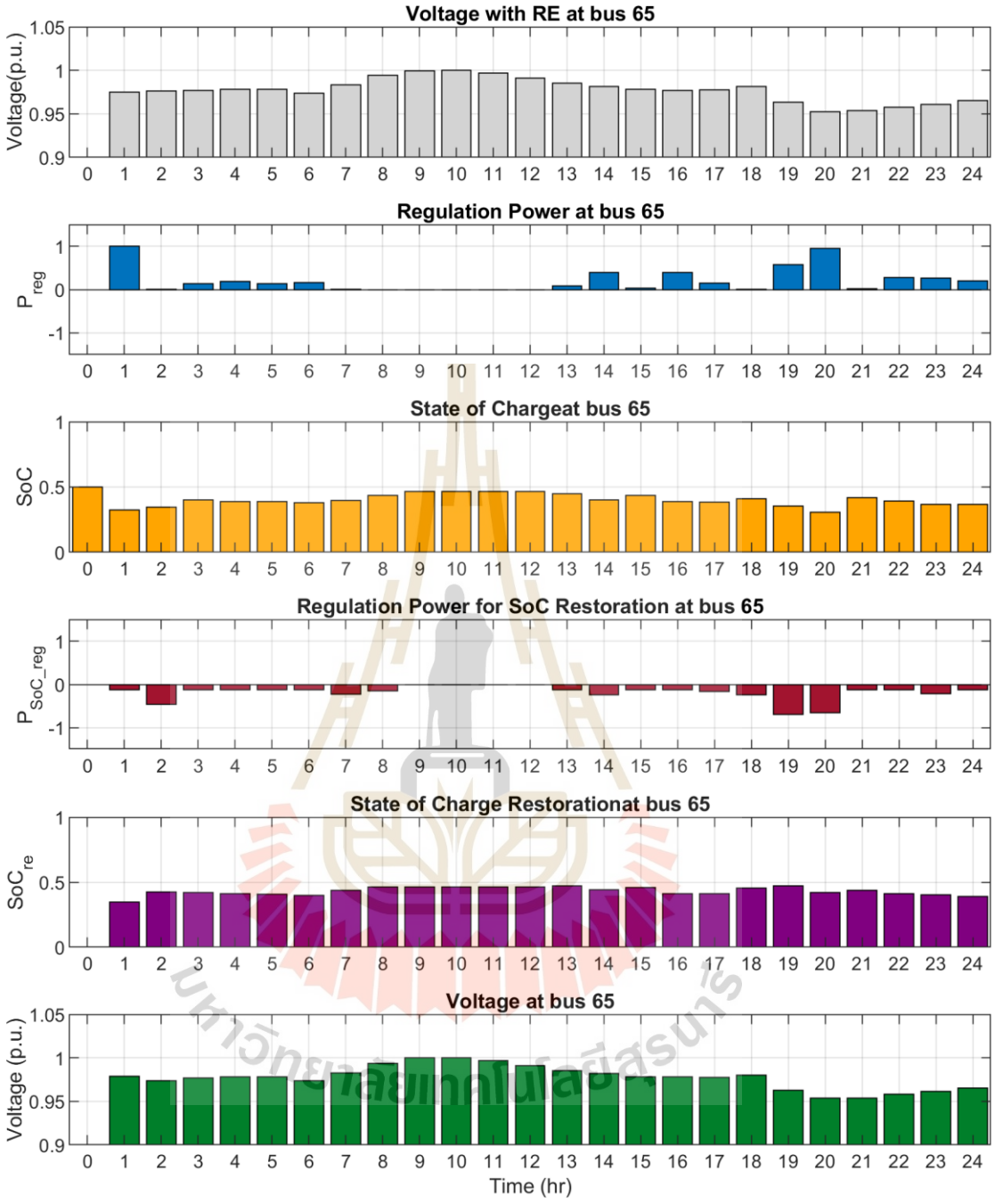

Figure 5.33 Time-Series Profiles of Voltage, Regulation Power and Battery SoC at Bus 65 Scenario 2

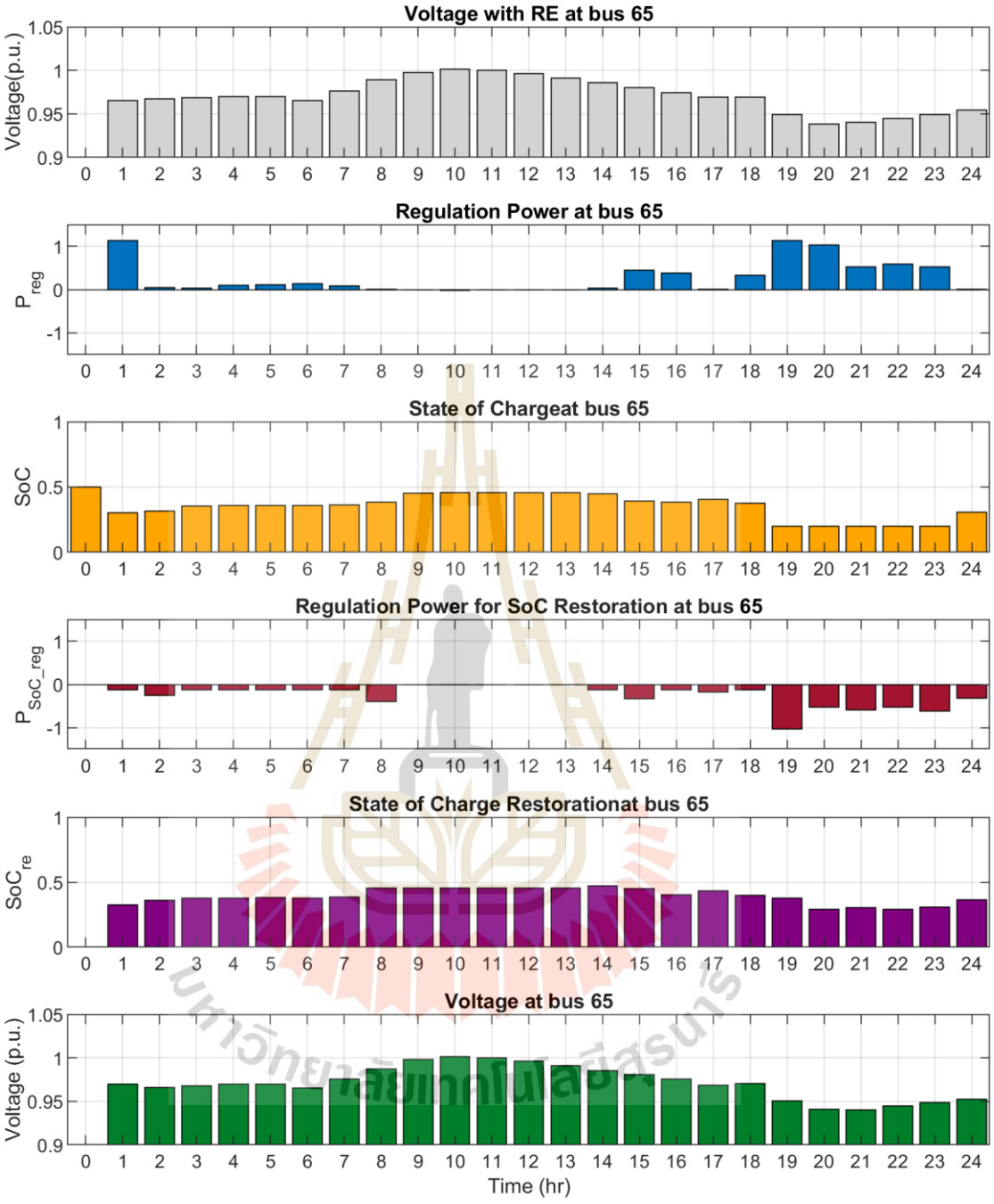

Figure 5.34 Time-Series Profiles of Voltage, Regulation Power and Battery SoC at Bus 65 Scenario 3

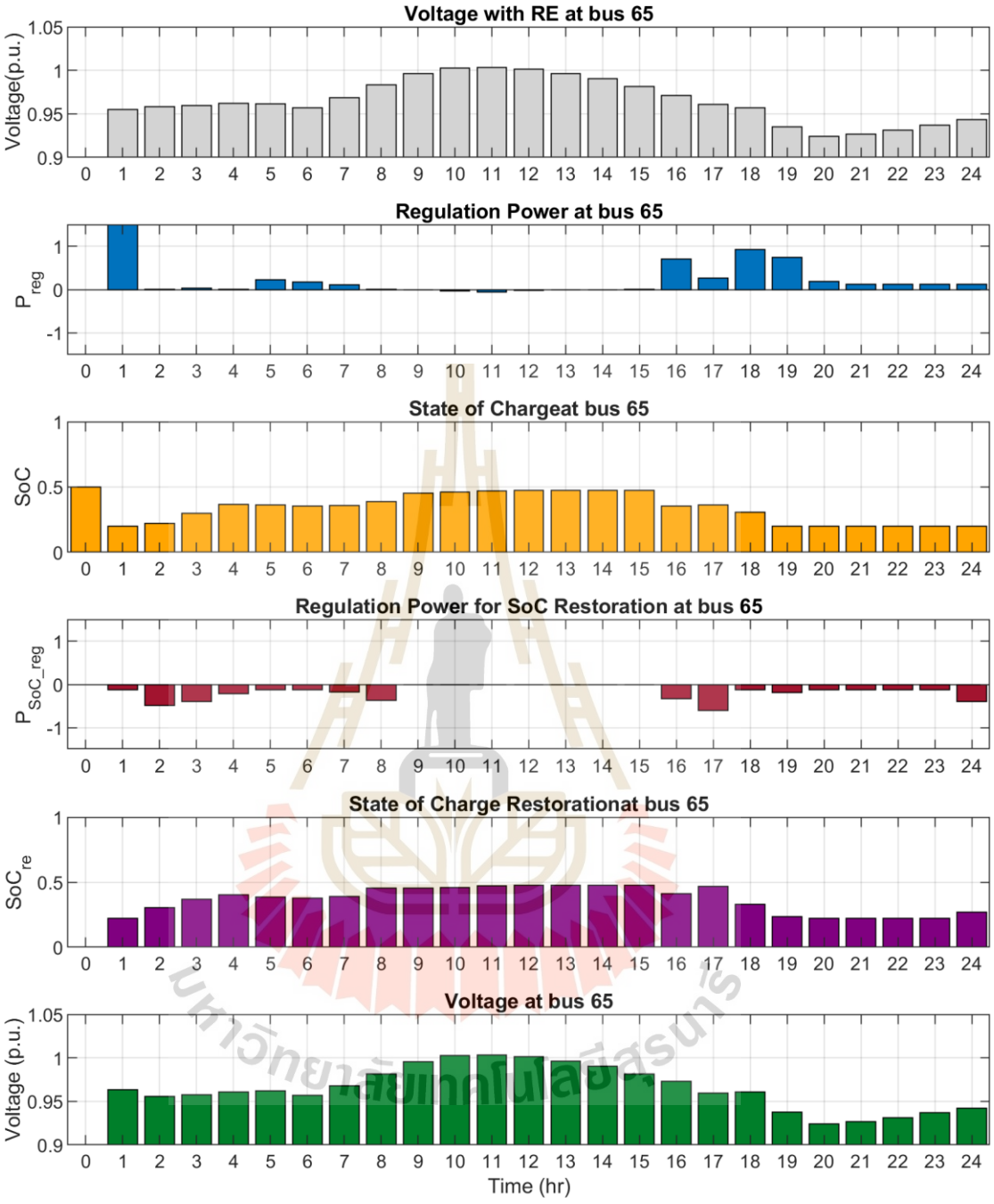

Figure 5.35 Time-Series Profiles of Voltage, Regulation Power and Battery SoC at Bus 65 Scenario 4

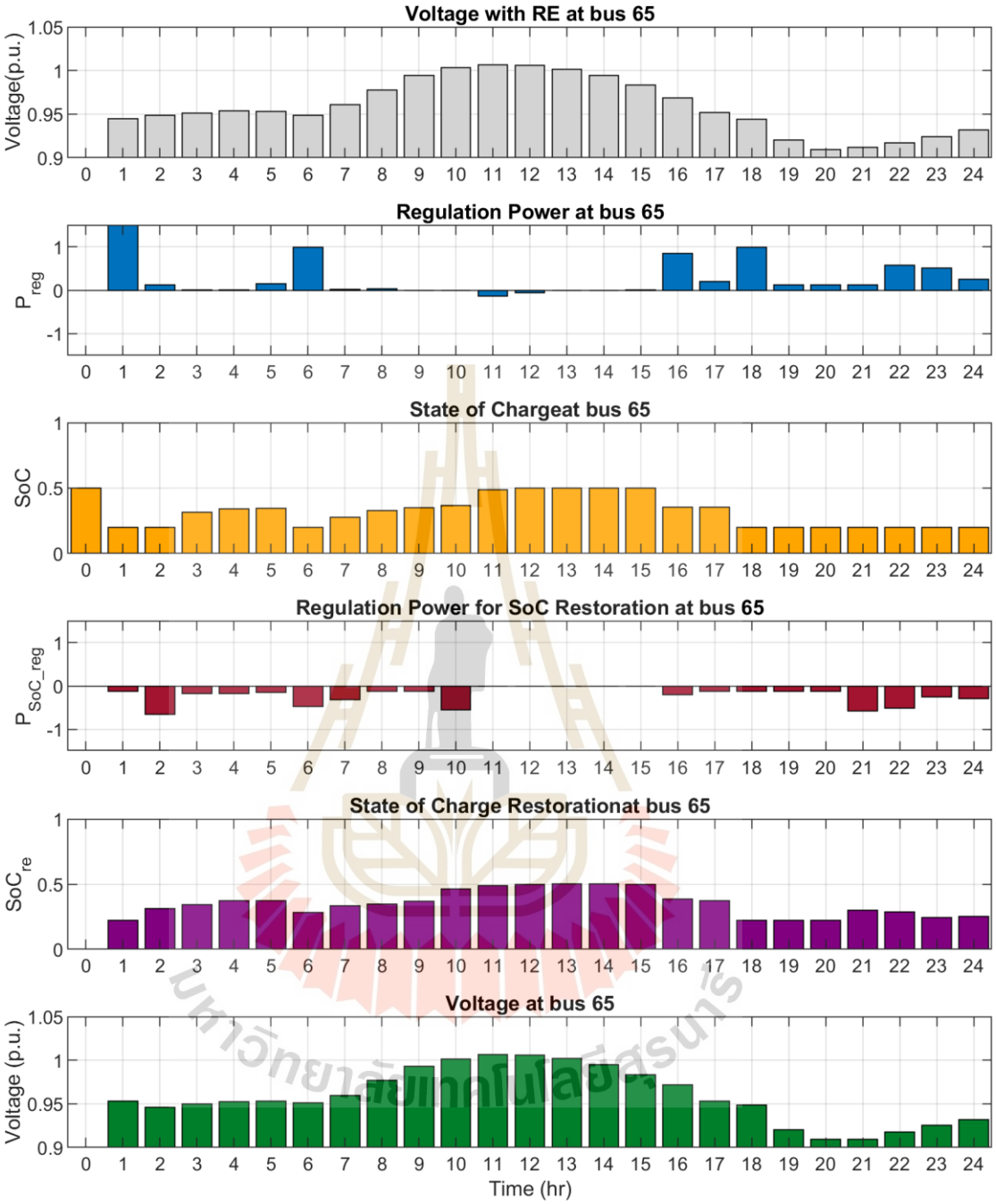

Figure 5.36 Time-Series Profiles of Voltage, Regulation Power and Battery SoC at Bus 65 Scenario 5

5.7 Chapter Summary

This chapter builds upon the previous chapter by introducing a more advanced control strategy for BESS that simultaneously manages voltage deviation and the battery's SoC. A key focus is the implementation of a SoC restoration mechanism, which ensures the BESS maintains an optimal charge level to guarantee its continuous availability for voltage regulation.

To address the competing objectives of minimizing TVD and TSoC, FMOO based on PSO was developed. This approach allows for a balanced trade-off between grid support and battery health. The methodology was rigorously tested on both the IEEE 33-bus and IEEE 69-bus systems under various scenarios with different combinations of PV and wind energy penetration.

The results consistently demonstrated the effectiveness of the FMOO-PSO controller. In all scenarios, the system successfully mitigated over-voltage during periods of high renewable generation and corrected under-voltage during low generation, while simultaneously guiding the SoC of the batteries back towards their nominal levels. The fuzzy multi-objective approach proved superior to single-objective optimization by finding a balanced solution that prevents excessive deviation in either voltage or SoC, thereby enhancing the overall reliability and resilience of the distribution network.

CHAPTER VI

CONCLUSION

This research developed and validated a comprehensive framework to enhance voltage stability in distribution networks with high renewable energy penetration. It began by refining the L-index method to efficiently identify weak buses prone to voltage instability, which helped guide the strategic placement of BESS.

Next, an adaptive voltage-droop control scheme was designed for BESS, where the droop parameters dynamically adjust based on the battery's SoC. Using PSO, the controller reduced voltage deviation and significantly cut power oscillations in the batteries.

To ensure long-term battery health alongside grid support, a FMOO layer was incorporated. This balanced minimizing voltage deviations with restoring SoC, successfully keeping battery charge within initial levels while voltage profiles improved when compared to only renewable energy.

While the study focused on steady-state analysis and used simplified battery aging models, it showed practical benefits by targeting only critical buses, avoiding unnecessary BESS deployment, and enabling implementation on commercial power converters.

In conclusion, this research demonstrates that integrating L-index-based siting, PSO-optimized adaptive droop control, and SoC-aware multi-objective dispatch provides an effective and practical solution to voltage stability challenges in renewable-rich distribution systems.

A key practical application of this integrated framework lies in its direct applicability to the day-ahead operational planning of BESS, transforming grid management from a purely reactive to a proactive and predictive model. By utilizing

day-ahead forecasts for renewable generation and load demand, grid operators can employ the developed tools to formulate an optimized 24-hour operational schedule. In essence, this work provides not just a solution for voltage stability, but a comprehensive scheduling methodology that enhances grid reliability while ensuring the operational and economic viability of energy storage assets in modern power systems.

REFERENCE

Adnan, A. Z., Yusoff, M. E., & Hashim, H. (2018, 08/01). Analysis on the Impact of Renewable Energy to Power System Fault Level. *Indonesian Journal of Electrical Engineering and Computer Science, 11*, 652-657. https://doi.org/10.11591/ijeecs.v11.i2.pp652-657

Alam, M. J. E., Muttaqi, K. M., & Sutanto, D. (2013). Mitigation of Rooftop Solar PV Impacts and Evening Peak Support by Managing Available Capacity of Distributed Energy Storage Systems. *IEEE Transactions on Power Systems, 28*(4), 3874-3884. https://doi.org/10.1109/TPWRS.2013.2259269

Chen, X., Wang, L., Sun, H., & Chen, Y. (2017). Fuzzy Logic Based Adaptive Droop Control in Multiterminal HVDC for Wind Power Integration. *IEEE Transactions on Energy Conversion, 32*(3), 1200-1208. https://doi.org/10.1109/TEC.2017.2697967

Danish, M. S., Senjyu, T., Danish, S. M., Sabory, N. R., K, N., & Mandal, P. (2019). A Recap of Voltage Stability Indices in the Past Three Decades. *Energies, 12*(8).

Ding, X., Chen, X., Cao, F., & Wang, B. (2024, 05/07). Multi-time-scale voltage control of the distribution network with energy storage equipped soft open points. *Frontiers in Energy Research, 12*. https://doi.org/10.3389/fenrg.2024.1374704

Dondariya, C., & Sakravdia, D. K. (2021, 10-11 Dec. 2021). Voltage Stability Assessment and Improvement in Power Systems with Solar Photovoltaic Penetration. 2021 IEEE 2nd International Conference On Electrical Power and Energy Systems (ICEPES)

Duan, F., Eslami, M., Khajehzadeh, M., Basem, A., Jasim, D., & Palani, S. (2024, 06/10). Optimization of a photovoltaic/wind/battery energy-based microgrid in distribution network using machine learning and fuzzy multi-objective improved Kepler optimizer algorithms. *Scientific Reports, 14*, 13354. https://doi.org/10.1038/s41598-024-64234-x

Isaiah, A., Jimoh, A.-G., & Yusuff, A. (2015). *Detection of weak bus through Fast Voltage Stability index and inherent structural characteristics of power system*. https://doi.org/10.1109/EPECS.2015.7368536

Jain, A., Joshi, K., Behal, A., & Mohan, N. (2006). Voltage regulation with STATCOMs: modeling, control and results. *IEEE Transactions on Power Delivery, 21*(2), 726-735. https://doi.org/10.1109/TPWRD.2005.855489

Jamroen, C., Pannawan, A., & Sirisukprasert, S. (2018, 4-7 Sept. 2018). Battery Energy Storage System Control for Voltage Regulation in Microgrid with High Penetration of PV Generation. 2018 53rd International Universities Power Engineering Conference (UPEC),

Jamroen, C., & Sirisukprasert, S. (2022, 2022/07/01/). A voltage regulation strategy with state of charge management using battery energy storage optimized by a self-learning particle swarm optimization. *Computers and Electrical Engineering, 101*, 108103. https://doi.org/https://doi.org/10.1016/j.compeleceng.2022.108103

Karn, A. K., Hameed, S., & Sarfraz, M. (2023, 10-12 Feb. 2023). Identification of Strong and Weak Bus and Optimal Bus Coupling by L —Index Coefficients For Voltage Regulation in Power System. 2023 International Conference on Power, Instrumentation, Energy and Control (PIECON),

Kessel, P., & Glavitsch, H. (1986). Estimating the Voltage Stability of a Power System. *IEEE Transactions on Power Delivery, 1*(3), 346-354. https://doi.org/10.1109/TPWRD.1986.4308013

Li, Y., Li, K., Fan, R., Chen, J., & Zhao, Y. (2024, 11/06). Multi-objective planning of distribution network based on distributionally robust model predictive control. *Frontiers in Energy Research, 12*. https://doi.org/10.3389/fenrg.2024.1478040

Liu, H., Hu, Z., Song, Y., & Lin, J. (2013). Decentralized Vehicle-to-Grid Control for Primary Frequency Regulation Considering Charging Demands. *IEEE Transactions on Power Systems, 28*(3), 3480-3489. https://doi.org/10.1109/TPWRS.2013.2252029

Malik, F. H., Khan, M. W., Rahman, T. U., Ehtisham, M., Faheem, M., Haider, Z. M., & Lehtonen, M. (2024). A Comprehensive Review on Voltage Stability in Wind-Integrated Power Systems. *Energies, 17*(3).

Maroua, B., Laid, Z., Benbouhenni, H., Fateh, M., Debdouche, N., & Colak, I. (2024, 2024/06/01/). Robust type 2 fuzzy logic control microgrid-connected photovoltaic system with battery energy storage through multi-functional voltage source inverter using direct power control. *Energy Reports, 11*, 3117-3134. https://doi.org/https://doi.org/10.1016/j.egyr.2024.02.047

Muangkhiew, P. a. C., K. (2022). Multi-objective Optimal Power Flow Using Fuzzy Satisfactory Stochastic Optimization. *International Energy Journal, 22*(September), 281–290.

Ota, Y., Taniguchi, H., Nakajima, T., Liyanage, K. M., Baba, J., & Yokoyama, A. (2012). Autonomous Distributed V2G (Vehicle-to-Grid) Satisfying Scheduled Charging. *IEEE Transactions on Smart Grid, 3*(1), 559-564. https://doi.org/10.1109/TSG.2011.2167993

Ram, T., & M, H. (2016). *Voltage stability analysis using L-index under various transformer tap changer settings*. https://doi.org/10.1109/ICCPCT.2016.7530331

Ramanareddy, I. K. ษ. P. (2011). Analysis of Voltage Stability using L-Index Method. *International Journal of Electrical Engineering, 4*(4), 483-498. http://www.irphouse.com

Renewables.ninja. Renewables.ninja: Simulate the power output from wind and solar power plants. https://www.renewables.ninja/

Rouzbehi, K., Miranian, A., Candela, J. I., Luna, A., & Rodriguez, P. (2015). A Generalized Voltage Droop Strategy for Control of Multiterminal DC Grids. *IEEE Transactions on Industry Applications, 51*(1), 607-618. https://doi.org/10.1109/TIA.2014.2332814

Soni, N., & Gaur, A. (2018, 05/12). A Literature Review on Voltage Regulation Techniques in Power System. *International Journal of Scientific and Research Publications (IJSRP), 8*. https://doi.org/10.29322/IJSRP.8.5.2018.p7739

Swe, P. L., Swe, W., & Lin, K. M. (2011, 03/01). Effects of tap changing transformer and shunt capacitor on voltage stability enhancement of transmission networks. *World Academy of Science, Engineering and Technology, 75*, 556-559.

Tan, Z., Li, X., He, L., Li, Y., & Huang, J. (2020, 2020/05/01/). Primary frequency control with BESS considering adaptive SoC recovery. *International Journal of Electrical Power & Energy Systems, 117*, 105588. https://doi.org/https://doi.org/10.1016/j.ijepes.2019.105588

Taylor, C. W. (2003, 2003/09/01/). Shunt Compensation for Voltage Stability. *IFAC Proceedings Volumes, 36*(20), 43-48. https://doi.org/https://doi.org/10.1016/S1474-6670(17)34440-3

Wang, Y., Cai, Y., Li, W., Tan, Z., Song, Z., Li, Y., Bai, H., & Liu, T. (2024). Static-Voltage-Stability Analysis of Renewable Energy-Integrated Distribution Power System Based on Impedance Model Index. *Energies, 17*(5).

Wang, Y., Tan, K. T., Peng, X. Y., & So, P. L. (2016). Coordinated Control of Distributed Energy-Storage Systems for Voltage Regulation in Distribution Networks. *IEEE Transactions on Power Delivery, 31*(3), 1132-1141. https://doi.org/10.1109/TPWRD.2015.2462723

Xu, X., Yan, Z., Shahidehpour, M., Wang, H., & Chen, S. (2018). Power System Voltage Stability Evaluation Considering Renewable Energy With Correlated Variabilities. *IEEE Transactions on Power Systems, 33*(3), 3236-3245. https://doi.org/10.1109/TPWRS.2017.2784812

Xu, Y., & Li, F. (2014). Adaptive PI Control of STATCOM for Voltage Regulation. *IEEE Transactions on Power Delivery, 29*(3), 1002-1011. https://doi.org/10.1109/TPWRD.2013.2291576

Yadav, L., Verma, M. K., Joshi, Agrawal, S., Alotaibi, M., Malik, H., García Márquez, F. P., & Hossaini, M. (2024, 01/01). A Framework for Qualitative Analysis of Voltage Stability Indices (VSIs). *IEEE Access, PP*, 1-1. https://doi.org/10.1109/ACCESS.2024.3438266

Zaheb, H., Danish, M. S., Senjyu, T., Ahmadi, M., Nazari, A. M., Wali, M., Khosravy, M., & Mandal, P. (2020). A Contemporary Novel Classification of Voltage Stability Indices. *Applied Sciences, 10*(5).

Zainal Abidin, M. A., & A. Danapalasingam, K. (2022). Fuzzy Logic in Battery Energy Storage System (BESS). In (pp. 45-72). https://doi.org/10.1007/978-981-16-8484-5_5

Zeraati, M., Hamedani Golshan, M. E., & Guerrero, J. (2016, 12/06). Distributed Control of Battery Energy Storage Systems for Voltage Regulation in Distribution Networks With High PV Penetration. *IEEE Transactions on Smart Grid, PP*, 1-1. https://doi.org/10.1109/TSG.2016.2636217

Zhang, Y., & Srivastava, A. (2021). Voltage Control Strategy for Energy Storage System in Sustainable Distribution System Operation. *Energies, 14*(4).

APPENDIX

APPENDIX A

The BESS Operating Result

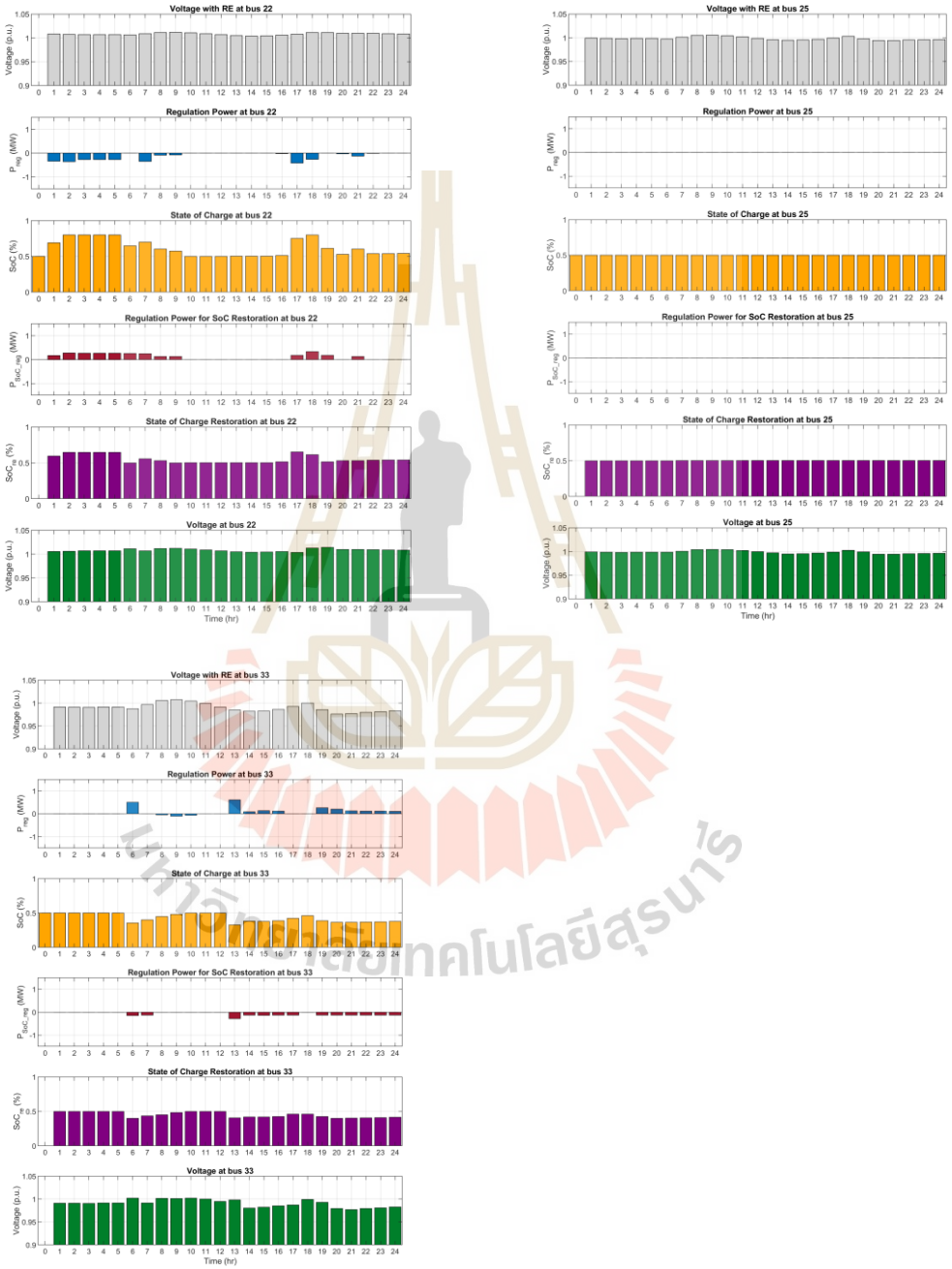

Figure A.1 Time-Series Profiles of Voltage, Regulation Power and Battery SoC at Bus 22, 25 and 33 in IEEE 33-bus system Scenario 1

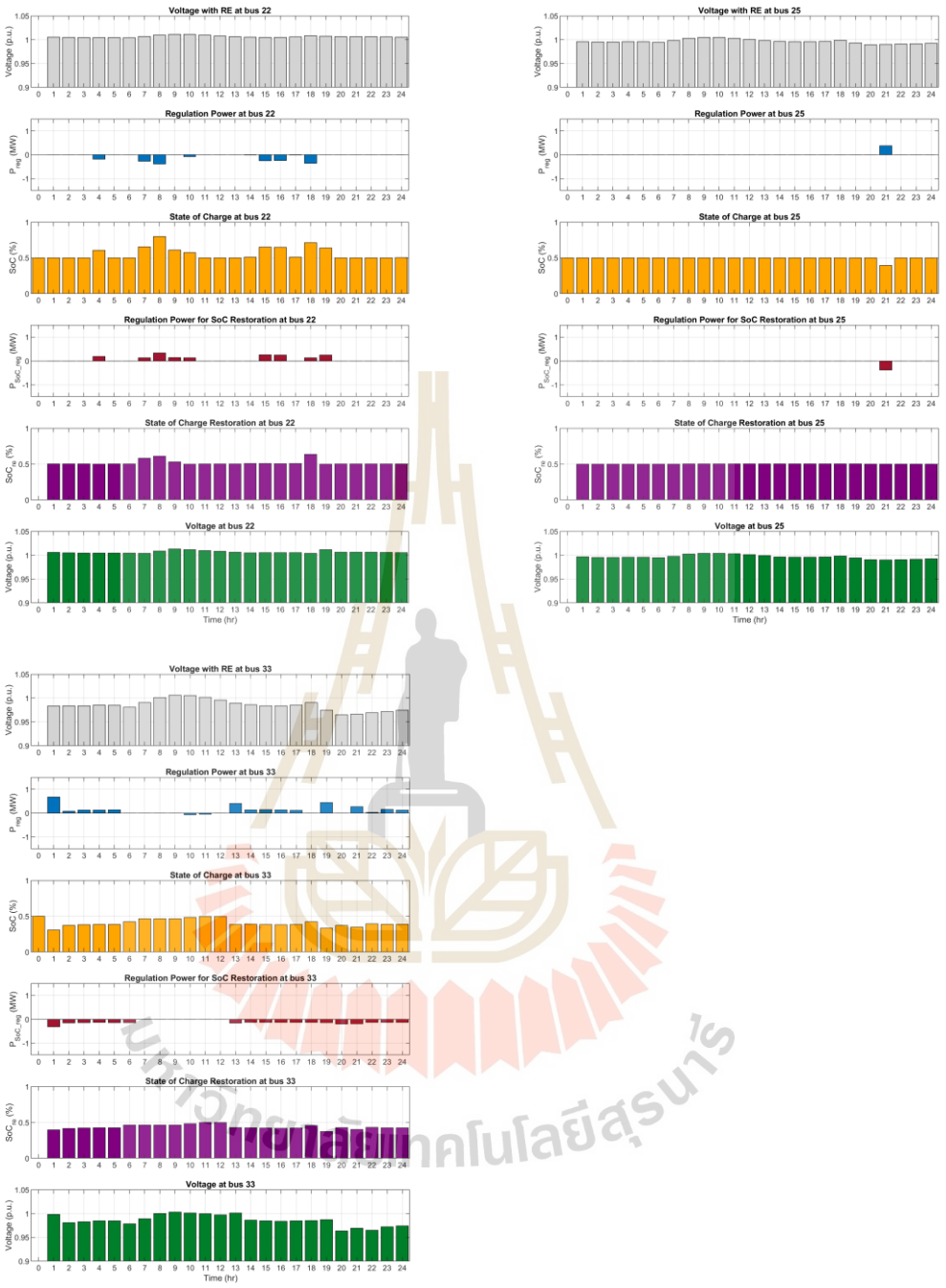

Figure A.2 Time-Series Profiles of Voltage, Regulation Power and Battery SoC at Bus 22, 25 and 33 in IEEE 33-bus system Scenario 2

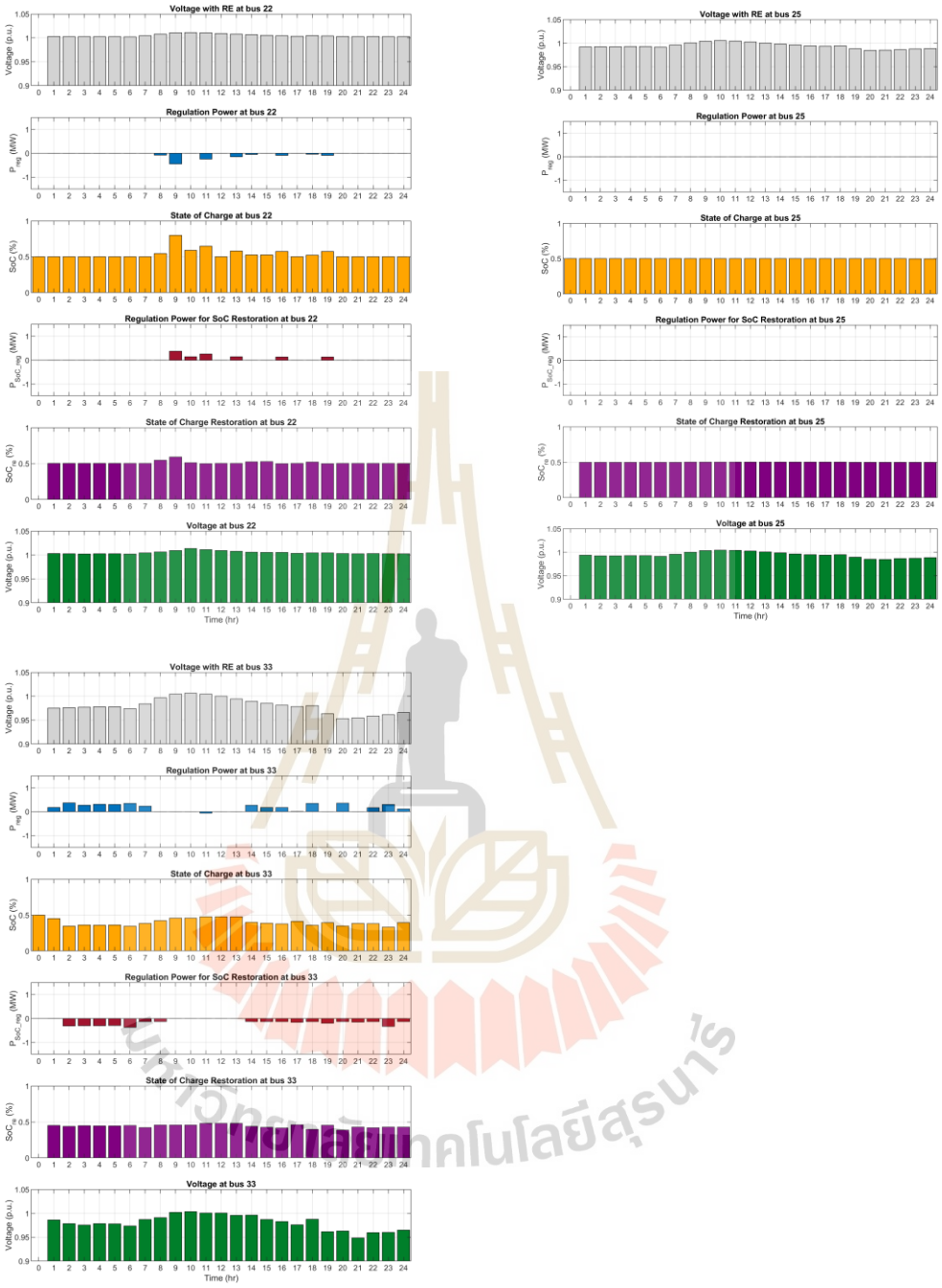

Figure A.3 Time-Series Profiles of Voltage, Regulation Power and Battery SoC at Bus 22, 25 and 33 in IEEE 33-bus system Scenario 3

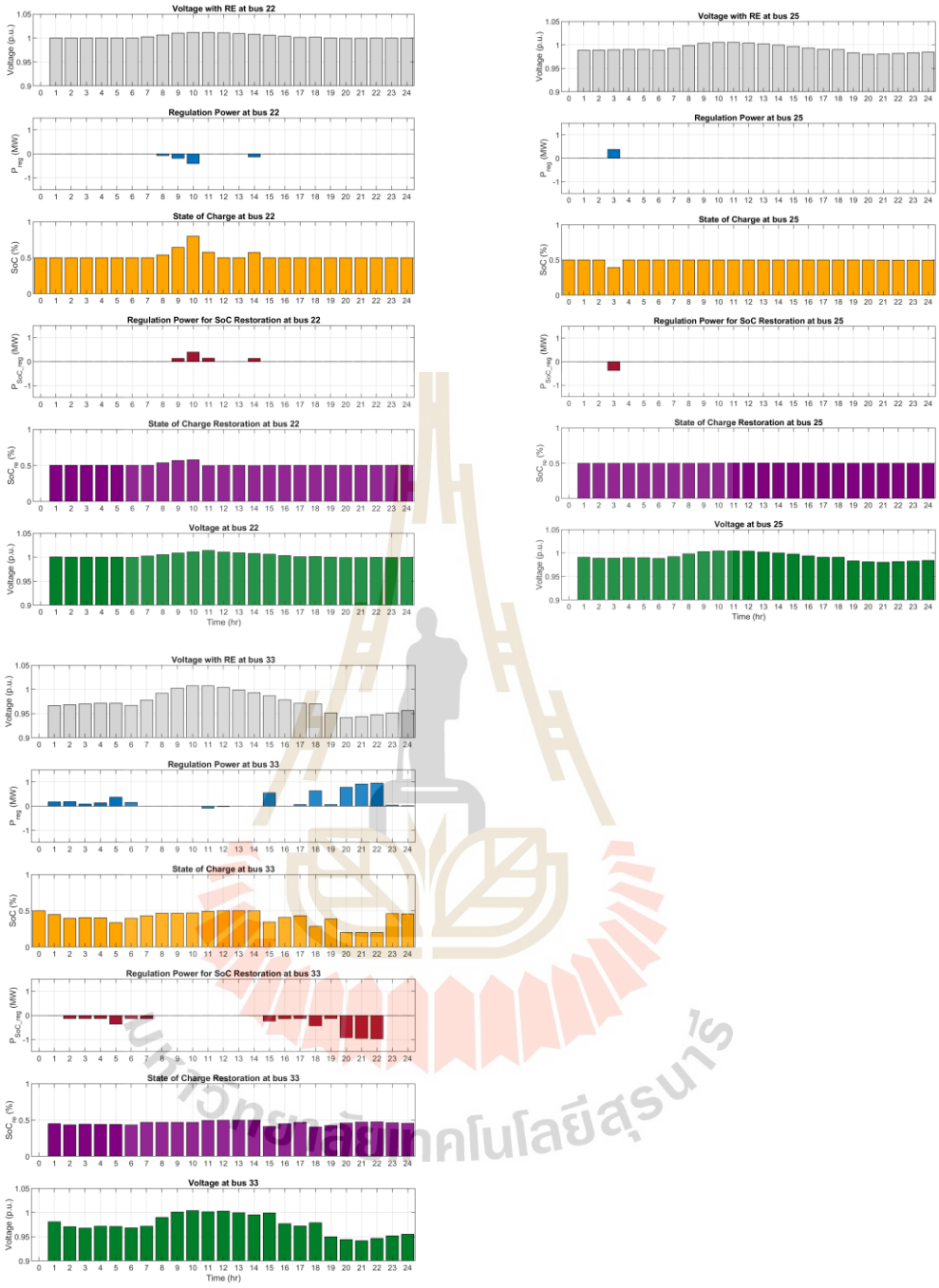

Figure A.4 Time-Series Profiles of Voltage, Regulation Power and Battery SoC at Bus 22, 25 and 33 in IEEE 33-bus system Scenario 4

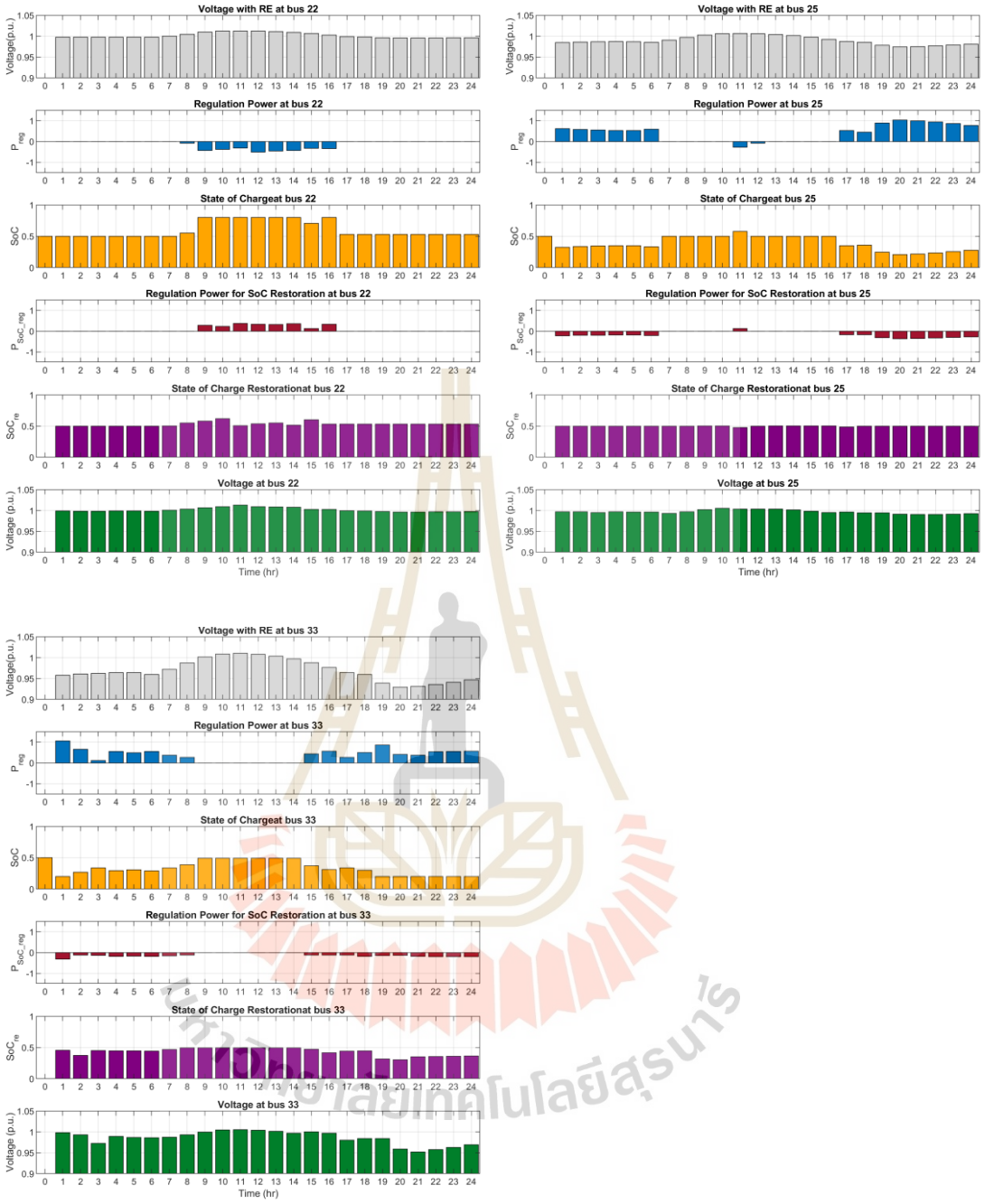

Figure A.5 Time-Series Profiles of Voltage, Regulation Power and Battery SoC at Bus 22, 25 and 33 in IEEE 33-bus system Scenario 5

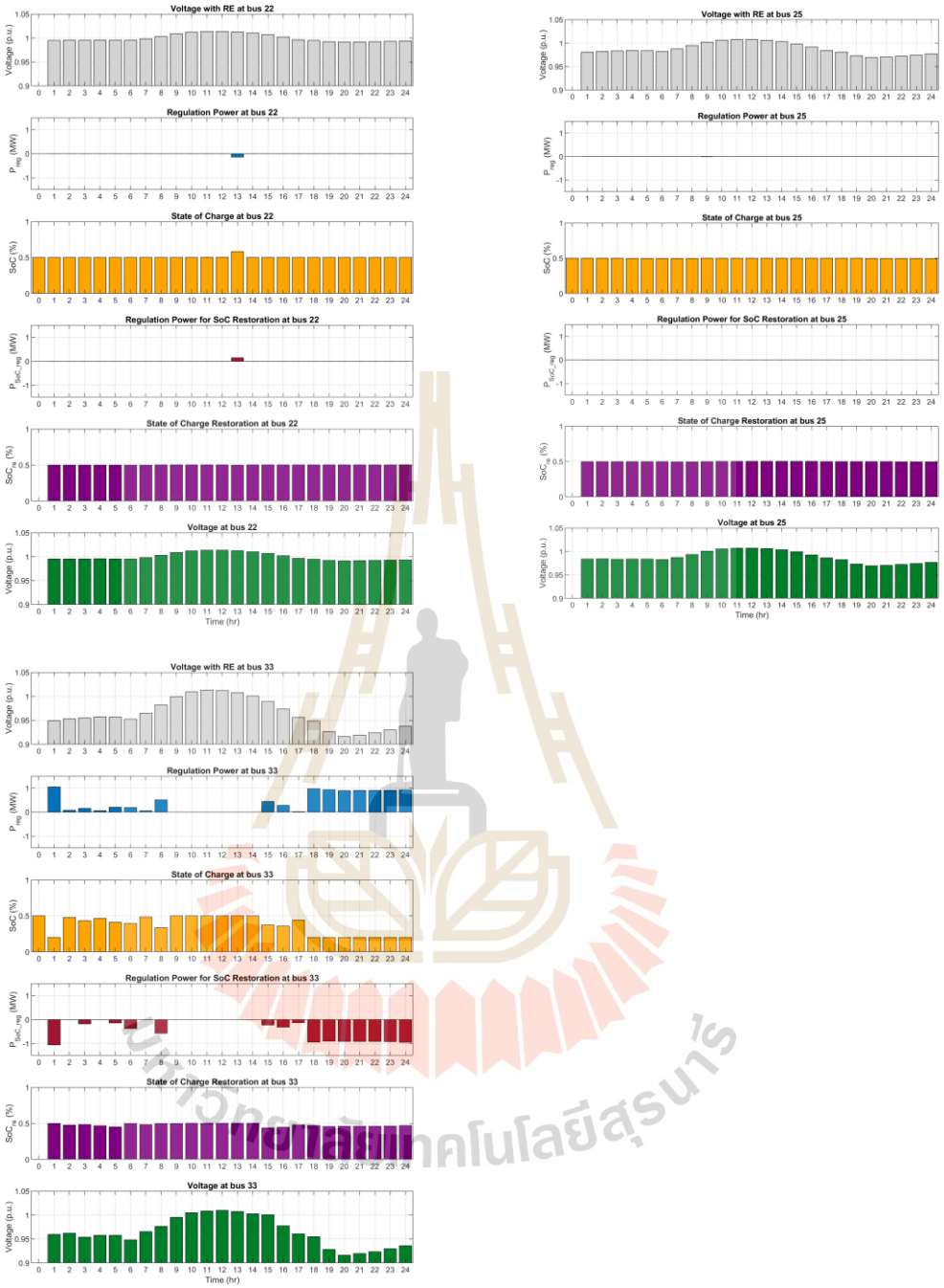

Figure A.6 Time-Series Profiles of Voltage, Regulation Power and Battery SoC at Bus 22, 25 and 33 in IEEE 33-bus system Scenario 6

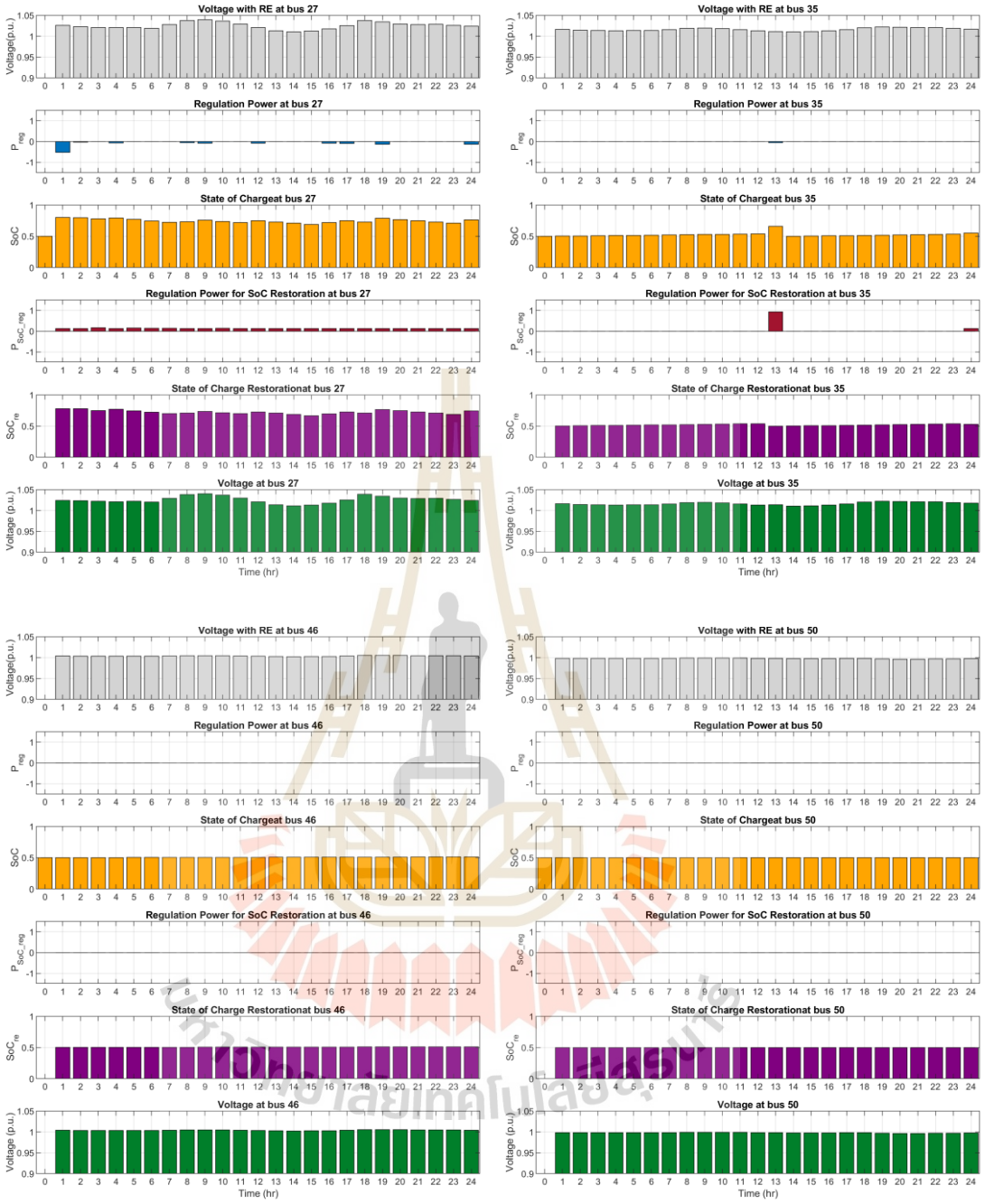

Figure A.7 Time-Series Profiles of Voltage, Regulation Power and Battery SoC at Bus 27, 35, 46 and 50 in IEEE 69-bus system Scenario 1

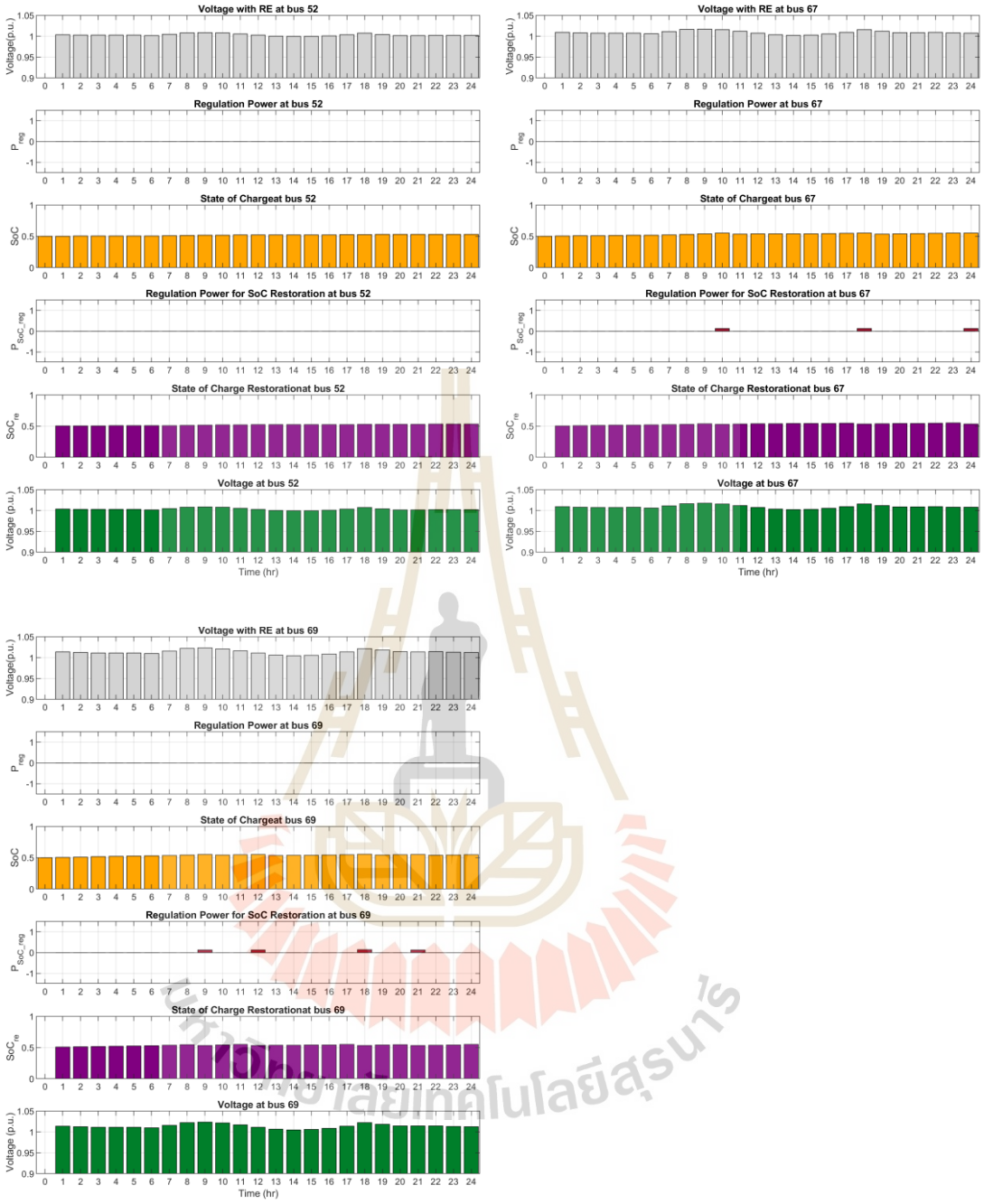

Figure A.8 Time-Series Profiles of Voltage, Regulation Power and Battery SoC at Bus 52, 67 and 69 in IEEE 69-bus system Scenario 1

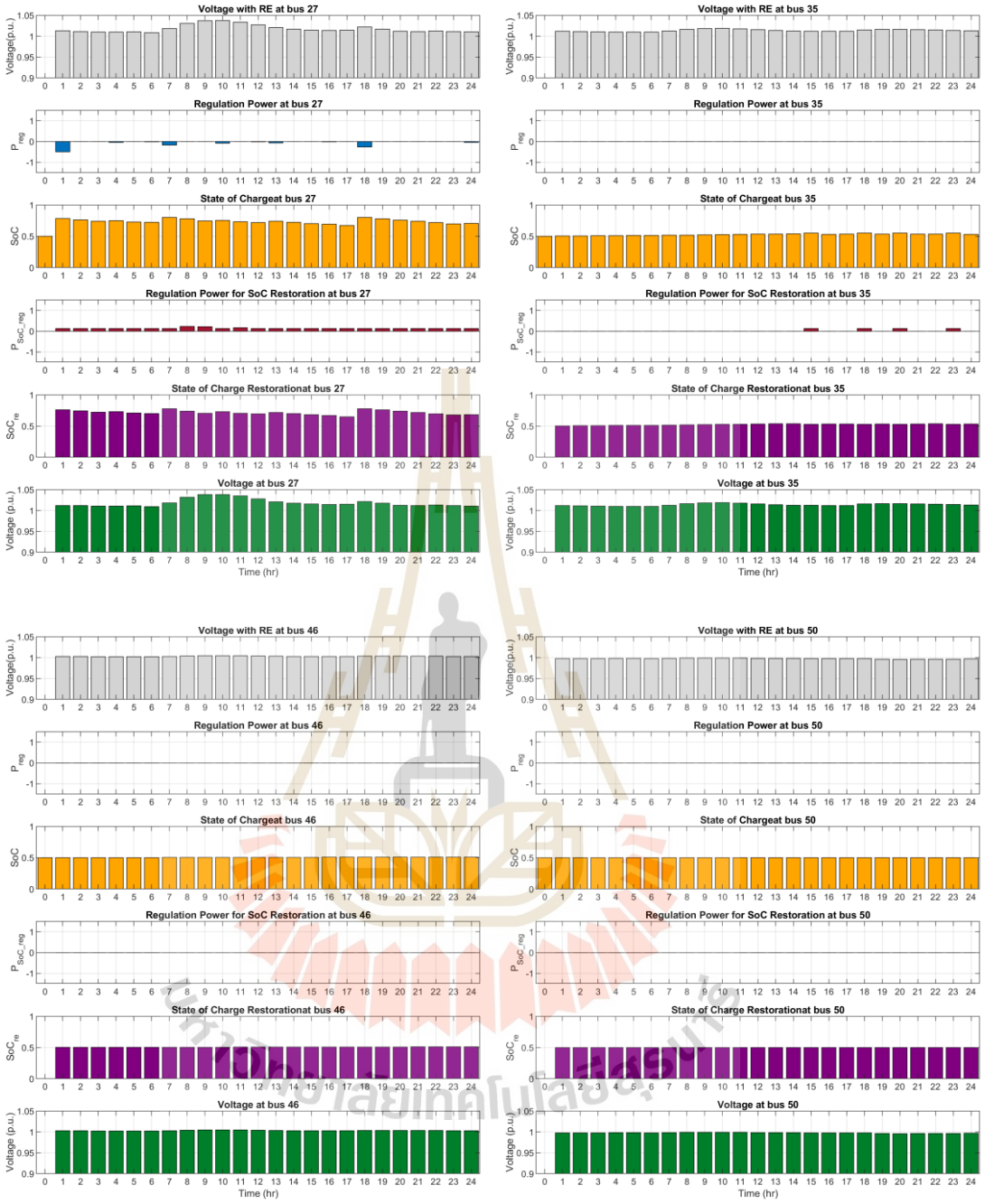

Figure A.9 Time-Series Profiles of Voltage, Regulation Power and Battery SoC at Bus 27, 35, 46 and 50 in IEEE 69-bus system Scenario 2

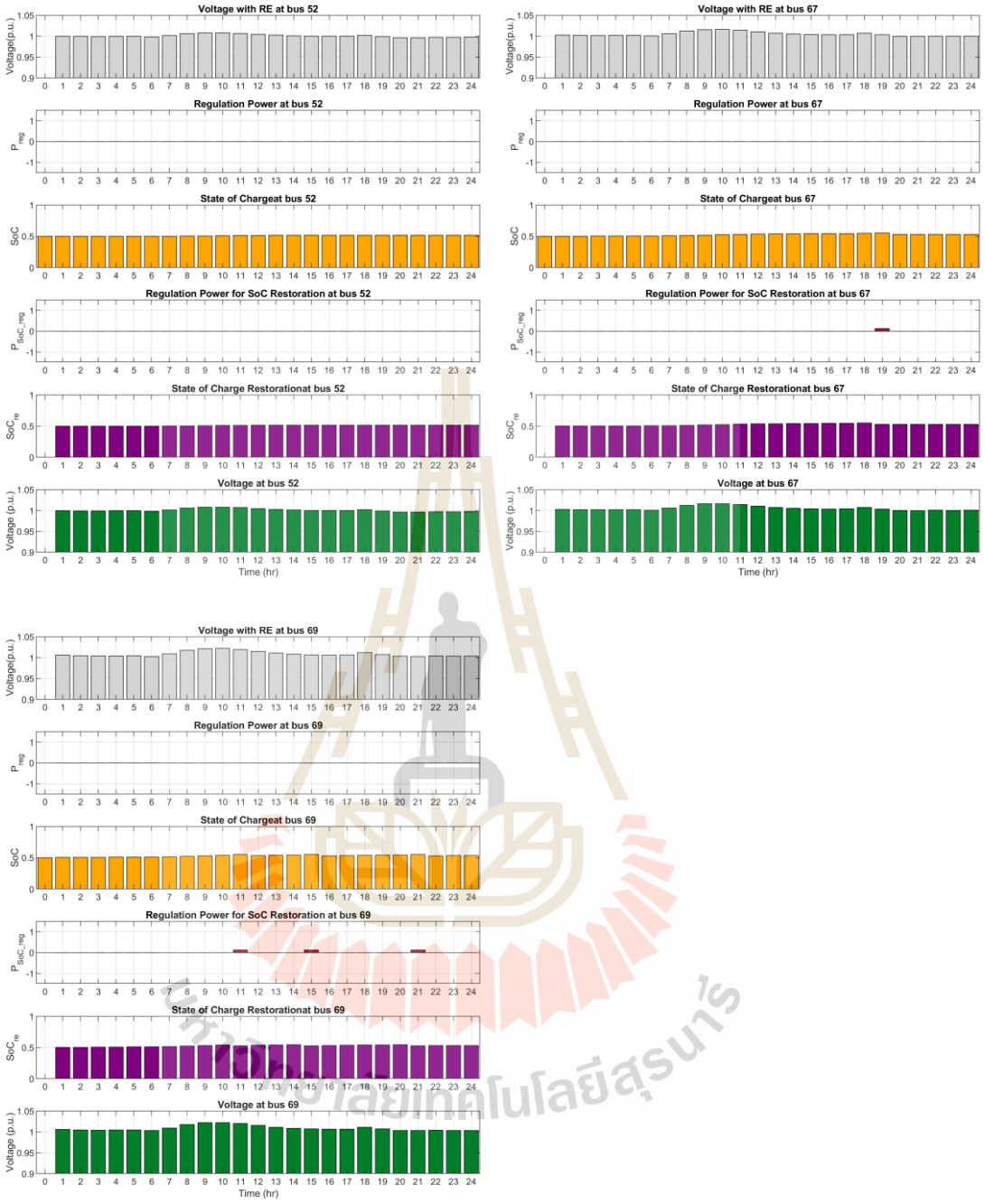

Figure A.10 Time-Series Profiles of Voltage, Regulation Power and Battery SoC at Bus 52, 67 and 69 in IEEE 69-bus system Scenario 2

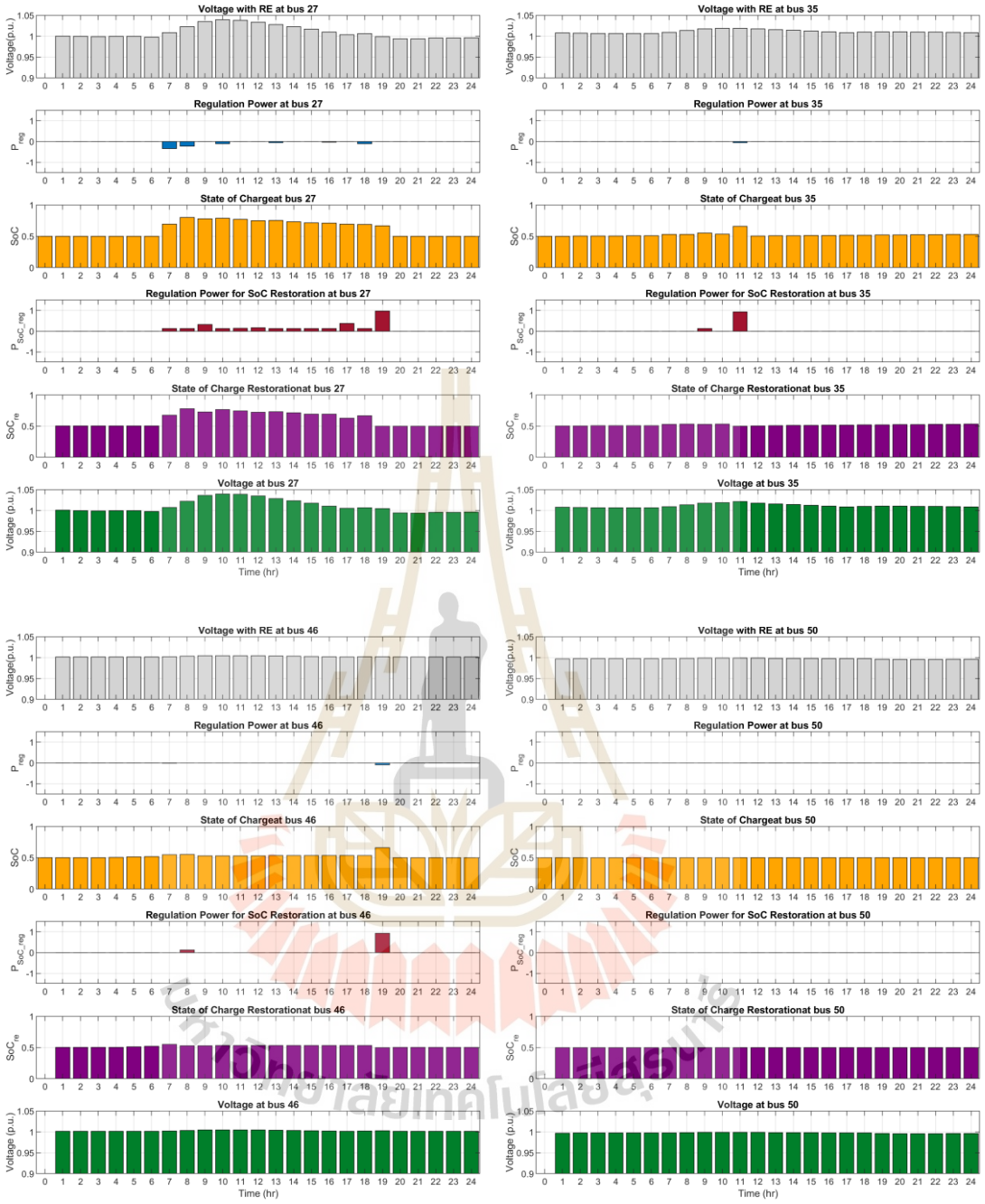

Figure A.11 Time-Series Profiles of Voltage, Regulation Power and Battery SoC at Bus 27, 35, 46 and 50 in IEEE 69-bus system Scenario 3

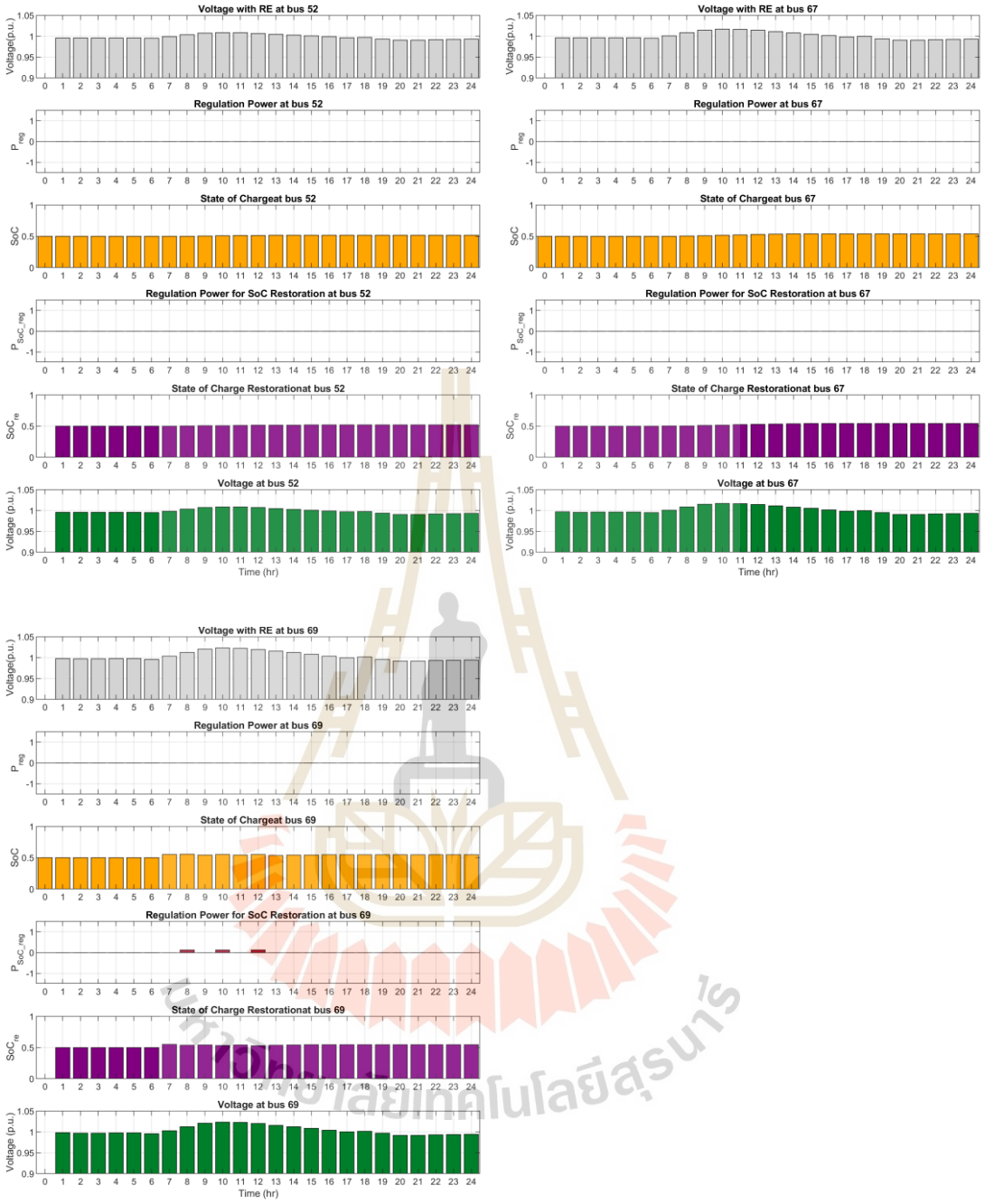

Figure A.12 Time-Series Profiles of Voltage, Regulation Power and Battery SoC at Bus 52, 67 and 69 in IEEE 69-bus system Scenario 3

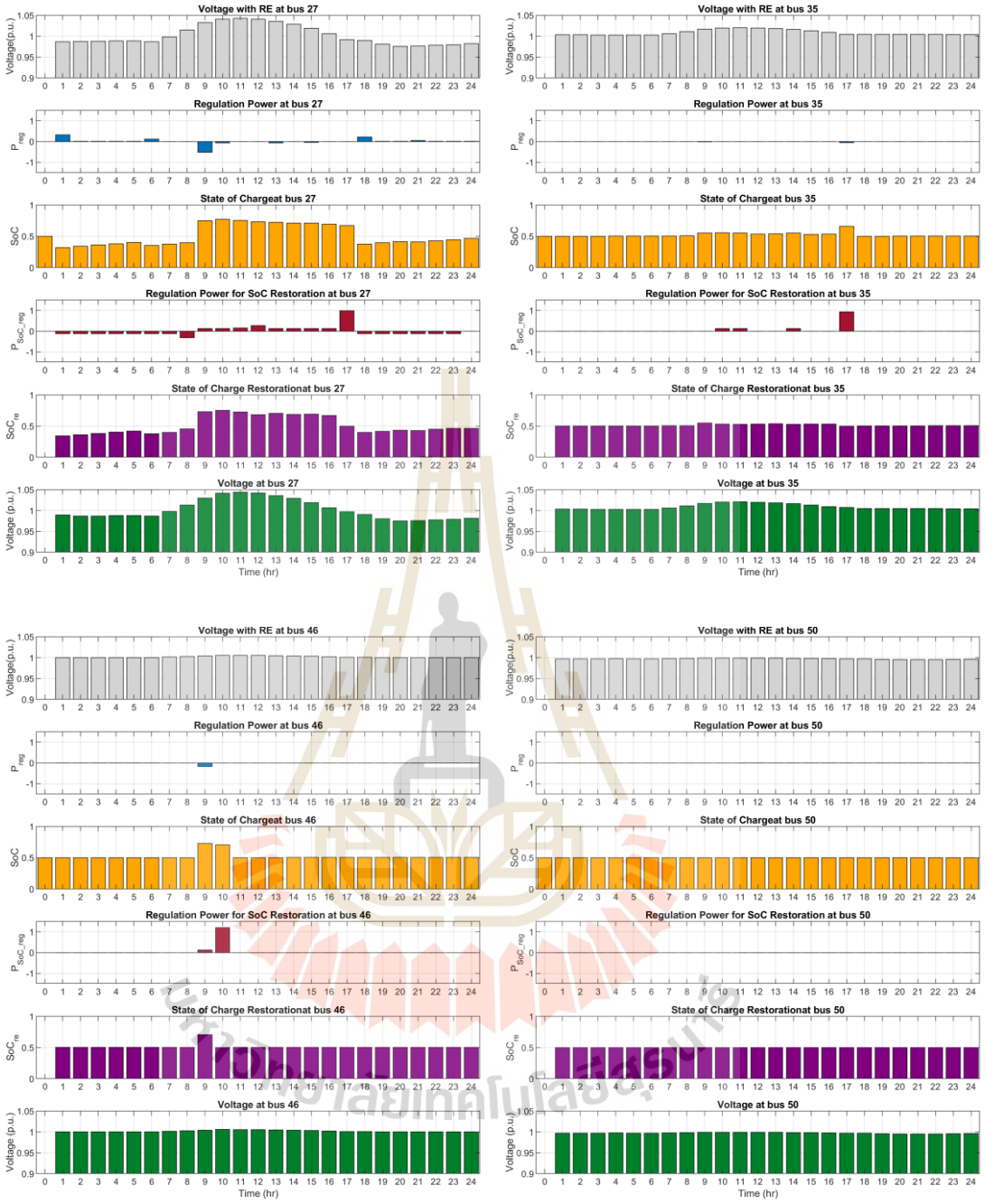

Figure A.13 Time-Series Profiles of Voltage, Regulation Power and Battery SoC at Bus 27, 35, 46 and 50 in IEEE 69-bus system Scenario 4

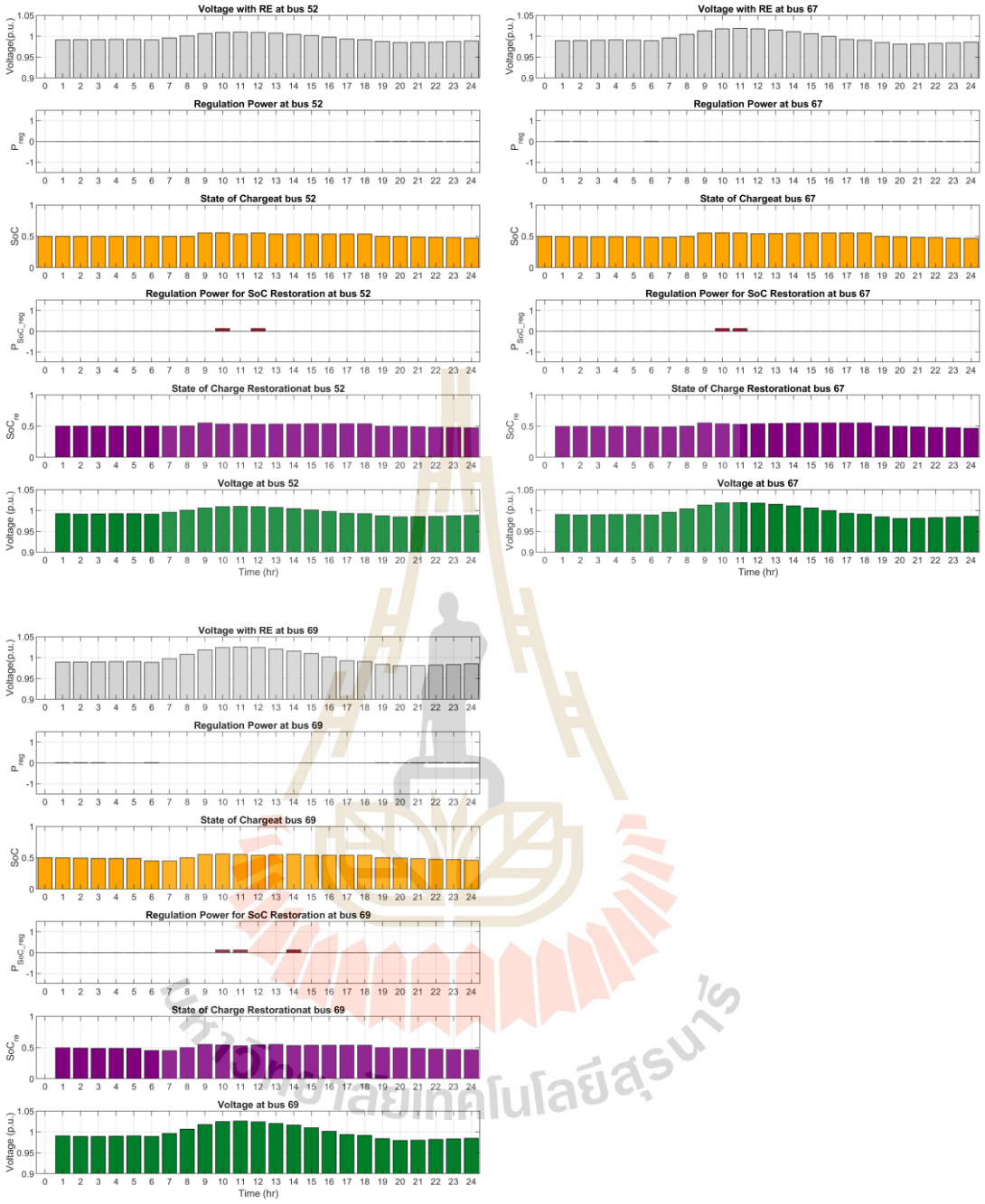

Figure A.14 Time-Series Profiles of Voltage, Regulation Power and Battery SoC at Bus 52, 67 and 69 in IEEE 69-bus system Scenario 4

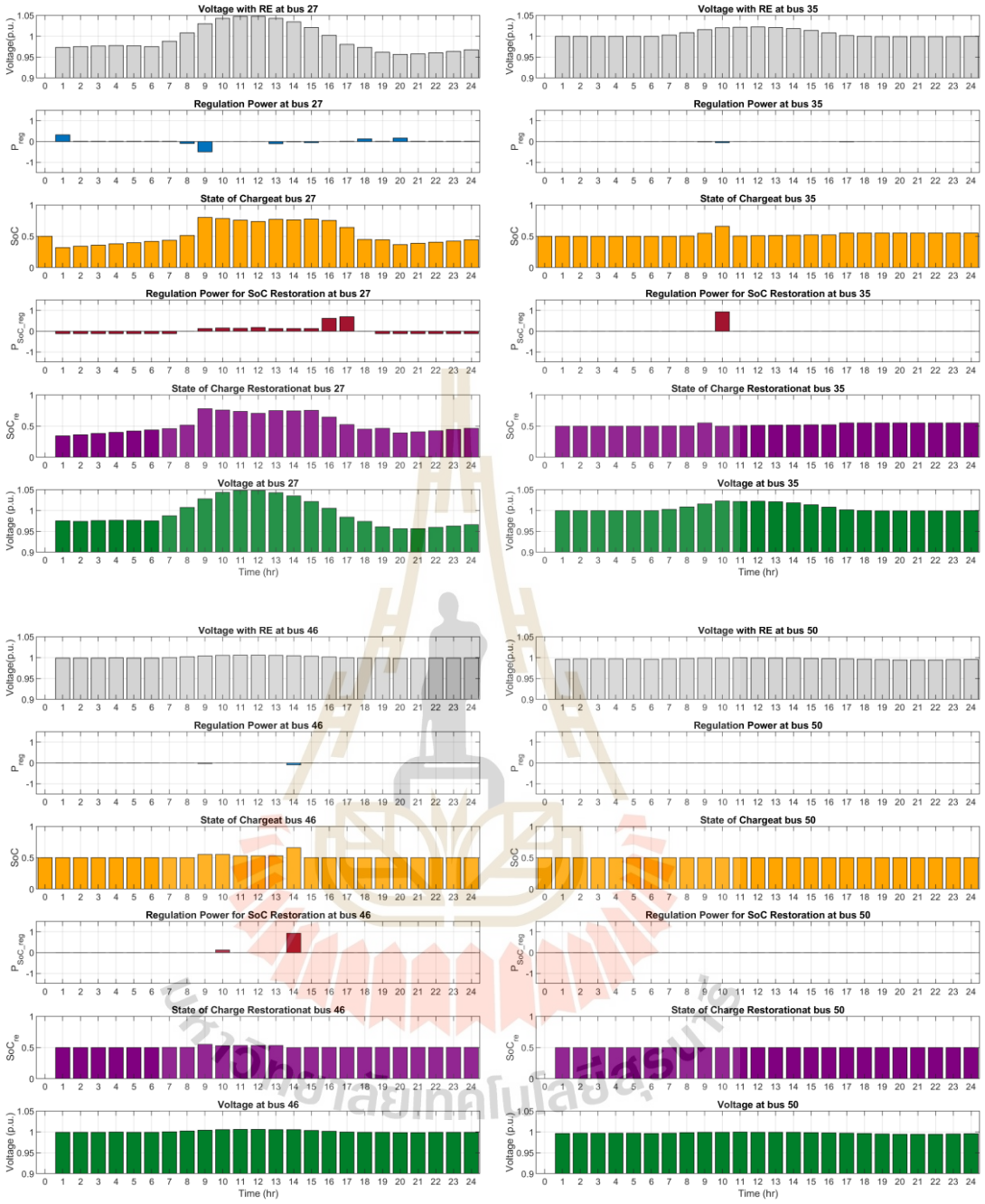

Figure A.15 Time-Series Profiles of Voltage, Regulation Power and Battery SoC at Bus 27, 35, 46 and 50 in IEEE 69-bus system Scenario 5

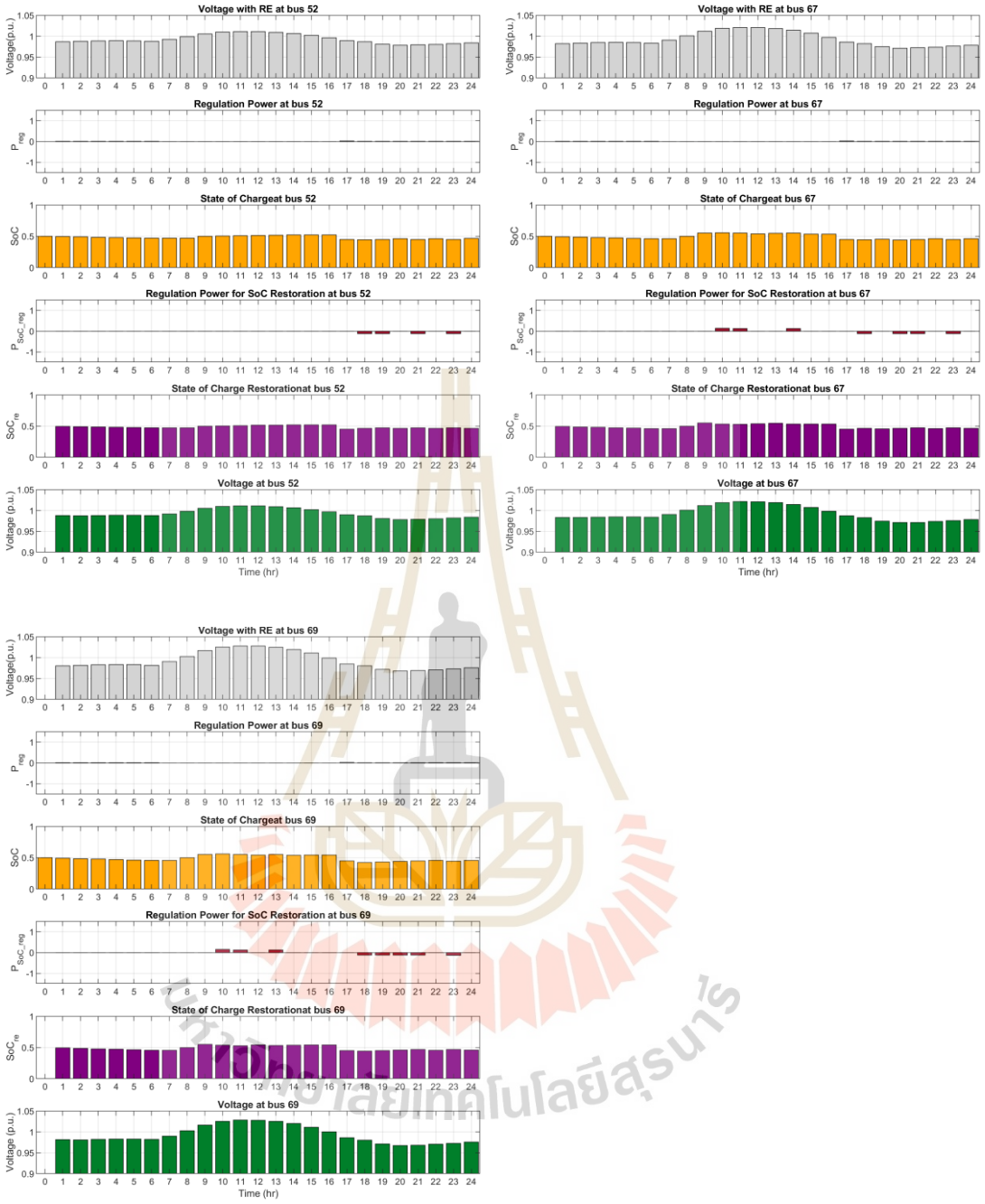

Figure A.16 Time-Series Profiles of Voltage, Regulation Power and Battery SoC at Bus 52, 67 and 69 in IEEE 69-bus system Scenario 5

APPENDIX B

Energy Profile for Test Simulation

Table B.1 Load profile

Hour	Load (p.u.)	Hour	Load (p.u.)	Hour	Load (p.u.)
1	0.6300	9	0.5132	17	0.5979
2	0.5864	10	0.5174	18	0.6374
3	0.5611	11	0.5200	19	0.8881
4	0.5348	12	0.5330	20	1.0000
5	0.5404	13	0.5506	21	0.9697
6	0.5936	14	0.5676	22	0.9192
7	0.5490	15	0.5897	23	0.8459
8	0.5139	16	0.5986	24	0.7669

Table B.2 PV profile, rated 0.25 MW

Hour	Generation (kW)	Hour	Generation (kW)	Hour	Generation (kW)
1	0.0000	9	135.7000	17	14.3000
2	0.0000	10	172.2000	18	0.0000
3	0.0000	11	185.2000	19	0.0000
4	0.0000	12	186.3000	20	0.0000
5	0.0000	13	175.6000	21	0.0000
6	0.9000	14	154.4000	22	0.0000
7	29.1000	15	119.9000	23	0.0000
8	76.0000	16	70.1000	24	0.0000

Table B.3 PV profile, rated 0.50 MW

Hour	Generation (kW)	Hour	Generation (kW)	Hour	Generation (kW)
1	0.0000	9	271.3000	17	28.5000
2	0.0000	10	344.4000	18	0.0000
3	0.0000	11	370.4000	19	0.0000
4	0.0000	12	372.6000	20	0.0000
5	0.0000	13	351.2000	21	0.0000
6	1.8000	14	308.9000	22	0.0000
7	58.3000	15	239.7000	23	0.0000
8	152.0000	16	140.3000	24	0.0000

Table B.4 PV profile, rated 0.75 MW

Hour	Generation (kW)	Hour	Generation (kW)	Hour	Generation (kW)
1	0.0000	9	407.0000	17	42.8000
2	0.0000	10	516.7000	18	0.0000
3	0.0000	11	555.6000	19	0.0000
4	0.0000	12	558.9000	20	0.0000
5	0.0000	13	526.8000	21	0.0000
6	2.6000	14	463.3000	22	0.0000
7	87.4000	15	359.6000	23	0.0000
8	227.9000	16	210.4000	24	0.0000

Table B.5 PV profile, rated 1.00 MW

Hour	Generation (kW)	Hour	Generation (kW)	Hour	Generation (kW)
1	0.0000	9	542.6000	17	57.1000
2	0.0000	10	688.9000	18	0.0000
3	0.0000	11	740.8000	19	0.0000
4	0.0000	12	745.2000	20	0.0000
5	0.0000	13	702.4000	21	0.0000
6	3.5000	14	617.8000	22	0.0000
7	116.5000	15	479.5000	23	0.0000
8	303.9000	16	280.6000	24	0.0000

Table B.6 PV profile, rated 1.25 MW

Hour	Generation (kW)	Hour	Generation (kW)	Hour	Generation (kW)
1	0.0000	9	678.3100	17	71.3390
2	0.0000	10	861.1150	18	0.0000
3	0.0000	11	926.0140	19	0.0000
4	0.0000	12	931.4830	20	0.0000
5	0.0000	13	877.9420	21	0.0000
6	4.3820	14	772.2040	22	0.0000
7	145.6720	15	599.3430	23	0.0000
8	379.9020	16	350.7060	24	0.0000

Table B.7 Wind profile, rated 0.25 MW

Hour	Generation (kW)	Hour	Generation (kW)	Hour	Generation (kW)
1	138.4000	9	163.5000	17	133.2000
2	125.2000	10	154.4000	18	172.1000
3	117.3000	11	135.1000	19	190.4000
4	113.5000	12	112.7000	20	188.0000
5	115.0000	13	95.0000	21	182.1000
6	115.8000	14	90.2000	22	178.3000
7	135.4000	15	97.5000	23	162.5000
8	158.2000	16	111.5000	24	148.4000

Table B.8 Wind profile, rated 0.50 MW

Hour	Generation (kW)	Hour	Generation (kW)	Hour	Generation (kW)
1	276.8000	9	327.0000	17	266.4000
2	250.4000	10	308.8000	18	344.3000
3	234.5000	11	270.1000	19	380.8000
4	226.9000	12	225.5000	20	376.0000
5	230.0000	13	190.1000	21	364.2000
6	231.5000	14	180.4000	22	356.5000
7	270.8000	15	194.9000	23	325.0000
8	316.5000	16	223.1000	24	296.7000

Table B.9 Wind profile, rated 0.75 MW

Hour	Generation (kW)	Hour	Generation (kW)	Hour	Generation (kW)
1	415.1000	9	490.5000	17	399.5000
2	375.5000	10	463.2000	18	516.4000
3	351.8000	11	405.2000	19	571.2000
4	340.4000	12	338.2000	20	564.0000
5	345.0000	13	285.1000	21	546.3000
6	347.3000	14	270.6000	22	534.8000
7	406.2000	15	292.4000	23	487.5000
8	474.7000	16	334.6000	24	445.1000

Table B.10 Wind profile, rated 1.00 MW

Hour	Generation (kW)	Hour	Generation (kW)	Hour	Generation (kW)
1	553.5000	9	654.0000	17	532.7000
2	500.7000	10	617.6000	18	688.5000
3	469.1000	11	540.3000	19	761.7000
4	453.9000	12	450.9000	20	752.0000
5	460.1000	13	380.2000	21	728.4000
6	463.0000	14	360.9000	22	713.0000
7	541.5000	15	389.9000	23	650.0000
8	633.0000	16	446.1000	24	593.4000

Table B.11 Wind profile, rated 1.25 MW

Hour	Generation (kW)	Hour	Generation (kW)	Hour	Generation (kW)
1	691.8920	9	817.5140	17	665.8940
2	625.8990	10	771.9730	18	860.6840
3	586.3450	11	675.3310	19	952.0810
4	567.3650	12	563.6320	20	939.9630
5	575.0730	13	475.2160	21	910.5220
6	578.7850	14	451.0680	22	891.2850
7	676.9350	15	487.3670	23	812.5470
8	791.1880	16	557.6670	24	741.7850

APPENDIX C

IEEE 33-bus system test data

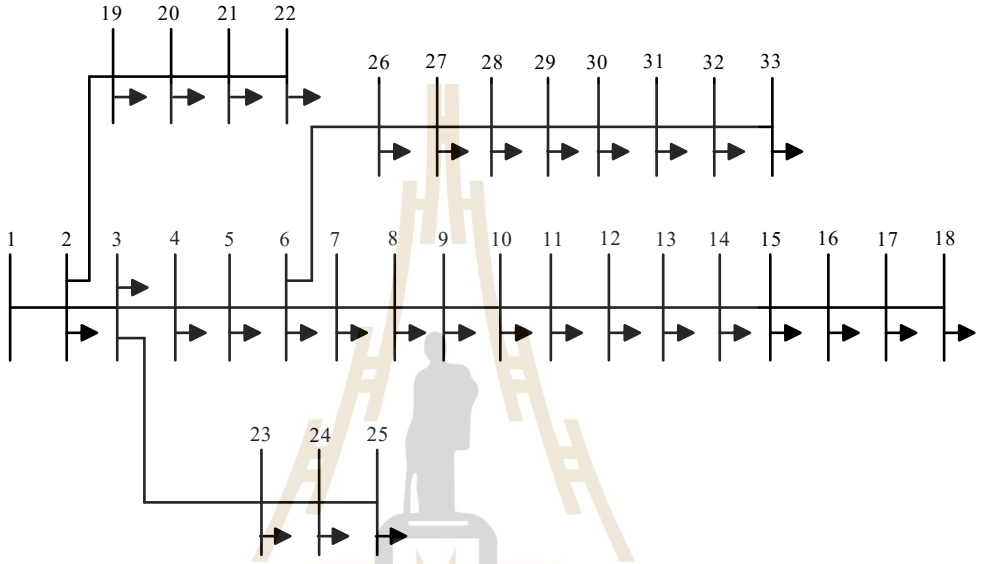

Figure C.1 IEEE 33-bus system data

Table C.1 Line parameter of IEEE 33-bus test system

From Bus	To Bus	R(p.u.)	X(p.u.)
1	2	0.0575	0.0298
2	3	0.3076	0.1567
3	4	0.2284	0.1163
4	5	0.2378	0.1211
5	6	0.5110	0.4411
6	7	0.1168	0.3861
7	8	1.0678	0.7706
8	9	0.6426	0.4617
9	10	0.6489	0.4617
10	11	0.1227	0.0406

Table C.1 Line parameter of IEEE 33-bus test system (Continued)

From Bus	To Bus	R(p.u.)	X(p.u.)
11	12	0.2336	0.0772
12	13	0.9159	0.7206
13	14	0.3379	0.4448
14	15	0.3687	0.3282
15	16	0.4656	0.3400
16	17	0.8042	1.0738
17	18	0.4567	0.3581
2	19	0.1023	0.0976
19	20	0.9385	0.8457
20	21	0.2555	0.2985
21	22	0.4423	0.5848
3	23	0.2815	0.1924
23	24	0.5603	0.4424
24	25	0.5590	0.4374
6	26	0.1267	0.0645
26	27	0.1773	0.0903
27	28	0.6607	0.5826
28	29	0.5018	0.4371
29	30	0.3166	0.1613
30	31	0.6080	0.6008
31	32	0.1937	0.2258
32	33	0.2128	0.3308

Table C.2 Power parameter of IEEE 33-bus test system

Bus	Type	P(MW)	Q(MVar)
1	slack	0.0000	0.0000
2	PQ	0.1000	0.0600
3	PQ	0.0900	0.0400
4	PQ	0.1200	0.0800
5	PQ	0.0600	0.0300
6	PQ	0.0600	0.0200
7	PQ	0.2000	0.1000
8	PQ	0.2000	0.1000
9	PQ	0.0600	0.0200
10	PQ	0.0600	0.0200
11	PQ	0.0450	0.0300
12	PQ	0.0600	0.0350
13	PQ	0.0600	0.0350
14	PQ	0.1200	0.0800
15	PQ	0.0600	0.0100
16	PQ	0.0600	0.0200
17	PQ	0.0600	0.0200
18	PQ	0.0900	0.0400
19	PQ	0.0900	0.0400
20	PQ	0.0900	0.0400
21	PQ	0.0900	0.0400
22	PQ	0.0900	0.0400
23	PQ	0.0900	0.0500
24	PQ	0.4200	0.2000
25	PQ	0.4200	0.2000
26	PQ	0.0600	0.0250
27	PQ	0.0600	0.0250
28	PQ	0.0600	0.0200

Table C.2 Power parameter of IEEE 33-bus test system (Continued)

Bus	Type	P(MW)	Q(MVar)
29	PQ	0.1200	0.0700
30	PQ	0.2000	0.6000
31	PQ	0.1500	0.0700
32	PQ	0.2100	0.1000
33	PQ	0.0600	0.0400

APPENDIX D

IEEE 69-bus system test data

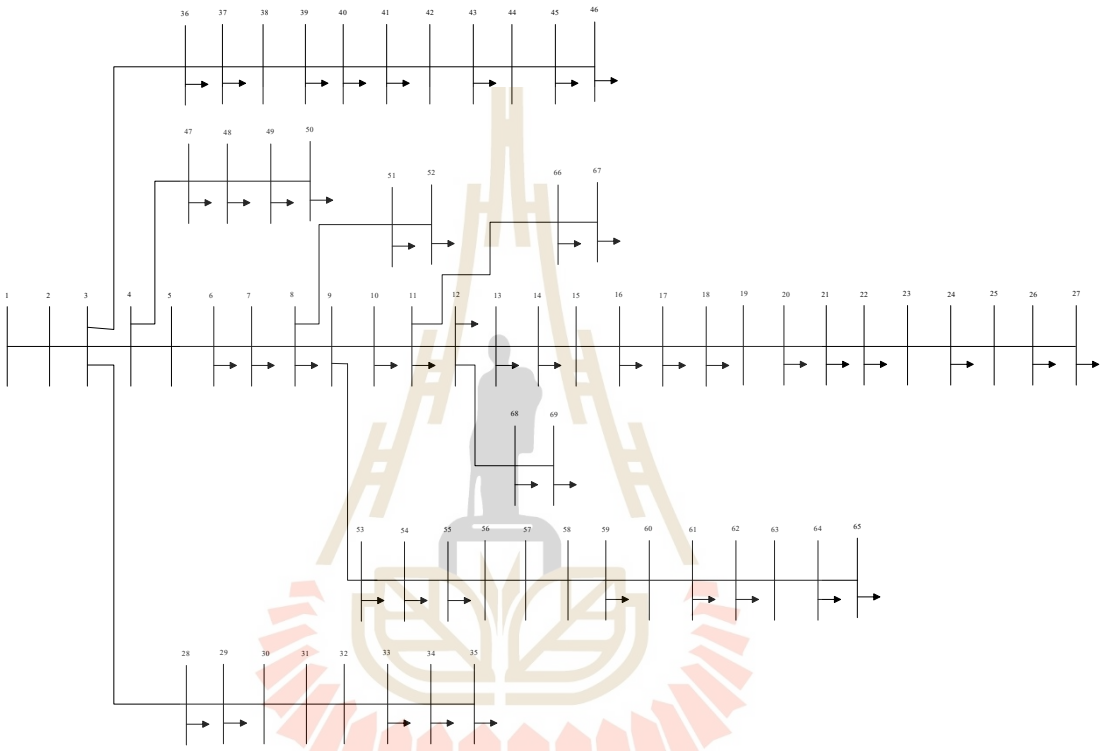

Figure D.1 IEEE 69-bus system data

Table D.1 Line parameter of IEEE 69-bus test system

From Bus	To Bus	R(p.u.)	X(p.u.)
1	2	3.12e-05	7.487e-05
2	3	3.12e-05	7.487e-05
3	4	9.359e-05	0.00022461
4	5	0.00156605	0.00183434
5	6	0.02283567	0.01162997
6	7	0.02377779	0.01211039
7	8	0.00575259	0.00293245

Table D.1 Line parameter of IEEE 69-bus test system (Continued)

From Bus	To Bus	R(p.u.)	X(p.u.)
8	9	0.00307595	0.00156605
9	10	0.05109948	0.01688966
10	11	0.01167988	0.0038621
11	12	0.04438605	0.01466848
12	13	0.0642643	0.02121346
13	14	0.0651378	0.02152542
14	15	0.0660113	0.02181243
15	16	0.01226637	0.00405551
16	17	0.02335976	0.0077242
17	18	0.00029324	9.983e-05
18	19	0.02043979	0.00675711
19	20	0.01313987	0.00434252
20	21	0.02131329	0.00704412
21	22	0.0008735	0.00028701
22	23	0.00992665	0.00328185
23	24	0.02160653	0.00714394
24	25	0.04671953	0.01544215
25	26	0.01927305	0.00637028
26	27	0.01080639	0.00356885
27	28	0.00027453	0.00067384
28	29	0.00399312	0.00976443
29	30	0.02481975	0.00820462
30	31	0.00437996	0.00144751
31	32	0.02189978	0.00723753
32	33	0.05234733	0.01756974
33	34	0.10656644	0.03522682
34	35	0.09196659	0.03040388
35	36	0.00027453	0.00067384

Table D.1 Line parameter of IEEE 69-bus test system (Continued)

From Bus	To Bus	R(p.u.)	X(p.u.)
36	37	0.00399312	0.00976443
37	38	0.00656993	0.00767428
38	39	0.00189673	0.00221493
39	40	0.00011231	0.00013102
40	41	0.04544048	0.0530898
41	42	0.01934168	0.02260481
42	43	0.00255809	0.00298236
43	44	0.00057401	0.00072375
44	45	0.00679455	0.00856649
45	46	5.615e-05	7.487e-05
46	47	0.00021213	0.0005241
47	48	0.0053096	0.01299636
48	49	0.01808135	0.04424254
49	50	0.00512867	0.01254714
50	51	0.00579003	0.00295117
51	52	0.02070808	0.00695053
52	53	0.0108563	0.00552798
53	54	0.01266568	0.00645139
54	55	0.01773196	0.0090282
55	56	0.01755102	0.00894085
56	57	0.09920412	0.03329889
57	58	0.04889702	0.01640924
58	59	0.01897981	0.00627669
59	60	0.02408976	0.0073124
60	61	0.03166421	0.01612847
61	62	0.00607703	0.00309467
62	63	0.00904692	0.00460457
63	64	0.04432989	0.02257986

Table D.1 Line parameter of IEEE 69-bus test system (Continued)

From Bus	To Bus	R(p.u.)	X(p.u.)
64	65	0.06495062	0.03308052
65	66	0.01255338	0.00381218
66	67	0.00029324	8.735e-05
67	68	0.04613304	0.01524873
68	69	0.00029324	9.983e-05

Table D.2 Power parameter of IEEE 69-bus test system

Bus	Type	P(MW)	Q(Var)
1	slack	0.0000	0.0000
2	PQ	0.0000	0.0000
3	PQ	0.0000	0.0000
4	PQ	0.0000	0.0000
5	PQ	0.0000	0.0000
6	PQ	0.0026	0.0022
7	PQ	0.0404	0.0300
8	PQ	0.0750	0.0540
9	PQ	0.0300	0.0220
10	PQ	0.0280	0.0190
11	PQ	0.1450	0.1040
12	PQ	0.1450	0.1040
13	PQ	0.0080	0.0055
14	PQ	0.0080	0.0055
15	PQ	0.0000	0.0000
16	PQ	0.0455	0.0300
17	PQ	0.0600	0.0350
18	PQ	0.0600	0.0350
19	PQ	0.0000	0.0000
20	PQ	0.0010	0.0006

Table D.2 Power parameter of IEEE 69-bus test system (Continued)

Bus	Type	P(MW)	Q(Var)
21	PQ	0.1140	0.0810
22	PQ	0.0053	0.0035
23	PQ	0.0000	0.0000
24	PQ	0.0280	0.0200
25	PQ	0.0000	0.0000
26	PQ	0.0140	0.0100
27	PQ	0.0140	0.0100
28	PQ	0.0260	0.0186
29	PQ	0.0260	0.0186
30	PQ	0.0000	0.0000
31	PQ	0.0000	0.0000
32	PQ	0.0000	0.0000
33	PQ	0.0140	0.0100
34	PQ	0.0195	0.0140
35	PQ	0.0060	0.0040
36	PQ	0.0260	0.0186
37	PQ	0.0260	0.0186
38	PQ	0.0000	0.0000
39	PQ	0.0240	0.0170
40	PQ	0.0240	0.0170
41	PQ	0.0012	0.0010
42	PQ	0.0000	0.0000
43	PQ	0.0060	0.0043
44	PQ	0.0000	0.0000
45	PQ	0.0392	0.0263
46	PQ	0.0392	0.0263
47	PQ	0.0000	0.0000
48	PQ	0.0790	0.0564

Table D.2 Power parameter of IEEE 69-bus test system (Continued)

Bus	Type	P(MW)	Q(Var)
49	PQ	0.3847	0.2745
50	PQ	0.3847	0.2745
51	PQ	0.0405	0.0283
52	PQ	0.0036	0.0027
53	PQ	0.0043	0.0035
54	PQ	0.0264	0.0190
55	PQ	0.0240	0.0172
56	PQ	0.0000	0.0000
57	PQ	0.0000	0.0000
58	PQ	0.0000	0.0000
59	PQ	0.1000	0.0720
60	PQ	0.0000	0.0000
61	PQ	1.2440	0.8880
62	PQ	0.0320	0.0230
63	PQ	0.0000	0.0000
64	PQ	0.2270	0.1620
65	PQ	0.0590	0.0420
66	PQ	0.0180	0.0130
67	PQ	0.0180	0.0130
68	PQ	0.0280	0.0200
69	PQ	0.0280	0.0200

APPENDIX E

List of publications

T. Phimtakhob and K. Chayakulkheeree (2024), Microgrid Voltage Stability Indices Improvement Using Particle Swarm Optimization., 2024 International Electrical Engineering Congress (iEECON2024), Pattaya, Thailand.

T. Phimtakhob and K. Chayakulkheeree (2024), Voltage Deviation Improvement in Active Distribution Network Using Battery Energy Storage System Optimal Voltage Droop Control., GMSARN International Journal.

2024 International Electrical Engineering Congress (iEECON 2024)
March 6-8, 2024, Pattaya Chonburi, THAILAND

Microgrid Voltage Stability Indices Improvement Using Particle Swarm Optimization

Thanarat Phimtakhob, Keerati Chayakulkheeree
School of electrical engineering
Institute of Engineering
Suranaree University of Technology
Nakhon Ratchasima, Thailand
Thanarat.ptk@gmail.com, keerati.ch@sut.ac.th

***Abstract*— This paper provides a strategy for improving microgrid voltage stability indices (VSI) using particle swarm optimization (PSO). The L-index value is used to assess the weak bus of the system. The IEEE 33-bus system is used for evaluating the proposed method, including four cases as follows; the IEEE 33-bus base case, the IEEE 33-bus with L-index improvement, the IEEE 33-bus as microgrid (MG), and the modified IEEE 33-bus as microgrid with L-index improvement. For VSI improvement, PSO is utilized to determine the generator bus voltages for minimizing the L-index. The proposed method can successfully minimize the L-index for both conventional distribution networks and MG systems, from the simulation results.**

Keywords— Voltage Stability, weak bus, L-index, PV-curve, optimization

I. INTRODUCTION

The electrical system operation has changed significantly in recent years. This is due to an increment in distributed energy resources (DERs) that drives the distribution networks to the active distribution network (ADNs) or microgrids (MGs) [1]. An MG is a small system that combines multiple generators and loads. In the MG system, most of the energy used is from Renewable energy resources include solar cells, wind power, and so on [2]. MG operation can help the system in terms of reliability by reducing the cost of producing electricity [3]. However, maintaining stability in the MG system is critical for both voltage and frequency stabilities. A microgrid system's operating mode has a significant impact on its performance and dependability. MG operating modes are classified into two types: grid-connected and isolated. In grid-connected mode, the MG system connects to the main grid and can exchange power and energy with it. In isolated mode, the microgrid is detached from the main grid, and supplying the load by its own distributed energy resources. MG systems may face abnormal conditions while transitioning from grid-connected to isolated mode. Specifically in terms of voltage stability. As a result, having the right tools and methodologies is critical for ensuring voltage stability in isolated MG systems [4]. As a result, rigorous monitoring and oversight are required to ensure that the electrical system is as stable as feasible [5]. The Countries that experienced voltage collapse and long-term power outages are occurs include Bangladesh, the United States, Japan, and Canada [6-7]. From history, it can be observed that no matter how complex the system that the voltage collapse can happen.

Voltage stability is a fundamental feature of power system functioning, and it refers to an electrical network's ability to maintain a stable and appropriate voltage profile under various operating conditions [8]. Voltage is a basic element in an electric power system that must be controlled within specific parameters to ensure the dependable and secure delivery of electricity to users. Voltage instability occurs when voltage levels in the electrical grid deviate significantly from their nominal values, which can cause a variety of problems such as voltage sags, voltage collapses, and even blackouts. The overall stability and dependability of the electrical system may be significantly impacted by this [9].

The voltage stability index (VSI), provides a sufficiently precise and more pragmatic approach to assessment, enabling the representation of stability analysis in a straightforward manner [10]. There are many indicators proposed to forecast or detect voltage collapse in the power system. Phanikumar and Kanta Rao use the model analysis method and sensitive method to observe the stability of the power system [11]. Reference [12] employs the fast voltage stability index to detect weak lines and weak buses. In addition, reference [13] determines the weak bus using the L-index. Vadivelu shows how to calculate the maximum load capacity of an electrical system using a line voltage stability index, such as the fast voltage stability index [14]. Salama and Vokony examine and analyze several voltage stability indexes, including the line index and bus index, presenting benefits, drawbacks, and calculation formulas [15].

This paper uses the L-index values to determine which bus in the system is the weakest. The voltage stability improves with a lower L-index value. Each load bus contains its own L-index based on the power network admittance characteristic. By using particle swarm optimization (PSO), the optimal generator voltage that minimizes the L-index value can be obtained. Finally, PV curves for the weakest buses of the system are determined to evaluate the system performance.

The paper is structured as follows: Section 1 addresses an introduction Section 2 illustrates the L-index computation Section 3 contains the proposed technique Section 4 provides and discusses the simulation results and Section 5 gives the conclusion.

II. L-INDEX

In this study, the L-index is used to predict the incidence of electrical collapse and it is a simple technique for calculating and identifying weak busses. therefore, it is a tool that may be improved to increase system stability. Using the following equation:

2024 12th International Electrical Engineering Congress (iEECON) | 979-8-3503-8359-1/24/$31.00 ©2024 IEEE | DOI: 10.1109/IEECON60677.2024.10537938

2024 International Electrical Engineering Congress (iEECON 2024)
March 6-8, 2024, Pattaya Chonburi, THAILAND

Before determining the indicator L, evaluate the current flow in the system using the following equation:

$$I_{bus} = Y_{bus} V_{bus} \tag{1}$$

And because the system includes multiple buses, we can consider them in the matrix.

$$\begin{bmatrix} \mathbf{I^G} \\ \mathbf{I^L} \end{bmatrix} = \begin{bmatrix} \mathbf{Y^{GG}} & \mathbf{Y^{GL}} \\ \mathbf{Y^{LG}} & \mathbf{Y^{LL}} \end{bmatrix} \begin{bmatrix} \mathbf{V^G} \\ \mathbf{V_L} \end{bmatrix} \tag{2}$$

$$\mathbf{I^G} = \mathbf{Y^{GG}V^G} + \mathbf{Y^{GL}V^L} \tag{3}$$

$$\mathbf{I^L} = \mathbf{Y^{LG}V^G} + \mathbf{Y^{LL}V^L} \tag{4}$$

Where $\mathbf{I^G}$ is current at generator bus, $\mathbf{I^L}$ is current at load bus, $\mathbf{V^G}$ is voltage at generator bus and $\mathbf{V^L}$ is voltage at load bus After some mathematical manipulation, equation (2) can be written as equations (5)–(7).

$$\mathbf{V^L} = [\mathbf{Y^{LL}}]^{-1}\mathbf{I^L} - [\mathbf{Y^{LL}}]^{-1}\mathbf{Y^{LG}V^G} \tag{5}$$

$$\mathbf{I^G} = \mathbf{Y^{GL}}[\mathbf{Y^{LL}}]^{-1}\mathbf{I^L} + (\mathbf{Y^{GG}} - \mathbf{Y^{GL}}[\mathbf{Y^{LL}}]^{-1}\mathbf{Y^{LG}})\mathbf{V^G} \tag{6}$$

Equations (5) and (6) in matrix form

$$\begin{bmatrix} \mathbf{V^L} \\ \mathbf{I^G} \end{bmatrix} = \begin{bmatrix} [\mathbf{Y^{LL}}]^{-1} & -[\mathbf{Y^{LL}}]^{-1}\mathbf{Y^{LG}} \\ \mathbf{Y^{GL}}[\mathbf{Y^{LL}}]^{-1} & \mathbf{Y^{GG}} - \mathbf{Y^{GL}}[\mathbf{Y^{LL}}]^{-1}\mathbf{Y^{LG}} \end{bmatrix} \begin{bmatrix} \mathbf{I^L} \\ \mathbf{V^G} \end{bmatrix} \tag{7}$$

Rearranging the above matrix we get,

$$\begin{bmatrix} \mathbf{V^L} \\ \mathbf{I^G} \end{bmatrix} = \begin{bmatrix} \mathbf{Z^{LL}} & \mathbf{F^{LG}} \\ \mathbf{K_{GL}} & \mathbf{Y^{GG}} \end{bmatrix} \begin{bmatrix} \mathbf{I^L} \\ \mathbf{V^G} \end{bmatrix} \tag{8}$$

$$\mathbf{F_{LG}} = -\mathbf{Y_{LL}}^{-1}\mathbf{Y_{LG}} \tag{9}$$

$$L_j = \left| 1 - \sum_{i=1}^{i=g} F_{ij} \frac{V_i}{V_j} \right| \tag{10}$$

Where,

g is the total number of generators,

L_j is the L-index value of the bus,

V_i is the voltage at the generator bus,

V_j is the voltage at the load bus j,

F_{ij} is the element of the $\mathbf{F_{LG}}$ matrix obtained by (9) [16].

$\mathbf{Y_{LL}}$ and $\mathbf{Y_{LG}}$ are the submatrix of $\mathbf{Y_{bus}}$ that rearranged to represent the correlation between load buses and between load and generator buses, respectively.

Prior to computing the L-Index, the voltage values for each system bus and Y-bus must be known. These are computed using the Newton-Raphson load flow (NRLF) method. Next, the matrix $\mathbf{F_{LG}}$ is obtained by converting it from Y-bus. Then (10) is used in order to obtain the value of the L-Index. Note that the L-Index holds the value for only load buses. Furthermore, if the L-Index value is closest to 1, it indicates that the bus is the weakest bus and could potentially cause the voltage collapse to the system. Conversely, the most powerful bus is indicated by the L-Index value closest to 0.

III. Voltage Stability Improvement Using PSO

PSO is a well-known metaheuristic approach inspired by birds flocking to find food. It iteratively searches the solution space by adjusting particle positions until it discovers the best-known and global best positions, with the goal of finding an optimal solution. as well as velocity updates [17].

PSO emerges as a potential method for improving voltage stability in microgrid systems. It accomplishes this by determining the appropriate generator bus voltage to reduce the L-index, which is a critical indicator of the voltage stability margin. PSO's intrinsic features, such as simplicity, computational efficiency, and adaptability, make it ideal for use in this case.

The objective function or fitness function to minimize the L-index value of the weakest bus can be written as,

$$\text{minimize} \qquad f(x_i^t) = \max\{\text{L-index}\}, \tag{11}$$

and the following equations are used to compute velocity and position,

$$v_i^{t+1} = wv_i^t + c_1 r_1 (pBest_i^t - x_i^t) + c_2 r_2 (gBest_i^t - x_i^t), \tag{12}$$

$$x_i^{t+1} = x_i^t + v_i^t. \tag{13}$$

Where,

$pBest$ is the best value of each particle, where $pBest$ used to update the population,

$gBest$ is the best value of all particles,

t and $t+1$ is the iteration,

v_i is the velocity for particle i,

c_1 and c_2 is a constant numbers,

r_1 and r_2 is a random parameters,

w is inertial weight, and

x_i is the population of particles that represent the generator's voltage values. The lowest and top limits of the generator's voltage are 0.9 and 1.1, respectively. The proposed PSO based VSI improvement computational procedure is illustrated in Fig. 1.

Another crucial instrument for assessing the stability of a system is the PV curve. PV curve is obtained by step-wise increasing the real power loading of the selected bus and calculating the load flow to obtain the bus voltage. The computational step is repeated until the load flow is infeasible. Then, the plot between the bus real power load and the bus voltage or PV curve can represent the voltage collapse characteristic of the system [18].

2024 International Electrical Engineering Congress (iEECON 2024)
March 6-8, 2024, Pattaya Chonburi, THAILAND

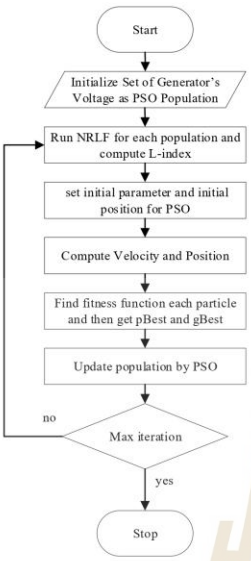

Fig. 1. Computation Procedure

IV. RESULTS AND DISCUSSION

This section displays the results of the suggested approach on the IEEE 33-bus system. It is separated into four cases, as shown below.

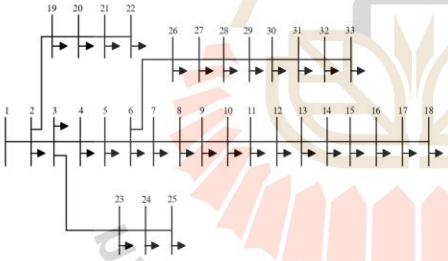

Fig. 2. IEEE 33-bus system

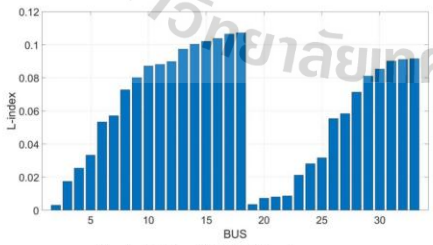

Fig. 3. L-index of IEEE 33-bus base case

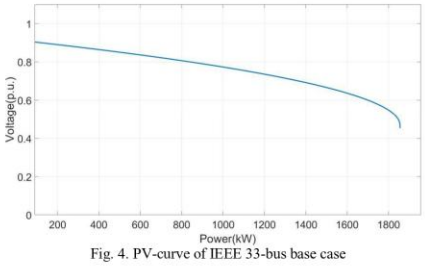

Fig. 4. PV-curve of IEEE 33-bus base case

A. *IEEE 33-bus base case*

As illustrated in Fig. 2, the base case IEEE 33-bus system consists of one slack bus and 32 load buses, with the voltage value at the slack bus set to 1 p.u.

Figure 3 depicts the L-Index values of each bus. Bus 18 provides the most L-Index value, so it is the weak bus. Meanwhile, bus 2 resulted in lower L-Index value and, therefore, it is a strong bus. Bus 18 has the highest possibility of voltage collapse of this system. Figure 4 shows the PV-curve of bus 18, where the voltage is collapsed at 1854.9 kW of power leading.

B. *IEEE 33-bus with L-index improvement*

With the proposed method, the optimal value for the generator voltage at the slack bus is 1.1 p.u.

Figure 5 shows that in this optimized system, the L-index value is reduced. Bus 18 is still a weak bus, as is Bus 2, which is still a strong bus. However, when compared with the previous case, the L-index value is lower. Figure 6 shows the PV curve of the optimized system. The maximum loading capability of bus 18 is increased to 2355.3 kW.

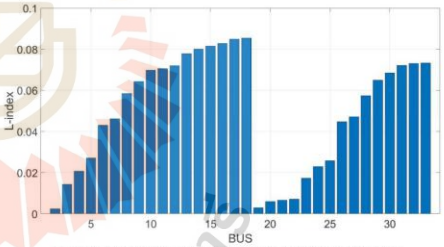

Fig. 5. L-index of IEEE 33-bus with L-index improvement

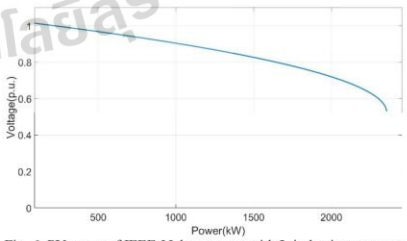

Fig. 6. PV-curve of IEEE 33-bus system with L-index improvement

2024 International Electrical Engineering Congress (iEECON 2024)
March 6-8, 2024, Pattaya Chonburi, THAILAND

C. IEEE 33-bus Modified

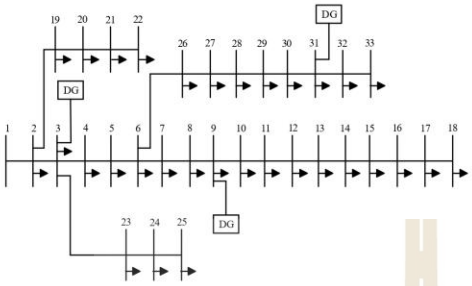

Fig. 7. Modified IEEE 33-bus system

In this case, the IEEE 33-bus system is modified by adding three distributed generators (DGs) at buses 3, 9, and 31 with power generators of 1.9 MW, 0.95 MW, and 1.69 MW, respectively [19]. Bus 1 is disconnected from the main power grid for the MGs case study. The values of the voltages at all generator buses are set to 1 p.u. Bus 3 is set to slack bus.

Figure 8 shows the L-index of the modified IEEE 33-bus, similarly Bus 18 is a weaker bus, while bus 2 is a stronger bus. As observed, the weak bus is the farthest bus from the power sources. On the other hand, the strong bus is the nearest to the power sources. Figure 9 shows the PV-curve of bus 18, The maximum loading capability is 3852.9 kW.

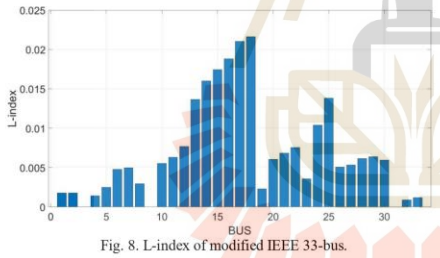

Fig. 8. L-index of modified IEEE 33-bus.

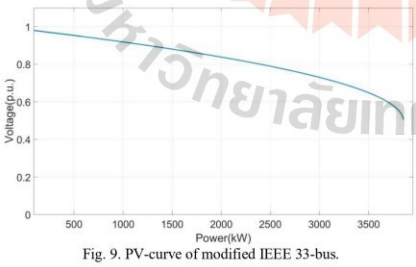

Fig. 9. PV-curve of modified IEEE 33-bus.

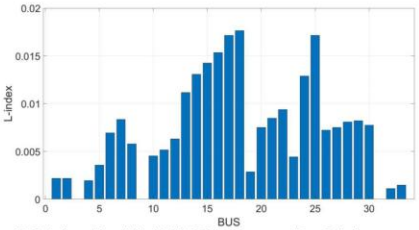

Fig. 10. L-index of modified IEEE 33-bus system with L-index improvement.

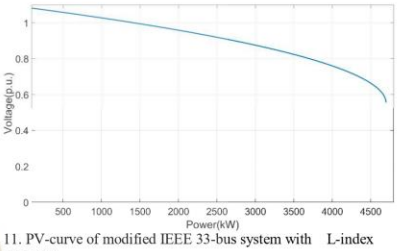

Fig. 11. PV-curve of modified IEEE 33-bus system with L-index improvement.

D. Modified IEEE 33-bus system with L-index improvement.

Figure 10 depicts the L-index values for each bus in the modified IEEE 33-bus system. The L-index value has decreased significantly when compared to previous cases. Bus 18 is a weak bus, while Bus 2 is a strong bus.

Figure 11 shows the PV curve of the modified IEEE 33-bus system with L-index improvement. It is found that in this case, the maximum loading is increased to 4698.9 kW, indicating that the system can handle a higher loading level. this system is very stable.

From Table 1, it is found that for systems voltage stability has been improving, with a reduction of the L-Index values. This reduction in L-Index values significantly improves system stability by the optimization process. The L-index values that are not presented in the table are those at the PV bus, where the L-index computation solely applies to bus loads. The PV buses are IEEE 33-bus base case system bus 1 and IEEE 33-bus Modified system buses 3, 9, and 31. In assessing the system stability, bus 18 emerges with the highest L-index value. This observation implies that bus 18 is the least reliable and possesses the greatest potential to induce system instability. Consequently, to uphold system stability, particular attention should be directed towards bus number 18 within the system. Addressing or optimizing the conditions associated with Bus 18 becomes critical in preserving the overall stability of the IEEE 33-bus system.

The PV curves also show that the modified IEEE 33-bus system is the most stable, as it can handle the highest load compared to other cases.

2024 International Electrical Engineering Congress (iEECON 2024)
March 6-8, 2024, Pattaya Chonburi, THAILAND

TABLE I. COMPARING L-INDEX VALUE

BUS	L-index			
	IEEE 33-bus base case	***IEEE 33-bus with L-index improvement***	***IEEE 33-bus Modified***	***IEEE 33-bus Modified with L-index improvement***
1	-	-	0.001772	0.00219
2	0.003004	0.002454	0.001772	0.00219
3	0.017498	0.014244	-	-
4	0.025411	0.020637	0.001415	0.00195
5	0.033364	0.02704	0.002505	0.003562
6	0.053276	0.042984	0.004789	0.00692
7	0.057172	0.046085	0.004961	0.008352
8	0.072771	0.05846	0.002968	0.005789
9	0.080183	0.064309	-	-
10	0.087129	0.069775	0.001415	0.00195
11	0.088143	0.070571	0.002505	0.003562
12	0.089917	0.071964	0.004789	0.00692
13	0.097415	0.077838	0.004961	0.008352
14	0.100304	0.080097	0.002968	0.005789
15	0.102096	0.081497	0.017461	0.014241
16	0.103813	0.082837	0.018828	0.015352
17	0.10646	0.084901	0.021021	0.017133
18	0.107227	0.085498	0.021628	0.017626
19	0.003527	0.002885	0.002313	0.00286
20	0.00723	0.005937	0.006068	0.007512
21	0.007993	0.006564	0.006841	0.008471
22	0.008698	0.007145	0.007558	0.009361
23	0.021172	0.017244	0.003574	0.004428
24	0.028149	0.022928	0.01038	0.012882
25	0.031696	0.025812	0.013806	0.017149
26	0.055454	0.044721	0.005074	0.007212
27	0.058377	0.047049	0.005345	0.00751
28	0.071425	0.057412	0.006137	0.008081
29	0.081028	0.065007	0.006387	0.008205
30	0.085367	0.068429	0.00597	0.007742
31	0.090123	0.072171	-	-
32	0.091174	0.072997	0.000907	0.00112
33	0.0915	0.073253	0.001192	0.001471

V. CONCLUSION

The proposed PSO based VSI improvement was tested with the IEEE 33-bus system, under the conventional distribution system, and modified to the MG system. The primary objective is to identify the bus exerting the most significant influence on system instability, utilizing the L-index. The results demonstrated that the proposed method could reduce the L-index of the system's weakest bus., leading to voltage stability improvement and loading capability increment. In future work, additional factors of voltage regulation could be studied using data from the reliable L-index as a consistent bus selection criterion to maintain system stability.

ACKNOWLEDGMENT

We want to offer our profound gratitude to Suranaree University of Technology for their invaluable assistance with scholarships and resources during the period of this research project. Their vast knowledge and unwavering support were critical in bringing this study to a successful conclusion.

REFERENCES

[1] I. G. Adebayo and Y. Sun, "A comparison of voltage stability indices for critical node identification in a power system," *2021 International Conference on Sustainable Energy and Future Electric Transportation (SEFET)*, Jan. 2021.

[2] L. Jimin and N. Ming, "Overview on microgrid research and development," in *Communications in computer and information science*, 2010, pp. 161–168.

[3] A. Kumar, M. Z. U. Khan, and D. M. A. Hussain, "Microgrids Technology: A Review paper," *Gyancity Journal of Electronics and Computer Science*, vol. 3, no. 1, pp. 11–20, Mar. 2018.

[4] R. Kljajić, P. Marić, H. Glavaš, and M. Žnidarec, "Microgrid Stability: A Review on Voltage and Frequency Stability," *2020 IEEE 3rd International Conference and Workshop in Óbuda on Electrical and Power Engineering (CANDO-EPE)*, Nov. 2020.

[5] Y. A. Mashhadany, A. K. Abbas, and S. Algburi, "Study and analysis of power system stability based on FACT Controller System," *Indonesian Journal of Electrical Engineering and Informatics*, vol. 10, no. 2, Jun. 2022.

[6] R. Gadal, A. Oukennou, F. Elmariami, A. Belfqih, and N. Agouzoul, "Voltage Stability Assessment and Control Using Indices and FACTS: A Comparative review," *Journal of Electrical and Computer Engineering*, vol. 2023, pp. 1–18, Aug. 2023.

[7] C. Dondariya, D.K. Sakravdia, "A comprehensive investigation on voltage stability indices for distributed generation placement and sizing," 2021.

[8] Ieee Committee Report, Voltage Stability of Power Systems: Concepts Analytical Tools and Industry Experience, Springer, Berlin, Germany, 1990.

[9] H. H. Alhelou, M. E. Hamedani-Golshan, T. C. Njenda, and P. Siano, "A survey on power system blackout and cascading Events: Research Motivations and challenges," *Energies*, vol. 12, no. 4, p. 682, Feb. 2019.

[10] E. Z. Yahia, M. Elsherif, and M. Zaggout, "Detection of proximity to voltage collapse byUsing 1 ÃçÂÂIndex," *International Journal of Innovative Research in Science, Engineering and Technology*, vol. 4, no. 3, pp. 1755–1765, Jul. 2015.

[11] M. S. V. Phanikumar and P. Rao, "Comparison of voltage stability and loss reduction by modal analysis and sensitivity methods," vol. 16, pp. 183-188, 01/01 2016.

[12] I. G. Adebayo, A. A. Jimoh, and A. A. Yusuff, "Detection of weak bus through Fast Voltage Stability index and inherent structural characteristics of power system," *2015 4th International Conference on Electric Power and Energy Conversion Systems (EPECS)*, Nov. 2015.

[13] A. K. Karn, S. Hameed, and M. Sarfraz, "Identification of Strong and Weak Bus and Optimal Bus Coupling by L —Index Coefficients For Voltage Regulation in Power System," *2023 International Conference on Power, Instrumentation, Energy and Control (PIECON)*, Feb. 2023.

[14] A. K. Sharma, A. Saxena, R. Tiwari, and R. Scholar, "Maximum Loadability Estimation for Weak Bus Identification using Line Stability Indices," *ResearchGate*, Jan. 2017.

[15] H. S. Salama and I. Vokony, "Voltage stability indices–A comparison and a review," *Computers & Electrical Engineering*, vol. 98, p. 107743, Mar. 2022.

[16] P. Kessel and H. Glavitsch, "Estimating the voltage stability of a power system," *IEEE Transactions on Power Delivery*, vol. 1, no. 3, pp. 346–354, Jan. 1986.

[17] J. Kennedy and R. C. Eberhart, "Particle swarm optimization," *Proceedings of ICNN'95 - International Conference on Neural Networks*, Nov. 2002.

[18] T. Van Cutsem and C. Vournas, Voltage stability of electric power systems. Springer, 1998.

[19] M. V. Kirthiga and S. A. Daniel, "Computational techniques for autonomous microgrid load flow analysis," *ISRN Power Engineering*, vol. 2014, pp. 1–12, May 2014.

Voltage Deviation Improvement in Active Distribution Network Using Battery Energy Storage System Optimal Voltage Droop Control

Thanarat Phimtakhob [1] and Keerati Chayakulkeeree [1,*]

ARTICLE INFO

Article history:
Received:
Revised:
Accepted:

Keywords:
Battery Energy Storage
Voltage Regulation
Voltage Deviation
Adaptive Droop Control
Particle Swarm Optimization

ABSTRACT

This work proposes the implementation of battery energy storage system (BESS) management for voltage regulation in the active distribution network (ADN). The primary goal is to minimize the overall voltage deviation of all buses in the power system. Adaptive droop control is employed to regulate BESS and optimize the efficiency of battery operation. In order to enhance the performance of the battery energy storage system, the study employs particle swarm optimization (PSO) to identify the most effective control parameters. To validate the efficacy of the proposed methodology, its performance is examined utilizing an IEEE 33-bus distribution system by testing scenarios both with and without renewable energy sources such as photovoltaic panels and wind turbines. The results demonstrate that the approach extensively decreases the voltage deviation in three scenarios, including with/without BESS. The optimization of BESS management can effectively confine the voltage within the established range of 0.95 – 1.05 and minimize the voltage deviation of all buses to a minimum of 0.0385 p.u. Consequently, this leads to an enhancement in the voltage profile, power quality, and system dependability.

1. INTRODUCTION

Voltage stability in the electrical system is extremely important and must be prioritized. In modern distribution network (DN), renewable energy is currently increasing rapidly, due to the increase in photovoltaic (PV) and wind power. Therefore, many DNs have been transformed into active distribution network (ADNs). The main issue with renewable energy is the discontinuity of the energy that can be generated [1]. These are the challenges that make ADN voltage control more difficult. One of the key indices for voltage stability is voltage deviation (VD). It measures the difference of voltage value from the nominal value. If it exceeds the specified standard, it may have an impact on system efficiency or even cause damage to electrical equipment [2-4]. As a result, many tools have been developed over time to help maintain voltage stability, including transformer load tap changes, shunt capacitor banks, and STATCOM [5]. These tools help to enhance the stability of the electrical system. For example, Sarithumu et al. [6] developed a strategy to regulate voltage in networks with a high level of renewable energy penetration, making the use of traditional tools or methods ineffective, Thus, a technique utilizing on-load tap changer voltage regulation was devised for voltage control. According to Abedini et al. [7], shunt capacitor banks can give a good solution for voltage profile problems in power systems by delivering reactive power to the system, but they still have the problem of transient signals, which might impact sensitive devices. According to Gurav and Mittal [8], STATCOM can supply fast reactive power, but it is not always effective due to the trial-and-error control strategy in controller configuration. Similarly, Xu and Li [9] claimed that classical STATCOM control should not be used in engineering or the real world, despite the fact that it has the advantage of providing fast reactive power.

As mentioned, most conventional devices still have several limitations compared to battery energy storage system (BESS), such as fast response, which can bring more benefits than just voltage regulation. As a result, the usage of BESS is intriguing and has great promise for controlling voltage in power systems and resolving VD issues [10]. BESS has several operating functions, for example, energy arbitrage that provides lowering electricity cost, peak shaving for reducing the peak demand, and even store the excess energy for utilizing in the shortage period [11]. In addition, BESS can also regulate the system frequency and voltage [12]. However, for batteries to function optimally, they must be properly managed or controlled. Several research studies have explored battery management strategies. Mohammed et al. [13] focus on improving the sizing of a stand-alone hybrid energy system that consists of three components: PV, diesel generator, and BESS. Saini and Gidwani [14] use BESS as an alternative load for charging and discharging. The objective is to minimize

[1] *School of Electrical Engineering, Institute of Engineering, Suranaree University of Technology, Nakhon Ratchasima, Thailand*
**Corresponding author:* Email: keerati.ch@sut.ac.th

yearly energy losses, alleviate reverse power flow, and resolve overvoltage challenges in an IEEE 69-bus system integrated with PV. Tamrakar et al. [15] suggest employing BESS to replace outdated equipment like on-load tap changer capacitor banks. To improve system dependability, Zhang et al. [16] presents a multi-agent system-based control approach for energy storage and PV inverters. Alam et al. [17] presents a novel charge and discharge control scheme that takes into account the status of the charging current. Considering the impact of solar cells in the system in terms of energy efficiency, the storage is utilized to catch the extra energy produced by PV during the PV peak and store it for peak load support. Tandon et al. [18] discovered the optimal allocation of BESS to increase system performance while taking into account load volatility, renewable energy sources, and network constraints. Alzahrani et al. [19] used BESS in a system with high PV deployment to explore system loss and power quality issues, employing a genetic algorithm-based placement methodology. Wang et al. [20] proposed employing BESS to address voltage instability issues in low-voltage grids with high rooftop PV penetration, considering the state of charge (SoC). Rouzbehi et al. [21] proposed a generalized voltage droop (GVD) control approach to address the voltage rise issue. GVD operates in three modes: fixed voltage control, fixed active power control, and traditional voltage droop control (VDC), all of which can be changed using the GVD characteristic of a voltage regulation inverter. Zeraati et al. [22] employed BESS to handle various voltage difficulties, such as voltage rise, and presented a collaboration between a local droop-based control approach for battery installation size and a distributed control system to manage SoC performance to prevent battery saturation. Chen et al. [23] suggested a fuzzy logic-based adaptive droop controller to alter the droop coefficient, resulting in a compromise between DC. Jamreon and Sirisukprasert [24] presented a voltage control technique integrating battery energy storage with SoC management. The battery control employs adaptive droop control as a power supply controller, as well as self-learning particle swarm optimization (PSO) to optimize the operational performance of BESS. Jamroen et al. [25] proposed an adaptive droop-based method that takes into account the SoC system to manage the functioning of BESS in a low voltage (LV) system. The objective is to mitigate voltage rise caused by high solar penetration by enhancing voltage regulation and power-sharing efficiency using fuzzy logic.

The literature research revealed that the current instability of renewable energy poses a variety of issues. This study presents a solution to mitigate the impact of renewable energy on VD in ADN. The optimum BESS management is achieved by adopting a VDC approach that employs BESS to charge and discharge energy to the system. The adaptive droop control approach was chosen for BESS management because it allows the droop coefficient to be chosen as desired and appropriate, as well as taking into account the SoC level. In addition, the PSO is used to get the most appropriate droop coefficient value for battery control. The IEEE 33-bus test system was chosen as a test system because it is a distribution system with voltage levels lower than the standard criterion, making it acceptable for testing.

The following sections of this paper are organized as follows: Section 2 presents a mathematical analysis of BESS management. Section 3 provides an explanation of the voltage regulation technique developed with the PSO algorithm. Section 4 details the simulation analysis and results, while Section 5 concisely summarizes the conclusion.

2. BESS WITH ADAPTIVE VOLTAGE DROOP CONTROL

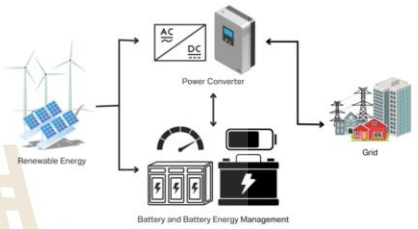

Fig. 1. BESS configuration

The BESS configuration is shown in Fig. 1, which includes the following main elements: a battery for storing energy, a battery energy management system for controlling BESS operation, and a power converter for energy conversion.

In this study, we focus on the battery and its energy management system. This study presents a method for controlling battery operations to resolve the VD issue. The battery can either provide or receive active power from the grid. When the BESS supplies active power to the grid, the voltage level rises, whereas when it absorbs active power from the grid, the voltage level drops. Thus, the BESS's operation can affect the voltage when the active power changes. Therefore, effective BESS operation relies heavily on battery energy management. According to a review, Fig. 2 shows that the VDC has three modes: (1) Mode 1 (Fixed Voltage): Keeps the voltage at a predetermined level and allows the battery power to adjust as needed, (2) Mode 2 (Fixed Power): Keeps the battery's power output constant, (3) Mode 3 (Droop Control): Uses a droop coefficient to determine how much power the battery delivers or consumes depending on the grid voltage.

This study uses the droop control method (Mode 3) to regulate battery operation because it can adjust the droop coefficient, allowing the voltage level to be freely regulated [24], [26]. Fig. 3 illustrates the operating concept as follows:

• 1: If the bus voltage of the battery exceeds the maximum voltage ($V_{\max}$), the battery will charge the maximum power into the system.
• 2: If the bus voltage value of the battery is less than the maximum voltage ($V_{\max}$) but larger than the maximum voltage thresholds ($V_{\text{th}}^{\max}$), the battery will charge power based on VD, which is governed by the droop coefficient.
• 3: If the battery's bus voltage value falls within the range of the minimum voltage thresholds ($V_{\text{th}}^{\min}$) and the maximum voltage thresholds ($V_{\text{th}}^{\max}$) or the deadband range, the battery will not charge or discharge at all.
• 4: If the bus voltage value of the battery is larger than the minimum voltage ($V_{\min}$) but less than the minimum voltage thresholds ($V_{\text{th}}^{\min}$), the battery will discharge the power based on VD, which is governed by the droop coefficient.
• 5: If the battery's bus voltage value is less than the minimum voltage ($V_{\min}$), it will discharge the maximum power back.

It can be represented mathematically as an equation given below:

$$P_{BES} = \begin{cases} -P_{BES}^{\max} & \text{if } V_i \geq V^{\max} \\ k_{BES,c(SoC)}\Delta V & \text{if } V_{\text{th}}^{\max} < V_i < V^{\max} \\ 0 & \text{if } V_{\text{th}}^{\min} \leq V_i \leq V_{\text{th}}^{\max} \\ k_{BES,d(SoC)}\Delta V & \text{if } V^{\min} < V_i < V_{\text{th}}^{\min} \\ P_{BES}^{\max} & \text{if } V_i \leq V^{\min} \end{cases} \quad (1)$$

$$\Delta V = V_i - V_0 \quad (2)$$

Since the battery may be saturated, it cannot be utilized further, causing the system to have a VD value that exceeds the required limit. As a result of the investigation, the SoC level was examined, as shown in the equation below.

$$k_{BES,d} = \begin{cases} 0 & \text{if } 0 < \text{SoC} \leq \text{SoC}_{\min} \\ \dfrac{K_{\max}K_{\min}e^{n_d(SoC-SoC_{\min})}}{K_{\max}+K_{\min}e^{n_d(SoC-SoC_{\min})}-1} & \text{if } \text{SoC}_{\min} < \text{SoC} \leq 1 \end{cases} \quad (3)$$

$$k_{BES,c} = \begin{cases} 0 & \text{if } \text{SoC}_{\max} \leq \text{SoC} < 1 \\ \dfrac{K_{\max}K_{\min}e^{n_c(SoC_{\max}-SoC)}}{K_{\max}+K_{\min}e^{n_c(SoC_{\max}-SoC)}-1} & \text{if } 0 < \text{SoC} < \text{SoC}_{\max} \end{cases} \quad (4)$$

$$SoC(t) = SoC(t-1) - \frac{1}{E}\int P_{BES}(t)dt \quad (5)$$

$$k_{droop} = \begin{cases} k_{BES,c}, \text{ charging} \\ k_{BES,d}, \text{ discharging} \end{cases} \quad (6)$$

$$n = \begin{cases} n_c, \text{ charging} \\ n_d, \text{ discharging} \end{cases} \quad (7)$$

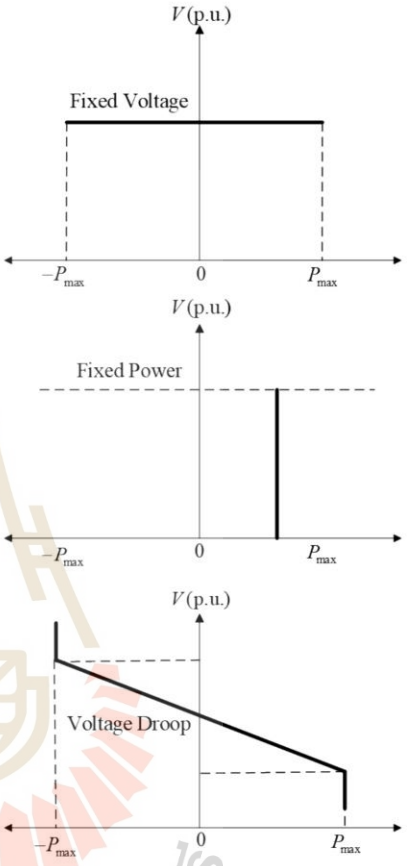

Fig. 2. VDC strategies

When evaluating k_{droop}, it is discovered that this value is related to the determination of $K_{\max}$, $K_{\min}$, SoC, and n As a result, while examining (1), (3), and (4), it can be represented in Fig. 4 and 5. From Fig. 4, it has been discovered that as the SoC of the battery increase, the $k_{BES,d}$ value gradually increases, the $k_{BES,c}$ value gradually decrease. This is because adaptive droop management is intended to protect the battery's

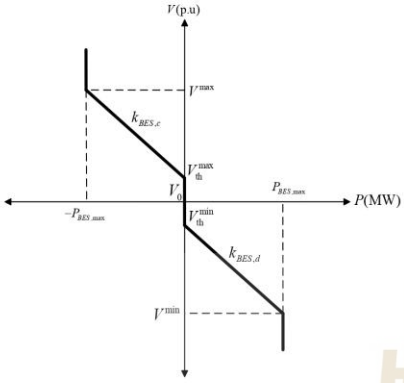

Fig. 3. Adaptive VDC strategy

functionality, which increases the SoC range, resulting in less charging and discharging. On the other hand, a low SoC level in the battery causes it to charge more and discharge less. The aforementioned relationship leads to the design of $K_{\max}$, $K_{\min}$ and n values, demonstrating that $K_{\max}$ and $K_{\min}$ will have a relationship with the desired power output, and n will be the factor determining the battery's power distribution, which is related to SoC, as shown in Fig. 5.

3. PSO BESED VOLTAGE DEVIATION IMPROVEMENT

PSO is a well-known metaheuristic method that mimics bird group's foraging activity. It accomplishes this by altering the locations of particles in search space, directing them toward the best solution discovered, similar to birds following the individual closest to a food source until the food is reached. Consequently, PSO is adept at determining optimal settings by iteratively updating particle positions.

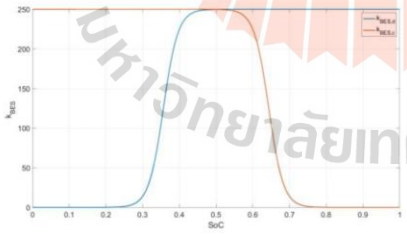

Fig. 4. The Relationship between SoC and k_{BES} with the SoC is within the range of $SoC_{\min}$ and $SoC_{\max}$

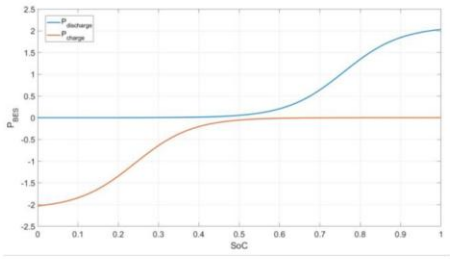

Fig. 5. The Relationship between SoC and n with the SoC is within the range of $SoC_{\min}$ and $SoC_{\max}$

Each parameter or particle updates its position iteratively until reaching the optimal value. The highest-performing value identified within the swarm is termed the global best, or $gBest$, while the best value found by an individual particle is known as the personal best, or $pBest_i$ [27]. This study uses PSO to change the adjustment exponent and calculate the droop efficient value, which is connected to battery operation, leading to the most efficient procedure based on the defined objective function.

This study aims to minimize the system's total voltage deviation (TVD) through the objective function. By reducing the TVD, the stability of the power system can be greatly enhanced. The objective function employed in this study is shown in the following equation.

$$\text{minimize } TVD = \sum_{i=1}^{N} (|V_i - V_0|) \tag{8}$$

and the constraints are defined as follows:

$$P_k^{gen} - P_k^{load} - \sum_{j=1}^{N} [V_k V_j (G_{kj} \cos\theta_{kj} + B_{kj} \sin\theta_{kj})] = 0 \tag{9}$$

$$Q_k^{gen} - Q_k^{load} - \sum_{j=1}^{N} [V_k V_j (G_{kj} \sin\theta_{kj} - B_{kj} \cos\theta_{kj})] = 0 \tag{10}$$

$$V_{\min} \le V_i \le V_{\max} \tag{11}$$

$$SoC_{\min} \le SoC \le SoC_{\max} \tag{12}$$

$$P_{BES,\min} \le P_{BES} \le P_{BES,\max} \tag{13}$$

$$k_{BES,d}^{\min} \le k_{BES,d} \le k_{BES,d}^{\max} \tag{14}$$

$$k_{BES,c}^{\min} \le k_{BES,c} \le k_{BES,c}^{\max} \tag{15}$$

The working equation of PSO is as follows:

$$v_i^{t+1} = wv_i^t + c_1 r_1 (pBest_i^t - x_i^t) + c_2 r_2 (gBest^t - x_i^t) \quad (16)$$

$$x_i^{t+1} = x_i^t + v_i^t \quad (17)$$

where x_i is the population of particles that represent the adjust exponent of $k_{BES,d}$ and $k_{BES,c}$, which are n_d and n_c, respectively. The proposed PSO-based VD improvement computational procedure is illustrated in Fig. 6.

4. RESULTS AND DISCUSSION

The test was conducted on the IEEE 33-bus system, which includes one generator bus and 32 load buses, where bus 1 is designated as the slack bus. The system's voltage restrictions range from 0.9 to 1.1 p.u. The system contains 3.715 MW of real power load and 2.3 MVar of reactive power load. The substation's nominal voltage is configured at 13.8 kV, with the transformer at bus 1 having a capacity of 3 MW. [28], [29]. In the simulation, the experiment is conducted as a single fixed-load test.

Table 1 also provides the study's parameters, which were evaluated and adjusted as needed, mostly through trial and error. The battery size was selected by using trial-and-error to adjust parameters, so they suit the operation of the IEEE 33-bus power system under both non-renewable and renewable energy conditions. From these trials, it was found that a 2 MWh size is appropriate for this system. The variable n specifies how quickly the battery can charge or discharge. A larger n allows faster charging or discharging when the BESS SoC is near its maximum or minimum, whereas a smaller n slows charging or discharging when the BESS SoC is near the nominal level. Therefore, we conducted trials to adjust these ranges, as illustrated in Fig 5.

The test is divided into three scenarios, as follows:

- case I: base case,
- case II: modified IEEE 33-bus with PV and wind power penetration, and
- case III: modified IEEE 33-bus with PV and wind power penetration and BESS with optimal VDC.

The system with renewable energy and BESS is shown on Fig. 7.

4.1 IEEE 33-bus base case

An initial test was conducted on an IEEE 33-bus distribution system. The voltage of each bus in the system ranges from 0.9038 p.u. to 1.0000 p.u., and the TVD is 1.8047 p.u., This significant deviation indicates that the bus voltages are not within the typical standard range of 0.95 p.u. to 1.05 p.u. The bus with the lowest value is Bus 18. Consequently, the lower-voltage bus should be prioritized to prevent power system instability, which could potentially lead to blackouts.

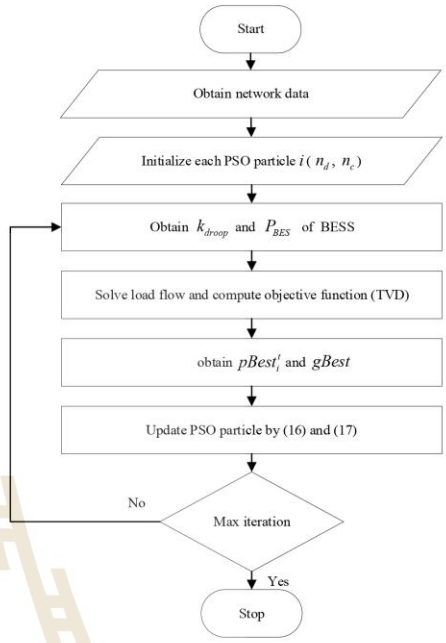

Fig. 6. The PSO based BESS optimal VDC computation procedure

Table 1. Specification of the BESS

Parameter	Specification
Range of the adjust exponent (n_d , n_c)	-100 to 100
The maximum power of battery (P_{BES}^{max})	2 MW
The maximum droop coefficient (K_{max})	250
The minimum droop coefficient (K_{min})	0.1
Nominal Voltage (V_0)	1.00 p.u.
Battery capacity (E)	2 MWh
The maximum voltage (V_{max})	1.10 p.u.
The minimum voltage (V_{min})	0.90 p.u.
Maximum state of charge (SoC_{max})	0.8 p.u.
Minimum state of charge (SoC_{min})	0.2 p.u.

4.2 *Modified IEEE 33-bus with PV and wind power penetration*

In this study, PV and wind power, as renewable energy sources, were integrated into an IEEE 33-bus distribution network. Two 1 MW wind turbine generators were installed at buses 18 and 24. Additionally, three 1 MW PV systems were deployed at buses 5, 21, and 31, while four 500 kW PV systems were positioned at buses 8, 12, 28, and 33 [30]. As a result of these renewable energy installations, the system's real power increased to 10.715 MW. It was observed that the system voltage ranged from 1.0000 p.u. to 1.0534 p.u. and that TVD was 0.6879 p.u. These findings indicate that high levels of renewable energy penetration impact the power system, causing over voltages and significant voltage fluctuations that negatively affect the electrical network. Therefore, appropriate energy management strategies should be implemented.

4.3 *Modified IEEE 33-bus with PV and wind power penetration and BESS with optimal VDC.*

In case III, the proposed method incorporates a battery into the system and employs PSO to optimize the system to obtain the best value that minimizes TVD. The PSO parameters are configured as follows w ranges from 0.1 to 1.1, both c_1 and c_2 are set to 1.49 and the maximum iterations is 100, which was selected through multiple trial runs. It was observed that the values generally start to converge around iterations 20-50, so this value was set accordingly. A 2 MWh battery has been installed on buses 18, 21, 24, and 32. The results show that the voltage levels on all buses in the system are within the prescribed range, with TVD being 0.0385 p.u. This adjustment was made using the variables presented in Table 2, specifically the values of the adjust exponent (n), droop coefficient (k_{droop}) and regulating power (P_{BES}) for each battery. The sign of P_{BES} for each value indicates whether the battery is charging or discharging. Specifically, a negative sign denotes that the BESS is charging, whereas a positive sign signifies that it is discharging.

Figure 8 illustrates the voltage profile for all three scenarios, showing that the proposed method maintains the voltage profile within the specified range through efficient battery charging and discharging. Table 3. depicts the 3 scenarios of TVD, indicating that the proposed method also

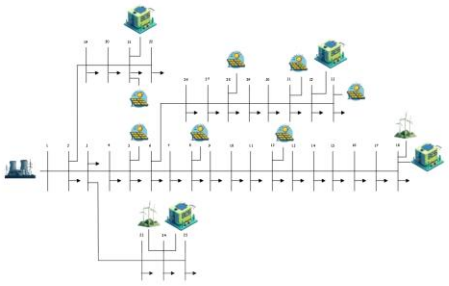

Fig. 7. The modified IEEE 33-bus with PV and wind power penetration and BESS

produces the best results by reducing VD compared to case 1 and 2. Furthermore, Fig. 9 shows the convergence plot of the proposed PSO-based BESS optimal VDC. it is clear that the value of the objective function progressively converges toward the optimal solution. Fig. 10 presents the results of 30 trials conducted using the proposed method that have the average value is 0.0409, standard deviation value is 0.0052, maximum value is 0.0524 and minimum value is 0.0385. The low standard deviation of the objective function values indicates that they are closely clustered, suggesting that the results obtained from PSO algorithm are reliable. The runtime of the proposed method was evaluated over 30 runs on a computer equipped with an AMD Ryzen 5 6600H CPU (3.30 GHz up to 4.50 GHz) and 16 GB of RAM. On average, the method took 774.45 seconds to complete, with a standard deviation of 178.33 seconds. The minimum runtime observed was 591.81 seconds, while the maximum reached 1490.75 seconds. Thus, although the PSO method typically requires about 774.45 seconds, it can occasionally take as long as 1490.75 seconds, likely due to unfavorable random initializations delaying convergence. These results are illustrated in Figure 11.

Table 2. Adjust exponent, Droop coefficient and BEES regulating power of BESS

Bus with Battery Installed	n	k_{droop}	P_{BES} (MW)
18	9.7258	12.3498	-0.6591
21	13.6507	67.4965	-0.6139
24	10.2878	16.0991	-0.0627
32	10.7010	19.5058	-0.5282

Table 3. Adjust exponent, Droop coefficient and BEES regulating power of BESS

Scenarios	TVD (p.u.)
IEEE 33-bus base case	1.8047
Modified IEEE 33-bus with PV and wind power penetration	0.6879
Modified IEEE 33-bus with PV and wind power penetration and BESS with optimal VDC.	0.0385

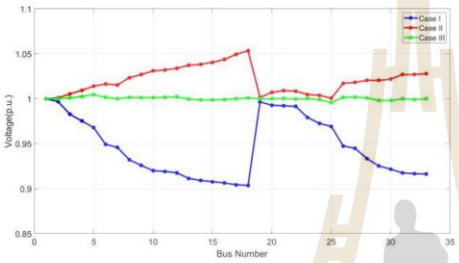

Fig. 8. Comparative Voltage Profile of modified IEEE 33-bus system

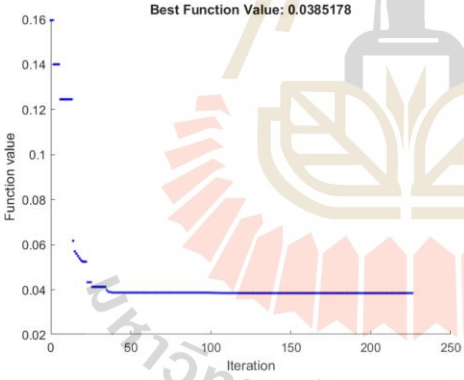

Fig. 9. the convergence plot of the proposed PSO-based BESS optimal VDC

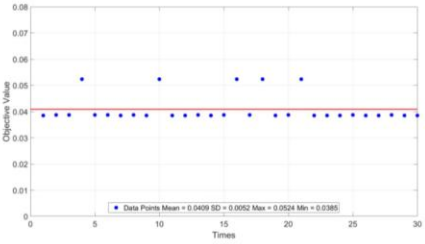

Fig. 10. The result of 30 trials of the proposed method

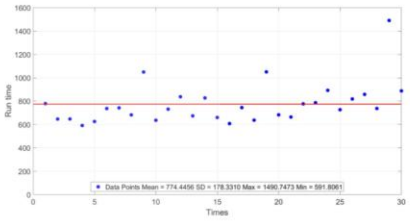

Fig. 11. The result of 30 trials of the computation time

5. Conclusion

This paper introduces a voltage regulation approach utilizing BESS management, tested on an IEEE 33-bus power distribution system. The primary goal is to determine the power value that will minimize TVD. The BESS management employed in this work is VDC, which is responsible for optimizing battery performance and responding to changes in electrical loads. In addition, the PSO approach is employed to determine the settings for BESS control. The results of this study indicate that the proposed method significantly reduces VD, resulting in a more stable power supply. Reducing voltage variation is critical for sustaining power quality and reliability across the power system.

ABBREVIATIONS

P_{BES}	The electrical power that a battery charges or discharges
P_{BES}^{max}	The maximum power that the battery can supply.
k_{droop}	The droop coefficient
$k_{BES,c}$	The droop coefficient controls energy charge.

$k_{BES,d}$	The droop coefficient controls energy discharge.
ΔV	voltage deviation
V_i	Bus voltage
V_0	Nominal voltage
TVD	Total voltage deviation
$V_{\text{th}}^{\max}$	The maximum voltage thresholds
$V_{\min}$	The minimum voltage
$V_{\max}$	The maximum voltage
$K_{\max}$	The maximum droop coefficient
$K_{\min}$	The minimum droop coefficient
n	The adjust exponent
n_d	The adjust exponent for $k_{BES,d}$
n_c	The adjust exponent for $k_{BES,c}$
$SoC(t)$	state of charge at the current step
$SoC(t-1)$	state of charge at the previous step
E	Battery capacity
N	Number of buses
SoC	State of charge
$SoC_{\min}$	Minimum state of charge
$SoC_{\max}$	Maximum state of charge
$P_{BES,\min}$	The minimum power that the battery can supply
$P_{BES,\max}$	The maximum power that the battery can supply
$pBest_i$	The best value of each particle i
$gBest$	The best value of all particles
t	The iteration
v_i	The velocity for a particle i
c_1 and c_2	Constant numbers
r_1 and r_2	Random parameters
w	Inertial weight
x_i	The population of particles i
P_k^{gen}	Active power generated at bus k
P_k^{load}	Active power consumed by the load at bus k
Q_k^{gen}	Reactive power generated at bus k
Q_k^{load}	Reactive power consumed by the load at bus k
G_{kj}	Conductance between bus k and j
B_{kj}	Susceptance between bus k and j
θ_{kj}	Phase angle difference between bus k and j

ACKNOWLEDGEMENTS

We would like to express our profound gratitude to Suranaree University of Technology for their invaluable assistance through scholarships and resources during this research project. Their extensive knowledge and unwavering support were instrumental in bringing this study to a successful conclusion.

REFERENCES

[1] Adetokun, B.B.; Muriithi, C.M.; Ojo, J.O.; and Oghorada, O. 2023. Impact assessment of increasing renewable energy penetration on voltage instability tendencies of power system buses using a QV-based index. Scientific Reports 13(1): 9782.

[2] Adegoke, S.A. and Sun, Y. 2023. Power system optimization approach to mitigate voltage instability issues: A review. Cogent Engineering 10(1): 2153416.

[3] Pachanapan, P.; Kaewchum, T.; and Somkun, S. 2023. Voltage Level Control by Grid-tied Hybrid Photovoltaic and Battery Controllers in Weak Distribution Networks with Electric Vehicles. GMSARN International Journal 17: 291-301.

[4] Pachanapan, P.; Tadthip, A.; and Somkun, S. 2021. Implementation of Single-Phase Grid-Tied Inverter with Voltage Controller for Preventing Over-Voltage Problem in Distribution Networks with Solar PV Rootftops. 15: 59-67.

[5] Sode-Yome, A.; Mithulananthan, N.; and Lee, K.Y. 2007. A Comprehensive Comparison of FACTS Devices for

Enhancing Static Voltage Stability. Proceedings of the 2007 IEEE Power Engineering Society General Meeting. 24-28 June 2007. pp. 1-8.

[6] Sarimuthu, C.; Ramachandaramurthy, V.K.; Ramasamy, A.; and Mokhlis, H. 2016. A review on voltage control methods using on-load tap changer transformers for networks with renewable energy sources. Renewable and Sustainable Energy Reviews 62: 1154-1161.

[7] Abedini, M.; Davarpanah, M.; Sepehr, A.; and Ajaei, F.B. 2020. Shunt capacitor bank: Transient issues and analytical solutions. International Journal of Electrical Power & Energy Systems 120: 106025.

[8] Gurav, P. and Mittal, S.K. 2016. Control of Voltage Regulation Using STATCOM. International Journal of Advanced Research in Electrical, Electronics and Instrumentation Engineering 5(6): 5589-5596.

[9] Xu, Y. and Li, F. 2014. Adaptive PI Control of STATCOM for Voltage Regulation. IEEE Transactions on Power Delivery 29(3): 1002-1011.

[10] Ahmed, H.M.A.; Awad, A.S.A.; Ahmed, M.H.; and Salama, M.M.A. 2020. Mitigating voltage-sag and voltage-deviation problems in distribution networks using battery energy storage systems. Electric Power Systems Research 184: 106294.

[11] Shi, Y.; Xu, B.; Wang, D.; and Zhang, B. 2018. Using Battery Storage for Peak Shaving and Frequency Regulation: Joint Optimization for Superlinear Gains. pp. 1-1.

[12] Shang, L.; Dong, X.; Liu, C.; and Gong, Z. 2022. Fast Grid Frequency and Voltage Control of Battery Energy Storage System Based on the Amplitude-Phase-Locked-Loop. IEEE Transactions on Smart Grid 13(2): 941-953.

[13] Mohammed, A.Q.; Al-Anbarri, K.A.; and Hannun, R.M. 2021. USING PARTICLE SWARM OPTIMIZATION TO FIND OPTIMAL SIZING OF PV-BS AND DIESEL GENERATOR. Journal of Engineering and Sustainable Development 25(3): 51-59.

[14] Saini, P. and Gidwani, L. 2022. An investigation for battery energy storage system installation with renewable energy resources in distribution system by considering residential, commercial and industrial load models. Journal of Energy Storage 45: 103493.

[15] Tamrakar, U.; Nguyen, T.A.; and Byrne, R.H. 2021. Model Predictive Dispatch of Energy Storage for Voltage Regulation in Active Distribution Systems. Proceedings of the 2021 IEEE 30th International Symposium on Industrial Electronics (ISIE). 20-23 June 2021. pp. 1-6.

[16] Zhang, Q.; He, J.; and Zhang, D. 2017. Coordinated control of energy storage devices and photovoltaic inverters for voltage regulation based on multi-agent system. Proceedings of the 2017 IEEE Conference on Energy Internet and Energy System Integration (EI2). 26-28 Nov. 2017. pp. 1-6.

[17] Alam, M.J.E.; Muttaqi, K.M.; and Sutanto, D. 2013. Mitigation of Rooftop Solar PV Impacts and Evening Peak Support by Managing Available Capacity of Distributed Energy Storage Systems. IEEE Transactions on Power Systems 28(4): 3874-3884.

[18] Tandon, A.; Jain, P.; Gauta, T.; Yadav, Y.; Arya, S.; and Solanki, Y. 2024. Battery Energy Storage System Allocation in the IEEE 33 Bus Test System for enhanced system performance. E3S Web of Conferences 559.

[19] Alzahrani, A.; Alharthi, H.; and Khalid, M. 2023. Minimization of Power Losses through Optimal Battery Placement in a Distributed Network with High Penetration of Photovoltaics. Energies 13(1).

[20] Wang, Y.; Tan, K.T.; Peng, X.Y.; and So, P.L. 2016. Coordinated Control of Distributed Energy-Storage Systems for Voltage Regulation in Distribution Networks. IEEE Transactions on Power Delivery 31(3): 1132-1141.

[21] Rouzbehi, K.; Miranian, A.; Candela, J.I.; Luna, A.; and Rodriguez, P. 2015. A Generalized Voltage Droop Strategy for Control of Multiterminal DC Grids. IEEE Transactions on Industry Applications 51(1): 607-618.

[22] Zeraati, M.; Hamedani Golshan, M.E.; and Guerrero, J. 2016. Distributed Control of Battery Energy Storage Systems for Voltage Regulation in Distribution Networks With High PV Penetration. IEEE Transactions on Smart Grid PP: 1-1.

[23] Chen, X.; Wang, L.; Sun, H.; and Chen, Y. 2017. Fuzzy Logic Based Adaptive Droop Control in Multiterminal HVDC for Wind Power Integration. IEEE Transactions on Energy Conversion 32(3): 1200-1208.

[24] Jamroen, C. and Sirisukprasert, S. 2022. A voltage regulation strategy with state of charge management using battery energy storage optimized by a self-learning particle swarm optimization. Computers and Electrical Engineering 101: 108103.

[25] Jamroen, C.; Pannawan, A.; and Sirisukprasert, S. 2018. Battery Energy Storage System Control for Voltage Regulation in Microgrid with High Penetration of PV Generation. Proceedings of the 2018 53rd International Universities Power Engineering Conference (UPEC). 4-7 Sept. 2018. pp. 1-6.

[26] Tan, Z.; Li, X.; He, L.; Li, Y.; and Huang, J. 2020. Primary frequency control with BESS considering adaptive SoC recovery. International Journal of Electrical Power & Energy Systems 117: 105588.

[27] Freitas, D.; Lopes, L.G.; and Morgado-Dias, F. 2020. Particle Swarm Optimisation: A Historical Review Up to the Current Developments. Entropy 22(3).

[28] Isong, U.; Okpura, N.; and Oritsetimeyin Tim, P. 2023. The IEEE 33 Bus Distribution System Load Flow Analysis Using Newton Raphson Method. 10: 2458-9403.

[29] Baran, M.E. and Wu, F.F. 1989. Network reconfiguration in distribution systems for loss reduction and load balancing. IEEE Transactions on Power Delivery 4(2): 1401-1407.

[30] Jayasekara, N.; Masoum, M.A.S.; and Wolfs, P.J. 2016. Optimal Operation of Distributed Energy Storage Systems to Improve Distribution Network Load and Generation Hosting Capability. IEEE Transactions on Sustainable Energy 7(1): 250-261.

BIOGRAPHY

Mr. Thanarat Phimtakhob was born in Nakhon Ratchasima, Thailand, in 2000. He received his Bachelor of Engineering degree in Electrical Engineering from Suranaree University of Technology in 2023. After graduation, he pursued his Master of Engineering in Electrical Engineering at the School of Electrical Engineering, Suranaree University of Technology.

During his graduate studies, his research focused on the improvement of voltage deviation in active distribution networks through the use of optimal voltage droop control with battery energy storage systems (BESS). His thesis integrates advanced optimization techniques, including Particle Swarm Optimization (PSO) and Fuzzy Multi-Objective Optimization (FMOO), to enhance voltage regulation and system stability under high renewable energy penetration.

In addition to his research work, Mr. Thanarat served as a teaching assistant for the undergraduate course Electric Circuits, where he supported laboratory sessions and assisted students in problem-solving. In 2024, he presented his research findings at the International Electrical Engineering Congress (IEECON 2024), gaining experience in academic communication and professional networking.

His academic interests include power system stability, energy storage integration, voltage control strategies, and the application of intelligent algorithms in electrical engineering.

Throughout his study, Mr. Thanarat has demonstrated strong analytical skills, effective communication, and a dedication to research in power system enhancement, with the goal of contributing to the development of more reliable and efficient smart grids.